# Hydrogen Isotopes from Lipid Biomarkers: Purification, Field Calibration, and Application to Reconstructing Galápagos Paleohydrology

Daniel B. Nelson

A dissertation

submitted in partial fulfillment of the

requirements for the degree of

Doctor of Philosophy

University of Washington

2013

Reading Committee:

Julian Sachs, Chair

Steven Emerson

Anitra Ingalls

Program Authorized to Offer Degree:

Oceanography

University of Washington

## Abstract

Hydrogen Isotopes from Lipid Biomarkers: Purification, Field Calibration, and Application to Reconstructing Galápagos Paleohydrology

Daniel B. Nelson

Chair of Supervisory Committee:

Associate Professor Julian Sachs

Oceanography

The tropics are centrally important in determining global climate patters as the primary heat and moisture source for atmosphere and ocean circulation. Understanding of the range of natural variability and the sensitivity to external change is limited by the short period of direct observation and the relative scarcity of paleoclimate records. In this thesis I develop and apply new methods to determine rainfall changes in the tropics based on the hydrogen isotopic composition of lipids from phytoplankton. Specifically, I enhance the capacity to measure the hydrogen isotopic composition of organic compounds preserved in sediments, calibrate the sensitivity of these values to modern lake water and salinity, and apply these tools to reconstruct hydrologic changes in the Galápagos. Several streamlined methods for purifying dinosterol, taraxerol, brassicasterol, and individual alkenones are presented using high performance liquid chromatography (HPLC). These techniques permit quantification of the hydrogen isotope fractionation in dinosterol, brassicasterol, individual alkenones, and *n*-alkanoic acids, from a

series of globally distributed lake surface sediments spanning a salinity range of 0 to 248 ppt. Dinosterol and brassicasterol hydrogen isotope fractionations decreased by approximately 1 ‰/unit change in salinity, which agrees with previous localized environmental transect studies, but individual alkenones and *n*-alkanoic acids are found to be relatively insensitive to changing salinity. These fractionation factors are then applied to reconstruct hydroclimate variations in the Galápagos islands during the past 2,000 years. Using a combination of $n$C$_{29}$-alkane, $n$C$_{24}$-alkanol, taraxerol and dinosterol hydrogen isotope data, as well as concentration profiles of *n*-alkanes, *n*-alkanols, and taraxerol, along with calibration data sets for mangrove- and algal-lipids, from three different saline lakes in the southern part of Isabela Island I quantitatively reconstruct lake water hydrogen isotope and salinity changes. The data imply that the region experienced significant hydrologic changes, with those occurring between approximately 0 and 1200 AD driven by shifts in the El Nino-Southern Oscillation system, and those between 1200 AD and the present driven predominantly by changes in position of the Intertropical Convergence Zone.

**Table of Contents**

# Chapter 1:

# Introduction

Observations inform us of the central role of the tropical Pacific in determining global climate conditions through the influence of the inter-tropical convergence zone (ITCZ) and its impact on Hadley circulation, as well as through interannual variability associated with the El Niño/Southern Oscillation (ENSO) and its global teleconnections. Reflecting this, the tropical Pacific is one of the most heavily instrumented regions of the world ocean. Unfortunately, despite this importance, when looking to the paleoclimate record the tropical Pacific is one of the most poorly constrained regions on the planet, owing largely to the lack of suitable paleoclimate archives and appropriate proxies. All aspects of my dissertation are tied together with the central goal of improving this situation by using compound specific hydrogen isotope analyses as a proxy for hydrology. My research can be divided into three general categories that include purification method development, field-based calibrations from surface sediments, and application of these methods and calibrations to provide new insight into paleohydrologic change in the eastern tropical Pacific.

The stable isotopes of hydrogen and oxygen have long served as useful indicators of a wide variety of processes within and relating to the hydrosphere, and in particular as sources of paleoclimate proxy data. Because the hydrogen and oxygen isotopic composition of water is a physical value that carries information related to transport history, which can then be preserved in materials in geologic archives on long timescales, measurements of these archives are outstanding indicators of past climate. Examples are numerous, but include applications to reconstruct near million-year records of polar air temperature (Jouzel et al., 2007), global sea surface temperatures spanning most of the Cenozoic Era (Zachos et al., 2001), Pleistocene ice volume changes (Shackleton, 1967), East Asian monsoon intensity (Wang et al., 2001), and mid-latitude storm track trajectories (Berkelhammer and Stott, 2008). However, in all cases accurate

interpretation of geologic oxygen and hydrogen isotope measurements requires a detailed understanding of which transport mechanisms are important for determining the water isotope composition and what other factors act to modify that value as it is recorded in a particular geologic archive since these will vary by geography and material type.

Understanding the processes that control the oxygen and hydrogen isotopic composition of precipitation in the tropics has lagged behind progress in polar regions. While it has been long recognized that the oxygen and hydrogen isotopic composition of precipitation is generally inversely correlated with amount of precipitation falling at sea-level sites in tropical marine environments (Dansgaard, 1964; Rozanski et al., 1993), robust theoretical frameworks to explain the empirical relationship have been limited. Recently, efforts have received renewed interest to explain this 'amount effect', which has resulted in advances in mechanistic explanations supported by atmospheric convection models and isotope-enabled general circulation models (GCMs) (Bony et al., 2008; Conroy et al., 2013; Risi et al., 2008). These efforts have been at least partially motivated by a combination of the relatively recent recognition of the importance of the tropics in paleoclimate (Chiang, 2009), advances in isotope-enabled general circulation models (GCMs) (Cole et al., 1999), and the advent of new sources of isotope proxy data in the form of speleothem carbonate and sedimentary biomarkers (e.g. Sachs et al., 2009; Wang et al., 2001).

Within the last decade, compound specific hydrogen isotope analyses by gas chromatography – isotope ratio mass spectrometry (GC-IRMS) have become more commonplace in biogeochemistry (Sessions et al., 1999). Hydrogen isotope values are reported as δD values, where $\delta D = [(D/H_{sample}/D/H_{standard}) - 1] \times 1000‰$, and D, and H stand for deuterium, and

hydrogen, respectively, and the reference standard is Vienna Standard Mean Ocean Water (VSMOW, δD = 0 ‰). This new analytical capacity generated considerable interest in the paleoclimate community since sedimentary biomarker records are often temporally continuous, span thousands of years, are of decadal-scale or better temporal resolution, and can be found in climatologically important regions, which is an exceedingly rare combination of traits among sources of paleoclimate data available from the tropics. Observations have demonstrated that δD values of lipids from photoautotrophs are well correlated with δD values of environmental water over large changes in water δD values, but with an offset, or 'fractionation factor', α ($\alpha = D/H_{lipid}/D/H_{water}$), that is usually larger than 100 ‰ (Hou et al., 2006; Huang et al., 2004; Sachse et al., 2004; Sessions et al., 1999; Zhang and Sachs, 2007). These robust correlations raised the possibility that lipid δD values in sedimentary archives might serve as a direct proxy for source water δD values. But subsequent calibration efforts have now conclusively demonstrated that this fractionation is not constant, and varies as a function of a variety of factors, including species type, growth rates, temperatures, and light levels for algal lipids (Romero-Viana et al., 2013; Sachs and Schwab, 2011; Sachse and Sachs, 2008; Schouten et al., 2006; Wolhowe et al., 2009; Zhang and Sachs, 2007; Zhang et al., 2009), and humidity, evapotranspiration rates, salinity, timing of leaf wax production, and changes in vegetation assemblage for lipids from terrestrial plants (Douglas et al., 2012; Hou et al., 2008; Kahmen et al., 2013a; Kahmen et al., 2013b; Ladd and Sachs, 2012; Liu and Yang, 2008; McInerney et al., 2011; Nelson et al., 2013; Polissar and Freeman, 2010; Sachse et al., 2009; Smith and Freeman, 2006; Tipple et al., 2013; Wang et al., 2013; Yang et al., 2011; Yang et al., 2009; Zhou et al., 2011). Although such secondary factors are a complication to reconstructing water δD values directly, they also provide an opportunity to recover additional environmental information. Sediments usually

contain dozens to several hundred lipids within the gas chromatography analyte window, which provides an opportunity to recover hydrogen isotope information from several compounds within a single sample. In lake or marine environments it can often be assumed that a variety of photoautotrophs synthesize lipids while drawing hydrogen from the same source water, so efforts to observe, quantify, and understand how these secondary factors modulate the biologic component of lipid δD values should permit quantitative recovery of the common water isotope signal from multiple analytes. At a minimum, calibration efforts allow for the most informed decisions to be made regarding which compounds are the best targets for qualitative climate reconstructions using hydrogen isotopes, and in a best case scenario they enable redundant and internally consistent quantitative reconstructions of water isotope δD values as well as other variables like salinity, temperature, humidity, and nutrient levels.

Most efforts to understand lipid δD values, and to apply these data as paleoclimate indicators to date have focused on *n*-alkanes or *n*-alkanoic acids, which are produced in high abundance by virtually all terrestrial higher plants as a part of the epicuticular wax in leaves (Eglinton and Hamilton, 1967). These compounds were logical first targets when lipid δD measurements became possible because they are relatively easy to purify from sediment lipid extracts and are found in most environments. But it is increasingly clear based on the growing recognition of secondary influences on lipid δD values outlined above that there are significant limitations on the information that can be recovered from this single biologic source, which reflects the amount-weighted average leaf wax δD value of all higher plants contributing these compounds to the sediment in a given environment. Logical augmenting targets come either from compounds that are more specific to a particular higher plant type, or that are representative

of a different class of organisms. Unfortunately, many such compounds are lipids that require more sophisticated and time-consuming purification procedures for hydrogen isotope analysis than leaf wax *n*-alkanes and *n*-alkanoic acids, which is precisely why they have received less attention. A primary focus of my research has therefore been aimed at improving and streamlining methods for purifying some of these more source specific lipids to enable more widespread investigation of the environmental significance of their δD values (Chapter 2).

Salinity has been shown to exert a major influence on the magnitude of D/H fractionation in algal lipids in laboratory cultures (Schouten et al., 2006), as well as in field studies that have targeted salinity gradients in isolated regions (Sachs and Schwab, 2011; Sachse and Sachs, 2008), but the extent and consistency of this relationship has not yet been assessed in the field at a global scale. In many ways this has limited more widespread implementation of algal lipid-based research, and the second major pillar of my work focused on reducing the uncertainty around this effect. I worked to compile and collect a series of surface sediment and/or suspended particle samples from more than 50 lakes and lagoons spanning a salinity range from ~ 0 – 248 ppt. I evaluated the distribution of compounds present at each site and then used available methods and new methods that I developed to purify and analyze the δD values of these compounds. I also recovered water samples from each lake and measured the δD value, which permitted me to calculate the α value for each target compound at each site to assess the extent to which changes in the magnitude of D/H fractionation were related to changes in salinity across diverse environments representing variable additional known influences on α values such as temperature, species distributions, and nutrients. This work was divided into three subcategories based on the nature of the compounds that were targeted.

The first group consisted of dinosterol (4α, 23, 24-trimethyl-5α-cholest-22E-en-3β-ol) and brassicasterol (24-methyl cholest-5, 22-dien-3β-ol) - two promising sedimentary biomarkers that are largely derived from aquatic photoautotrophs, the presence of which in sediments has been interpreted as a marker for dinoflagellates and diatoms, respectively, albeit also with some caveats (Rampen et al., 2010; Volkman, 2003; Volkman et al., 1998). Dinosterol δD values have been investigated previously to determine how salinity affects isotopic fractionation in this compound in the Chesapeake Bay (Sachs and Schwab, 2011) and also applied a paleohydrologic indicator in Palau (Smittenberg et al., 2011), but these are the first measurements of brassicasterol δD values. The second group of compounds used in the salinity calibration work were alkenones ($C_{37\text{-}39}$ di-, tri- and tetra-unsaturated methyl- and ethyl-ketones). These compounds are highly source specific in marine settings, and changes in their relative abundances have become a proven and reliable indicator of sea surface temperature (Brassell et al., 1986; Conte et al., 2006). Given the widely recognized importance and significance of these compounds, and previous experiments from laboratory batch cultures to investigate the influence of salinity on D/H fractionation (Schouten et al., 2006; van der Meer et al., 2013), these were targeted despite a lack of widespread occurrence in the compiled sample set. *n*-alkanoic acids were the final category of compounds. Although not highly source specific, long chain *n*-alkanoic acids are primarily derived from leaf wax, middle-chain *n*-alkanoic acids from submerged aquatic vegetation, and short-chain acids deriving from algae and higher plants, the widespread occurrence and application of these compounds in paleoclimate studies, combined with the fact that the influence of salinity on D/H fractionation during their biosynthesis had never been evaluated, prompted me to investigate this category. Collectively, the salinity

calibration work forms the second chapter of my dissertation (Chapters 3-5) that I expect will result in 3 separate publications.

The third chapter of my dissertation focuses on an application of biomarker δD values to provide insight on paleoclimate in the Galapagos over the past 2 kyr. The work is focused on sediment cores collected from Poza del Diablo, a brackish coastal lagoon on Isabela Island. The Diablo sediment record has sub-centennial scale resolution based on a radiocarbon chronology, and target compounds include $n$C$_{29}$ alkane, a common leaf wax compound, taraxerol, a triterpenoid specific to *Rhizophora* mangroves in this type of environment (Versteegh et al., 2004), dinosterol, from dinoflagellates, and an $n$C$_{24}$ alkanol that is derived from tetracosanyl 3-O-methyl-α-rhamnopyranoside in this lake, a glycolipid marker compound for cyanobacteria (Castañeda et al., 2011; Sinninghe-Damste et al., 2001). In addition, I developed complimenting records of the changing concentrations of these compounds in the sediments, and by combining all sources of lipid abundance and δD data, was able to produce an internally consistent and quantitative record of lake water δD values and salinity through time that is consistent with a recently published salinity reconstruction from the same location based on diatom assemblages (Seddon et al., 2011). I also developed shorter sediment records from two neighboring lakes – dinosterol and taraxerol δD records from Poza Verde, and dinosterol, taraxerol, and $n$C$_{29}$ alkane δD records from Poza Escondida – that span approximately the past 500 and 100 years, respectively, to compare with the data from Poza del Diablo. These records mirror the changes in the longer Diablo records, and corroborate the interpretation of the isotope signal as indicative of regional, rather than local changes that might be unique to a particular lake and not indicative of climate. These results are detailed in the final chapter of my dissertation (Chapter 6). The

individual components of my dissertation therefore build on one another and together represent an important step forward in advancing the capability to measure the δD values of new compounds, to understand the meaning of these measurements, and improve our understanding of tropical paleoclimate by applying these techniques in a climatologically important location.

**Chapter 1 References**

Berkelhammer, M.B., Stott, L.D., 2008. Recent and dramatic changes in Pacific storm trajectories recorded in d18O from Bristlecone Pine tree ring cellulose. Geochemistry, Geophysics, Geosystems 9, Q04008.

Bony, S., Risi, C., Vimeux, F., 2008. Influence of convective processes on the isotopic composition (d18O and dD) of precipitation and water vapor in the tropics: 1. Radiative-convective equilibrium and Tropical Ocean–Global Atmosphere–Coupled Ocean-Atmosphere Response Experiment (TOGA-COARE) simulations. Journal of Geophysical Research 113, D19305.

Brassell, S.C., Brereton, R.G., Eglinton, G., Grimalt, J., Liebezeit, G., Marlowe, I.T., Pflaumann, U., Sarnthein, M., 1986. Palaeoclimatic signals recognized by chemometric treatment of molecular stratigraphic data. Organic Geochemistry 10, 649-660.

Castañeda, I.S., Werne, J.P., Johnson, T.C., Powers, L.A., 2011. Organic geochemical records from Lake Malawi (East Africa) of the last 700 years, part II: Biomarker evidence for recent changes in primary productivity. Palaeogeography, Palaeoclimatology, Palaeoecology 303, 140-154.

Chiang, J.C.H., 2009. The Tropics in Paleoclimate. Annual Review of Earth and Planetary Sciences 37, 263-297.

Cole, J.E., Rind, D., Webb, R.S., Jouzel, J., Healy, R., 1999. Climatic controls on interannual variability of precipitation d18O: Simulated influence of temperature, precipitation amount, and vapor source region. Journal of Geophysical Research 104, 14,223 - 214,235.

Conroy, J.L., Cobb, K.M., Noone, D., 2013. Comparison of precipitation isotope variability across the tropical Pacific in observations and SWING2 model simulations. Journal of Geophysical Research: Atmospheres 118, 5867-5892.

Conte, M.H., Sicre, M.-A., Ruhlemann, C., Weber, J.C., Schulte, S., Schulz-Bull, D., Blanz, T., 2006. Global temperature calibration of the alkenone unsaturation index (Uk'37) in surface waters and comparison with surface sediments. Geochemistry, Geophysics, Geosystems 7.

Dansgaard, W., 1964. Stable Isotopes in Precipitation. Tellus 16, 436-468.

Douglas, P.M.J., Pagani, M., Brenner, M., Hodell, D.A., Curtis, J.H., 2012. Aridity and vegetation composition are important determinants of leaf-wax dD values in southeastern Mexico and Central America. Geochimica et Cosmochimica Acta 97, 24-45.

Eglinton, G., Hamilton, R.J., 1967. Leaf Epicuticular Waxes. Science 156, 1322-1335.

Hou, J., D'Andrea, W.J., Huang, Y., 2008. Can sedimentary leaf waxes record D/H ratios of continental precipitation? Field, model, and experimental assessments. Geochimica et Cosmochimica Acta 72, 3503-3517.

Hou, J., Huang, Y., Wang, Y., Shuman, B., Oswald, W.W., Faison, E., Foster, D.R., 2006. Postglacial climate reconstruction based on compound- specific D/H ratios of fatty acids from Blood Pond, New England. Geochemistry, Geophysics, Geosystems 7, Q03008.

Huang, Y., Shuman, B., Wang, Y., III, T.W., 2004. Hydrogen isotope ratios of individual lipids in lake sediments as novel tracers of climatic and environmental change: a surface sediment test. Journal of Paleolimnology 31, 363-375.

Jouzel, J., Masson-Delmotte, V., Cattani, O., Dreyfus, G., Falourd, S., Hoffmann, G., Minster, B., Nouet, J., Barnola, J.M., Chappellaz, J., Fischer, H., Gallet, J.C., Johnsen, S., Leuenberger, M., Loulergue, L., Luethi, D., Oerter, H., Parrenin, F., Raisbeck, G., Raynaud, D., Schilt, A., Schwander, J., Selmo, E., Souchez, R., Spahni, R., Stauffer, B., Steffensen, J.P., Stenni, B., Stocker, T.F., Tison, J.L., Werner, M., Wolff, E.W., 2007. Orbital and Millennial Antarctic Climate Variability over the Past 800,000 Years. Science 317, 793-796.

Kahmen, A., Hoffmann, B., Schefuß, E., Arndt, S.K., Cernusak, L.A., West, J.B., Sachse, D., 2013a. Leaf water deuterium enrichment shapes leaf wax n-alkane dD values of angiosperm plants II: Observational evidence and global implications. Geochimica et Cosmochimica Acta 111, 50-63.

Kahmen, A., Schefuß, E., Sachse, D., 2013b. Leaf water deuterium enrichment shapes leaf wax n-alkane dD values of angiosperm plants I: Experimental evidence and mechanistic insights. Geochimica et Cosmochimica Acta 111, 39-49.

Ladd, S.N., Sachs, J.P., 2012. Inverse relationship between salinity and n-alkane dD values in the mangrove Avicennia marina. Organic Geochemistry 48, 25-36.

Liu, W., Yang, H., 2008. Multiple controls for the variability of hydrogen isotopic compositions in higher plant n-alkanes from modern ecosystems. Global Change Biology 14, 2166-2177.

McInerney, F.A., Helliker, B.R., Freeman, K.H., 2011. Hydrogen isotope ratios of leaf wax n-alkanes in grasses are insensitive to transpiration. Geochimica et Cosmochimica Acta 75, 541-554.

Nelson, D.M., Henderson, A.K., Huang, Y., Hu, F.S., 2013. Influence of terrestrial vegetation on leaf wax dD of Holocene lake sediments. Organic Geochemistry 56, 106-110.

Polissar, P.J., Freeman, K.H., 2010. Effects of aridity and vegetation on plant-wax dD in modern lake sediments. Geochimica et Cosmochimica Acta 74, 5785-5797.

Rampen, S.W., Abbas, B.A., Schouten, S., Sinninghe-Damsté, J.S., 2010. A comprehensive study of sterols in marine diatoms (Bacillariophyta): Implications for their use as tracers for diatom productivity. Limnology and Oceanography 55, 91-105.

Risi, C., Bony, S., Vimeux, F., 2008. Influence of convective processes on the isotopic composition (δ18O andδD) of precipitation and water vapor in the tropics: 2. Physical interpretation of the amount effect. Journal of Geophysical Research 113.

Romero-Viana, L., Kienel, U., Wilkes, H., Sachse, D., 2013. Growth-dependent hydrogen isotopic fractionation of algal lipid biomarkers in hypersaline Isabel Lake (Mexico). Geochimica et Cosmochimica Acta 106, 490-500.

Rozanski, K., Araguas-Araguas, L., Gonfiantini, R., 1993. Isotopic patterns in modem global precipitation, in: Swart, P.K., Lohman, K.C., McKenzie, J., Savin, S. (Eds.), Climate Change in Continental Isotopic Records - Geophysical Monograph 78. American Geophysical Union, Washington, D.C., pp. 1-36.

Sachs, J.P., Sachse, D., Smittenberg, R.H., Zhang, Z., Battisti, D.S., Golubic, S., 2009. Southward movement of the Pacific intertropical convergence zone AD 1400–1850. Nature Geoscience 2, 519-525.

Sachs, J.P., Schwab, V.F., 2011. Hydrogen isotopes in dinosterol from the Chesapeake Bay estuary. Geochmica et Cosmochimica Acta 75, 444-459.

Sachse, D., Kahmen, A., Gleixner, G., 2009. Significant seasonal variation in the hydrogen isotopic composition of leaf-wax lipids for two deciduous tree ecosystems (Fagus sylvativa and Acer pseudoplatanus). Organic Geochemistry 40, 732-742.

Sachse, D., Radke, J., Gleixner, G., 2004. Hydrogen isotope ratios of recent lacustrine sedimentary n-alkanes record modern climate variability. Geochimica et Cosmochimica Acta 68, 4877-4889.

Sachse, D., Sachs, J.P., 2008. Inverse relationship between D/H fractionation in cyanobacterial lipids and salinity in Christmas Island saline ponds. Geochim. Cosmochim. Acta 72, 793-806.

Schouten, S., Ossebaar, J., Schreiber, K., Kienhuis, M.V.M., Langer, G., Benthien, A., Bijma, J., 2006. The effect of temperature, salinity and growth rate on the stable hydrogen isotopic composition of long chain alkenones produced by *Emiliania huxleyi* and *Gephyrocapsa oceanica*. Biogeosciences 3, 113-119.

Seddon, A.W.R., Froyd, C.A., Leng, M.J., Milne, G.A., Willis, K.J., 2011. Ecosystem Resilience and Threshold Response in the Galápagos Coastal Zone. Plos One 6, e22376.

Sessions, A.L., Burgoyne, T.W., Schimmelmann, A., Hayes, J.M., 1999. Fractionation of hydrogen isotopes in lipid biosynthesis. Organic Geochemistry 30, 1193-1200.

Shackleton, N.J., 1967. Oxygen Isotope Analyses and Pleistocene Temperatures Re-assessed. Nature 215, 15-17.

Sinninghe-Damste, J.S., Dongen, B.E.v., Rijpstra, W.I.C., Schouten, S., Volkman, J.K., Geenevasen, J.A.J., 2001. Novel intact glycolipids in sediments from an Antarctic lake (Ace Lake). Organic Geochemistry, 321-332.

Smith, F.A., Freeman, K.H., 2006. Influence of physiology and climate on delta D of leaf wax n-alkanes from C-3 and C-4 grasses. Geochimica et Cosmochimica Acta 70, 1172-1187.

Smittenberg, R.H., Saenger, C., Dawson, M.N., Sachs, J.P., 2011. Compound-specific D/H ratios of the marine lakes of Palau as proxies for West Pacific Warm Pool hydrologic variability. Quaternary Science Reviews 30, 921-933.

Tipple, B.J., Berke, M.A., Doman, C.E., Khachaturyan, S., Ehleringer, J.R., 2013. Leaf-wax n-alkanes record the plant–water environment at leaf flush. Proceedings of the National Acadamy of Sciences of the United States of America 110, 2659-2664.

van der Meer, M.T.J., Benthien, A., Bijma, J., Schouten, S., Sinninghe-Damsté, J.S., 2013. Alkenone distribution impacts the hydrogen isotopic composition of the C37:2 and C37:3 alkan-2-ones in *Emiliania huxleyi*. Geochimica et Cosmochimica Acta 111, 162-166.

Versteegh, G.J.M., Schefuss, E., Dupont, L., Marret, F., Damste, J.S.S., Jansen, J.H.F., 2004. Taraxerol and Rhizophora pollen as proxies for tracking past mangrove ecosystems. Geochimica et Cosmochimica Acta 68, 411-422.

Volkman, J.K., 2003. Sterols in microorganisms. Applied Microbiology and Biotechnology 60, 495-506.

Volkman, J.K., Barrett, S.M., Blackburn, S.I., Mansour, M.P., Sikes, E.L., Gelin, F., 1998. Microalgal biomarkers: A review of recent research developments. Organic Geochemistry 29, 1163-1179.

Wang, Y.J., Cheng, H., Edwards, R.L., An, Z.S., Wu, J.Y., Shen, C.-C., Dorale, J.A., 2001. A High-Resolution Absolute-Dated Late Pleistocene Monsoon Record from Hulu Cave, China. Science 294, 2345-2348.

Wang, Y.V., Larsen, T., Leduc, G., Andersen, N., Blanz, T., Schneider, R.R., 2013. What does leaf wax dD from a mixed C3/C4 vegetation region tell us? Geochimica et Cosmochimica Acta 111, 128-139.

Wolhowe, M.D., Prahl, F.G., Probert, I., Maldonado, M., 2009. Growth phase dependent hydrogen isotopic fractionation in alkenone-producing haptophytes. Biogeosciences 6, 1681-1694.

Yang, H., Liu, W., Leng, Q., Hren, M.T., Pagani, M., 2011. Variation in n-alkane dD values from terrestrial plants at high latitude: Implications for paleoclimate reconstruction. Organic Geochemistry 42, 283-288.

Yang, H., Pagani, M., Briggs, D.E.G., Equiza, M.A., Jagels, R., Leng, Q., LePage, B.A., 2009. Carbon and hydrogen isotope fractionation under continuous light: implications for paleoenvironmental interpretations of the High Arctic during Paleogene warming. Oecologia 160, 461-470.

Zachos, J., Pagani, M., Sloan, L., Thomas, E., Billups, K., 2001. Trends, Rhythms, and Aberrations in Global Climate 65 Ma to Present. Science 292, 686-693.

Zhang, Z., Sachs, J.P., 2007. Hydrogen isotope fractionation in freshwater algae: I. Variations among lipids and species. Organic Geochemistry 38, 582-608.

Zhang, Z., Sachs, J.P., Marchetti, A., 2009. Hydrogen isotope fractionation in freshwater and marine algae: II. Temperature and nitrogen limited growth rate effects. Organic Geochemistry 40, 428-439.

Zhou, Y., Grice, K., Chikaraishi, Y., Stuart-Williams, H., Farquhar, G.D., Ohkouchi, N., 2011. Temperature effect on leaf water deuterium enrichment and isotopic fractionation during leaf lipid biosynthesis: Results from controlled growth of C3 and C4 land plants. Phytochemistry 72, 207-213.

# Chapter 2:

# Concurrent Purification of Sterols, Triterpenols and Alkenones from Sediments for Hydrogen Isotope Analysis using High Performance Liquid Chromatography

[*In Revision at Organic Geochemistry, Aug. 21, 2013*]

**Concurrent Purification of Sterols, Triterpenols and Alkenones from Sediments for Hydrogen Isotope Analysis using High Performance Liquid Chromatography**

Daniel B. Nelson[1*], Julian P. Sachs[1]

1. University of Washington, School of Oceanography, Box 355351, Seattle, WA 98195, USA

*Corresponding author. Tel: 1-206-685-9879; email: dbnelson@uw.edu

**Abstract**

Three methods are presented to purify acetylated sterols, acetylated triterpenols, and individual alkenones for hydrogen isotope analysis from marine and lacustrine sediments using reverse-phase high performance liquid chromatography (RP-HPLC). The main advantages over previous HPLC methods are reduced operator time, increased automation, and the ability to simultaneously purify multiple target compounds from a sample. These gains are achieved primarily by acetylating compounds prior to purification rather than after, and also by using a fraction collector with semi-preparatory configuration rather than analytic. The effectiveness of the method is demonstrated for (i) dinosterol and taraxerol in sediment from the brackish pond Poza del Diablo, Galápagos, (ii) for di- and tri-unsaturated $C_{37}$ and $C_{38}$ alkenones in cultured *Emiliania huxleyi*, (iii) for brassicasterol, and di-, tri-, and tetra-unsaturated $C_{37}$ alkenones in sediment from Manito Lake, Saskatchewan, Canada, and (iv) for brassicasterol, dinosterol, and di-, tri-, and tetra-unsaturated $C_{37}$ alkenones in sediment from The Great Salt Lake, Utah. The purification process yields 80-90 % recoveries and results in no measurable hydrogen isotope alteration.

**Keywords:** hydrogen isotopes; biomarkers; lipids; dinosterol; taraxerol; brassicasterol; alkenones; HPLC-MS; GC-IRMS.

## 1. Introduction

Selecting appropriate compounds for hydrogen isotope analysis of biomarkers in sediments for paleoenvironmental applications is often a balance between the biological source, its specificity, and the relative ease of purification. The hydrogen isotopic composition of both terrestrial and aquatic lipid biomarkers are increasingly being used as hydrologic indicators. But their value is offset from the hydrogen isotopic composition of the environmental water due to a combination of biologically controlled isotopic fractionations, many of which are sensitive to secondary environmental parameters such as humidity, salinity or the growth rate of the organism (e.g. Douglas et al., 2012; Sachse and Sachs, 2008; Schouten et al., 2006; Wolhowe et al., 2009; Zhang and Sachs, 2007; Zhang et al., 2009). Many applications of hydrogen isotope measurements for paleoenvironmenal investigation have attempted to work around these issues by targeting compounds that are produced by a wide range of organisms, such as leaf waxes, with the hope that the biological factors average out and that the isotope signal is reflective of the precipitation signal common to each compound-producing organism. Long chain *n*-alkanes and *n*-alkanoic acids are the most common leaf wax compounds measured. These are produced in high abundance by terrestrial higher plants, are relatively easy to purify from sedimentary lipid extracts, and many calibration studies have been performed in modern environments to demonstrate an empirical link between their hydrogen isotopic composition and that of local precipitation (Sachse et al., 2012). However, some calibration efforts have identified additional controls on the hydrogen isotopic composition of these compounds including humidity, salinity, and shifting vegetation assemblages (Douglas et al., 2012; Ladd and Sachs, 2012; Nelson et al., 2013).

Although many of these shortcomings are not unique to leaf wax compounds, it is increasingly clear that the isotope signal recovered from any single molecule may not always be a reliable indicator of past hydrologic conditions. Nevertheless, the hydrogen isotopic composition of biomarkers remains a useful hydrologic indicator, provided that the complicating issues are understood and managed appropriately. Additional paleohydrologic proxy data may therefore be of value in providing supporting and complimentary information on which to interpret an isotope record from a single compound. One such strategy is to extend the investigation to include additional biomarkers since laboratories that are equipped to measure the hydrogen isotopic composition of one compound are well positioned to measure additional compounds. Lipids with higher degrees of source specificity and alternate sources are likely to be effective compliments.

Sterols and triterpenols tend to be more source-specific than *n*-alkanes and *n*-alkanoic acids. Examples among these include dinosterol (4α,23,24-trimethyl-5α-cholest-22E-en-3 $\beta$ -ol), which is produced primarily by dinoflagellates (Volkman, 2003; Volkman et al., 1998), and has been the target of previous hydrogen isotope calibration (Sachs and Schwab, 2011), and paleoclimate studies (Sachs et al., 2009; Smittenberg et al., 2011). Brassicasterol (24-methyl cholest-5,22-dien-3 $\beta$ -ol) has been applied as a biomarker in sediments to indicate the presence of diatoms, although it is also produced by other microalgae including haptophytes and cryptophytes, and can also be found in some higher plants (Volkman, 2003). However, the viability of the hydrogen isotopic composition of brassicasterol as a paleoenvironmental indicator has not been thoroughly evaluated. Taraxerol (3 $\beta$ -D-friedoolean-14-en-3-ol) is a pentacyclic triterpenoid that is produced in high abundance by *Rhizophora* mangroves, and has

been shown to covary in sediments with *Rhizophora* pollen (Versteegh et al., 2004). This highly source-specific compound presents an attractive target for evaluating the hydrogen isotope signal from higher plants in coastal tropical and subtropical environments, particularly given the recently demonstrated complexity associated with the hydrogen isotopic composition of leaf waxes from mangroves, and the potential for mixed mangrove and non-mangrove sources of *n*-alkanes and *n*-alkanoic acids (Ladd and Sachs, 2012). Alkenones (unsaturated $C_{37\text{-}39}$ methyl and ethyl ketones), though not sterols or triterpenols, are specific to a relatively small number of haptophyte algae in both marine and lacustrine environments (Conte et al., 2006; Theroux et al., 2010; Volkman et al., 1980). Alkenones are the basis of the well-established $U^{k'}_{37}$ sea surface temperature proxy (Brassell et al., 1986; Conte et al., 2006), have been the focus of previous hydrogen isotope investigations (Englebrecht and Sachs, 2005; Leduc et al., 2013; Pahnke et al., 2007; Schwab and Sachs, 2011; van der Meer et al., 2007), and are therefore also attractive targets for continued application. The potential for added perspective on paleoenvironmental conditions from δD measurements on algal biomarkers is already well-documented, particularly when paired with δD measurements from higher plants, which together may reveal greater insight on paleoaridity than would be possible from either type of compound on its own (Mügler et al., 2008; Sachse et al., 2004).

Unfortunately, sterols and triterpenols that are specific to a particular organism or class of organisms such as those described above are not well resolved by gas chromatography-isotope ratio mass spectrometry (GC-IRMS) after a single extraction or compound-class fractionation by aminopropyl or silica column chromatography. Existing methods developed for geochemical application using high performance liquid chromatography (HPLC) have proven effective for

purifying dinosterol (Atwood and Sachs, 2012; Smittenberg and Sachs, 2007) and individual alkenones (Schwab and Sachs, 2009) from some sediment matrices, but these methods are all time consuming, require near constant operator attention and extensive post-purification handling procedures, and include multiple steps where mishandling can induce isotopic fractionation. They are each also not well developed for purifying multiple target compounds from the same sample injection. Applications of HPLC-based purification strategies for compound-specific hydrogen isotope analysis by geochemists have been somewhat limited, but the approach has recently gained ground in the sports doping testing field (e.g. Piper et al., 2011; Piper et al., 2013; Piper et al., 2012). Literature reviews of other disciplines suggest that HPLC-purification for compound-specific hydrogen isotope analysis has not yet been implemented, although examples of HPLC purification for bulk isotope analysis exist, such as vanilla purification for food science applications (Lamprecht et al., 1994). HPLC-based steroid purification techniques for purposes other than hydrogen isotope analysis have been applied more widely, including purification of steroids from coral (Jin et al., 2005) and mushrooms (Mattilaa et al., 2002), although many applications are analytical rather than semi-preparatory (e.g. McDonald et al., 2012).

Continued improvement of HPLC-based compound purification procedures is important for eliminating the risk of compromising the sample, and also for increasing sample throughput since paleoenvironmental applications require large numbers of analyses. Toward these ends we present a series of new HPLC-based methods for purifying sterols, triterpenols, and alkenones from complex sample matrices typical of lacustrine and marine sediment lipid extracts. Isotope measurements are discussed in standard δ-notation $[(R_{sample}/R_{standard})-1]*1000‰$, where R

represents the raw isotopic ratio. Hydrogen isotope measurements are discussed as δD values, and are referenced to VSMOW.

## 2. Methods

### *2.1 Samples and Lipid Extraction*

Four samples were used to demonstrate the new HPLC methods that we present. A sediment sample from Poza del Diablo was collected in June 2008 using a Livingstone-type coring device (Geocore, Columbus, OH). Surface sediment from Manito Lake, Saskatchewan, Canada, was collected in 2007 using a Van Veen sediment sampler (Bowman and Sachs, 2008), and surface sediments from the Great Salt Lake were collected as a part of the same field campaign. Excess material from an *Emiliania huxleyi* culturing experiment was collected after the conclusion of controlled conditions and passed through a 0.7 μm glass fiber filter (Whatman GF/F). This material was used only as a known source of readily available alkenones for method development purposes, and is not representative of any known temperature, or culture water δD value. All samples were freeze dried and extracted in a 9:1 mixture of dichloromethane (DCM) and methanol (MeOH) on an accelerated solvent extractor (ASE) Dionex 200 operated at 100 °C and 1500 psi with three five-minute static phases. Excess solvent was evaporated under $N_2$ from the total lipid extract (TLE) on a Turbo-vap system (Caliper, Hopkinton, MA, USA).

*2.2. Pre-HPLC compound class separations*

The sediment samples used to demonstrate the methods presented here were each a part of separate studies with independent goals, while the culture material was used only for HPLC method development. Due to the varied nature of the samples and their associated projects, pre-HPLC sample cleanup differed between the samples, but we note that no particular pre-sample cleanup is preferred over another provided that the sample is soluble in the HPLC injection solvent when the target compounds are present at adequate concentration for hydrogen isotope analysis after purification. Galápagos, Great Salt Lake and *Emiliania huxleyi* TLEs were eluted from glass solid phase extraction columns that were hand-packed with 1 g of silica gel 60 (5 % deactivated by weight; EMD chemicals, 35-75 μm). Hydrocarbon fractions were eluted with 10 mL of hexane, ketones with 6mL DCM/hexane (1:1), alcohols with 8mL ethyl acetate (EtOAc)/hexane (1:4), followed by a polar fraction with 6mL methanol. The Galápagos alcohol fraction, the *Emiliania huxleyi* ketone fraction, and the combined ketone-alcohol fraction from The Great Salt Lake were purified further by HPLC. The Manito Lake TLE was separated into polar and non-polar fractions using a liquid-liquid extraction by dissolution in 2 mL of methanol, to which 2 mL of hexane was added. The mixture was then agitated and sonicated to ensure complete dissolution of the TLE. The solvents were allowed to separate, after which the hexane supernatant was removed by Pasteur pipet. This was repeated ten times with the supernatants combined. To assess recovery, 5 % aliquots of the methanol and hexane fractions were removed and evaluated by gas chromatography mass spectrometry (GC-MS), which revealed no remaining GC-amenable compounds in the methanolic mother liquor.

*2.3 Gas Chromatography-Mass Spectrometry*

GC-MS analyses of all sample aliquots were conducted with an Agilent 6890N GC with 5975 inert mass selective detector equipped with an Agilent (formerly Varian) VF-17ms column (60 m X 0.32 mm X 0.25 μm). Samples were injected in splitless mode at 300 °C using helium carrier gas at 1.5 mL/min. For most injections, the GC oven was held at the initial temperature of 110 °C for 3 minutes after sample injection, then increased to 170 °C at 15 °C/min, then to 325 °C at 5 °C/min and held for 24 minutes. For some purified sterol and triterpenol samples the GC oven was held at an initial temperature of 120 °C for 10 minutes, then increased to 260 °C at 20 °C/min, then to 300 °C at 1 °C/min, then to 325 °C at 20°C/min and held for 8 minutes. All samples were run in full scan mode (*m/z* 50-700). Compound quantification was approximated based on the relative areas of unknown peaks to that of a 5α-cholestane internal standard added to each sample prior to GC-MS analysis.

*2.4 High-Performance Liquid Chromatography purification*

HPLC purifications were performed with an Agilent 1100 HPLC-MSD equipped with a solvent degasser, quaternary pump, autoinjector, fraction collector, and mass selective detector. Samples were injected in 25 μL of 2:1 DCM/MeOH. An Agilent ZORBAX Eclipse XDB $C_{18}$ column (4.6 mm X 250 mm X 5 μm) equipped with matching guard column was used at a constant temperature of 30 °C and flow rate of 1.5 mL/min. Column effluent was directed to an adjustable flow splitter (Analytical Science Instruments), where 2 % was diverted to the mass spectrometer and 98 % to the fraction collector. The fraction collector was equipped with a

semi-preparatory needle and fractions tray, which permitted recovery of up to 28.5 mL of column effluent per vial. The 2 % split flow to the MSD was augmented with 0.3 mL/min methanol supplied from an HPLC pump (Waters 510) to improve ionization. The MSD was operated in positive atmospheric pressure chemical ionization mode (APCI+) with the following specifications: gas temperature 350 °C, vaporizer 250 °C, drying gas 12.0 L/min, nebulizer pressure 20 psig. The methods we present are semi-preparatory rather than analytical, so extensive efforts to optimize detection or to determine the limit of detection for each compound on the MSD were not undertaken, although we may make the general statement that dinosterol-acetate was significantly more difficult to detect than taraxerol-acetate, brassicasterol-acetate, or individual alkenones. Samples containing sterols or triterpenols intended for purification were acetylated prior to injection on the HPLC by heating to 70 °C for 30 minutes in a mixture of 20 μL acetic anhydride of known δD value and 20 μL pyridine.

Mobile phase composition varied for each of the three samples and methods discussed. In order to purify dinosterol and taraxerol from the Galápagos sediment sample (Figures 1 & 2), an initial mobile phase of 5 % MeOH in acetonitrile (ACN) was maintained for 10 minutes, followed by a ramp to 5:10:85 MeOH:EtOAc:ACN from 10-20 minutes, and an isocratic phase to 65 minutes. After 65 minutes the column was cleaned by transitioning to 100 % EtOAc from 65-75 minutes and maintaining from 75-85 minutes. The column was transitioned back to 5 % MeOH in ACN from 85-95 minutes, and re-equilibrated under these conditions from 95-105 minutes in preparation for the next sample injection. Under these conditions, taraxerol-acetate was typically eluted between 35-41 minutes, and dinosterol-acetate between 56-62 minutes, although precise retention times varied slightly over time and as a function of column loading.

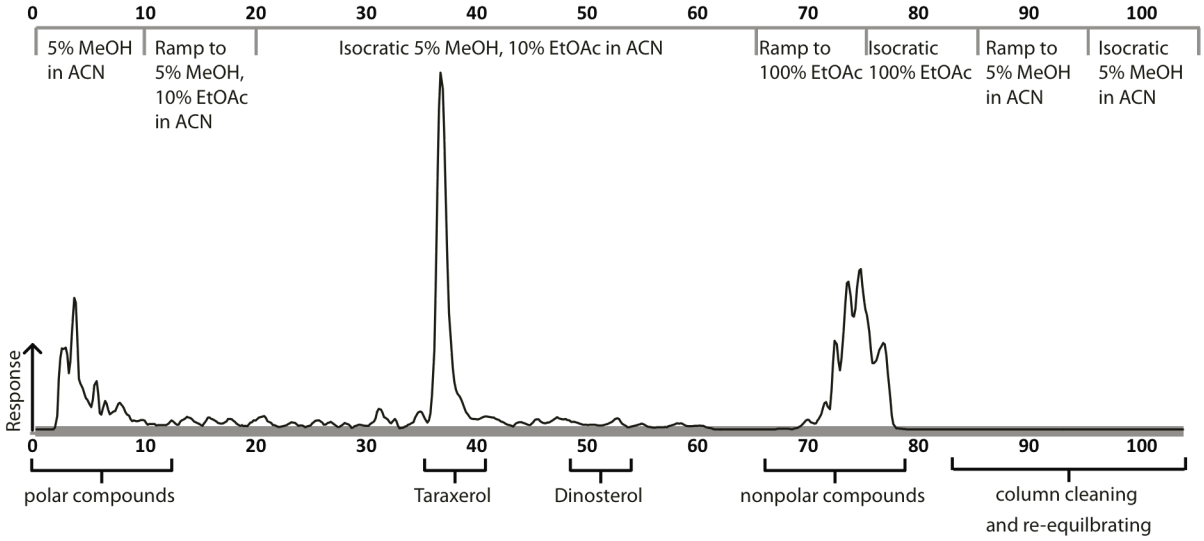


**Figure 1:** HPLC-MS total ion chromatogram of taraxerol- and dinosterol-acetate purification from lake sediments from the Galápagos with run time listed in minutes on the x-axes. Mobile phase makeup listed below the upper x-axis, and compound elution and column cleaning and re-equilibration events listed below the lower x-axis.

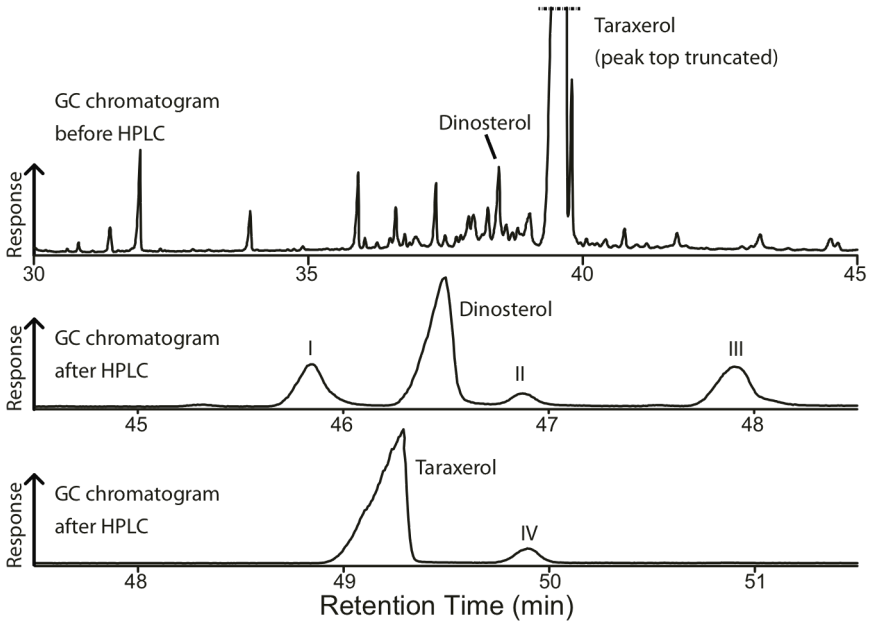


**Figure 2:** GC chromatograms comparing pre- and post-HPLC purification of dinosterol- and taraxerol-acetate. Taraxerol peak top is truncated in the pre-HPLC chromatogram in order to facilitate visualization of dinosterol and other unwanted peaks. Non-target compounds tentatively identified in lower panels: I) 4α-24-dimethylcholestanol-acetate, II) 4α-methyl-24-ethyl-5α-cholest-22E-en-3β-ol-acetate, III) 24-ethyl-5α-cholestan-3β-ol-acetate (sitostanol), IV) olean-12-en-3β-ol-acetate (β-amyrin). Retention time shifts between pre- and post-HPLC samples occur as a result of the GC method; pre-HPLC uses faster temperature ramp.

For the *Emiliania huxleyi* sample (Figure 3), where individual alkenones were the only target compounds, initial mobile phase composition was 5:30:65 MeOH:EtOAc:ACN. These conditions were maintained from 0-60 minutes, with approximate elution windows of individual alkenones as follows: $C_{37:3}$ from 27-30 minutes, $C_{38:3}$ from 32-36 minutes, $C_{37:2}$ from 37-39 minutes, and $C_{38:2}$ from 45-48 minutes. After 60 minutes the column was cleaned and re-equilibrated following a similar procedure to the sterol/triterpenols method: ramp to 100 % EtOAc from 60-70 minutes, hold from 70-80 minutes, ramp back to the initial blend of 5:30:65 MeOH:EtOAc:ACN from 80-90 minutes, and then hold from 90-100 minutes.

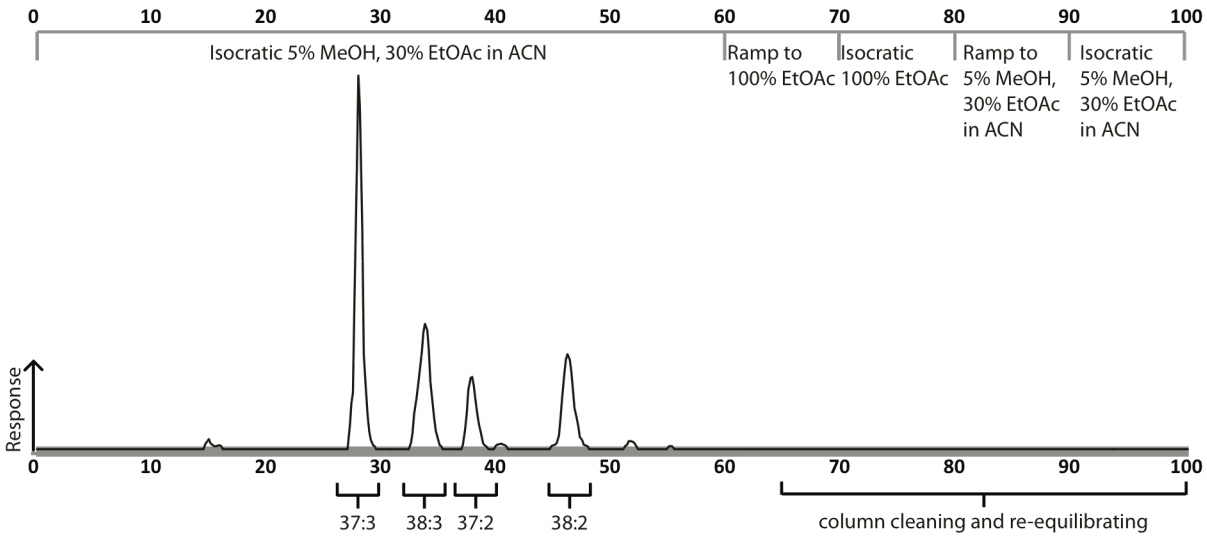


**Figure 3:** HPLC-MS total ion chromatogram of stand-alone alkenone purification from biomass from a chemostat culture of *Emiliania huxleyi* with run time listed in minutes on the x-axes. Mobile phase makeup listed below the upper x-axis, and compound elution and column cleaning and reconditioning events listed below the lower x-axis.

The Manito Lake and Great Salt Lake sediment samples (Figures 4 - 6) consisted of a complex mixture of coeluting sterols on GC, as well as alkenones and hopanoids. In order to purify brassicasterol, dinosterol and alkenones from a single sample using one HPLC injection, the methods described above were combined with minor modification. The initial mobile phase makeup was identical to that used for sterol and triterpenol purification from the Galápagos samples, but following this the mobile phase was transitioned to 5:20:75 MeOH:EtOAc:ACN from 65-75 minutes and maintained until 145 minutes as individual alkenones were eluted (Figure 4). A 20-minute column cleaning with ethyl acetate from 145-165 and a 20-minute re-equilibration interval with the initial mobile phase composition from 165-185 minutes again followed target compound elution. Brassicasterol, was eluted as its acetyl-ester from 28-32 minutes, acetylated dinosterol eluted with similar retention time as compared to the method described for the Galápagos sample, while the individual alkenones were eluted as follows: $C_{37:4}$ from 76-82 minutes, $C_{37:3}$ from 97-103 minutes, $C_{38:3}$ from 113-119 minutes, $C_{37:2}$ from 121-128 minutes, and $C_{38:2}$ from 143-149 minutes.

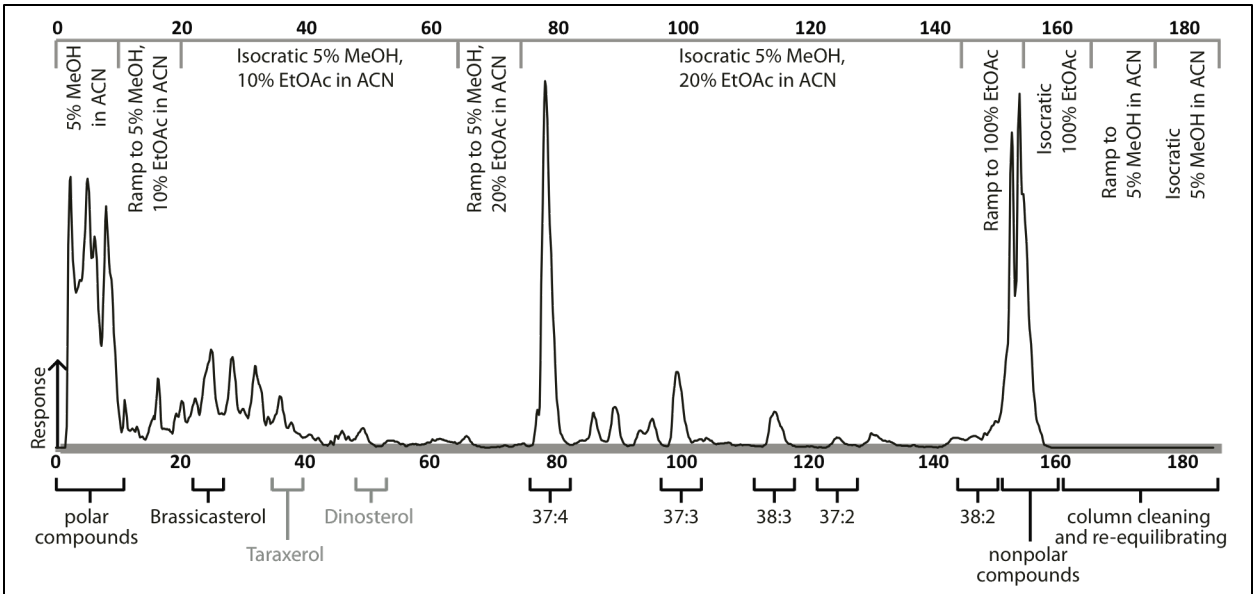


**Figure 4:** HPLC-MS total ion chromatogram and method outline for sterol-, triterpenol-acetate and alkenone purification from sediments. Example shows Manito Lake, Saskatchewan, Canada sample, but the Great Salt Lake sample was processed following the same procedure. Run time is listed in minutes on the x-axes, mobile phase makeup is listed below the upper x-axis, and compound elution and column cleaning and re-equilibration events listed below the lower x-axis. Dinosterol- and taraxerol-acetate are listed in gray below the lower x-axis to indicate their approximate retention time using this method, although they were not present in the Manito Lake example. $C_{38}$ alkenones are also indicated on this example, but note that $C_{38:2}$ is highly retained, and did not elute until column cleaning commenced.

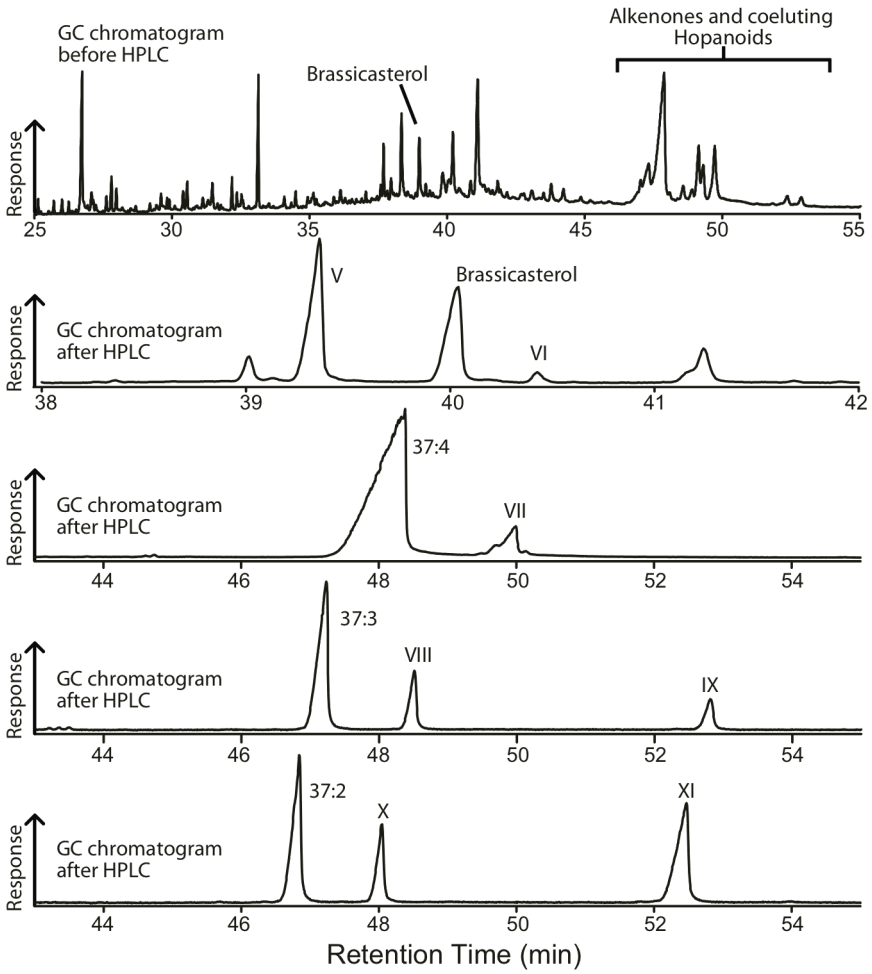


**Figure 5:** GC chromatograms comparing pre- and post-HPLC purification of brassicasterol-acetate, and tetra-, tri-, and di-unsaturated $C_{37}$ alkenones. Note the difference in scale of the x-axis in the pre-HPLC chromatogram. Non-target compounds tentatively identified in lower panels: V) cholesterol-acetate, VI) 5α-cholest-8(14)-en-3β-ol-acetate (doristerol), VII) $C_{38:4}$ alkenone ($MeC_{38:4}$), VIII) $C_{37:4}$ ethyl-alkenoate ($EtOC_{37:4}$), IX) $C_{39:4}$ alkenone ($MeC_{39:4}$), X) $C_{37:3}$ ethyl-alkenoate ($EtOC_{37:3}$), XI) $C_{39:3}$ alkenone ($MeC_{39:3}$). All chromatograms shown used the same fast-oven ramp GC method.

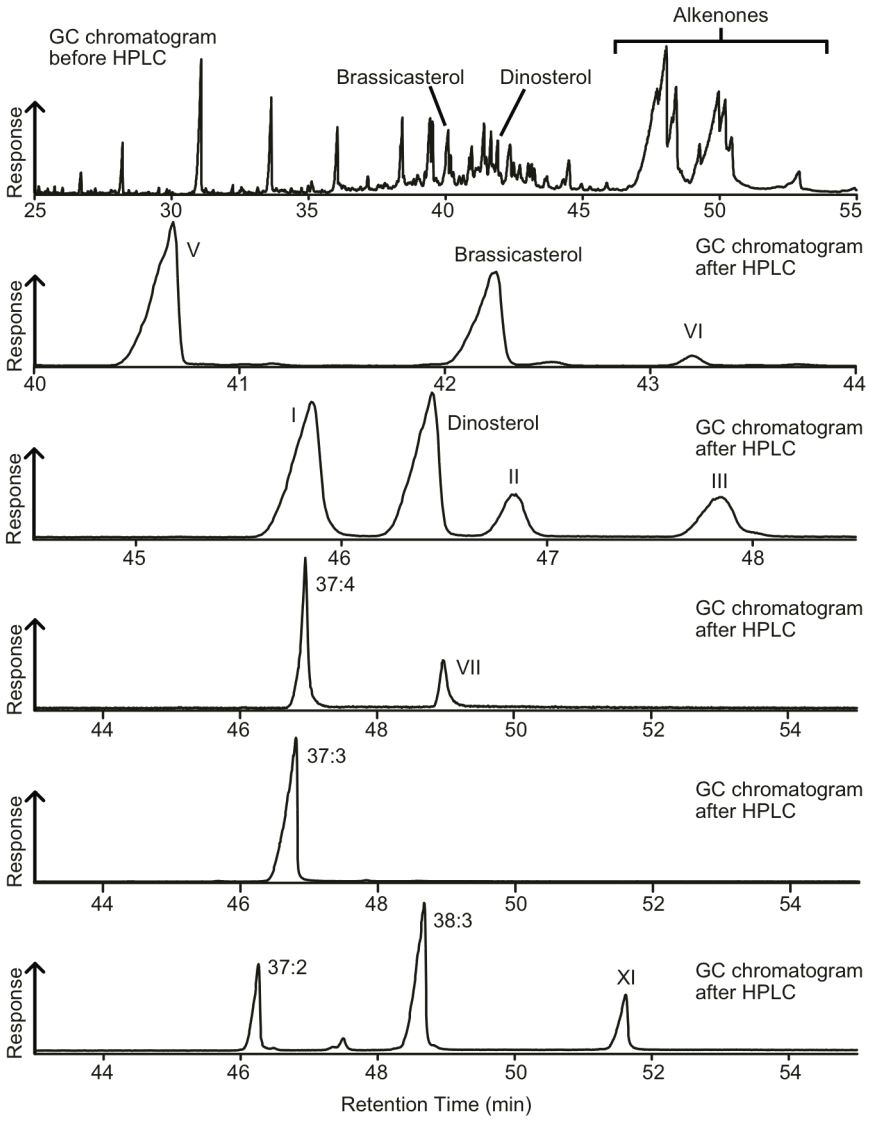


**Figure 6:** GC chromatograms comparing pre- and post-HPLC purification of brassicasterol-acetate, dinosterol-acetate, and tetra-, tri-, and di-unsaturated $C_{37}$ alkenones. Note the difference in scale of the x-axes between chromatograms. Non-target compounds are as in previous figures. Pre-HPLC and alkenone chromatograms used a fast-oven ramp GC method, while dinosterol and brassicasterol chromatograms are from a slow-oven ramp method.

*2.5 Gas Chromatography-Isotope Ratio Mass Spectrometry*

Purified target compound δD values were measured by gas chromatography-isotope ratio mass spectrometry (GC-IRMS) using a Thermo Delta V Plus isotope ratio mass spectrometer and Thermo Trace GC Ultra interfaced to a gas chromatography combustion interface III. Samples were injected in splitless mode at 330 °C using helium carrier gas at 1.5 mL/min. The GC was equipped with either an identical column to the GC-MS, or a similar VF-17ms with slightly narrower diameter (60 m X 0.25 mm X 0.25 μm). The GC-IRMS oven program for sterols and triterpenols was identical to the GC-MS sterol/triterpenol program with the exception of the initial oven temperature and hold time, which was 120 °C for 2 minutes. Alkenones were injected with an initial oven temperature of 120 °C, which was then increased to 230 °C at 20 °C/min, then to 325 °C at 8 °C/min and held for 17 minutes. GC column effluent was directed through the pyrolysis reactor and combustion interface prior to introduction to the mass spectrometer. The $H_3^+$ factor was measured prior to every sample sequence, and was stable at less than 5 (Sessions et al., 2001).

External isotope standard mixes were analyzed between approximately every six samples (standards from Arndt Schimmelmann at Indiana University, Bloomington, IN, USA). Two standard mixes were typically run for sterols, the first of which used *n*$C_{26}$, *n*$C_{38}$, and *n*$C_{40}$ and the second of which used *n*$C_{39}$, and *n*$C_{41}$. Samples and external standards were both also injected with a co-injection standard, which included *n*$C_{21}$, *n*$C_{23}$, *n*$C_{28}$, *n*$C_{32}$ and *n*$C_{34}$. For alkenones, the external standard used *n*$C_{26}$, *n*$C_{38}$, and *n*$C_{41}$, while the co-injection standard included *n*$C_{21}$, *n*$C_{23}$, *n*$C_{28}$, *n*$C_{32}$, *n*$C_{34}$, and *n*$C_{39}$. Initial isotopic evaluations of all peaks were performed within the Isodat software relative to a calibrated reference gas. Secondary corrections were performed

based on the regression of Isodat-reported δD values of external standard *n*-alkanes and their accepted values in order to maintain like treatments of samples and standards, as well as to correct for potential scale compression or stretching as a result of the one-point referencing to VSMOW performed by the Isodat software. Mixtures of external standards were prepared from individual alkane standards in order to ensure adequate baseline separation between peaks to avoid potential biasing of compounds used in the calibration due to short-term memory effects in the pyrolysis reactor (Wang and Sessions, 2008). Co-injection standards in samples were measured as unknown peaks to verify the accuracy of the correction procedure, and most samples were analyzed at least three times. Measurement precision for samples run using the sterol/triterpenol GC oven program was typically 4-6 ‰, and average co-injection standard accuracy was 1-3 ‰. For samples run using the alkenone GC oven program, precision was typically 3 ‰, and average co-injection standard accuracy was 1-3 ‰. Peak areas less than 15 V·s were below the cutoff identified on this GC-IRMS to avoid size dependent δD effects, and were not considered (Polissar et al., 2009). δD values for acetylated compounds were corrected by mass balance calculation based on the number of total hydrogen atoms analyzed per compound and the weighted δD value contribution of the hydrogen of known isotopic composition in the acetyl group to the measured δD value.

## 3. Results and Discussion

Previous HPLC-based methods for purifying dinosterol and individual alkenones from sediments are described in detail in Smittenberg and Sachs (2007), Schwab and Sachs (2009), and Atwood and Sachs (2012) (hereafter SS07-SS09-AS12). These methods have been

successfully applied in several studies (Leduc et al., 2013; Sachs and Schwab, 2011; Schwab and Sachs, 2009; Schwab and Sachs, 2011; Smittenberg et al., 2011). Our goal with this study was to decrease the time and number of steps required to process a sample, while expanding the range of lipids that could be purified with a single HPLC method, all while minimizing the potential for isotope fractionation, since large isotope effects are known to occur across an HPLC peak (Atwood and Sachs, 2012; Schwab and Sachs, 2009; Smittenberg and Sachs, 2007). Given this last fact, we consider it necessary to collect the entire HPLC peak to avoid isotopic fractionation and chose not to repeat the experiments to demonstrate that the magnitude of this effect is large. We adopted several new procedures and instrumental adaptations that are unique from SS07-SS09-AS12. As a starting point we replaced the analytical configuration in the fraction collector with a semi-preparatory configuration. This permitted several complete samples to be collected within a single fractions tray, and thus permitted automated sequences of samples to be run unattended, which was previously not possible. The change also made it possible to collect entire target compounds within a single collection vial, thereby eliminating the potential for isotopic fractionation in the event of mishandling during recombination of fractions.

*3.1 Derivatization*

Compounds that contain exchangeable hydrogen must be derivatized prior to hydrogen isotope analysis by GC-IRMS. Derivatization replaces active hydrogen with hydrogen of known isotopic composition, and improves chromatography. For sterols and triterpenols, which typically contain one hydroxyl group, acetylation—i.e. the replacement of the hydroxyl hydrogen with an acetate ester—is the preferred method of derivatization for its procedural ease and

permanence. Acetylation also limits the total number of hydrogen atoms to three that are added to the target compound that must then be isotopically corrected for (as opposed to 9 for a silyl ether).

The HPLC-based methods developed by SS07 and AS12 were aimed at purification of sterols or triterpenols as free alcohols for hydrogen isotope analyses. Following purification, it was therefore necessary to individually transfer each HPLC fraction to vials suitable for analysis by gas chromatography, and then to individually derivatize each compound fraction, as well as each bracketing fraction. Because acetylation is not easily reversible and no methods existed for purifying acetylated compounds prior to this study, test aliquots of individual LC fractions were typically first sub-sampled, derivatized, and analyzed by GC-MS to identify which fractions contained the target compound. The remainder of the LC fractions were then recombined, derivatized, and analyzed by GC-IRMS. The time required for this procedure, and the potential for H-isotope alteration through partial sample loss, make acetylation prior to HPLC-based separation a better alternative.

### *3.2 The mobile phase*

#### *3.2.1 Pre-acetylation of sterols and triterpenols*

By acetylating the sterols and triterpenols prior to injection on the HPLC they are immediately ready for GC-MS or GC-IRMS following elution from the HPLC column. But their reduced polarity required changes to the mobile phase from the RP-HPLC method in Atwood and Sachs (2012). Our changes to the mobile phase ameliorated two other complications with

the AS12 method, inconsistent recoveries of dinosterol and high operating pressures when using 5 % $H_2O$ in methanol as the mobile phase on a $C_{18}$ column (Atwood and Sachs, 2012).

We investigated a variety of alternate mobile phases working with underivatized sterols and triterpenols and found promising initial separations with acetonitrile, but with unacceptable peak tailing. The requirement for near-complete chromatographic recoveries to guard against isotopic fractionation required additional mobile phase experimentation. Even directly after manufacture, some residual silanol sites exist within the stationary phase of a $C_{18}$ column that remain free and unreacted due to steric interactions among the bonded phase ligands (Snyder et al., 1997). Column specifications indicate that in the mid pH range these are more active, and that tailing interactions are more likely. Peak tailing problems were corrected when the mobile phase was modified with 5 % methanol in acetonitrile, which resulted in symmetric peaks under normal column loads and adequate chromatographic resolution. This may result from the lower pKa of methanol, compared to acetonitrile, and its increased affinity for active silanol sites.

An isocratic mobile phase of 5 % methanol in acetonitrile at 1.5 mL/min was effective for purifying brassicasterol, taraxerol, and dinosterol as free alcohols (results not discussed here). In order to elute acetyl-esters of these compounds we introduced 10 % ethyl acetate to the mobile phase at the expense of acetonitrile. Nevertheless, it was advantageous to begin the method with 5 % methanol in acetonitrile in order to remove polar compounds from the column so that when the solvent was transitioned to 5:10:85 MeOH:EtOAc:ACN, the acetyl-esters of the sterols and triterpenols eluted in cleaner fractions. Although we did not evaluate the purification of other alcohols directly, it is likely that the method will work for many sterols and triterpenols based on peripheral assessment of the fractions collected from the HPLC. This sterol/triterpenol

purification method has now been applied to a wide diversity of sediment samples, and has been used to prepare approximately 150 dinosterol, 80 taraxerol, and 10 brassicasterol samples for hydrogen isotope analysis (Table 1). Taraxerol purification by normal phase HPLC was demonstrated in Smittenberg and Sachs (2007), but was never extensively applied or tested. We therefore cannot evaluate the relative effectiveness of our method compared to this one. Instead, we present an alternate approach with the goal of minimizing column changes and operator time through the use of a $C_{18}$ column and pre-acetylated taraxerol. The Smittenberg and Sachs (2007) method has also not been shown to be compatible with brassicasterol or individual alkenone purification.

**Table 1:** Summary of applications of the methods described in this study. Columns indicate the number of purifications performed for each compound at each of the sites listed.

| | **Dinosterol** | **Taraxerol** | **Brassicasterol** | **Alkenones** |
|---|---|---|---|---|
| Poza del Diablo, Galápagos | 23 | 26 | | |
| Pozas Verdes, Galápagos | 14 | 11 | | |
| Poza Escondida, Galápagos | 5 | 5 | 2 | |
| Clear Lake, Palau | 62 | 40 | | |
| Galápagos suspended particles | 4 | | 3 | |
| North American Lakes | 7 | | 9 | 4 |
| Lake Tulane, Florida | 38 | | | |
| Total | 153 | 82 | 14 | 4 |

*3.2.2 Alkenones*

Existing methods for purifying individual alkenones for hydrogen isotope analysis are based on silver nitrate-impregnated silica gel column chromatography (D'Andrea et al., 2007) and normal-phase HPLC (Schwab and Sachs, 2009). These methods are effective, but are both designed with alkenone purification as the only goal, and cannot be readily combined with a procedure to purify other compounds. The silver nitrate column method is also a manual procedure and as such it cannot be run unattended, while the separation time between individual alkenones with the NP-HPLC method is often 30-seconds or less, requiring that numerous 30-second intervals are collected to ensure adequate purification (Schwab and Sachs, 2009). Our new reverse-phase HPLC methods for alkenone purification on a $C_{18}$ HPLC column can be run as part of the sterol/triterpenol purification described above (Figure 4), or independently (Figure 3). Although the independent application has not been tested on sediment samples, the primary concern regarding alkenone purification is the presence of other alkenones rather than other unknown compounds, which suggests that the method will be adequate as long as alkenones with the same carbon number but different degrees of unsaturation may be separated from one another, which is shown to occur in Figure 3. This point is especially true in consideration of the fact that a method has been developed for separation using silver-nitrate silica gel (D'Andrea et al., 2007), which will be even less selective for individual compounds as compared to an HPLC-based approach. As compared to the Prevail Cyano column used in the normal phase HPLC purification method (Schwab and Sachs, 2009), we have found the $C_{18}$ column to perform more consistently over time, and to require less equilibration time between samples and less frequent cleaning. The example shown in Figure 4 and 5 is from the injection of the product of a liquid-liquid extraction, but we have also successfully applied the procedure to neutral fractions from

aminopropyl column chromatography as well as a combined ketone/alcohol fraction from silica gel column chromatography since as noted previously, there is no specific and preferred method for pre-HPLC sample cleanup, and the results will be similar in each case. However, for comparative purposes we also show the results from dinosterol-acetate, brassicasterol-acetate, and individual alkenone purification from a combined ketone/alcohol fraction from the Great Salt Lake (Figure 6).

HPLC retention times are widely spaced, with $C_{37}$ alkenones separated from one another by more than 15 min when run in combination with sterol/triterpenol purification. The large separation windows are desirable for ensuring complete chromatographic recovery, as well as separation of the $C_{37:2}$ from the $C_{38:3}$ alkenones, although the latter point is not a strict requirement for analysis by GC-IRMS. This alkenone method has not yet been as extensively applied to a wide diversity of samples as the sterol/triterpenol method, but it has proven effective at four lacustrine settings in North America (Table 1), and should work just as well in other settings. Although our alkenone methods were not optimized for complete and individual purification of all $C_{38}$ and $C_{39}$ alkenones, purification of these compounds is probably attainable with only minor modification to the method since the $C_{38:3}$ and $C_{38:2}$ alkenones are already well separated from one another (Figure 5), as are the $C_{39:4}$ and $C_{39:3}$ (Figure 5). The $C_{38:2}$ alkenone in the Manito Lake sample can be seen eluting at the earliest stage of HPLC column cleaning, so it is likely that were there a detectible $C_{39:2}$ alkenone in our samples that it would elute even later since the RP-HPLC procedures separate alkenones as a function of both chain length and degree of unsaturation. Extending the isocratic 5:20:75 MeOH:EtOAc:ACN time or increasing the percentage of ethyl acetate slightly might permit recovery of these compounds. However, it is likely that a choice would have to be made between purifying $C_{37}$ or $C_{39}$ alkenones, since some

of these currently partially coelute on HPLC despite the large separation distances as a function of the number of points of unsaturation.

*3.3 Recoveries and isotopic effects*

In order to assess the potential isotopic biasing that the new HPLC purification methods might introduce, we selected the $C_{37:3}$ alkenone to use as a test compound. $C_{37:3}$ is highly retained on the $C_{18}$ HPLC column, eluting near the end of a sterol/triterpenol/alkenone purification run. As a result, the peaks tend to be broad, suggesting an elevated risk of unintended isotope effects. To evaluate this, we purified a sample of $C_{37:3}$ from cultured *Emiliania huxleyi*. The purified $C_{37:3}$ fraction was split into control and method evaluation aliquots. The latter was re-purified using the stacked sterol/triterpenol/alkenone RP-HPLC method (Figure 4), and both $C_{37:3}$ alkenone samples were quantified by GC-FID, and analyzed in triplicate by GC-IRMS. Recovery was 89%, and the control sample δD value was -299±0.5 ‰, while the method evaluation $C_{37:3}$ alkenone was -298±2 ‰, with the stated uncertainty representing the standard deviation of triplicate measurements.

In order to compare recoveries using an acetonitrile/methanol-based mobile phase more directly with recovery experiments performed using underivatized cholesterol with a methanol/water mobile phase (Atwood and Sachs, 2012), we performed recovery experiments using underivatized brassicasterol and dinosterol. The free alcohols were first purified by HPLC using 5% methanol in acetonitrile, then quantified by FID, then purified a second time and re-quantified. Brassicasterol recovery was 80 % and dinosterol recovery was 80 % with this

approach. To test recovery of acetylated sterols, we performed similar repeat-purifications of dinosterol using the acetylated sterol HPLC method (Figure 1) and compared pre- and post-HPLC quantities by GC-MS. In these samples the dinosterol recoveries were 82 % and 84 %. Application of combinations of the sterol, triterpenol, and alkenone HPLC methods to sample sets from Palau, the Galápagos, and continental lakes in North America also yielded qualitatively consistent recovery and minimal losses of target compounds (Table 1). Although we do not achieve 100 % recovery, these losses are within the range of what might be expected through multiple transferring steps, and we are confident that losses do not occur as a result of partial collection of an HPLC peak.

*3.4 Hydrogen Isotope Measurements of Dinosterol*

Although Atwood and Sachs (2012) reported that compounds I (4α-24-dimethylcholestanol-acetate) and II (4α-methyl-24-ethyl-5α-cholest-22E-en-3β-ol-acetate) (Figure 2) eluted too closely to dinosterol on GC for accurate isotope measurement, we have found that through our modified GC method we are able to attain satisfactory chromatographic separation between these steroidal compounds and dinosterol. The slower temperature ramp of 1 °C/min as opposed to 2 °C/min and the reduced flow rate of 1.5 mL/min as opposed to 2.6 mL/min used by Atwood and Sachs (2012) results in improved separation by GC. Peak shapes are broad and asymmetric due to loading demands and the GC method conditions, but this strategy for isotope measurements in complex chromatograms is not uncommon (e.g. Freeman et al., 1990). In order to assess the adequacy of the LC purified dinosterol, we calculated percent valley values for the minima preceding and following the dinosterol peak on the IRMS *m/z* 2

trace for the sample shown in Figure 2 (% valley = valley height/peak height *100%) (Goodman and Brenna, 1994; Jeansonne and Foley, 1989) Values are 2.4% and 0.29%, and although greater than zero, are small enough to be comparable to what could be expected from variable baseline conditions due to factors other than coeluting compounds, such as column bleed. In addition, there is a short, but observable 'flat' baseline in the ratio trace immediately preceding and following the dinosterol peak, which is another method that has been employed to identify adequate chromatographic conditions (Freeman et al, 1990).

Although the chromatography is not ideal, and compound I is not separated enough from the dinosterol peak to prevent the potential for memory effects (Wang and Sessions, 2008), it is adequate. We also point out that the normal phase HPLC purification method developed by Smittenberg and Sachs (2007) does not remove compounds I and II, but that it was nevertheless successfully applied in Palau and the Chesapeake Bay to produce hydrogen isotope records from dinosterol that were consistent with palmitic acid δD values, as well as water δD values and salinity (Sachs and Schwab, 2011; Smittenberg et al., 2011). In these cases, samples were even analyzed on GC columns other than VF-17ms, although in both cases reduced carrier gas flow rates similar to those that we use as compared to those employed by Atwood and Sachs (2012) may have been centrally important in delivering adequate chromatography. We also note that our new reverse-phase HPLC method results in similar separation on the $C_{18}$ column as compared to the method of Atwood and Sachs (2012). However, since in both cases the separation is minimal (< 1 minute), and given that LC retention time can vary from sample to sample or over days of analyses owing to variable sample matrices and column wear, we choose to err on the side of caution from the perspective of being certain that we have collected 100 %

of the primary dinosterol peak, even if it means that we also include compounds I and II, since these are separated by our GC conditions.

*3.5 Applications*

As a demonstration of the effectiveness and applicability of the methods described herein we present three examples from surface sediments in saline lakes in the tropical Pacific from which we purified dinosterol and taraxerol using the method employed for the Galápagos sample (Figures 2 & 3). Following purification we performed δD measurements of these compounds, as well as modern lake water δD values, and used these together to calculate an isotopic fractionation factor, α, where $\alpha = (\delta D_{lipid}+1000)/(\delta D_{water} + 1000)$ (Figure 7). We compare our α values from dinosterol with previously published α values from other algal lipids, including dinosterol from the Chesapeake Bay (Sachs and Schwab, 2011), as well as hydrocarbons from ponds on Christmas Island (Sachse and Sachs, 2008). The three new dinosterol data points plot in general agreement with the dinosterol values from the Chesapeake Bay, and suggest a similar relationship between D/H fractionation and salinity as described by Sachs and Schwab (2011) and Sachse and Sachs (2008), amounting to about a 1‰ decrease in D/H fractionation (and increase in $\delta D_{lipid}$) per unit increase in salinity. We compare the taraxerol α values with the *n*-alkanes from mangrove leaves collected in the Brisbane River Estuary (Ladd and Sachs, 2012) and find that although the magnitude of α values are lower overall, due to the different biosynthetic pathways for *n*-alkanes as opposed to taraxerol (Sessions et al., 1999), the taraxerol δD data imply a similar sensitivity of D/H fractionation to salinity in mangroves, that is opposite to that in microalgae and amounts to an increase in D/H fractionation in mangrove lipids of about

1.5 ‰ per unit increase in salinity (Ladd and Sachs, 2012) (Figure 7). That these data show general agreement with previous investigations on the influence of salinity on the magnitude of D/H fractionation in algal- and mangrove-derived lipids serves as a useful validation of the methods, but a detailed analysis of the significance of these results are beyond the scope of the present study.

**Figure 7:** (next page) Comparison of example data from dinosterol (checkered circles) and taraxerol (checkered diamonds) using the methods presented here with previously published isotope data. Fractionation factor is calculated from δD measurements of lipids and water, and plotted against salinity. Open circles are dinosterol from the Chesapeake Bay (Sachs and Schwab, 2011), black, gray and white triangles are $n$C$_{17}$, total lipid extract, and phytene, respectively, from Christmas Island (Sachse and Sachs, 2008), and black and white squares are $n$C$_{31}$ and $n$C$_{33}$ , respectively, from the Brisbane River Estuary (Ladd and Sachs, 2012). Regression lines shown for each compound type, but taraxerol line is dashed due to the limited

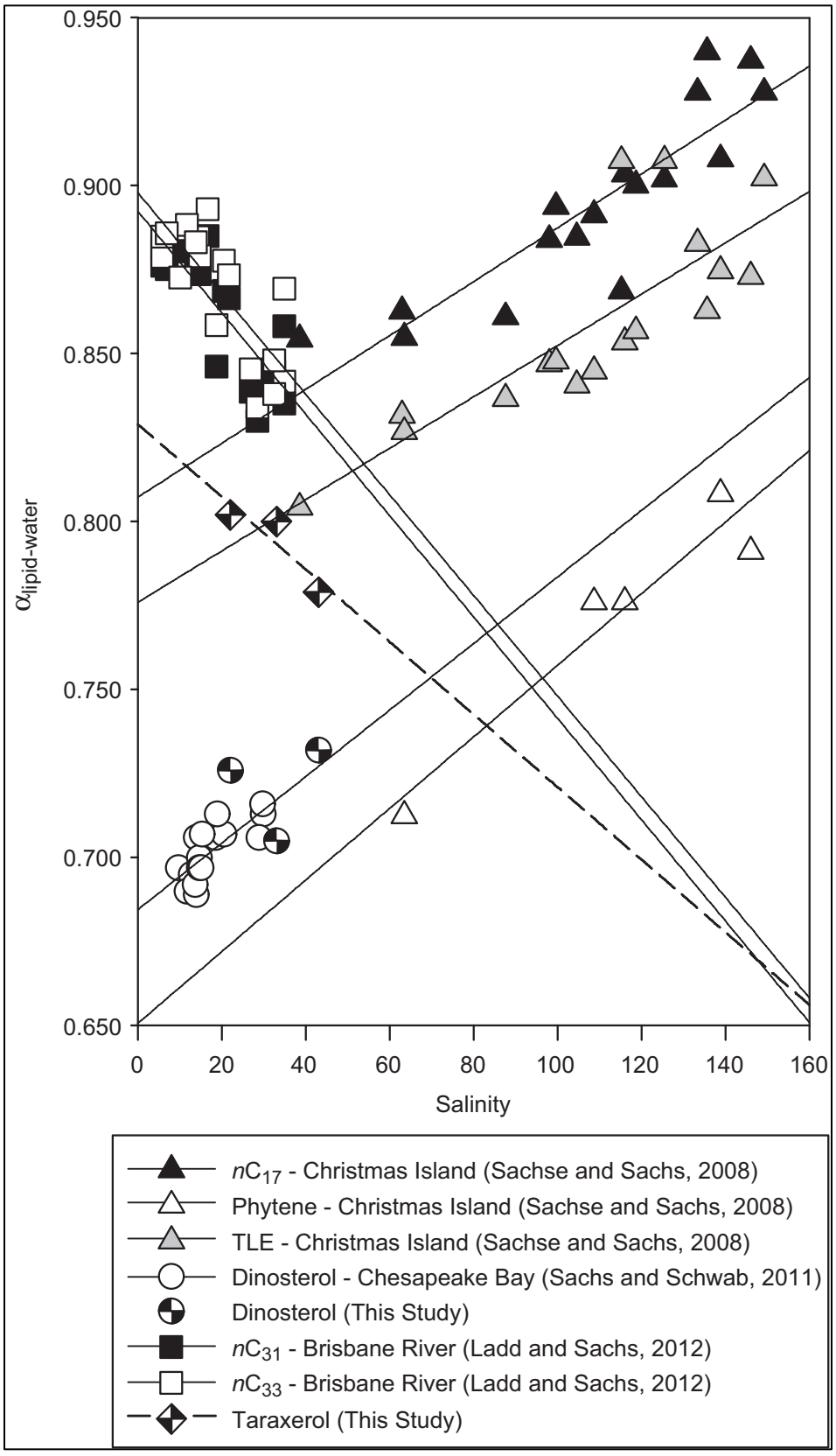
0.950
0.900
0.850
0.800
0.750
0.700
0.650
$\alpha_{lipid\text{-}water}$
0
20
40
60
80
100
120
140
160
Salinity
$nC_{17}$ - Christmas Island (Sachse and Sachs, 2008)
Phytene - Christmas Island (Sachse and Sachs, 2008)
TLE - Christmas Island (Sachse and Sachs, 2008)
Dinosterol - Chesapeake Bay (Sachs and Schwab, 2011)
Dinosterol (This Study)
$nC_{31}$ - Brisbane River (Ladd and Sachs, 2012)
$nC_{33}$ - Brisbane River (Ladd and Sachs, 2012)
Taraxerol (This Study)

There is potential for further applications of the presented methods beyond isotope analysis. For example, it might be possible to use our methods as a tool for evaluating the presence of various sterols, triterpenols or alkenones in marine sediments as a screening tool for paleoceanography, and perhaps even to calculate alkenone unsaturation ratios for sea surface temperature reconstruction (Brassell et al., 1986; Conte et al., 2006) using HPLC-MS peaks, and as a part of alkenone purification for hydrogen isotope analysis. However, we also note that purely analytical applications of our method would probably be optimized by greatly reducing the column loading, which would sharpen the peaks and permit faster elution for cases where post-column collection of sufficient material for hydrogen isotope analysis is not a requirement.

**4. Conclusion**

Three methods are presented for purifying individual sterols, triterpenols and alkenones from sediments using $C_{18}$ HPLC. The methods improve the purification speed, reduce the use of laboratory consumables, and virtually eliminate the risk of inadvertent isotopic fractionation of target compounds over previous methods for purifying lipid biomarkers by HPLC. The most significant gains in efficiency come from pre-acetylating the sterols and triterpenols, but the use of a semi-preparatory fraction collector also resulted in improved efficiency as well as reduced potential for inadvertent isotopic fractionation of the sample. Through these improvements we estimate that we have achieved an approximately 50 % reduction in the time required per sample and have eliminated more than ten potential steps where isotopic fractionation might be possible (Supplemental Materials). We have demonstrated the effectiveness of the methods through

applications in three selected samples, but the techniques have been applied in a wider range of environments (Table 1). Despite the gains that these methods have achieved, continued room for improvement exists. Although equally as effective in dinosterol purification as previous HPLC methods (Atwood and Sachs, 2012), hydrogen isotope analysis of this compound still specifically requires a VF-17ms GC column to achieve adequate chromatographic resolution for isotope analysis, as well as a relatively slow GC oven heating rate, causing broadened peaks and degraded analytical precision. Improved purification through alternative stationary phases and/or alternative derivatization methods might therefore offer opportunities to further improve the measurement. Regardless, continued application of these approaches will facilitate an expanded view of the hydrogen isotopic composition of biomarkers, and further our understanding of their environmental significance, which may eventually lead to true quantitative reconstructions of past rainfall and hydrologic variability.

**Supplemental Material**

*Increased efficiency of lipid purification*

We attempted to make a quantitative estimate of the increases in efficiency offered by our HPLC methods by comparing the time required for purification of one target alcohol from an HPLC injection to the methods in SS07 and AS12 (Figure S1). We assumed that each manual sample transfer between vials requires five minutes to complete, and instrument analysis times were derived from the individual HPLC, GC-MS, and GC-IRMS methods. Purification activities were categorized as either active, where the analyst must be present and engaged in the procedure, or passive, where the analyst must be in the vicinity of a process, but immediate involvement is not required. We also calculated the maximum time the HPLC may run unattended, and the maximum number of samples that may be run while unattended. We identified the number of steps where potential exists for causing isotopic fractionation of the target compound, with the assumptions that the instrument is operating as intended, and that the target compound is distributed over five 4 mL vials in the analytical configuration of the fraction collector. In summary, we estimate that the new approach cuts active time from 163 to 80 minutes per sample, passive time from 16.8 to 8.5 hours, and instrument time from 8.7 to 3.3 hours. The maximum time that the HPLC may be left unattended is increased from 40 minutes to 8.3 hours, and the number of steps where mishandling could potentially cause isotopic fractionation is reduced from 14 to 0 (Figure S1).

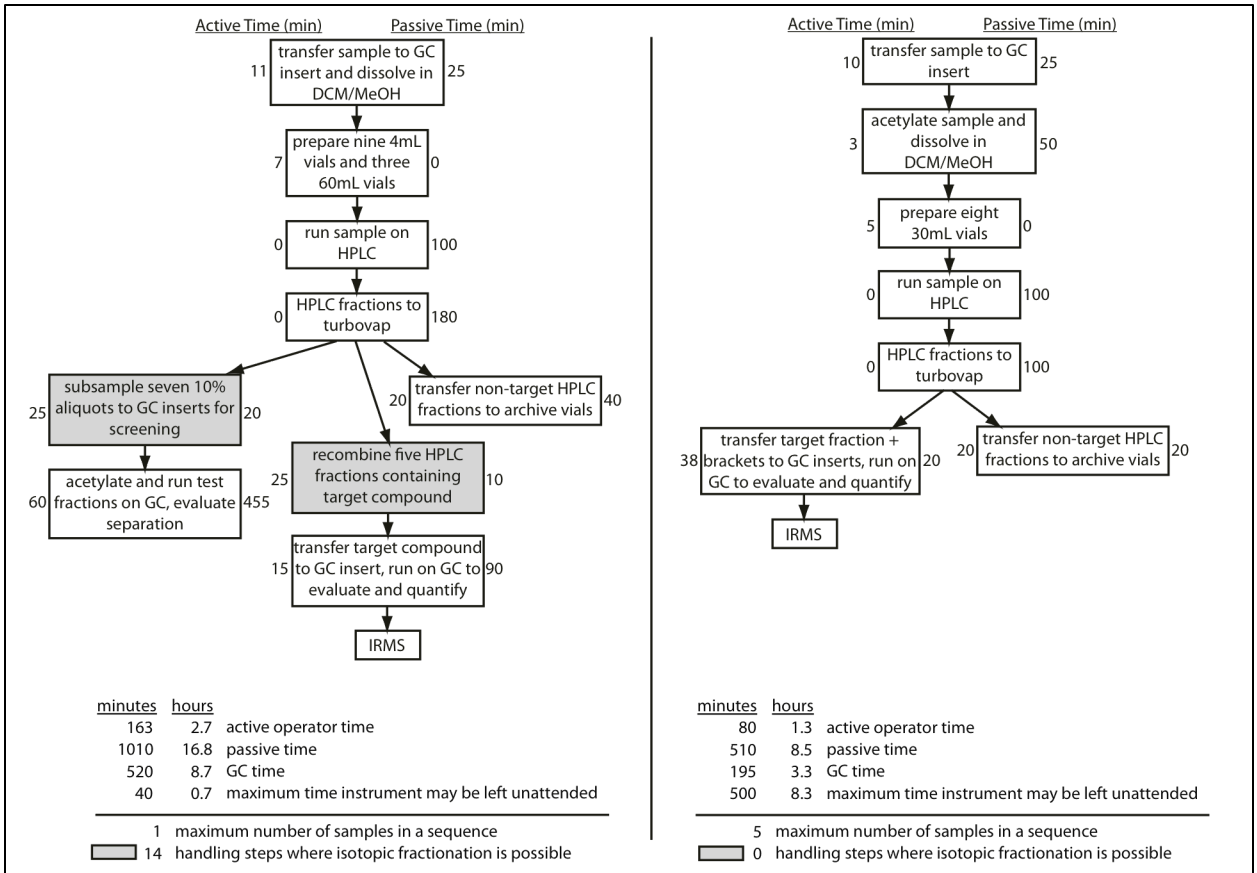


**Figure S1:** Comparison of HPLC-based purification strategies using an analytical fraction collector configuration and post-HPLC derivatization (left), with a semi-preparatory fraction collector and pre-HPLC derivatization (right). Boxes with gray shading indicate handling stages where mishandling has potential to cause isotope fractionation. Active and passive time differentiates between tasks requiring active analyst intervention and those that do not. Time estimates assume five minutes per manual sample transfer.

**Acknowledgments**

This material is based upon work supported by the U.S. National Science Foundation under Grants NSF-EAR-0745982, EAR-0823503 and ESH-0639640, and the U.S. National Oceanic and Atmospheric Administration under Grant No. NA08OAR4310685 to J. Sachs. The authors would like to thank Orest Kawka, Josh Gregersen, Nemiah Ladd, Alyssa Atwood, and Julie Richey for useful discussions, advice and assistance in the lab. We thank Ariel Townsend for her careful assistance in the lab. We thank Alyssa Atwood, Jeff Bowman, and Simon Haberle for assistance in the field, and Orest Kawka for providing culture samples. We also thank Associate Editor Stefan Schouten and two anonymous reviewers for their constructive comments, which helped to greatly improve the quality of this manuscript.

**Chapter 2 References**

Atwood, A.R., Sachs, J.P., 2012. Purification of dinosterol from complex mixtures of sedimentary lipids for hydrogen isotope analysis. Organic Geochemistry 48, 37-46.

Bowman, J.S., Sachs, J.P., 2008. Chemical and physical properties of some saline lakes in Alberta and Saskatchewan. Saline Systems 4.

Brassell, S.C., Brereton, R.G., Eglinton, G., Grimalt, J., Liebezeit, G., Marlowe, I.T., Pflaumann, U., Sarnthein, M., 1986. Palaeoclimatic signals recognized by chemometric treatment of molecular stratigraphic data. Organic Geochemistry 10, 649-660.

Conte, M.H., Sicre, M.-A., Ruhlemann, C., Weber, J.C., Schulte, S., Schulz-Bull, D., Blanz, T., 2006. Global temperature calibration of the alkenone unsaturation index (Uk'37) in surface waters and comparison with surface sediments. Geochemistry, Geophysics, Geosystems 7.

D'Andrea, W.J., Liu, Z., Alexandre, M.D.R., Wattley, S., Herbert, T.D., Huang, Y., 2007. An Efficient Method for Isolating Individual Long-Chain Alkenones for Compound-Specific Hydrogen Isotope Analysis. Analytical Chemistry 79, 3430-3435.

Douglas, P.M.J., Pagani, M., Brenner, M., Hodell, D.A., Curtis, J.H., 2012. Aridity and vegetation composition are important determinants of leaf-wax dD values in southeastern Mexico and Central America. OBJOBJGeochimica et Cosmochimica Acta 97, 24-45.

Englebrecht, A.C., Sachs, J.P., 2005. Determination of sediment provenance at drift sites using hydrogen isotopes and unsaturation ratios in alkenones. Geochim. Cosmochim. Acta 69, 4253-4265.

Freeman, K., Hayes, J.M., Trendel, J.-M., Albrecht, P., 1990. Evidence from cabon isotope measurements for diverse origins of sedimentary hydrocarbons. Nature 343, 254-256.

Goodman, K.J., Brenna, J.T., 1994. Curve Fitting for Restoration of Accuracy for Overlapping Peaks in Gas Chromatography/Combustion Isotope Ratio Mass Spectrometry. Analytical Chemistry 66, 1294-1301.

Jeansonne, M.S., Foley, J.P., 1989. Measurement Of Statistical Moments Of Resolved And Overlapping Chromatographic Peaks. Journal of Chromatography 461, 149-163.

Jin, P., Deng, Z., Peib, Y., Fua, H., Lia, J., Van Ofwegend, L., Proksche, P., Lina, W., 2005. Polyhydroxylated steroids from the soft coral Sinularia dissecta. Steroids 70, 487-493.

Ladd, S.N., Sachs, J.P., 2012. Inverse relationship between salinity and n-alkane dD values in the mangrove Avicennia marina. Organic Geochemistry 48, 25-36.

Lamprecht, G., Pichlmayer, F., Schmidt, E.R., 1994. Determination of the Authenticity of Vanilla Extracts by Stable Isotope Ratio Analysis and Component Analysis by HPLC. Journal of Agriculture and Food Chemistry 42, 1722-1727.

Leduc, G., Sachs, J.P., Kawka, O.E., Schneider, R.R., 2013. Holocene changes in eastern equatorial Atlantic salinity as estimated by water isotopologues. Earth and Planetary Science Letters 362, 151-162.

Mattilaa, P., Lampib, A.-M., Ronkainenb, R., Toivob, J., Piironenb, V., 2002. Sterol and vitamin D2 contents in some wild and cultivated mushrooms. Food Chemistry 76, 293-298.

McDonald, J.G., Smith, D.D., Stiles, A.R., Russell, D.W., 2012. A comprehensive method for extraction and quantitative analysis of sterols and secosteroids from human plasma. Journal of Lipid Research 53, 1399-1409.

Mügler, I., Sachse, D., Werner, M., Xu, B., Wu, G., Yao, T., Gleixner, G., 2008. Effect of lake evaporation on dD values of lacustrine n-alkanes: A comparison of Nam Co (Tibetan Plateau) and Holzmaar (Germany). Organic Geochemistry 39, 711-729.

Nelson, D.M., Henderson, A.K., Huang, Y., Hu, F.S., 2013. Influence of terrestrial vegetation on leaf wax dD of Holocene lake sediments. Organic Geochemistry 56, 106-110.

Pahnke, K., Sachs, J.P., Keigwin, L., Timmermann, A., Xie, S.-P., 2007. Eastern tropical Pacific hydrologic changes during the past 27,000 years from D/H ratios in alkenones. PALEOCEANOGRAPHY 22.

Piper, T., Emery, C., Saugy, M., 2011. Recent developments in the use of isotope ratio mass spectrometry in sports drug testing. Analytical and Bioanalytical Chemistry 401, 433-447.

Piper, T., Emery, C., Thomas, A., Saugy, M., Thevis, M., 2013. Combination of carbon isotope ratio with hydrogen isotope ratio determinations in sports drug testing. Analytical and Bioanalytical Chemistry 405, 5455-5466.

Piper, T., Thomas, A., Thevis, M., Saugy, M., 2012. Investigations on hydrogen isotope ratios of endogenous urinary steroids: reference-population-based thresholds and proof-of-concept. Drug Testing and Analysis 9, 717-727.

Polissar, P.J., Freeman, K.H., Rowley, D.B., McInerney, F.A., Currie, B.S., 2009. Paleoaltimetry of the Tibetan Plateau from D/H ratios of lipid biomarkers. Earth and Planetary Science Letters 287, 64-76.

Sachs, J.P., Sachse, D., Smittenberg, R.H., Zhang, Z., Battisti, D.S., Golubic, S., 2009. Southward movement of the Pacific intertropical convergence zone AD 1400–1850. Nature Geoscience 2, 519-525.

Sachs, J.P., Schwab, V.F., 2011. Hydrogen isotopes in dinosterol from the Chesapeake Bay estuary. Geochmica et Cosmochimica Acta 75, 444-459.

Sachse, D., Billault, I., Bowen, G.J., Chikaraishi, Y., Dawson, T.E., Feakins, S.J., Freeman, K.H., Magill, C.R., McInerney, F.A., van der Meer, M.T.J., Polissar, P., Robins, R.J., Sachs, J.P., Schmidt, H.-L., Sessions, A.L., White, J.W.C., West, J.B., Kahmen, A., 2012. Molecular Paleohydrology: Interpreting the Hydrogen-Isotopic Composition of Lipid Biomarkers from Photosynthesizing Organisms. Annual Review of Earth and Planetary Sciences 40.

Sachse, D., Radke, J., Gleixner, G., 2004. Hydrogen isotope ratios of recent lacustrine sedimentary n-alkanes record modern climate variability. Geochimica et Cosmochimica Acta 68, 4877-4889.

Sachse, D., Sachs, J.P., 2008. Inverse relationship between D/H fractionation in cyanobacterial lipids and salinity in Christmas Island saline ponds. Geochim. Cosmochim. Acta 72, 793-806.

Schouten, S., Ossebaar, J., Schreiber, K., Kienhuis, M.V.M., Langer, G., Benthien, A., Bijma, J., 2006. The effect of temperature, salinity and growth rate on the stable hydrogen isotopic composition of long chain alkenones produced by *Emiliania huxleyi* and *Gephyrocapsa oceanica*. Biogeosciences 3, 113-119.

Schwab, V.F., Sachs, J.P., 2009. The measurement of D/H ratio in alkenones and their isotopic heterogeneity. Organic Geochemistry 40, 111-118.

Schwab, V.F., Sachs, J.P., 2011. Hydrogen isotopes in individual alkenones from the Chesapeake Bay estuary. Geochimica et Cosmochimica Acta 75, 7552-7565.

Sessions, A.L., Burgoyne, T.W., Hayes, J.M., 2001. Determination of the H3 Factor in Hydrogen Isotope Ratio Monitoring Mass Spectrometry. Analytical Chemistry 73, 200-207.

Sessions, A.L., Burgoyne, T.W., Schimmelmann, A., Hayes, J.M., 1999. Fractionation of hydrogen isotopes in lipid biosynthesis. Organic Geochemistry 30, 1193-1200.

Smittenberg, R.H., Sachs, J.P., 2007. Purification of dinosterol for hydrogen isotopic analysis using high-performance liquid chromatography–mass spectrometry. Journal of Chromatography A 1169, 70-76.

Smittenberg, R.H., Saenger, C., Dawson, M.N., Sachs, J.P., 2011. Compound-specific D/H ratios of the marine lakes of Palau as proxies for West Pacific Warm Pool hydrologic variability. Quaternary Science Reviews 30, 921-933.

Snyder, L.R., Kirkland, J.J., Glajch, J.L., 1997. Practical HPLC Method Development, 2nd ed. John Wiley & Sons, Inc.

Theroux, S., D'Andrea, W.J., Toney, J., Amaral-Zettler, L., Huang, Y., 2010. Phylogenetic diversity and evolutionary relatedness of alkenone-producing haptophyte algae in lakes: Implications for continental paleotemperature reconstructions. Earth and Planetary Science Letters 300, 311-320.

van der Meer, M.T.J., Baas, M., Rijpstra, W.I.C., Marino, G., Rohling, E.J., Sinninghe-Damsté, J.S., Schouten, S., 2007. Hydrogen isotopic compositions of long-chain alkenones record freshwater flooding of the Eastern Mediterranean at the onset of sapropel deposition. Earth and Planetary Science Letters 262, 594-600.

Versteegh, G.J.M., Schefuss, E., Dupont, L., Marret, F., Sinninghe-Damsté, J.S., Jansen, J.H.F., 2004. Taraxerol and Rhizophora pollen as proxies for tracking past mangrove ecosystems. Geochimica et Cosmochimica Acta 68, 411-422.

Volkman, J.K., 2003. Sterols in microorganisms. Applied Microbiology and Biotechnology 60, 495-506.

Volkman, J.K., Barrett, S.M., Blackburn, S.I., Mansour, M.P., Sikes, E.L., Gelin, F., 1998. Microalgal biomarkers: A review of recent research developments. Organic Geochemistry 29, 1163-1179.

Volkman, J.K., Eglinton, G., Corner, E.D.S., Sargent, J.R., 1980. Novel unsaturated straight-chain C37-C39 methyl and ethyl ketones in marine sediments and a coccolithophore *Emiliania huxleyi*. Elsevier, New York.

Wang, Y., Sessions, A.L., 2008. Memory Effects in Compound-Specific D/H Analysis by Gas Chromatography/Pyrolysis/Isotope-Ratio Mass Spectrometry. Analytical Chemistry 80, 9162-9170.

Wolhowe, M.D., Prahl, F.G., Probert, I., Maldonado, M., 2009. Growth phase dependent hydrogen isotopic fractionation in alkenone-producing haptophytes. Biogeosciences 6, 1681-1694.

Zhang, Z., Sachs, J.P., 2007. Hydrogen isotope fractionation in freshwater algae: I. Variations among lipids and species. Organic Geochemistry 38, 582-608.

Zhang, Z., Sachs, J.P., Marchetti, A., 2009. Hydrogen isotope fractionation in freshwater and marine algae: II. Temperature and nitrogen limited growth rate effects. Organic Geochemistry 40, 428-439.

# Chapter 3:

# The influence of salinity on D/H fractionation in dinosterol and brassicasterol from globally distributed saline and hypersaline lakes

[*Submitted to Geochimica et Cosmochimica Acta*]

**The influence of salinity on D/H fractionation in dinosterol and brassicasterol from globally distributed saline and hypersaline lakes**

Daniel B. Nelson[1*], Julian P. Sachs[1]

1. University of Washington, School of Oceanography, Box 355351, Seattle, WA 98195, USA

*Corresponding author. Tel: 1-206-685-9879; email: dbnelson@uw.edu

**Abstract**

Salinity, growth rate, growth stage, nutrient limitation and temperature have all been shown to influence the magnitude of D/H fractionation in algal lipids through laboratory and field studies. Of these factors, salinity has been studied most extensively in the field, but to date all such investigations have focused on transect studies within specific and isolated environments. Here we seek to test the relationship between salinity and the magnitude of D/H fractionation in algal lipids through paired analyses of sedimentary and suspended particulate lipid and water hydrogen isotope values at a wide range of continental and coastal lake sites spanning salinities from 0 to 133 ppt. Our results demonstrate broad consistency between D/H fractionations in dinosterol and brassicasterol at our sample sites with those from previous work, with salinity changes of 1 ppt resulting in lipid δD changes of 0.6 to 0.9 ‰. Although our results also show variability in D/H fractionation among sites that are not related to salinity, the fact that any relationship emerges above the influences of other factors known to influence D/H fractionation in algal lipids suggests that the salinity effect may be dominant in the majority of saline to hypersaline environments. Extending the number of algal lipids within which a consistent relationship between D/H fractionation and salinity has been identified also supports the idea that the relationship is widespread among unicellular photoautotrophs.

## Introduction

The hydrogen isotopic composition of organic compounds offers unique insights on a variety of processes in the natural world, including biosynthetic pathways and paleohydrology. Paleohydrologic applications target organic compounds that are well preserved in sediments and can be traced to a particular biologic source. But typical lipid extracts from sediments contain a diverse assortment of compounds that vary by environment, and the significance of the hydrogen isotope signal preserved in most compounds is only beginning to be understood. Calibration efforts have routinely demonstrated that in most environments, the hydrogen isotopic composition of lipids from terrestrial and aquatic autotrophic organisms tracks the hydrogen isotopic composition of environmental water (Sachse et al., 2012 for a review). However, sediment based records that seek to exploit this relationship through measurements of changing biomarker hydrogen isotope values over time are limited to qualitative interpretations due to an incomplete understanding of the degree to which various additional factors, such as humidity, evapotranspiration rates, salinity, timing of leaf wax production, and vegetation assemblage for higher plant lipids (Douglas et al., 2012; Hou et al., 2008; Kahmen et al., 2013; Ladd and Sachs, 2012; Liu and Yang, 2008; McInerney et al., 2011; Nelson et al., 2013; Polissar and Freeman, 2010; Sachse et al., 2009; Smith and Freeman, 2006; Tipple et al., 2013; Yang et al., 2009; Zhou et al., 2011) and salinity, nutrient stress, growth phase, and temperature for aquatic photoautotrophs (Sachs and Schwab, 2011; Sachse and Sachs, 2008; Schouten et al., 2006; van der Meer et al., 2013; Wolhowe et al., 2009; Zhang and Sachs, 2007; Zhang et al., 2009) act to modulate the magnitude of isotopic fractionation between source water and lipid hydrogen isotope values.

While the variety of secondary effects on the hydrogen isotope signal preserved in lipids may be complex and numerous, there are also numerous lipids preserved in any given sediment sample, all of which incorporate hydrogen from the same external pool of environmental water. Continued study of the secondary influences on hydrogen isotope fractionation in biomarkers should thus lead to improved paleohydrologic applications, either by making quantitative paleoprecipitation records possible through the use of multiple calibrated biomarkers, or at a minimum by helping to confirm that the most appropriate biomarkers are targeted for qualitative applications.

Hydrogen isotope ratios are measured and reported in terms of delta notation, where $\delta D = [(D/H_{sample}/D/H_{standard}) - 1] \times 1000‰$, and D, and H stand for deuterium, and hydrogen, respectively, and the reference standard is Vienna Standard Mean Ocean Water (VSMOW, $\delta D = 0$ ‰). The magnitude of the isotopic change imparted over any reaction or series of reactions from substrate to product is defined in terms of a fractionation factor, $\alpha$. For lipids synthesized by aquatic photoautotrophs, the source of all hydrogen is environmental water, and the combined sequence of biochemical reactions including initial uptake of environmental water into the cell and photolysis to later elongation and desaturation steps that transfer hydrogen from water to an end product lipid can be represented as $\alpha = (D/H_{lipid})/(D/H_{water}) = (\delta D_{lipid} + 1000)/(\delta D_{water} + 1000)$. The further the $\alpha$ value is from unity, the greater the magnitude of D/H fractionation for a given reaction. Lipids are almost always depleted relative to their source water ($\alpha < 1$), so decreasing fractionation is described by increasing $\alpha$ values.

An increase in the salinity of environmental water has been shown to correlate with decreasing D/H fractionation (increased $\alpha$ values) for algal lipids in laboratory culture

experiments (Schouten et al., 2006), and in field calibration studies (Sachs and Schwab, 2011; Sachse and Sachs, 2008). Sachs and Schwab (2011) observed that the relationship between dinosterol $\alpha$ values and salinity in the Chesapeake Bay displayed a near identical slope, but different intercept, from the relationship observed for hydrocarbons from hypersaline ponds on Christmas Island (Sachse and Sachs, 2008), suggesting that the influence of salinity on $\alpha$ values may be universal among unicellular photoautotrophs. Notably, these observations differed in magnitude, but not sign, from a batch culture experiment with *Emiliania huxleyi* and *Gephyrocapsa oceanica*, whose alkenone $\alpha$ values were also shown to increase with increasing salinity (Schouten et al., 2006; van der Meer et al., 2013). More recently, analysis of a 60-year sediment record from a hypersaline lake in Mexico documented $\delta$D values of a 1,15-$C_{32}$ diol that are inversely correlated with precipitation, and presumably salinity as well (Romero-Viana et al., 2013). This compound is suspected to derive from algae from the class Eustigmatophyta, and the authors interpreted this relationship as a growth rate effect. They suggested that increasing salinity in this system plays a key role in limiting carbon solubility leading to carbon limited growth rates during dry periods. If so, this would indicate that in certain environments such effects may be more important than salinity in determining the magnitude of D/H fractionation.

In the present study we sought to evaluate the relationship between $\alpha_{lipid\text{-}water}$ and salinity through paired analyses of water $\delta$D values and $\delta$D values from lipids in surface sediments and suspended particles in a wide range of saline and hypersaline lakes. The environments that we targeted encompassed salinities from 0 to 133, $\delta D_{water}$ values from -81.1 ‰ to +13.2 ‰, latitudes from 1 °S to 53 °N, and distances from the ocean of $10^{-2}$ to $10^{3}$ km. By examining such a large diversity of aquatic systems we aimed to incorporate a wide range of algal species, growth rates,

temperatures, and light levels, all of which have been identified as additional factors that can influence the magnitude of D/H fractionation during algal lipid synthesis (Romero-Viana et al., 2013; Sachs and Schwab, 2011; Sachse and Sachs, 2008; Schouten et al., 2006; Wolhowe et al., 2009; Zhang and Sachs, 2007; Zhang et al., 2009). In so doing we sought to evaluate whether the effect of salinity on D/H fractionation in algal lipids was discernible above the 'noise' from other known modulators of D/H fractionation in algal lipid synthesis, and hence the universality of this relationship.

We report on D/H fractionation in dinosterol (4α,23,24-trimethyl-5α-cholest-22E-en-3β-ol) and brassicasterol (24-methyl cholest-5,22-dien-3β-ol). Dinosterol is primarily produced by dinoflagellates, although it has also been shown to occur in some diatoms (Rampen et al., 2010; Volkman, 2003; Volkman et al., 1998). Brassicasterol is the most commonly used diatom marker, and has been referred to as 'diatomsterol' although it has been reported in other algal groups including Haptophyceae, Cryptophyceae, Chrysophyceae, Bangiophyceae, and in some dinoflagellates (Rampen et al., 2010; Volkman, 2003; Volkman et al., 1998). These lipids were selected due to their relatively high degree of source specificity and widespread distribution among the lacustrine environments that were sampled, although many sediment and suspended particle samples contained neither dinosterol nor brassicasterol. We estimate that dinosterol occurred at detectable levels in approximately 34 % of sites that were assessed, while brassicasterol occurred in approximately 67 %, although brassicasterol was not purified from every site where it was found to occur (Table 1). Another benefit of our sample set is the paired assessment from multiple algal biomarkers, which should act to improve confidence in the idea of extrapolating conclusions based on one algal biomarker to other compounds with similar origins.

| Site | Dinosterol | Brassicasterol |
|---|---|---|
| **Canada** | | |
| Unnamed Fresh Pond , Saskatchewan, Canada | | N |
| Manito Lake, Saskatchewan, Canada | | x |
| Redberry Lake, Saskatchewan, Canada | x | x |
| Patience Lake, Saskatchewan, Canada | | x |
| Little Manitou West, Saskatchewan, Canada | | x |
| Big Quill Lake, Saskatchewan, Canada | | x |
| Muskiki Lake, Saskatchewan, Canada | | x |
| West of West Chaplin Lake NE Division, Saskatchewan, Canada | | x |
| East of West Chaplin Lake NE Division, Saskatchewan, Canada | | x |
| Hughes Bay, Saskatchewan, Canada | | x |
| Midtskogen Bay, Saskatchewan, Canada | | x |
| West Chaplin West Division 1, Saskatchewan, Canada | | x |
| Chaplin Salt Mine, Saskatchewan, Canada | | x |
| West Chaplin Center Division, Saskatchewan, Canada | | x |
| West Chaplin Lake SE Division, Saskatchewan, Canada | | x |
| Freefight Lake, Saskatchewan, Canada | | x |
| Ingebright Lake, Saskatchewan, Canada | | x |
| Bitter Lake, Saskatchewan, Canada | | x |
| Chappice Lake, Saskatchewan, Canada | | x |
| **USA** | | |
| Mono Lake, California, USA | | x |
| Great Salt Lake (North), Utah, USA | | |
| Great Salt Lake (South), Utah, USA | x | x |
| Great Pond, Massachusetts, USA | x | |
| Soap Lake , Washington, USA | | x |
| Salton Sea, California, USA | x | x |
| *Cargill Salt Ponds, San Francisco Bay, California, USA* | | |
| Cargill Salt Pond 1 | x | x |
| Cargill Salt Pond 2 | x | x |
| Cargill Salt Pond 3 | x | x |
| Cargill Salt Pond 4 | | |
| Cargill Salt Pond 5 | | |
| Cargill Salt Pond 6 | | |
| Cargill Salt Pond 7 | | x |
| Cargill Salt Pond 8 | | |
| Cargill Salt Pond 9 | | |
| Cargill Salt Pond 10 | | |
| Cargill Salt Pond 11 | | |
| Cargill Salt Pond 12 | x | x |
| Cargill Salt Pond 13 | | |
| Cargill Salt Pond 14 | | |
| Cargill Salt Pond 15 | | |
| Cargill Salt Pond 16 | | |
| **Tropical Pacific Island Lakes** | | |
| Poza Verdes, Galápagos | x | x |
| Poza del Diablo, Galápagos | x | x |
| Poza Escondida, Galápagos | x | x |
| Flamingo Lagoon, Galápagos | x | x |
| Lib Pond, Marshall Islands | x | N |
| Clipperton Lagoon | x | N |
| Spooky Lake, Palau | x | N |
| Clear Lake, Palau | x | N |
| El Junco Lake, Galápagos | x | N |
| Bainbridge, Galápagos | | |
| **Other** | | |
| The Large Aral Sea | x | x |
| The Small Aral Sea | x | x |
| Laguna Pumacocha, Peru | | |
| Tswaing Crater, South Africa | | x |
| The Dead Sea | | N |
| Number of sites analyzed | 56 | 49 |
| Number of sites with compound in sediments or suspended particles | 19 | 33 |
| Percentage of sites where compound found | 34% | 67% |

**Table 1:** (previous page) Summary of all sites where sediments and/or suspended particles were screened for the presence of dinosterol and/or brassicasterol. Sites where compound was found are marked with 'x'. Sites where the compound was not found are blank. Sites where the presence of the compound was not assessed are marked with 'N'.

Dinosterol has been the focus of investigation in a previous study of the effect of salinity on D/H fractionation in phytoplankton (Sachs and Schwab, 2011), and dinosterol δD values have been used as a paleohydrologic indicator in Spooky Lake, Palau (Sachs et al., 2009; Smittenberg et al., 2011). We include all known sites where paired dinosterol and surface water δD measurements are available in our analysis, which includes the new measurements that we have made in addition to any others that were available from other studies including freshwater sites. To our knowledge, this is the first report of brassicasterol δD values.

## Methods

### *Sediment and water sampling*

Samples discussed in the present study are divided into broad categories based on provenance and sample collection techniques. Surface sediment samples from tropical Pacific island lakes were taken from sediment cores at each site, recovered with either a universal corer (Aquatic Research, Hope, ID), or a modified Livingstone-type corer (Geocore, Columbus, OH). Sediment cores were sectioned in the field at 1 cm-thick intervals and the sectioned material was frozen prior to analysis. Suspended particle samples were collected from the water column at

sites in the tropical Pacific by filtering lake water through 0.7 μm glass fiber filters (Whatman GF/F), which were stored frozen until analysis. Surface sediment samples from the Cargill salt ponds were collected from the Cargill Salt Works facility in the San Francisco Bay area in June of 2008 using a hand sampler deployed in shallow water and stored frozen until analysis. Sediments from remaining lakes from continental interior sites were sampled either by Van Veen dredge, or by hand sampler deployed in shallow water and were also frozen until analysis. Sediment samples collected by Van Veen dredge or similar methods typically resulted in the recovery of material from ~5-20 cm deep in the surface sediments. Many of the sediment samples from the continental interior lake sites were sampled during the fieldwork described in Bowman and Sachs (2008). Lake water conductivity was measured at most sites at the time of sampling with a hand held conductivity sensor, and salinities were calculated based on the relationship between conductivity and salinity in seawater. For continental brines, water samples were collected and salinity was determined as describe in Bowman and Sachs (2008). In all cases, lake water samples were collected for $\delta D_{water}$ measurements in screw cap glass vials that were sealed with electrical tape on site at the time of sediment recovery.

### *$\delta D_{water}$ measurements*

Two separate measurement techniques were applied to the water samples used in this study depending on the time of sample collection and processing. Some were determined at the University of Washington using a Thermal Conversion Elemental Analyzer (TCEA) interfaced with a Delta V Plus Isotope Ratio Mass Spectrometer (IRMS) (Thermo Scientific, Waltham, MA), and the $H_3^+$ factor was evaluated at the beginning of each sample sequence (Sessions et al.,

2001). Each sample was analyzed over six consecutive injections with the first three omitted from reported values due to memory effects from the previous sample. δD values were determined in the Isodat 2.0 software platform relative to monitoring gas hydrogen, and then post-processed using measured values of two standards (0 ‰, and -189.5 ‰) analyzed in the same sequence to reference the data to the VSMOW. Additional water samples were analyzed at the University of Hawaii in the laboratory of Dr. Brian Popp by Cavity Ring Down Spectroscopy (CRDS) (Picarro, Inc., Santa Clara, CA), and are also reported in δD notation. Average analytical precision for all water samples was less than 1 ‰, but individual standard deviations of the triplicate analyses were calculated for each sample.

*Lipid extraction, saponification and column chromatography*

Sediment samples were freeze dried and extracted in a 9:1 mixture of dichloromethane (DCM) and methanol (MeOH) on an accelerated solvent extractor (ASE) Dionex 200 operated at 100 °C and 1500 psi with three five-minute static phases. Excess solvent was evaporated under $N_2$ from the total lipid extract (TLE) on a Turbo-vap system (Caliper, Hopkinton, MA, USA). TLEs were each processed with additional compound class separation or purification methods depending on the number of additional compounds of interest that were targeted for other applications. These are described below in detail, but generally, TLEs were saponified, then separated into neutral and acid fractions using aminopropyl silica gel ($NH_2$) columns, and the neutral fraction was then separated into hydrocarbon, ketone/ester, alcohol, and polar fractions using silica gel columns. Some of these steps were omitted when the complexity of the sample matrix permitted less rigorous purification protocols.

Saponifications were performed by reacting the TLE with 1 N potassium hydroxide (KOH) in MeOH and Nanopure water (Barnstead nanopure infinity water system) at 70 °C overnight. The saponified TLE was then acidified to pH ~2 with HCl to protonate the acid and alcohol potassium salts and then recovered from the aqueous MeOH using a series of hexane liquid-liquid extractions. The hexane was then rinsed once with Nanopure water to dilute the small quantity of low pH water dissolved in this phase, and then dried over sodium sulfate.

Neutral and acid compounds were separated using 0.5 g of aminopropyl (Supelco) in hand-packed glass solid phase extraction (SPE) columns. Neutral compounds were eluted with 8 mL of DCM/isopropyl alcohol (IPA) (3:1), acids were eluted with 6 mL of 4% acetic acid in diethyl ether, and a polar fraction was eluted with 6 mL MeOH. Neutral fractions or TLEs were separated using the same type of glass hand-packed column with 1 g of silica gel 60 (5 % deactivated by weight; EMD chemicals, 35-75 μm). Hydrocarbon fractions were eluted with 10 mL of hexane, ketones/esters with 6 mL DCM/hexane (1:1), alcohols with 8mL ethyl acetate (EtOAc)/hexane (1:4), followed by a polar fraction with 6 mL methanol.

*HPLC-MS purification of Dinosterol and Brassicasterol*

HPLC-MS purifications of initial dinosterol samples used in this study were performed using the methods described in Atwood and Sachs (2012). Briefly, alcohol fractions from silica gel columns were injected on an Agilent 1100 series HPLC using an Agilent ZORBAX Eclipse XDB $C_{18}$ column (4.6 mm X 250 mm X 5 μm) equipped with matching guard column operated at a constant temperature of 30 °C. Dinosterol was eluted with 5 % MeOH in water at a flow rate of 1.5 mL/min (Atwood and Sachs, 2012). HPLC-purified dinosterol was then acetylated at 70 °C for 30 minutes in a mixture of 20 μL acetic anhydride of known δD value and 20 μL

pyridine. This purification procedure was modified during the course of the present study in favor of a more streamlined approach, which also enabled the concurrent purification of brassicasterol (Nelson and Sachs, *Chapter 2*). For these samples, alcohol fractions from silica gel, or neutral fractions from aminopropyl columns were acetylated as described above prior to injection on the HPLC. The same HPLC column was used, but eluting acetylated brassicasterol and dinosterol required a mobile phase composition of 5 % MeOH, 10 % EtOAc, and 85% acetonitrile (ACN).

*Gas Chromatography –Mass spectrometry*

At each purification stage and prior to hydrogen isotope analysis, sample aliquots were analyzed by gas chromatography-mass spectrometry (GC-MS) to identify compounds of interest, assess the efficacy of separation procedures, and to determine subsequent handling steps. Samples were injected in splitless mode at 300°C using helium carrier gas at 1.5 mL/min on an Agilent 6890N GC with 5975 inert mass selective detector. Optimal sterol GC separation was achieved with an Agilent (formerly Varian) VF-17ms column (60 m X 0.32 mm X 0.25 μm). Initial sample screening was performed with an oven temperature program that held the initial temperature of 110 °C for 3 minutes after sample injection, then increased to 170 °C at 15 °C/min, then to 325 °C at 5 °C/min where it was held for 24 min. For purified dinosterol and brassicasterol samples the GC oven was held at an initial temperature of 120 °C for 10 minutes, then increased to 260 °C at 20 °C/min, then to 300 °C at 1 °C/min, then to 325 °C at 20°C/min and held for 8 minutes. All samples were run in full scan mode (*m/z* 50-700). Compound quantification was approximated based on the relative areas of unknown peaks to that of a 5α-

cholestane internal standard of known concentration that was added to each sample prior to GC-MS analysis.

*Gas Chromatography-Isotope Ratio Mass Spectrometry*

Purified dinosterol and brassicasterol δD values were measured by gas chromatography-isotope ratio mass spectrometry (GC-IRMS) using a Thermo Delta V Plus isotope ratio mass spectrometer and Thermo Trace GC Ultra coupled to a gas chromatography combustion interface III. Samples were injected in splitless mode at 330 °C using helium carrier gas at 1.5 mL/min. The GC was equipped with either an identical column to the GC-MS, or a similar VF-17ms with slightly narrower diameter (60 m X 0.25 mm X 0.25 μm). The GC-IRMS oven program was identical to the GC-MS program for purified sterols with the exception of the initial oven temperature and hold time, which was 120 °C for 2 minutes. GC column effluent was directed through the pyrolysis reactor and combustion interface to convert organic column effluents to $H_2$ gas prior to introduction to the mass spectrometer. The $H_3^+$ factor was measured prior to every sample sequence (Sessions et al., 2001), and was stable and less than 5.

All samples were analyzed with a mix of coinjection standards of known isotopic composition, which included a combination of $n$C$_{21}$, $n$C$_{23}$, $n$C$_{28}$, $n$C$_{32}$ and $n$C$_{34}$ (standards from Arndt Schimmelmann at Indiana University, Bloomington, IN, USA). Most samples were also analyzed in sequences that included an external standard with $n$C$_{26}$, $n$C$_{38}$, and $n$C$_{41}$ (standards from Arndt Schimmelmann at Indiana University, Bloomington, IN, USA). Initial isotopic evaluations of all peaks were performed within the Isodat 2.0 software relative to a calibrated

reference gas. Secondary corrections were performed based on the regression of Isodat-reported δD values of *n*-alkane standards and their accepted values in order to maintain like treatments of samples and standards, as well as to correct for potential scale compression or stretching as a result of the one-point referencing to VSMOW performed by the Isodat software. Most samples were analyzed at least three times, and measurement precision calculated as the standard deviation of multiple analyses was typically 4-6 ‰. Individual sample uncertainties were calculated as the standard deviation of replicate measurements. For some samples only one injection was possible, to which uncertainties of 10 ‰ were assigned, which is near the maximum error reported for any sample with multiple injections. Peak areas less than 15 V·s were below the cutoff identified on this GC-IRMS to avoid size dependent δD effects, and were not considered (Polissar et al., 2009). δD values for acetylated compounds were corrected by mass balance calculation based on the number of total hydrogen atoms analyzed per compound and the weighted δD value contribution of the hydrogen of known isotopic composition in the acetyl group to the measured δD value.

## Results and Discussion

### *Salinity*

The preferred modern oceanographic method for determining the salinity of water is by measuring electrical conductivity and applying a calibration equation to convert these values to salinity on the practical salinity scale. This proxy measurement has proven accurate and reliable in seawater because the relative abundances of the major ions do not change with respect to one

another. In continental interior lake settings this assumption is invalid, and salinity is often measured in g/L or ppt determined by alternate methods such as evaporite residue weight or direct independent measurement of all major ions. Although g/L and ppt are not directly comparable owing to the influence of salinity and temperature on water density, in most cases in our sample set g/L and ppt values are virtually identical to within the uncertainty required for our purposes of ~ ± 5 (Bowman and Sachs, 2008). We therefore use these values interchangeably where appropriate unless otherwise specified. For lakes in close proximity to seawater, we use the common oceanographic approach of conductivity based salinity estimates.

*Historical salinity changes*

Within our sample set, many lakes from continental interior sites are known to have experienced large changes in salinity in the recent past. Below we describe how representative salinities were determined from each site, and the final salinity estimates are listed in Table 2. Despite these efforts, it is likely that the snapshot measurements or historical estimates of salinity are only generally matched with the conditions that correctly represent the conditions that the source organism experienced when the lipids preserved in the sediments were biosynthesized.

The Large and Small Aral Sea salinities were both 10 g/L in 1960, but by 1989 they had risen to 30 g/L due to diversion of inflowing waters, and by 2006 the large Aral Sea salinity was as high as 80 g/L while the Small Aral Sea salinity had decreased to 12 g/L due to a restoration project (Micklin, 2007). Sedimentation rates in the Aral Sea over the past 1.3 meters of deposition are estimated at 3 mm/yr (Nourgaliev et al., 2003), so we report our measurements

relative to time-weighted average salinities of 55 ± 25 g/L and 20 ± 10 g/L for the Large and Small Aral Seas, respectively.

The Salton Sea was formed in 1905-1907 by accidental flooding of the Colorado River. Since that time, more than 23 cm of sediment have accumulated at a rate of ~2.3 mm/yr, while over the same interval salinity increased from 0 to ~40 g/L by ~1930, and has remained relatively constant at these levels since that time (Schroeder et al., 2002). We report our results using a salinity of 30 ± 10 for the Salton Sea.

Manito and Redberry Lakes displayed less variability in salinity over the 20$^{th}$ century compared to other continental lakes (Bowman and Sachs, 2008; Hammer, 1978), but for consistency, we also report our results from these sites relative to a time-weighted estimate of 20 ±15 g/L for Redberry Lake, and 24 ± 10 for Manito Lake. We also report our measurements from Big Quill Lake relative to time-weighted average salinity of 43 ± 20 since 20$^{th}$ century variability was from 16 to 71 ppt (Bowman and Sachs, 2008; Hammer, 1978).

Chappice Lake conductivity and total dissolved solids (TDS) were measured in 2007 at 110.9 mS/cm at 25°C, and 193.58 g/L, respectively (Bowman and Sachs, 2008). In addition to these parameters Bowman and Sachs (2008) calculated an absolute salinity value of 163.6 ppt, which is a more accurate indicator of salinity than conductivity estimates in lakes where the relative ion abundances differ significantly from seawater (Anati, 1999). Although each of these parameters were determined at every site from the continental interior lakes described by Bowman and Sachs (2008), of the sites within that sample set discussed in the present study only Chappice Lake TDS and absolute salinity differed from one another significantly. Given that absolute salinity is a more reliable indicator in such systems, we use these values at this site.

However, in order to compare to the historical record of conductivity (Vance et al., 1993 *and references therein*), we use the ratio between absolute salinity and conductivity measured in 2007 (Bowman and Sachs, 2008) to convert the pre-1990 conductivity record to absolute salinity. Chappice Lake is known to have become significantly saltier after the installation of a nearby weir in 1976 that diverted inflow. Prior to this, available conductivity data are low (~18 mS/cm; 27 ppt) and show minimal variability (Vance et al., 1993). We therefore assume pre-weir conductivity prior to the 1950s in order to calculate a time-weighted 20$^{th}$ century average salinity value of 49 ppt. We assign uncertainties to this estimate at half the range between this value and the minimum and maximum extremes, or 49 (+57, -15) ppt.

The southern section of the Great Salt Lake experienced large changes in salinity in its history from a minimum of 50 ppt in 1986 to a maximum of 270 ppt in 1961 (Arnow and stephens, 1990; USGS, 2013). A causeway was constructed across the lake in the 1950s to create the modern north and south sub-basins. After this time, annual records of salinity are available from the USGS, so we use the post-causeway time-weighted average salinity of 133 ppt, and include uncertainty estimates spanning half the range between this average value and the 50 ppt and 270 ppt extremes, or 133 (+69, -41) ppt.

We are unaware of extensive published records of historical salinity changes at the coastal lakes used in this study where conductivity-based salinity measurements were used, but we also note that the majority of these samples were collected from sediment cores, or with a hand-sampler, and therefore are more representative of the upper 1-2 cm of sediment than the continental interior lake samples, which were collected by Van Veen dredge.

*Salinity - $\delta D_{water}$ relationships*

In marine environments salinity is highly correlated with δD and $\delta^{18}O$ of seawater, but for continental saline lakes the relationship between salinity and δD values of water is inconsistent, and forms much of the motivation behind our chosen sample set (Figure 1). By targeting sites that exhibit no relationship between salinity and $\delta D_{water}$ values, we are able to clearly isolate the influence of salinity on D/H fractionation from any correlation that might exist between water and lipid δD values as a result of the influence of source water δD values on lipid δD values.

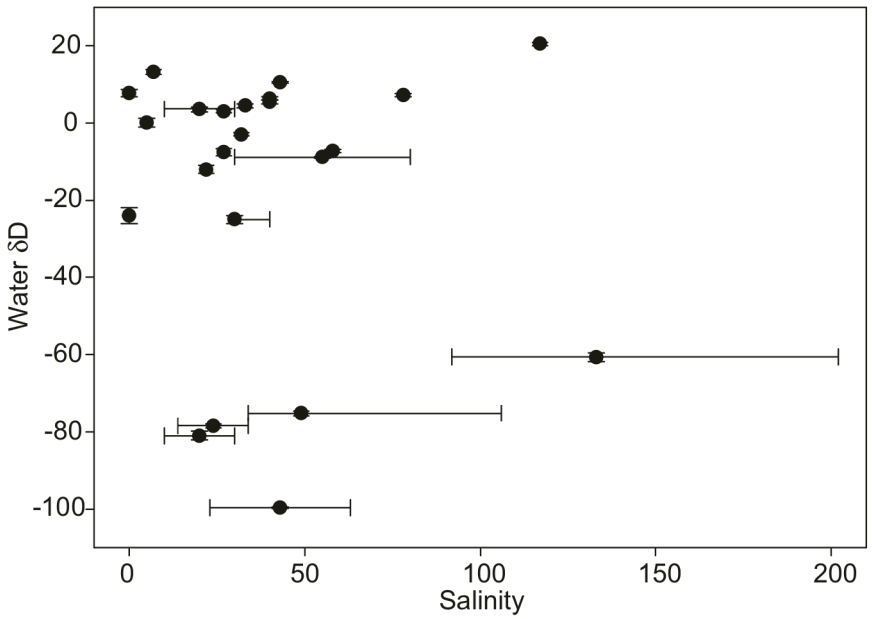


**Figure 1:** Salinity vs. δD values of lake water from all tropical and continental sites. Salinity error bars indicate known historical changes in salinity and continental interior sites (see text).

### $\delta D_{lipid} - \delta D_{water}$ relationships

Virtually all published paleoclimate applications of lipid δD values rely on the generally robust relationship between δD values of source water and those of the targeted sedimentary biomarker. Indeed, numerous calibration efforts have demonstrated the reliability of this approach (Sachse et al., 2012 *and references therein*). As more calibration studies are completed, it is increasingly clear that this assumption is not universally valid across all depositional environments (e.g. Douglas et al., 2012; Ladd and Sachs, 2012; Nelson et al., 2013; Romero-Viana et al., 2013). One goal of the present study was to assess the extent to which algal lipid δD values are applicable as indicators of source water δD values over a wide range of salinities and geographic distribution (Table 2). At most sample locations an effort was made to use lipid values from suspended particles rather than surface sediments since the measured lake water δD value and salinity should be more representative of these lipids than of lipids in the surface sediments, which were deposited over longer periods of time and therefore represent average lake water conditions over that interval. In many cases the total abundance of dinosterol and/or brassicasterol recovered from the suspended particle samples was too low to permit δD measurements so sediment lipids are used instead. In the two cases where dinosterol or brassicasterol from both sediments as well as suspended particles were analyzed, only the suspended particle δD value is plotted and included in the regression of lipid and water δD values in order to avoid over representing a single site. This applies to Poza del Diablo dinosterol, where the suspended particle δD value was -250 ‰ compared to the surface sediment value of -263 ‰, and Poza Escondida brassicasterol, where the suspended particle δD value was -237 ‰ as compared to the surface sediment value of –228 ‰ (Table 2).

In examining the relationship between dinosterol and water δD values (Figure 2a) and between brassicasterol and water δD values (Figure 2b) it is apparent that universal application of a direct water δD value to lipid δD value calibration across all environments may be problematic. Whole data set dinosterol δD values are only weakly correlated to water δD values ($R^2 = 0.20$, $P = 0.06$; Figure 2a). Within specific sub-sets of the data, correlation either worsens as in the case of the continental samples ($R^2 = 0.12$, $P = 0.32$; Figure 2a), or improves as in the case of the tropical Pacific ($R^2 = 0.40$, $P = 0.07$; Figure 2a,c), and in particular in the eastern and central tropical Pacific ($R^2 = 0.78$, $P = 0.008$, Figure 2c). The relationship between brassicasterol and water δD values is more complicated. On the one hand, whole data set correlation is stronger ($R^2 = 0.62$, $P = 0.001$; Figure 2b) than for dinosterol. On the other hand, within the tropical Pacific sample set, brassicasterol δD values are negatively correlated with water δD values ($R^2 = 0.64$, $P = 0.2$, Figures 2b,c). The number of samples driving this relationship is limited ($n = 4$) and results in a high P-value for the regression, so any conclusions drawn from these observations are therefore tenuous. However, it might suggest the possibility that the magnitude of D/H fractionation in brassicasterol is either inversely correlated with salinity, or is influenced by some other parameter such as growth rates or species assemblages that is correlated with water δD values at these sites. Taken together, the comparison of lipid and water δD values from brassicasterol and dinosterol seem to indicate that the water δD value signal is significantly obscured in the lipid δD values. At regional scales such as within the eastern tropical Pacific dinosterol or continental brassicasterol subsets, our calibration assessment supports the qualitative interpretation of δD values as indicators of δD values of source water.

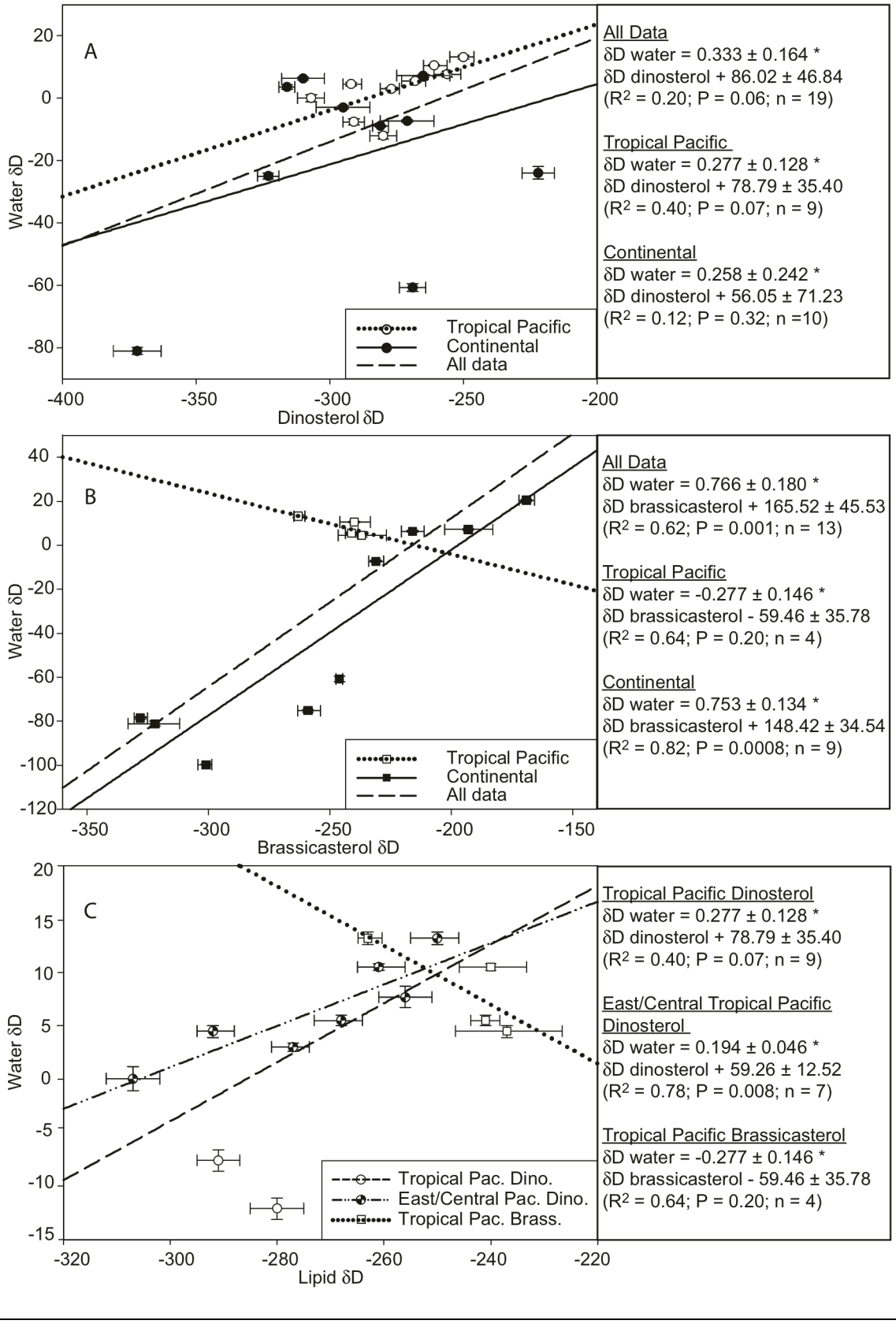
A
Water δD
Dinosterol δD
Tropical Pacific
Continental
All data
All Data
δD water = 0.333 ± 0.164 *
δD dinosterol + 86.02 ± 46.84
(R2 = 0.20; P = 0.06; n = 19)
Tropical Pacific
δD water = 0.277 ± 0.128 *
δD dinosterol + 78.79 ± 35.40
(R2 = 0.40; P = 0.07; n = 9)
Continental
δD water = 0.258 ± 0.242 *
δD dinosterol + 56.05 ± 71.23
(R2 = 0.12; P = 0.32; n =10)
B
Water δD
Brassicasterol δD
Tropical Pacific
Continental
All data
All Data
δD water = 0.766 ± 0.180 *
δD brassicasterol + 165.52 ± 45.53
(R2 = 0.62; P = 0.001; n = 13)
Tropical Pacific
δD water = -0.277 ± 0.146 *
δD brassicasterol - 59.46 ± 35.78
(R2 = 0.64; P = 0.20; n = 4)
Continental
δD water = 0.753 ± 0.134 *
δD brassicasterol + 148.42 ± 34.54
(R2 = 0.82; P = 0.0008; n = 9)
C
Water δD
Lipid δD
Tropical Pac. Dino.
East/Central Pac. Dino.
Tropical Pac. Brass.
Tropical Pacific Dinosterol
δD water = 0.277 ± 0.128 *
δD dinosterol + 78.79 ± 35.40
(R2 = 0.40; P = 0.07; n = 9)
East/Central Tropical Pacific Dinosterol
δD water = 0.194 ± 0.046 *
δD dinosterol + 59.26 ± 12.52
(R2 = 0.78; P = 0.008; n = 7)
Tropical Pacific Brassicasterol
δD water = -0.277 ± 0.146 *
δD brassicasterol - 59.46 ± 35.78
(R2 = 0.64; P = 0.20; n = 4)

**Figure 2:** $\delta D_{lipid}$-$\delta D_{water}$ relationships. A) $\delta D_{dinosterol}$ vs. $\delta D_{water}$. Weak positive correlations are observed across the entire data set, as well as within the tropical Pacific and continental lakes subsets. B) $\delta D_{brassicasterol}$ vs. $\delta D_{water}$. Positive correlation across the entire data set, but within the continental subset the correlation is very strong, and acts to counter the negative correlation within the tropical Pacific subset. C) Rescaled plot showing all tropical Pacific dinosterol and brassicasterol δD values vs. $\delta D_{water}$. Eastern and central tropical Pacific dinosterol data are also plotted independently from the complete tropical Pacific data set, which includes Spooky Lake and Clear Lake from Palau (Smittenberg et al., 2011). All tropical Pacific brassicasterol sites are located on Isabela Island, Galápagos.

*$\delta D_{lipid}$ and Salinity*

Comparison of the δD values of dinosterol and brassicasterol with the salinity at each sample site reveals generally weak to no correlation, especially for dinosterol ($R^2 = 0.006$, $P = 0.76$; Figure 3). This contrasts with previous dinosterol calibration work in the Chesapeake Bay, where salinity was well correlated with dinosterol δD values (Sachs and Schwab, 2011). The relatively poor correlation at our sites occurs as a result of the poor correlation between salinity and water δD values (Figure 1), although brassicasterol δD values are better correlated with water δD values ($R^2 = 0.34$, $P = 0.04$; Figure 3).

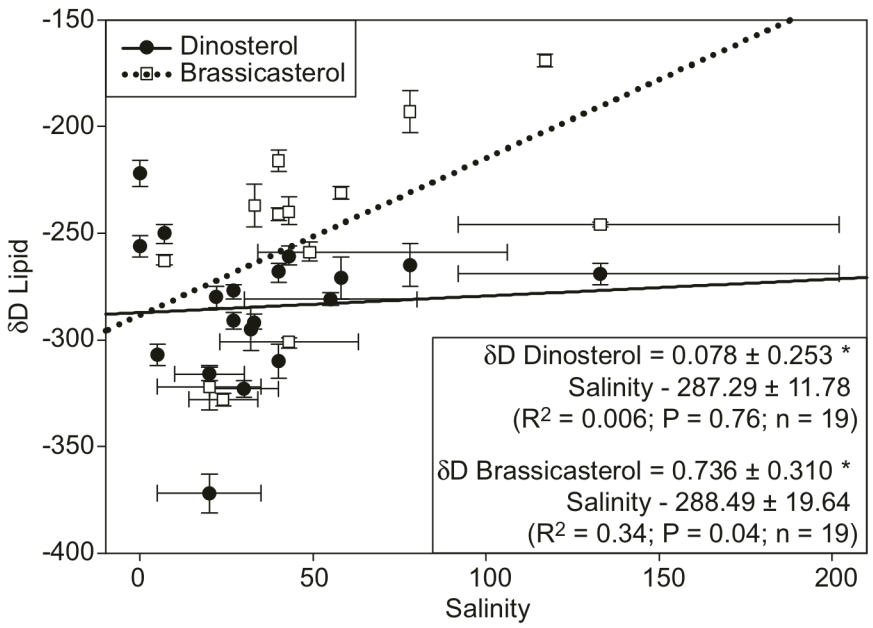


**Figure 3:** Salinity vs. brassicasterol and dinosterol δD values. Salinity error bars are as in figure 2. Lipid δD error bars represent the standard deviation of replicate measurements, or in cases where only one isotope measurement was possible error bars of ± 10 ‰ were assigned, representing a greater range of uncertainty than for any standard deviation of triplicate measurements on other samples.

*D/H fractionation and Salinity*

The magnitude of D/H fractionation, discussed here in terms of the fractionation factor, α, is better correlated with salinity for both dinosterol and brassicasterol than any of the relationships previously discussed (Figures 4). Whole data set correlation is higher for brassicasterol ($R^2 = 0.69$, $P = 0.0004$) than for dinosterol from saltwater environments ($R^2 = 0.48$, $P = 0.002$), although we also point out that there are more brassicasterol samples from higher salinity environments to influence the regression.

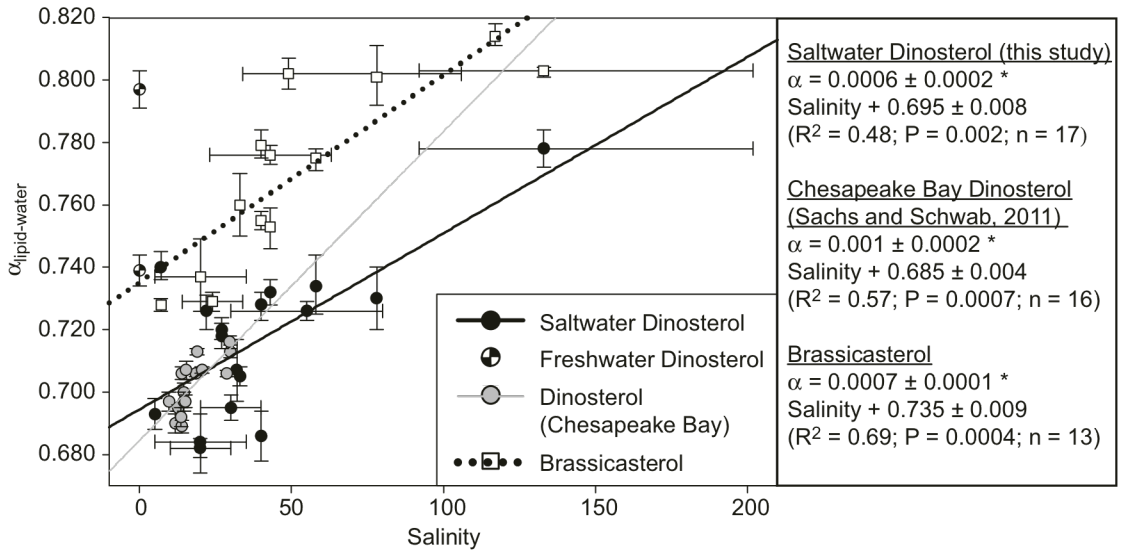


**Figure 4:** Salinity vs. $\alpha_{lipid\text{-}water}$ for dinosterol and brassicasterol from all sample locations. Dinosterol α-salinity data from the Chesapeake Bay plotted for comparison (Sachs and Schwab, 2011). Salinity error bars are as in figure 2. α error bars represent the propagated uncertainty from the paired lipid and water δD measurements used to calculate each α value.

We have omitted the dinosterol samples from freshwater environments (Table 2 and references therein) in the regression analysis of $\alpha_{dinosterol}$ values and salinity in Figure 4 due to the obvious lack of relationship. These two freshwater dinosterol samples, one from El Junco Lake in the Galápagos and the other from Great Pond, MA (Sauer et al., 2001) are apparently totally separate from the α-salinity relationship identified in saline systems. We also note that one of the largest outliers from the α-salinity relationship for dinosterol is from the brackish Lake Diablo, Galápagos (S = 7), but that the other eastern tropical Pacific brackish water dinosterol alpha value, from Clipperton Lagoon (S = 5) plots in accordance with the regression from higher salinity environments. Exclusion of this brackish water outlier improves the correlation ($R^2$ =

0.67, P = 0.0001; Figure 5), and subdivision of the dinosterol data presented in this study into tropical Pacific ($R^2$ = 0.56, P = 0.05; Figure 5) and continental ($R^2$ = 0.90, P = 0.0001; Figure 5) sets demonstrated improved correlation and steeper slopes, but different intercepts for each. The steeper slopes of the salinity-$\alpha_{dinosterol}$ relationships after removal of the outliers agree more closely with the slope observed in the Chesapeake Bay dinosterol (Figure 5) (Sachs and Schwab, 2011). Incorporating all known $\alpha_{dinosterol}$ values into a single regression with salinity with the exception of the three outliers mentioned above leads to the most robust relationship with the lowest P-values ($R^2$ = 0.68, P < 0.0001, N = 32; Figure 6).

The deviation from the $\alpha$-salinity relationship in fresh and some brackish water samples for dinosterol would seem to either suggest that alternate factors become more dominant at controlling $\alpha$ values at lowered salinity ranges, or that the magnitude of D/H fractionation during dinosterol synthesis differs significantly between most halotolerant species of dinoflagellates and some species with limited or no halotolerance. Of these two possibilities, we view the latter as more likely because the $\alpha_{brassicasterol}$ value from Lake Diablo, the brackish dinosterol outlier site, plots directly in accordance with the regression defined by the higher salinity $\alpha_{brassicasterol}$ samples (Figure 7). Were the discrepancy to be caused by a nutrient limitation or temperature effects, the brassicasterol producing diatoms and the dinosterol producing dinoflagellates might be expected to respond similarly. The fact that they do not argues in favor of a species effect for dinosterol at low salinities, although we also point out that tropical and especially eastern tropical Pacific dinosterol $\delta$D values including the fresh and brackish water sites are well correlated with water $\delta$D values (Figure 2c), and that application as a qualitative indicator to assess the sign of hydrologic change (i.e. wetter vs. drier) is likely valid.

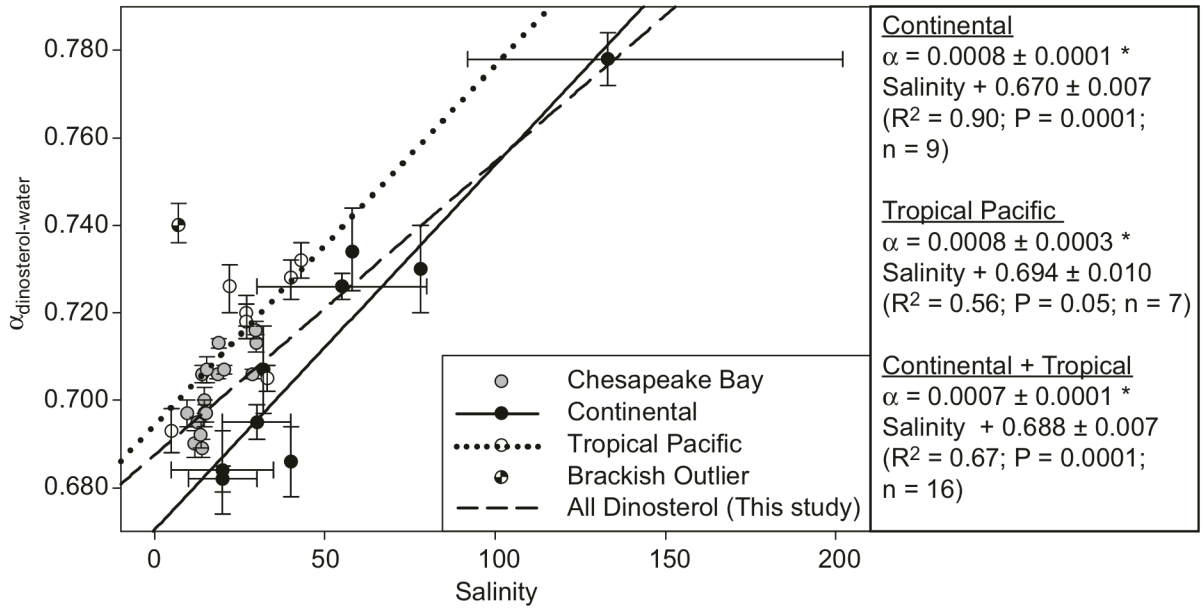


**Figure 5:** Salinity vs. $\alpha_{dinosterol\text{-}water}$ as in figure 4, but subdivided to highlight features of regional data sets. Salinity error bars are as in previous figures, α error bars are as in figure 4. Data plotted to highlight salinity - α relationship for all available salt-water samples within the tropical Pacific (open circles) and continental (black circles) sample sets. Chesapeake Bay dinosterol included for comparison (gray circles) (Sachs and Schwab, 2011). Regression lines plotted for the separate tropical (dotted line) and continental (solid line) data subsets, as well as for the combination of the two (dashed line). Brackish water outlier plotted (checkered circle), but not included in any regressions on this figure.

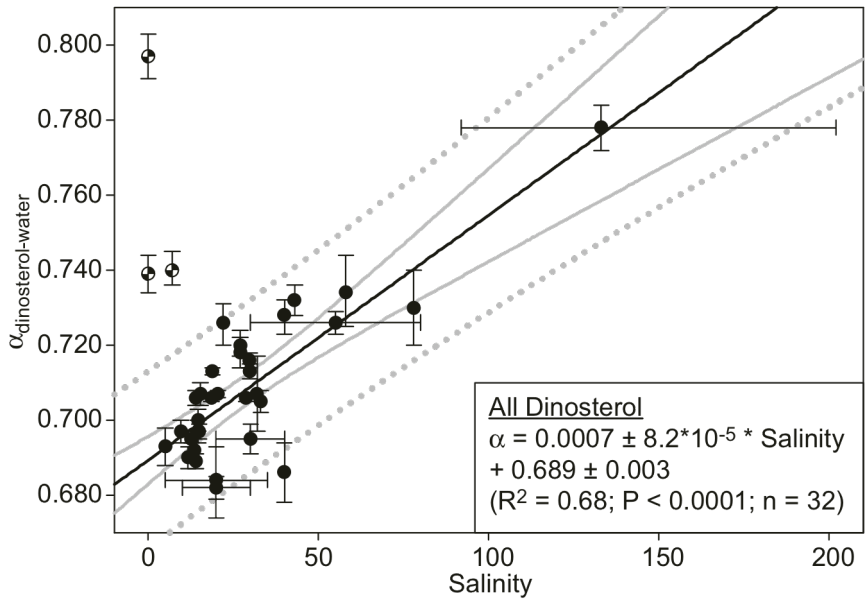


**Figure 6:** All known salinity vs. $\alpha_{dinosterol\text{-}water}$ data from this study (Table 2) and the Chesapeake Bay (Sachs and Schwab, 2011) (black circles). Error bars are as in previous figures. Confidence and prediction bands for whole dataset dinosterol $\alpha$-salinity values plotted at 95% level (gray solid and dotted lines). Fresh and brackish water outliers from this study, and Sauer et al., 2001 shown for comparison, but not included in regression (checkered circles).

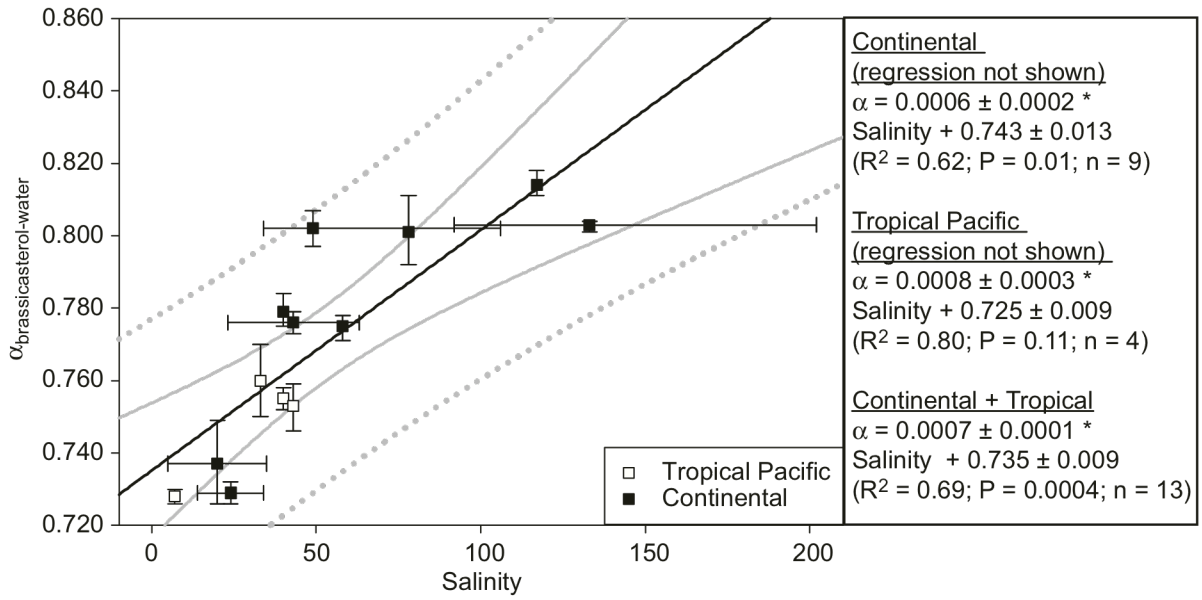


**Figure 7:** Salinity vs. $\alpha_{brassicasterol\text{-}water}$ as in figure 4, but subdivided to highlight features of regional data sets. Salinity error bars are as in previous figures, α error bars are as in figure 4. Data plotted to highlight salinity - α relationship for all available salt-water samples within the tropical Pacific (open squares) and continental (black squares) sample sets. Regression line (black) plotted for combined data sets, with 95% confidence (gray solid lines) and prediction bands (gray dotted lines).

*α vs salinity slopes are similar in all environments studied*

It is especially noteworthy that the slope of each of the regressions of brassicasterol and dinosterol α values with salinity are identical to one another within the range of uncertainty (Figure 4), and also very near to that observed in the Chesapeake Bay (Sachs and Schwab, 2011) as well as for algal lipids from hypersaline ponds on Christmas Island (Sachse and Sachs, 2008). Although the slopes of some of these previously published studies are slightly steeper than the

results identified in the current study, there is considerable scatter in our data owing to the uncertainty in salinity and water δD changes over the integrated time interval represented by our sediment samples, as well as the additional variability in the magnitude of D/H fractionation introduced by factors such as variable growth rates, species assemblages, and temperatures. We also note that the Chesapeake Bay study referenced the measured dinosterol δD values to the VSMOW scale using coinjection standards within the Isodat software package. By definition this is only a one-point calibration (Ricci et al., 1994), and therefore fails to take into account the possibility of any scale stretching or compression, which can produce systematic biases in measured δD values (Coplan, 1988; Meier-Augenstein et al., 2013). Conversely, our data were post-processed to ensure no scale stretch or compression was present, both of which are capable of slightly biasing the slope and intercept of an alpha salinity regression. If these factors were present in the previous algal lipid-salinity studies, they would have resulted in only minor changes in the slope of α-salinity regressions (slope ± ~0.00015), which is still within the uncertainty in the slope of the dinosterol and brassicasterol α-salinity regressions presented here. The differences in the slope of salinity-$\alpha_{\text{dinosterol-water}}$ regressions between the Chesapeake Bay dinosterol and those presented in this study of 0.001 vs. 0.0006 therefore appear to be in broad agreement.

*Potential mechanisms for the influence of salinity on D/H fractionation*

The agreement between previously published algal lipid α-salinity relationships and the dinosterol and brassicasterol α-salinity relationships presented here from a globally distributed

sample set significantly strengthens the case for salinity as the dominant factor responsible for modulating D/H fractionation in algal sterol synthesis. Although other factors are certainly relevant and are one likely explanation for why we do not observe salinity - $\alpha_{lipid\text{-}water}$ regressions with $R^2 = 1$, our results offer strong support for interpretation of algal lipid δD values as a function of both changing salinity and water δD values. Without targeted mechanistic studies under controlled laboratory conditions we can offer no additional insight on the underlying mechanism to cause the observed salinity modulation of D/H fractionation beyond those discussed in previous calibration studies of dinosterol (e.g. Sachs and Schwab, 2011). We do suggest that given the similarity of the observations from our widely dispersed sample set spanning a large range of salinities and geographic distributions, that the dependence of α values on salinity is likely to be the dominant effect in saline to hypersaline systems.

**Conclusion**

We have attempted to evaluate the extent to which salinity is a dominant control on the magnitude of D/H fractionation in algal lipids through an evaluation of dinosterol and brassicasterol $\alpha_{lipid\text{-}water}$ values over a widely distributed and diverse range of lake and lagoon systems. Our results demonstrate the broad consistency of patterns identified previously from algal lipids grown in batch culture (Schouten et al., 2006), and from field studies in the Chesapeake Bay (Sachs and Schwab, 2011) and from hypersaline ponds on Christmas Island (Sachse and Sachs, 2008). Interestingly, this relationship does not appear to extend to freshwater systems, although the number of sample sites on which we base this conclusion is limited (n = 3) and therefore is in need of additional study. The data presented here represent progress towards

the goal of a more complete characterization of the degree and magnitude to which environmental factors act to influence the magnitude of D/H fractionation in algal lipid synthesis.

A more complete understanding of the impact of the influences on D/H fractionation in biomarkers will improve the potential for extracting a quantitative record of the δD value of precipitation from multiple biomarkers from a single sediment record. Although targeting numerous compounds for high-temporal resolution paleoclimate work may be impractical in many cases or over meters-long sediment records, a multiple lipid approach at selected intervals might prove useful for anchoring a proxy record from a single biomarker in quantitative space, or to confirm or evaluate the magnitude of certain key climatic events of interest.

**Acknowledgments**

This material is based upon work supported by the U.S. National Science Foundation under Grants NSF-EAR-0745982, EAR-0823503 and ESH-0639640, and the U.S. National Oceanic and Atmospheric Administration under Grant No. NA08OAR4310685 to J. Sachs. The authors would like to thank Alyssa Atwood, Ines Mugler, and Julie Richey for providing surface sediment dinosterol δD values. We thank Hedi Oberhänsli for providing samples from the Aral Sea, and Robert Baskin for providing samples from the Salton Sea. We thank Orest Kawka, Josh Gregersen, S. Nemiah Ladd, Alyssa Atwood, Ines Mügler, and Julie Richey for useful discussions, advice and assistance in the lab. We thank Ariel Townsend for her careful assistance in the lab. We thank Jeff Bowman, Alyssa Atwood, Simon Haberle, S. Nemiah Ladd, Olivier Cartapanis, Fran Janny, and Conor Myhrvold for assistance in the field.

**Chapter 3 References**


Anati, D.A. (1999) The salinity of hypersaline brines: Concepts and misconceptions. *International Journal of Salt Lake Research* **8,** 55-70.

Arnow, T., stephens, D. (1990) Hydrologic Characteristics of the Great Salt Lake, Utah: 1847-1986, United States Geological Survey Water-Supply. U.S. Geological Survey.

Atwood, A.R., Sachs, J.P. (2012) Purification of dinosterol from complex mixtures of sedimentary lipids for hydrogen isotope analysis. *Organic Geochemistry* **48,** 37-46.

Bowman, J.S., Sachs, J.P. (2008) Chemical and physical properties of some saline lakes in Alberta and Saskatchewan. *Saline Systems* **4**.

Coplan, T.B. (1988) Normalization Of Oxygen And Hydrogen Isotope Data. *Chemical Geology (Isotope Geoscience Section)* **72,** 293-297.

Douglas, P.M.J., Pagani, M., Brenner, M., Hodell, D.A., Curtis, J.H. (2012) Aridity and vegetation composition are important determinants of leaf-wax dD values in southeastern Mexico and Central America. *Geochimica et Cosmochimica Acta* **97,** 24-45.

Hammer, U.T. (1978) The Saline Lakes of Saskatchewan III. Chemical Characterization. *Internationale Revue der gesamten Hydrobiologie und Hydrographie* **63,** 311-335.

Hou, J., D'Andrea, W.J., Huang, Y. (2008) Can sedimentary leaf waxes record D/H ratios of continental precipitation? Field, model, and experimental assessments. *Geochimica et Cosmochimica Acta* **72,** 3503-3517.

Kahmen, A., Schefuß, E., Sachse, D. (2013) Leaf water deuterium enrichment shapes leaf wax n-alkane dD values of angiosperm plants I: Experimental evidence and mechanistic insights. *Geochimica et Cosmochimica Acta* **111,** 39-49.

Ladd, S.N., Sachs, J.P. (2012) Inverse relationship between salinity and n-alkane dD values in the mangrove Avicennia marina. *Organic Geochemistry* **48,** 25-36.

Liu, W., Yang, H. (2008) Multiple controls for the variability of hydrogen isotopic compositions in higher plant n-alkanes from modern ecosystems. *Global Change Biology* **14,** 2166-2177.

McInerney, F.A., Helliker, B.R., Freeman, K.H. (2011) Hydrogen isotope ratios of leaf wax n-alkanes in grasses are insensitive to transpiration. *Geochimica et Cosmochimica Acta* **75,** 541-554.

Meier-Augenstein, W., Hobson, K.A., Wassenaar, L.I. (2013) Critique: measuring hydrogen stable isotope abundance of proteins to infer origins of wildlife, food and people *Bioanalysis* **5,** 751-767.

Micklin, P. (2007) The Aral Sea Disaster. *Annual Review of Earth and Planetary Sciences* **35,** 47-72.

Nelson, D.B., Sachs, J.P. (*Chapter 2*) Concurrent Purification of Sterols, Triterpenols and Alkenones from Sediments for Hydrogen Isotope Analysis using High Performance Liquid Chromatography.

Nelson, D.M., Henderson, A.K., Huang, Y., Hu, F.S. (2013) Influence of terrestrial vegetation on leaf wax dD of Holocene lake sediments. *Organic Geochemistry* **56,** 106-110.

Nourgaliev, D.K., Heller, F., Borisov, A.S., Hajdas, I., Bonani, G., Iassonov, P.G., Oberhänsli, H. (2003) Very high resolution paleosecular variation record for the last 1200 years from the Aral Sea. *Geophysical Research Letters* **30**.

Polissar, P.J., Freeman, K.H. (2010) Effects of aridity and vegetation on plant-wax dD in modern lake sediments. *Geochimica et Cosmochimica Acta* **74,** 5785-5797.

Polissar, P.J., Freeman, K.H., Rowley, D.B., McInerney, F.A., Currie, B.S. (2009) Paleoaltimetry of the Tibetan Plateau from D/H ratios of lipid biomarkers. *Earth and Planetary Science Letters* **287,** 64-76.

Rampen, S.W., Abbas, B.A., Schouten, S., Sinninghe-Damsté, J.S. (2010) A comprehensive study of sterols in marine diatoms (Bacillariophyta): Implications for their use as tracers for diatom productivity. *Limnology and Oceanography* **55,** 91-105.

Ricci, M.P., Merritt, D.A., Freeman, K., Hayes, J.M. (1994) Acquisition and processing of data for isotope-ratio-monitoring mass spectrometry. *Organic Geochemistry* **21,** 561-571.

Romero-Viana, L., Kienel, U., Wilkes, H., Sachse, D. (2013) Growth-dependent hydrogen isotopic fractionation of algal lipid biomarkers in hypersaline Isabel Lake (Mexico). *Geochimica et Cosmochimica Acta* **106,** 490-500.

Sachs, J.P., Sachse, D., Smittenberg, R.H., Zhang, Z., Battisti, D.S., Golubic, S. (2009) Southward movement of the Pacific intertropical convergence zone AD 1400–1850. *Nature Geoscience* **2,** 519-525.

Sachs, J.P., Schwab, V.F. (2011) Hydrogen isotopes in dinosterol from the Chesapeake Bay estuary. *Geochmica et Cosmochimica Acta* **75,** 444-459.

Sachse, D., Billault, I., Bowen, G.J., Chikaraishi, Y., Dawson, T.E., Feakins, S.J., Freeman, K.H., Magill, C.R., McInerney, F.A., van der Meer, M.T.J., Polissar, P., Robins, R.J., Sachs, J.P., Schmidt, H.-L., Sessions, A.L., White, J.W.C., West, J.B., Kahmen, A. (2012) Molecular Paleohydrology: Interpreting the Hydrogen-Isotopic Composition of Lipid Biomarkers from Photosynthesizing Organisms. *Annual Review of Earth and Planetary Sciences* **40,** null.

Sachse, D., Kahmen, A., Gleixner, G. (2009) Significant seasonal variation in the hydrogen isotopic composition of leaf-wax lipids for two deciduous tree ecosystems (Fagus sylvativa and Acer pseudoplatanus). *Organic Geochemistry* **40,** 732-742.

Sachse, D., Sachs, J.P. (2008) Inverse relationship between D/H fractionation in cyanobacterial lipids and salinity in Christmas Island saline ponds. *Geochim. Cosmochim. Acta* **72,** 793-806.

Sauer, P.E., Eglinton, T.I., Hayes, J.M., Schimmelmann, A., Sessions, A.L. (2001) Compound-specific D/H ratios of lipid biomarkers from sediments as a proxy for environmental and climatic conditions. *Geochimica et Cosmochimica Acta* **65,** 213-222.

Schouten, S., Ossebaar, J., Schreiber, K., Kienhuis, M.V.M., Langer, G., Benthien, A., Bijma, J. (2006) The effect of temperature, salinity and growth rate on the stable hydrogen isotopic composition of long chain alkenones produced by *Emiliania huxleyi* and *Gephyrocapsa oceanica*. *Biogeosciences* **3,** 113-119.

Schroeder, R.A., Orem, W.H., Kharaka, Y.K. (2002) Chemical evolution of the Salton Sea, California: nutrient and selenium dynamics. *Hydrobiologia* **473,** 23-45.

Sessions, A.L., Burgoyne, T.W., Hayes, J.M. (2001) Determination of the H3 Factor in Hydrogen Isotope Ratio Monitoring Mass Spectrometry. *Analytical Chemistry* **73,** 200-207.

Smith, F.A., Freeman, K.H. (2006) Influence of physiology and climate on delta D of leaf wax n-alkanes from C-3 and C-4 grasses. *Geochimica et Cosmochimica Acta* **70,** 1172-1187.

Smittenberg, R.H., Saenger, C., Dawson, M.N., Sachs, J.P. (2011) Compound-specific D/H ratios of the marine lakes of Palau as proxies for West Pacific Warm Pool hydrologic variability. *Quaternary Science Reviews* **30,** 921-933.

Tipple, B.J., Berke, M.A., Doman, C.E., Khachaturyan, S., Ehleringer, J.R. (2013) Leaf-wax n-alkanes record the plant–water environment at leaf flush. *Proceedings of the National Acadamy of Sciences of the United States of America* **110,** 2659-2664.

USGS (2013) Great Salt Lake - Salinity and Water Quality (http://ut.water.usgs.gov/greatsaltlake/salinity/index.html). Utah Water Science Center, U.S. Department of the Interior.

van der Meer, M.T.J., Benthien, A., Bijma, J., Schouten, S., Sinninghe-Damsté, J.S. (2013) Alkenone distribution impacts the hydrogen isotopic composition of the C37:2 and C37:3 alkan-2-ones in *Emiliania huxleyi*. *Geochimica et Cosmochimica Acta* **111,** 162-166.

Vance, R.E., Clague, J.J., Mathewes, R.W. (1993) Holocene Paleohydrology of a hypersaline lake in southeastern Alberta. *Journal of Paleolimnology* **8,** 103-120.

Volkman, J.K. (2003) Sterols in microorganisms. *Applied Microbiology and Biotechnology* **60,** 495-506.

Volkman, J.K., Barrett, S.M., Blackburn, S.I., Mansour, M.P., Sikes, E.L., Gelin, F. (1998) Microalgal biomarkers: A review of recent research developments. *Organic Geochemistry* **29,** 1163-1179.

Wolhowe, M.D., Prahl, F.G., Probert, I., Maldonado, M. (2009) Growth phase dependent hydrogen isotopic fractionation in alkenone-producing haptophytes. *Biogeosciences* **6,** 1681-1694.

Yang, H., Pagani, M., Briggs, D.E.G., Equiza, M.A., Jagels, R., Leng, Q., LePage, B.A. (2009) Carbon and hydrogen isotope fractionation under continuous light: implications for paleoenvironmental interpretations of the High Arctic during Paleogene warming. *Oecologia* **160,** 461-470.

Zhang, Z., Sachs, J.P. (2007) Hydrogen isotope fractionation in freshwater algae: I. Variations among lipids and species. *Organic Geochemistry* **38,** 582-608.

Zhang, Z., Sachs, J.P., Marchetti, A. (2009) Hydrogen isotope fractionation in freshwater and marine algae: II. Temperature and nitrogen limited growth rate effects. *Organic Geochemistry* **40,** 428-439.

Zhou, Y., Grice, K., Chikaraishi, Y., Stuart-Williams, H., Farquhar, G.D., Ohkouchi, N. (2011) Temperature effect on leaf water deuterium enrichment and isotopic fractionation during leaf lipid biosynthesis: Results from controlled growth of C3 and C4 land plants. *Phytochemistry* **72,** 207-213.

# Chapter 4:

# The influence of salinity on D/H fractionation in alkenones from saline and hypersaline lakes in continental North America

[*Submitted to Organic Geochemistry*]

**The influence of salinity on D/H fractionation in alkenones from saline and hypersaline lakes in continental North America**

Daniel B. Nelson[1*], Julian P. Sachs[1]

1. University of Washington, School of Oceanography, Box 355351, Seattle, WA 98195, USA

*Corresponding author. Tel: 1-206-685-9879; email: dbnelson@uw.edu

**Abstract**

We present a preliminary assessment of the hydrogen isotopic composition of individual alkenones ($C_{37-39}$ di-, tri- and tetra-unsaturated methyl- and ethyl-ketones) purified from surface lake sediment from sites spanning a range of salinities from 20 to 133 ppt. Combining these measurements with measurements of the hydrogen isotopic composition of modern lake water, we determine the magnitude of D/H fractionation across our sample set, and observe reduced sensitivity to salinity compared to observations from *Emiliania huxleyi* and *Gephyrocapsa oceanica*. This lends support to the hypothesis that D/H fractionation during biosynthesis is less sensitive to changes in salinity in alkenone producers from continental interior sites than in producers from open marine environments. We also observe stronger correlations between the tetra-unsaturated alkenone δD values with water δD values, and associated α values with salinity than we do for the di- and tri-unsaturated compounds, and suggest that this may result from increased number of lacustrine haptophyte species producing the di- and tri- unsaturated as compared to the tetra-unsaturated.

**Keywords:** hydrogen isotopes; δD, biomarkers; lipids; alkenones; lakes; saline; HPLC-MS; GC-IRMS.

## Introduction

Alkenones ($C_{37-39}$ di-, tri- and tetra-unsaturated methyl- and ethyl-ketones) have been extensively researched in the geochemical and paleoclimate communities owing to their high degree of source specificity, and the strong relationship between the relative abundances of di- and tri-unsaturated homologues and sea surface temperature (Brassell et al., 1986; Conte et al., 2006). Efforts to apply the marine based SST indices ($U^{k}_{37}$ and $U^{k'}_{37}$) in coastal oceans and lakes have been hindered by the broader range of water chemistries and comparatively large number of alkenone producing haptophytes in these systems as compared to open marine environments (Chu et al., 2005; Pearson et al., 2008; Sun et al., 2007; Theroux et al., 2010; Toney et al., 2010), where the producers are primarily limited to *Emiliania huxleyi* and *Gephyrocapsa oceanica* (Conte et al., 1995; Marlowe et al., 1990; Volkman et al., 1980). Although some non-calcifying alkenone producers have been described in coastal oceans and lakes, such as *Isochrysis galbana* and *Chrysotila lamellose* (Cranwell, 1985; Sun et al., 2007), species level identification in these systems has proven difficult, and new phylogenetic work has identified several unknown species in continental lakes (Theroux et al., 2010; Theroux et al., 2012). As a result, marine-based saturation indices are generally not correlated with surface temperature in lacustrine systems. Efforts to develop laboratory or regional lacustrine calibrations have proven somewhat successful, as have efforts to develop alternative saturation indices (e.g. $U^{k}_{3738}$, $U^{k}_{38}$, $U^{k'}_{38}$), but these efforts have also revealed additional challenges (Chu et al., 2005; D'Andreaa et al., 2011; Pearson et al., 2008; Sun et al., 2007; Toney et al., 2010; Versteegh et al., 2001). Work in saline lakes has identified patterns in the distribution of $C_{37:4}$ alkenones, or the ratio of $C_{37}$ to $C_{38}$ alkenones that were suggested to be indicative of salinity or the types of haptophytes present in a given location (Chu et al., 2005; Liu et al., 2011; Pearson et al., 2008). Further evaluation in

other locations revealed inconsistencies with these patterns, and it is now established that no known measure of the distribution pattern of alkenones present in a given lake environment is a reliable indicator of species composition, but rather that this information must come from phylogenetic work (Theroux et al., 2010).

The hydrogen isotopic composition of alkenones has been studied to a lesser degree than have alkenone distribution patterns. Although alkenones are attractive targets for hydrogen isotope analysis owing to their high degree of source specificity and widespread occurrence in the environment, analytical capacity for δD measurements ($\delta D = [(D/H_{sample}/D/H_{standard}) - 1]*1000‰$) on alkenones was only developed in the late 1990s (Sessions et al., 1999), and individual alkenones are not resolved adequately by gas chromatography (GC) when sufficient analyte is introduced for hydrogen isotope analysis. Initial efforts circumvented this issue by integrating all coeluting $C_{37}$ alkenone signals into one GC peak to determine the bulk $C_{37}$ alkenone δD value (e.g. Englebrecht and Sachs, 2005; Schouten et al., 2006; van der Meer et al., 2007). This approach was later questioned after methods were published and applied to purify individual alkenones using $AgNO_3$ column chromatography (D'Andrea et al., 2007) and high performance liquid chromatography (Schwab and Sachs, 2009), and revealed large differences in the δD values of individual alkenones. However, it has recently been suggested that the difference in δD values between alkenones with varying degrees of unsaturation occurs as a result of the desaturation process during biosynthesis, and should therefore be correlated with $U^{k'}_{37}$ temperature index (van der Meer et al., 2013). Whether this relationship is consistent across all environments, including among the less extensively studied lacustrine alkenone producers is currently unknown.

Calibration studies performed in the laboratory (Benthien et al., 2009; Englebrecht and Sachs, 2005; Schouten et al., 2006; van der Meer et al., 2013; Wolhowe et al., 2009) and field (Englebrecht and Sachs, 2005; Schwab and Sachs, 2011) have demonstrated that alkenone δD values reflect the δD value of environmental water, but that other factors can influence the magnitude of D/H fractionation, including growth stage, salinity, and light levels. Species effects are also known to be large in marine alkenone producers, with *E. huxleyi* and *G. oceanica* producing $C_{37}$ alkenone δD values that differed by up to 30 ‰ between similar cultures (Schouten et al., 2006). Evaluating the relationship between D/H fractionation and salinity has yielded contradictory results; a batch culture study revealed the strongest salinity effect yet observed for an algal lipid (Sachse et al., 2012; Schouten et al., 2006), and a field transect study identified no changes in D/H fractionation along the Chesapeake Bay in response to salinity, or any other environmental parameter (Schwab and Sachs, 2011).

Here we report on an assessment of δD values from individual alkenones from Manito, Chappice, and Redberry Lakes in Saskatchewan, Canada, and the Great Salt Lake in Utah, USA which span a range of salinities from 20 to 133 ppt. The goal of the present study was to evaluate the extent to which hydrogen isotope ratios of alkenones in terrestrial systems are useful environmental indicators, and particularly the extent to which they are sensitive to changes in salinity and the δD values of environmental water over a large geographic area and a probable diversity of species types, nutrient conditions, light levels, and water chemistries. The sites targeted in this study were part of a larger effort to evaluate the influence of salinity on D/H fractionation in algal lipids in saline and hypersaline environments. Results from assessments performed for the algal sterols dinosterol and brassicasterol form the basis of a separate paper

(Nelson and Sachs, *Chapter 3*). The magnitude of D/H fractionation is discussed in terms of the fractionation factor, $\alpha$, where $\alpha = D/H_{product}/D/H_{substrate} = (\delta D_{product}+1000)/(\delta D_{substrate}+1000)$.

## Methods

### *Sediment and water sampling*

All samples were recovered during the fieldwork described in Bowman and Sachs (2008). Sediments were collected by Van Veen dredge or hand sampler and frozen prior to analysis. This collection method typically resulted in the recovery of material from ~5-20 cm deep in the surface sediments. Lake water conductivity was measured at most sites at the time of sampling with a hand held conductivity sensor, and salinities were calculated based on the relationship between conductivity and salinity in seawater. Water samples were also collected to determine salinity by evaporite residue as described in Bowman and Sachs (2008). In all cases, lake water samples were collected for $\delta D_{water}$ measurements in screw cap glass vials that were sealed with electrical tape on site at the time of sediment recovery.

### *$\delta D_{water}$ measurements*

Water samples were measured at the University of Washington using a Thermal Conversion Elemental Analyzer (TCEA) interfaced with a Delta V Plus Isotope Ratio Mass Spectrometer (IRMS) (Thermo Scientific, Waltham, MA), and the $H_3^+$ factor (Sessions et al., 2001) was evaluated at the beginning of each sample sequence. Each sample was analyzed over

six consecutive injections with the first three omitted from reported values due to memory effects from the previous sample. δD values were determined in the Isodat 2.0 software platform relative to monitoring gas hydrogen, and then post-processed using measured values of two standards (0 ‰, and -189.5 ‰) analyzed in the same sequence to reference the data to the VSMOW.

*Lipid extraction and pre-HPLC sample procedures*

Sediment samples were freeze dried and extracted in a 9:1 mixture of dichloromethane (DCM) and methanol (MeOH) on an accelerated solvent extractor (ASE) Dionex 200 operated at 100 °C and 1500 psi with three five-minute static phases. Excess solvent was evaporated under $N_2$ from the total lipid extract (TLE) on a Turbo-vap system (Caliper, Hopkinton, MA, USA). In order to validate the high performance liquid chromatography – mass spectrometry (HPLC-MS) method that was developed and applied for this sample set (Nelson and Sachs, *Chapter 2*), several HPLC-MS procedural duplicates were prepared using varying pre-HPLC-MS clean up procedures. TLEs were separated into neutral and acid fractions using glass solid phase extraction (SPE) columns that were hand packed with 0.5 g of aminopropyl silica gel ($NH_2$) (Suppelco). Neutral compounds were eluted with 8 mL of dichloromethane (DCM) and isopropyl alcohol (IPA) (3:1), followed by an acid fraction with 6 mL of 4 % acetic acid in ethyl ether, followed by a polar fraction with 6 mL of methanol (MeOH). Subsamples of the neutral fraction from Chappice, Redberry and the Great Salt Lake were further separated into hydrocarbon, ketone/ester, alcohol, and polar fractions using the same glass hand-packed SPE columns with 1 g of silica gel 60 (5 % deactivated by weight; EMD chemicals, 35-75μm).

Hydrocarbon fractions were eluted with 10 mL of hexane, ketones with 6mL DCM/hexane (1:1), alcohols with 8mL ethyl acetate (EtOAc)/hexane (1:4), followed by a polar fraction with 6mL methanol. A subsample of the Manito Lake TLE was separated into polar and non-polar fractions using a liquid-liquid extraction by dissolution in 2 mL of methanol, to which 2 mL of hexane was added. The mixture was then agitated and sonicated to ensure complete dissolution of the TLE. The solvents were allowed to separate, after which the hexane supernatant was removed by Pasteur pipet. This was repeated ten times with the supernatants combined. To assess recovery, 5 % aliquots of the methanol and hexane fractions were removed and evaluated by gas chromatography mass spectrometry (GC-MS), which revealed no remaining GC-amenable compounds in the methanolic mother liquor.

*HPLC-MS purification of individual alkenones*

All HPLC-MS purifications of individual alkenones were performed using a reverse phase method designed for concurrent purification of sterols, triterpenols, and individual alkenones from a single sample injection (Nelson and Sachs, *Chapter 2*). Briefly, prior to injection on the HPLC samples were acetylated at 70 °C for 30 minutes in a mixture of 20 μL acetic anhydride of known δD value and 20 μL pyridine in order to derivitize the non-alkenone target alcohols which were purified from the same HPLC injection. In cases where silica fractions were used, ketone and alcohol fractions were recombined prior to acetylation and HPLC injection. Sterols and triterpenols were eluted first in an isocratic mobile phase of 5 % MeOH, 10 % EtOAc, and 85 % acetonitrile (ACN), after which the mobile phase composition was transitioned to 5:20:75 MeOH:EtOAc:ACN and held isocratic to elute individual alkenones.

The samples used in this study were also used in the final stage of developing the HPLC-MS method (Nelson and Sachs, *Chapter 2*). As a result, duplicate HPLC injections were performed for three of the four independent sample sites that we report on in order to finalize the correct collection intervals for all individual alkenones. These resulted in duplicate purifications of some, but not all, targeted alkenones. In cases where this occurred the injection was repeated with additional material, but all available purified alkenones from repeat injections were incorporated into the sample set to serve as HPLC-MS purification procedural duplicates. Only $C_{37:4}$, $C_{37:3}$, $C_{37:2}$, $C_{38:3}$ and $C_{38:2}$ alkenones were targeted for analysis.

*Gas Chromatography-Mass Spectrometry*

At each purification stage and prior to hydrogen isotope analysis, GC-MS analyses of sample aliquots were conducted with an Agilent 6890N GC with 5975 inert mass selective detector equipped with an Agilent (formerly Varian) VF-17ms column (60 m X 0.32 mm X 0.25 μm). Samples were injected in splitless mode at 300 °C using helium carrier gas at 1.5 mL/min. The GC oven was held at the initial temperature of 110 °C for 3 minutes after sample injection, then increased to 170 °C at 15 °C/min, then to 325 °C at 5 °C/min and held for 24 minutes. All samples were run in full scan mode (*m/z* 50-700). Compound quantification was approximated based on the relative areas of unknown peaks to that of a 5α-cholestane internal standard added to each sample prior to GC-MS analysis.

*Alkenone distribution ratios*

Subsamples of the neutral fractions from aminopropyl SPE columns were analyzed with an Agilent 6890N GC using a flame ionization detector (GC-FID). Samples were injected in splitless mode using a programmable temperature vaporization inlet with helium carrier gas at 2.0 mL/min onto a DB-5ms capillary column (60 m X 0.32 mm X 0.32 μm). The GC oven was held at 110 °C for 4 minutes after sample injection, then increased to 150 °C at 15 °C/min, then increased to 320 °C at 6 °C/min and held for 28 minutes. $U^{k}_{37}$ ($[C_{37:2} - C_{37:4}]/[C_{37:2} + C_{37:3} + C_{37:4}]$) and $U^{k'}_{37}$ ($[C_{37:2}]/[C_{37:3} + C_{37:2}]$) ratios, as well as $\%C_{37:4}$, $\%C_{37:3}$, and $\%C_{37:2}$ ($[C_{37:x}]/[C_{37:2} + C_{37:3} + C_{37:4}]$) were calculated based on the relative areas of each of the respective peaks.

*Gas chromatography-isotope ratio mass spectrometry*

Purified $C_{37:4}$, $C_{37:3}$, $C_{37:2}$, $C_{38:3}$ and $C_{38:2}$ alkenone δD values were measured by gas chromatography-isotope ratio mass spectrometry (GC-IRMS) using a Thermo Delta V Plus isotope ratio mass spectrometer and Thermo Trace GC Ultra interfaced to a gas chromatography combustion interface III. Samples were injected in splitless mode at 330 °C using helium carrier gas at 1.5 mL/min. The GC was equipped with a VF-17ms (60 m X 0.25 mm X 0.25 μm). Alkenones were injected with an initial oven temperature of 120 °C, which was then increased to 230 °C at 20 °C/min, then to 325 °C at 8 °C/min and held for 17 minutes. GC column effluent was directed through the pyrolysis reactor and combustion interface to convert all hydrogen to

$H_2$ prior to introduction to the mass spectrometer. The $H_3^+$ factor (Sessions et al., 2001) was measured prior to every sample sequence, and was stable and less than 5.

All samples were analyzed with a mix of coinjection standards of known isotopic composition, which included a combination of $n$C$_{21}$, $n$C$_{23}$, $n$C$_{32}$, $n$C$_{34}$ and $n$C$_{39}$ (standards from Arndt Schimmelmann at Indiana University, Bloomington, IN, USA). Samples were also analyzed in sequences that included an external standard with $n$C$_{26}$, $n$C$_{29}$, $n$C$_{38}$, and $n$C$_{41}$ (standards from Arndt Schimmelmann at Indiana University, Bloomington, IN, USA). Initial isotopic evaluations of all peaks were performed within the Isodat 2.0 software relative to a calibrated reference gas. Secondary corrections were performed based on the regression of Isodat-reported δD values of *n*-alkane standards and their accepted values in order to maintain like treatments of samples and standards, as well as to correct for potential scale compression or stretching as a result of the one-point referencing to VSMOW performed by the Isodat software. Samples were analyzed at least three times, and measurement precision calculated as the standard deviation of multiple analyses was typically 3 ‰. Individual sample uncertainties were calculated as the standard deviation of replicate measurements. Peak areas less than 15 V·s were below the cutoff identified on this GC-IRMS to avoid size dependent δD effects, and were not considered (Polissar et al., 2009). Individual $C_{37}$ alkenone δD values were then used with $\%C_{37:x}$ values determined by GC-FID to calculate a weighted sum δD value of pooled $C_{37}$ alkenones ($C_{\Sigma 37}$) for each site to facilitate comparison with other data sets.

*Post-IRMS saponification*

HPLC-purified $C_{37:3}$ samples each contained the target alkenone and an internal 5α-cholestane standard, but in addition, a $C_{37:4}$ ethyl-alkenoate that was well resolved from the $C_{37:3}$ alkenone. In order to confirm that two apparently anomalous $C_{37:3}$ δD values from Redberry and Manito Lake were not biased by any potential coeluting alkenoates that were somehow not removed by HPLC, after δD measurements were completed the remaining $C_{37:3}$ material from these two samples were each split into two fractions. One half of each sample was then saponified with 1 mL 1 N potassium hydroxide in MeOH and 0.5 mL Nanopure water (Barnstead Nanopure infinity water system) in order to remove any potential coeluting alkanoates. Following saponification, these aliquots were analyzed on the GC-MS to confirm that the mass spectra did not indicate the presence of coeluting compounds, and to confirm that the known $C_{37:4}$ ethyl-alkenoate was removed and therefore that the saponification was successful. Both the saponified and unsaponified aliquots were then analyzed by GC-FID. The ratio of the $C_{37:3}$ peak area to that of the internal 5α-cholestane standard, which was present in the sample prior to the pre-saponification split, were compared between the pre- and post-saponification aliquots and found to be unchanged, further confirming the purity of the measured δD values of the $C_{37:3}$ alkenone peaks.

## Results and Discussion

### *Salinity*

Recovery of surface samples by Van Veen dredge results in the collection of material from up to 20 cm deep in the sediments. Lake water salinity was measured during the time of sample collection (Bowman and Sachs, 2008), but these values are unlikely to be representative of the average salinity over the many decades required for the recovered sediment to accumulate in each basin. In order to compensate for this issue, we used historical salinity and sedimentation rates to calculate time-weighted average salinities (Tables 1-3). This results in significant uncertainty, but these estimates are still likely to be more representative of the salinity that corresponds with the sedimentary lipid chemistry than are the snapshot field measurements. This approach is outlined in detail in our related study of dinosterol and brassicasterol samples purified from this sample set (Nelson and Sachs, *Chapter 3*). Despite the large uncertainties in our salinity estimates, by targeting a very large range of salinities (20 – 133 ppt), our sample set still represents a large and detectable salinity gradient over which to evaluate alkenone chemistry.

**Table 1:** Salinity and hydrogen isotope data from water samples and individual purified alkenones from each lake site. At three of four sites, duplicate HPLC purifications were performed for some compounds. In these cases, the average of the two δD values were used. Values plotted in Figure 1 and used in the discussion are indicated in bold.

| Site | Salinity | estimated salinity error + | estimated salinity error - | δD-water | σ | δD-$C_{37:4}$ | σ | n | δD-$C_{37:3}$ | σ | n | δD-$C_{37:2}$ | σ | n | δD-$\Sigma C_{37}$ | σ | δD-$C_{38:3}$ | σ | n | δD-$C_{38:2}$ | σ | n |
|---|---|---|---|---|---|---|---|---|---|---|---|---|---|---|---|---|---|---|---|---|---|---|
| Manito Lake, Canada | 24 | 10 | 10 | -78.5 | 0.6 | -229 | 3 | 5 | -174 | 3 | 3 | -173 | 6 | 8 | | | -235 | 2 | 3 | -206 | 3 | 5 |
| HPLC duplicates | 24 | 10 | 10 | -78.5 | 0.6 | | | | -175 | 2 | 3 | | | | | | | | | | | |
| **average** | **24** | **10** | **10** | **-78.5** | **0.6** | **-229** | **3** | | **-175** | **2** | | **-173** | **6** | **8** | **-214** | **3** | **-235** | **2** | **3** | **-206** | **3** | **5** |
| Redberry Lake, Canada | 20 | 15 | 15 | -81.1 | 1.2 | -238 | 2 | 5 | -189 | 2 | 7 | -201 | 6 | 6 | | | | | | | | |
| HPLC duplicates | 20 | 15 | 15 | -81.1 | 1.2 | -235 | 2 | 5 | -183 | 3 | 8 | -187 | 6 | 6 | | | | | | | | |
| **average** | **20** | **15** | **15** | **-81.1** | **1.2** | **-237** | **2** | | **-186** | **3** | | **-194** | **6** | **6** | **-225** | **2** | | | | | | |
| Chappice Lake, Canada | 49 | 57 | 15 | -75.2 | 0.6 | **-231** | **3** | **6** | **-204** | **5** | **5** | **-184** | **4** | **4** | **-219** | **4** | **-232** | **3** | **3** | **-215** | **2** | **4** |
| Great Salt Lake (South), USA | 133 | 69 | 41 | -60.7 | 1.2 | -184 | 4 | 5 | -176 | 3 | 9 | -153 | 4 | 4 | | | -194 | 5 | 8 | -175 | 3 | 5 |
| HPLC duplicates | 133 | 69 | 41 | -60.7 | 1.2 | | | | -177 | 3 | 6 | | | | | | -198 | 3 | 7 | -177 | 4 | 6 |
| **average** | **133** | **69** | **41** | **-60.7** | **1.2** | **-184** | **4** | | **-176** | **3** | | **-153** | **4** | **4** | **-175** | **3** | **-196** | **4** | | **-176** | **4** | |

**Table 2:** Salinity and calculated alkenone distribution ratios from each lake site.

| Site | Salinity | estimated salinity error + | estimated salinity error - | $U^{k}_{37}$ | $U^{k'}_{37}$ | %$C_{37:4}$ | %$C_{37:3}$ | %$C_{37:2}$ |
|---|---|---|---|---|---|---|---|---|
| Manito Lake, Canada | 24 | 10 | 10 | -0.67 | 0.24 | 0.74 | 0.20 | 0.06 |
| Redberry Lake, Canada | 20 | 15 | 15 | -0.71 | 0.17 | 0.76 | 0.20 | 0.04 |
| Chappice Lake, Canada | 49 | 57 | 15 | -0.51 | 0.21 | 0.60 | 0.32 | 0.09 |
| Great Salt Lake (South), USA | 133 | 69 | 41 | -0.13 | 0.21 | 0.28 | 0.57 | 0.15 |

**Table 3:** Salinity and calculated α values from δD values of water and individual purified alkenones from each lake site. At three of four sites, duplicate HPLC purifications were performed for some compounds. In these cases, the average of the two calculated α values were used. Values plotted in Figure 1 and used in the discussion are indicated in bold.

| Site | Salinity | estimated salinity error + | estimated salinity error - | α ($C_{37:4}$-water) | σ | α ($C_{37:3}$-water) | σ | α ($C_{37:2}$-water) | σ | α ($C_{38:3}$-water) | σ | α ($C_{38:2}$-water) | σ |
|---|---|---|---|---|---|---|---|---|---|---|---|---|---|
| Manito Lake, Canada | 24 | 10 | 10 | 0.837 | 0.003 | 0.896 | 0.003 | 0.897 | 0.006 | 0.830 | 0.002 | 0.862 | 0.004 |
| HPLC duplicates | 24 | 10 | 10 | | | 0.895 | 0.002 | | | | | | |
| **average** | **24** | **10** | **10** | **0.837** | **0.003** | **0.896** | **0.003** | **0.897** | **0.006** | **0.830** | **0.002** | **0.862** | **0.004** |
| Redberry Lake, Canada | 20 | 15 | 15 | 0.829 | 0.002 | 0.882 | 0.002 | 0.869 | 0.007 | | | | |
| HPLC duplicates | 20 | 15 | 15 | 0.833 | 0.002 | 0.889 | 0.004 | 0.884 | 0.007 | | | | |
| **average** | **20** | **15** | **15** | **0.831** | **0.002** | **0.886** | **0.003** | **0.877** | **0.007** | | | | |
| **Chappice Lake, Canada** | **49** | **57** | **15** | **0.831** | **0.004** | **0.860** | **0.005** | **0.883** | **0.004** | **0.830** | **0.003** | **0.849** | **0.003** |
| Great Salt Lake (South), USA | 133 | 69 | 41 | 0.869 | 0.004 | 0.878 | 0.003 | 0.902 | 0.004 | 0.858 | 0.006 | 0.879 | 0.004 |
| HPLC duplicates | 133 | 69 | 41 | | | 0.876 | 0.003 | | | 0.854 | 0.004 | 0.876 | 0.005 |
| **average** | **133** | **69** | **41** | **0.869** | **0.004** | **0.877** | **0.003** | **0.902** | **0.004** | **0.856** | **0.005** | **0.877** | **0.004** |

*Salinity - $\delta D_{water}$ relationships*

Within the subset of continental interior lakes discussed in the present study, δD values of water are highly correlated with historic average salinity ($R^2 = 0.99$, $P = 0.004$) (Figure 1; Table 1). This is expected within sub-regions of the oceans, and in regions of lakes where waters are derived from similar sources and subjected to varying degrees of subsequent evaporative enrichment. While we suspect that this may be the case for the lakes in Saskatchewan, which are within a few hundred kilometers of one another, it is perhaps more surprising that the salinity-$\delta D_{water}$ relationship in these systems appears quite similar to that in the Great Salt Lake. Nevertheless, this appears to be the case, and must therefore be considered when evaluating the potential causes of the relationships between alkenone δD values and salinity.

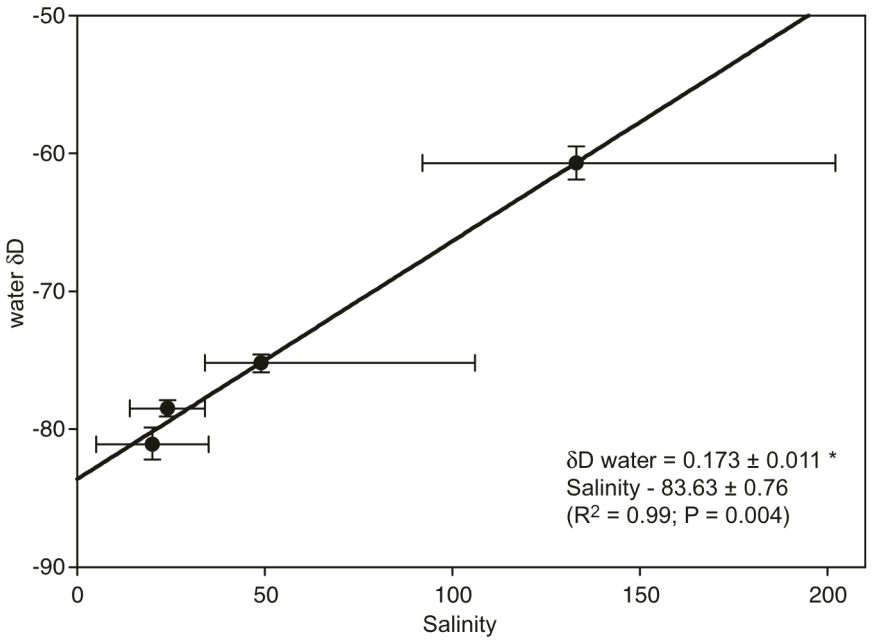


**Figure 1:** Salinity vs. δD water at all sites. Salinity error bars indicate known historical changes in salinity at continental interior sites (Nelson and Sachs, *Chapter 3*).

*Salinity - %$C_{37:4}$ relationships*

Salinity shows a strong negative correlation with %$C_{37:4}$ in our data set ($R^2$ = 0.99, P = 0.003) (Figure 2; Table 2). Although the $C_{37:4}$ alkenone is not always present in saline lakes where alkenones are detectable (Toney et al., 2010), the sites in our study support the idea that $C_{37:4}$ concentrations decrease with increasing salinity (Chu et al., 2005; Liu et al., 2011), which is in disagreement with observations from the Chesapeake Bay (Schwab and Sachs, 2011). Schwab and Sachs (2011) suggested that this discrepancy might result from physiological or species changes along the Chesapeake Bay that differ from other settings, which might suggest that the sites we report on also contain different alkenone producers.

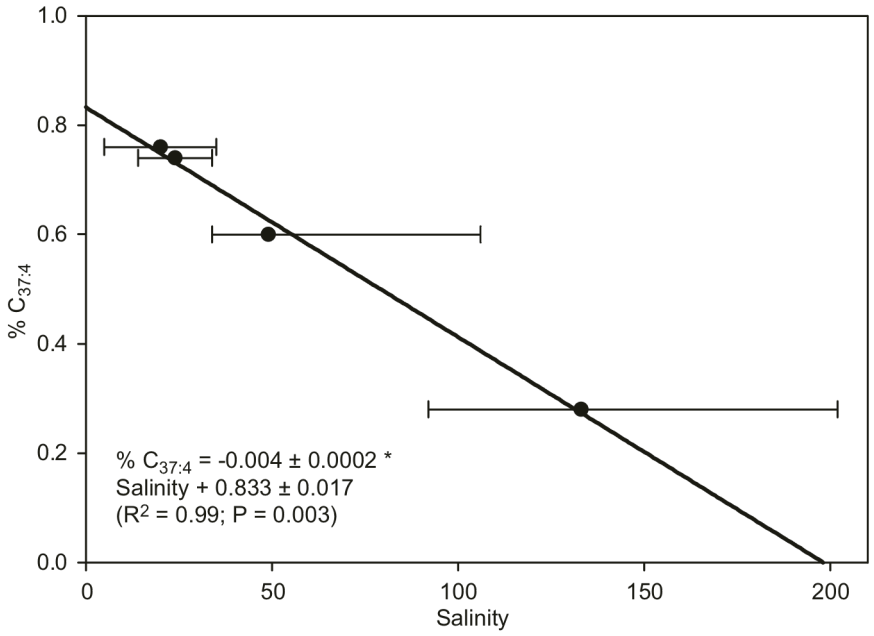


**Figure 2:** Salinity vs. % $C_{37:4}$ at all sites. Salinity error bars indicate known historical changes in salinity at continental interior sites (Nelson and Sachs, *Chapter 3*).

### *$\delta D_{alkenones} - \delta D_{water}$ relationships*

The relationships between the δD values of individual alkenones and the calculated pooled $C_{\Sigma 37}$ with $\delta D_{water}$ values display almost universally high $R^2$ values, with the notable exception of $C_{37:3}$ (Table 1, Figure 3). The fact that the slopes for most regressions are similar suggests that this is likely to be a real environmental signal despite the relatively high P values, which are largely attributable to the low number of samples, particularly for $C_{38}$ alkenones since purification of these compounds from Redberry Lake was unsuccessful. We explore some ideas about the cause for the lack of consistency in the $C_{37:3}$ data in more detail later in the text, but disregarding for the moment, we point out that all remaining slopes are below 0.5, implying that more than half of an observed change in the δD value of an individual alkenone δD value must be driven by factors other than changes in the δD of the water.

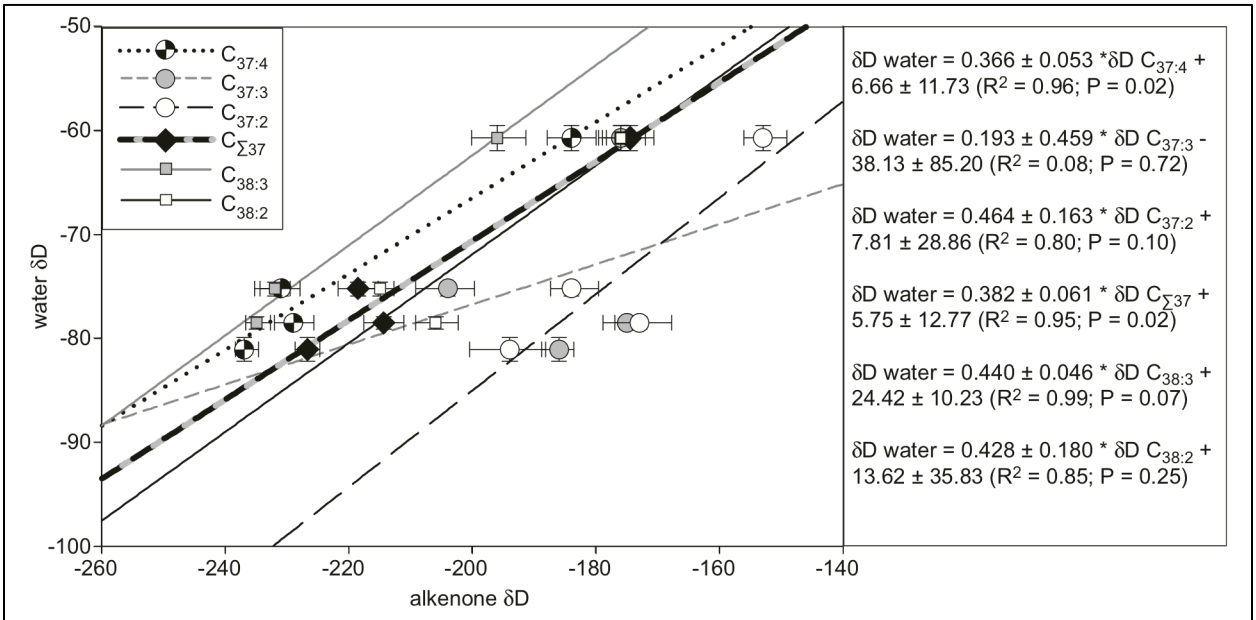


**Figure 3:** Alkenone and water δD relationships. Error bars represent the standard deviation of replicate measurements, or propagated standard deviations in the case of $C_{\Sigma 37}$ data.

*α - Salinity relationships*

The average range of δD values for an individual alkenones in our sample set is ~35 ‰, but water changes are limited to ~20 ‰ (Figure 3, Table 1). The larger difference in lipid δD values occurs due to changes in α values over the range of the sample set, which average 0.033 per alkenone (Table 3). As is the case for $\delta D_{alkenone}$-$\delta D_{water}$ relationships, although $R^2$ values are for the most part relatively high between α values and salinity (Figure 4), the limited number of data points also results in relatively high P values, and therefore limited statistical significance.

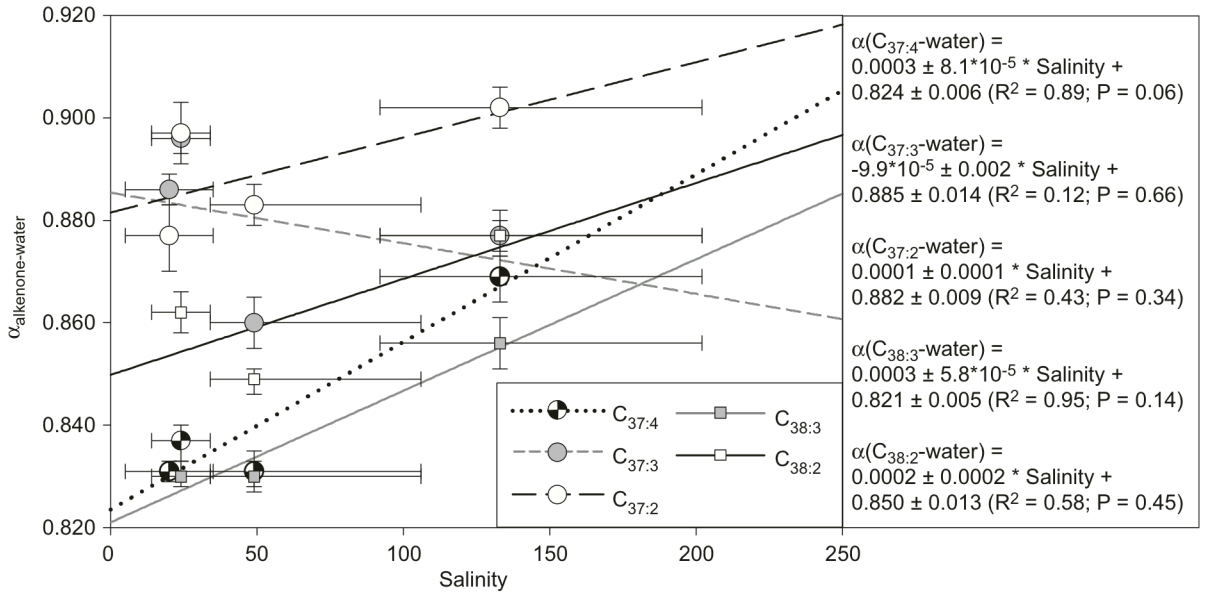


**Figure 4:** Salinity vs. α values for alkenone-water hydrogen isotope product-substrate pairs. Salinity error bars are as in Figure 1, α error bars are the propagated standard deviations of replicate measurements of water and alkenone δD values.

Nevertheless, the fact that most α values are positively correlated with salinity suggests that there may be a salinity dependence on D/H fractionation in alkenone biosynthesis by non-marine producers. This is in contrast to alkenone-water α values in the Chesapeake Bay (Schwab and Sachs, 2011), which showed no salinity dependence. These results also disagree with those from batch culture experiments with *E. huxleyi* and *G. oceanica* (Schouten et al., 2006; van der Meer et al., 2013), for which the observed α-salinity relationship of approximately 0.0033 per unit change in salinity was an order of magnitude larger than the 0.0003 α-salinity slope that we observe for the $C_{37:4}$ alkenone. However, in these experiments salinity likely also influenced the growth rates of the organisms, which causes a separate isotope effect (Zhang et al., 2009), and may therefore have resulted in a larger apparent α dependence to salinity than is directly attributable to salinity alone.

$\alpha_{C37:3\text{-}C37:2}$ - $U^{k'}_{37}$ relationships

Van der Meer et al., 2013 recently noted that the difference between δD values of $C_{37:3}$ and $C_{37:2}$ vary as a function of $U^{k'}_{37}$. In order to make this comparison, they calculate a ΔδD value ($\delta D_{C37:2}$ - $\delta D_{C37:3}$). This approach will yield different ΔδD values for different substrate δD values (i.e. changing water δD values in this case) for reactions that proceed under otherwise identical conditions due to the nature of δ-notation. In order to assess the relationship between differences in δD values between $C_{37:3}$ and $C_{37:2}$ alkenones, we favor α notation, which does not suffer from the dependence on substrate δD values. Comparing $\alpha_{C37:3\text{-}C37:2}$ values with the $U^{k'}_{37}$ values from our current study, as well as with those from other published data sets (D'Andrea et

al., 2007; Schwab and Sachs, 2011; van der Meer et al., 2013; Wolhowe et al., 2009), we observe that the Chappice Lake and Great Salt Lake samples follow the relationship defined by most of the available data. However, the data from Redberry and Manito Lake do not, nor does the value from D'Andrea et al. (2007). The relationship between δD value differences and $U^{k'}_{37}$ values is best described by a linear fit when using α notation and excluding the three outlier points ($R^2$ = 0.84; P < 0.001) (Figure 5).

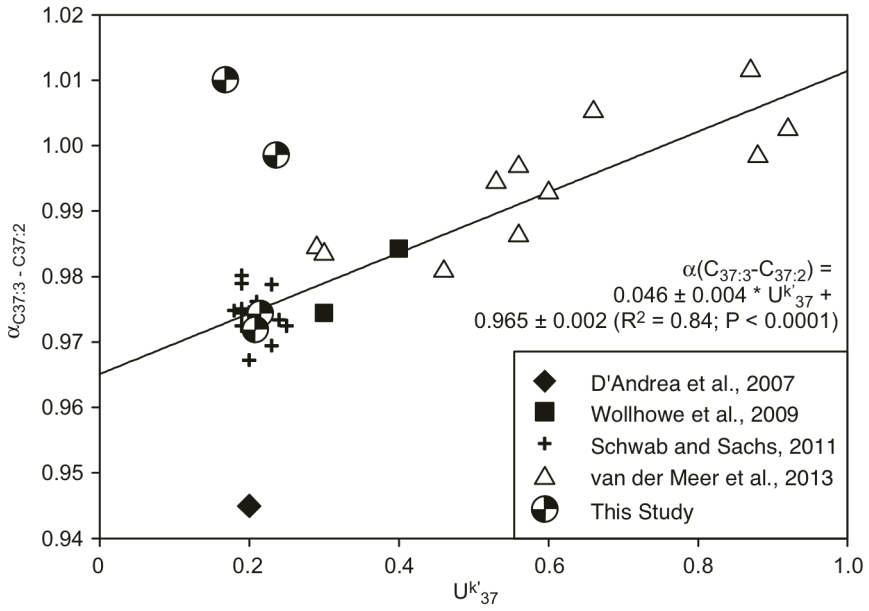


**Figure 5:** Hydrogen isotopic fractionation between $C_{37:3}$ and $C_{37:2}$ plotted against $U^{k'}_{37}$ values for all available records. Regression line excludes outlier points from Redberry and Manito Lake, as well as the value from D'Andrea et al. (2007).

The original explanation put forth to explain the relationship between $\alpha_{C37:3\text{-}C37:2}$ and $U^{k'}_{37}$ was that the biosynthetic pathway of desaturation from $C_{37:2}$ to $C_{37:3}$ was unidirectional and contained no major branch points, and that therefore it is best described by a Rayleigh distillation type fractionation (van der Meer et al., 2013). Were this to be the case, then there would be no

mechanism for changes in the offset between product $C_{37:2}$ and substrate $C_{37:3}$ δD values. Instead, the initial δD value of $C_{37:3}$ produced from $C_{37:2}$ would be depleted by whatever the magnitude of D/H fractionation is at this step, but as progressively more and more $C_{37:2}$ were converted to $C_{37:3}$, the δD value of the growing $C_{37:3}$ pool would gradually approach the initial δD value of the $C_{37:2}$ pool, with the offset between the δD values of each of the respective alkenones remaining constant at any stage of the process regardless of the relative sizes of the pools, and therefore of the $U^{k'}_{37}$ values (e.g. Hayes, 2001). We suggest that the fact that $\alpha_{C37:3\text{-}C37:2}$ do vary as a function of $U^{k'}_{37}$ values instead implies either that there is a direct temperature dependence of the magnitude of D/H fractionation that occurs during the desaturation, or that there are branch points in the biosynthetic pathway that are currently unknown. This latter point might argue in favor of controlled experiments to evaluate and potentially refine current ideas regarding alkenone biosynthesis (Rontani et al., 2006). In either case, it is clear that the sensitivity of $\alpha_{C37:3\text{-}C37:2}$ to $U^{k'}_{37}$ is intriguing and currently unexplained. Given the incomplete understanding, despite the apparently strong empirical fit between $\alpha_{C37:3\text{-}C37:2}$ and $U^{k'}_{37}$ values we are still of the opinion that individual alkenone δD values are preferable to measuring pooled $C_{37}$, at least until a valid mechanism can be identified or the empirical fit is substantiated with more data. This is especially true when considering that pooled $C_{37}$ δD values may be calculated from individual alkenone δ values and concentration data while the reverse cannot.

*$\delta D_{alkenone}$ species effects in lakes*

Although lacustrine alkenones have received relatively less attention than those in marine systems, rather extensive alkenone distribution and phylogenetic studies have been conducted on the lakes of interior North America, including at two lakes within our sample set – The Great Salt Lake, Utah, and Redberry Lake, Saskatchewan (Theroux et al., 2010; Toney et al., 2010; Toney et al., 2011; Toney et al., 2012). Genetic analyses of the alkenone producers in the Great Salt Lake identified one operational taxonomic unit, which was also identified in other lakes in continental North America, that are most closely related to the known coastal haptophyte species in the *Chrysotilia*, *Isochrysis*, and *Pseudoisochrysis* genera, which are all more closely related to the marine alkenone producers in the *Emiliania* and *Gephyrocapsa* genera than either are to most alkenone producers in Greenland lakes (Theroux et al., 2010). Efforts to grow lacustrine alkenone producing haptophytes in laboratory cultures have recently proven successful with two organisms that display strong genetic similarity to the operational taxonomic units identified in the Great Salt Lake and the lakes of North Dakota and other Great Plains Lakes (Toney et al., 2012). These cultured haptophytes were both observed to produce the $C_{37:4}$ alkenone, although to a lesser degree in the haptophyte that was genetically similar to the sequences recovered from the Great Salt Lake, which showed the lowest % $C_{37:4}$ value in our sample set (Table 2) . Although the distribution patterns of alkenones have been shown to be an unreliable indicator of the exact species assemblage at a particular sample site (Theroux et al., 2010), based on the extensive genetic and alkenone survey work that has been conducted on the lakes in continental North America, we suggest that the alkenone species assemblages at our sites are likely to be primarily comprised of a mix of species closely related to the cultured $C_{37:4}$ producing Hap-A and Hap-B phylotypes (Toney et al., 2012).

The $C_{37:3}$ alkenone δD data from our study and related α values are uncorrelated with water δD values and salinity, respectively (Figures 3 & 4). In order to confirm that these data are not biased by laboratory handling error, we point out that three of the four $C_{37:3}$ samples were processed in duplicate on the HPLC (Table 1). Of these, two of the separate measurements differ by only 1 ‰, and most were analyzed more than three times each by IRMS. The greatest discrepancy between HPLC duplicates is from Redberry Lake, where the HPLC duplicates measured -189 ± 2 ‰ and -183 ± 3 ‰, while this difference may be the result of an inadvertent sample preparation error, it is nowhere near the magnitude that would be required to explain the scatter in the $C_{37:3}$ δD and α data. We also performed post–IRMS saponifications on the samples from Redberry and Manito Lakes in order to confirm that no coeluting alkenones were biasing these measurements (see Methods).

Alkenones with increasing degrees of unsaturation usually show decreasing δD values (Figure 5), yet the δD values of the $C_{37:3}$ alkenones in Redberry and Manito Lake are virtually equivalent to or more enriched than the δD values of the $C_{37:2}$ alkenone. We suggest that the apparently anomalous $C_{37:3}$ relationships may occur as a result of variable species distributions in each of our lakes. The $C_{37:3}$ compound is produced in high abundance at the surface temperatures typical of inland continental lakes, and is therefore the compound that is most likely to be derived from multiple producers. In contrast, $C_{37:4}$ is produced in much greater abundance by one of the two species types that are suspected to dominate at these sites (Toney et al., 2012), so the hydrogen isotope data derived from it is likely to be more indicative of the lipids from a single alkenone producer, or at least a reduced diversity and more closely related group of alkenone producing organisms. This may explain the fact that the highest $R^2$ values and

lowest P values are observed for the $C_{37:4}$ alkenone relationships (both water vs. lipid δD values, and α vs. salinity values), and substantiates the argument that species effects are influencing these relationships for the di- and tri- unsaturated alkenones at these sites.

*Comparing the wide range of α-salinity relationships in alkenones*

The differences in slopes of the $\alpha_{alkenone\text{-}water}$ – salinity relationships among the separate available data sets are striking. While the slopes for each of the individual alkenones from this study are broadly similar with the exception of the $C_{37:3}$, at ~0.0003 these are much shallower than those observed in *E. huxleyi* and *G. oceanica* batch cultures (0.003), either for the integrated $C_{37}$ peak (Schouten et al., 2006), or for individual alkenones that were later purified from the same samples (van der Meer et al., 2013), although as indicated above, some of this difference may be due to the influence of salinity on growth rates. Figure 6 compares the α-salinity slopes from each of these studies using only one representative type of alkenone measurement for each study to highlight the differences since the slopes of individual alkenones and/or species were far more similar within than between the three data sets.

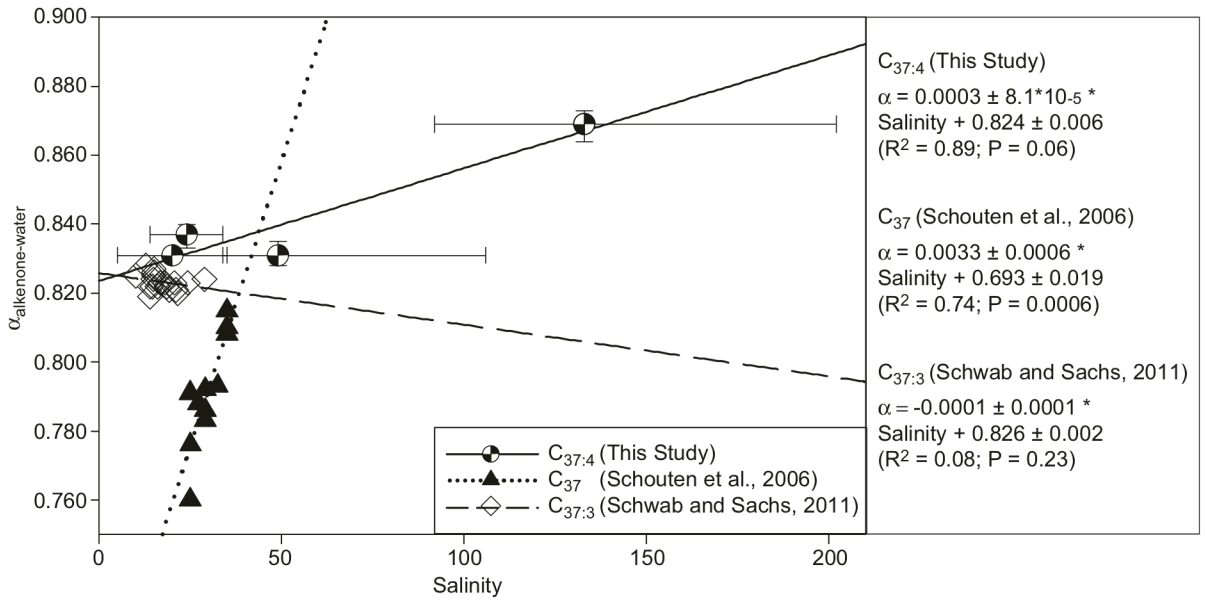


**Figure 6:** Comparison of $\alpha_{alkenone\text{-}water}$ values and salinity from the representative $C_{37:4}$ alkenone from this study with representative pooled $C_{37}$ alkenone values from *E. huxleyi* grown in batch cultures (Schouten et al., 2006) and $C_{37:3}$ purified from suspended particles in the Chesapeake Bay (Schwab and Sachs, 2011).

If the Schouten et al. (2006) and Van der Meer et al. (2013) trends were linear over the range of salinities represented in the present research the $\alpha$ value would cross unity as salinity approaches 100 (Figure 6). It may be that the relationship would cease to be linear over a larger range of salinities, although *E. huxleyi* and *G. oceanica* are thought to be intolerant of salinities approaching 50 (Winter et al., 1983). The steepness of the slope in these data is also likely to be partially related to varying growth rates among the batch cultures, which are also known to influence the magnitude of D/H fractionation (Zhang et al., 2009). Nevertheless, this is unlikely to offer a complete explanation for the discrepancy between the steep slopes from the *E. huxleyi* and *G. oceanica* batch culture experiments (Schouten et al., 2006; van der Meer et al., 2013) and the near zero slope from the Chesapeake Bay transect study (Schwab and Sachs, 2011), or the

shallow α-salinity relationship that we observe in the present study. If D/H fractionation during alkenone biosynthesis were universally sensitive to environmental stresses across all alkenone producing organisms we would expect to observe a much larger range of α values in our data since the differences in growth environments across our sample set is almost certainly larger than those in the *E. huxleyi* and *G. oceanica* batch cultures (Schouten et al., 2006).

We also note that application of the 0.0033 α-salinity relationship has provided realistic paleosalinity estimates in a sapropel formation from the Mediterranean Sea, where independent estimates of seawater $\delta^{18}O$ were derived from paired planktonic foraminifera $\delta^{18}O$ and $U^{k'}_{37}$ measurements, and converted into δD values for seawater to constrain the degree of δD variability that was attributable to isotopic changes in the water (van der Meer et al., 2007). The authors assert that the remaining δD response in alkenones must have occurred as a result of changing α values, and application of the 0.0033 α-salinity relationship provided estimates of salinity changes from 39 to 33. Although directly applying the 0.0033 α-salinity relationship may be somewhat dubious due to the likely contributing effect of salinity-induced growth rate changes in determining that value, it may be valid when consideration is given to the fact that similar salinity induced growth rate changes could have occurred in the environment in association with the measured change in pooled alkenone δD values. This salinity reconstruction also seems more realistic than the change that would have been required if the shallower slope that we observe in the present study of 0.0003 were applied, which would require that salinity changes were on the order of 60 ppt. The near zero α-salinity slope observed in the Chesapeake Bay (Schwab and Sachs, 2011) would require that the Mediterranean Sea record be explained entirely by factors other than salinity, with changing growth rates as an obvious possibility.

However, were this to be the cause, it seems difficult to reconcile the observation that α values were essentially unchanged along the Chesapeake Bay despite significant salinity changes and probable growth rate changes (Schwab and Sachs, 2011).

Another paleoclimate application of δD values from alkenones over time intervals during which very large salinity changes are suspected is from sediments from the Black Sea from the Messinian Salinity Crisis, when the basin became isolated from the Mediterranean and subject to intensely negative precipitation-evaporation balance (Vasiliev et al., 2013). Here, the authors are unable to differentiate between changes in water δD values and changes in α driven by salinity, or other factors, but note that the 60 ‰ enrichment of alkenone δD values is exceptionally large, and would require that water δD values increase by 110 ‰, or that salinity increase from ~25 to 41 if the 0.0033 α-salinity relationship is applied. They avoid a discussion of the relative contributions of each, and instead simply argue that either would indicate significant drying, but at least some change in α values, probably as a result of salinity changes, would seem to be more likely than a 110 ‰ increase in water δD values. Although more paleoclimate applications of alkenone δD values exist (e.g. Kasper et al., 2013; Leduc et al., 2013; Pahnke et al., 2007), we restrict our paleoclimate examples to only those studies targeting extremely large salinity changes for brevity.

We suggest that species differences offer the most plausible explanation for the apparent discrepancies between the α-salinity relationship observed in *E. huxleyi* and *G. oceanica* batch cultures (Schouten et al., 2006; van der Meer et al., 2013) and the paleoclimate applications of alkenone δD values spanning apparently large changes in salinity (van der Meer et al., 2007; Vasiliev et al., 2013) as compared to the shallow and near zero α-salinity slope that we observe

and that which was identified in the Chesapeake Bay (Schwab and Sachs, 2011). Schwab and Sachs (2011) suggested three hypotheses to explain the near zero slopes that they observed in the Chesapeake Bay transect: (i) that a variety of environmental factors including salinity, growth rates, and temperatures were perfectly balanced to produce no measured change in $\alpha$ values along the axis of the bay, (ii) that the assemblages of alkenone producing haptophytes changed along the axis of the bay in response to changing environmental factors so that each of these competing causes of changes in $\alpha$ values offset perfectly or (iii) that coastal haptophytes have an enhanced osmoregulative capacity that circumvents the mechanisms that cause changes in $\alpha$ values in marine haptophytes. In light of our results, we suggest that reduced sensitivity in non-marine alkenone producing haptophytes offers the most logical explanation of the observed shallow to near zero slopes in the $\alpha$-salinity relationship for alkenones. Although the number of independent sample sites in our study is limited and the uncertainties in the estimates of salinity at any given site is large, it may be stated with confidence that the sites span a large range of salinities of at least 34 to 92, and at most 14 to 202 (Tables 1 - 3). Over this range we observe an average change in individual alkenone $\alpha$ values of 0.033, or possible $\alpha$-salinity relationships from 0.0006 to 0.0002 per unit change in salinity. The uncertainty in the magnitude of our $\alpha$-salinity slope is high since it is being driven by one data point from the Great Salt Lake, however, were the 0.0033 $\alpha$-salinity slope constant (Schouten et al., 2006), or even close to similar among all alkenone producers then the measured $\delta$D value of all alkenones in the Great Salt Lake would be enriched relative to VSMOW. This is clearly not the case, so although we cannot confidently quantify the influence of factors such as growth rates or species assemblages in the resulting $\alpha$-

salinity relationships with the limited sample set that we present, it is clear that the 0.0033 α-salinity relationship as not common among all alkenone producing haptophytes.

Should the reduced salinity sensitivity that we observe be substantiated with additional data, it may be reconciled with the Chesapeake Bay data after consideration of the limited 18 unit range in salinities targeted in that study (Schwab and Sachs, 2011). Applying the 0.0003 α-salinity relationship derived from our $C_{37:4}$ data over a salinity range of 18 units would result in a difference in α values of only 0.005 over the length of the bay, or a measured δD value difference of only 5 ‰. This is very close to the analytical error of δD measurements, and given the likely competing influences of variable growth rates, light levels, temperatures, and other environmental factors that may influence α values, it is not surprising that this salinity signal did not emerge.

**Conclusion**

We have presented a preliminary study of alkenone hydrogen isotope data from surface lake sediments spanning a very large range of salinities. Although the sample set is limited, we have offered compelling evidence that there are significant differences in the salinity sensitivity of coastal and lacustrine alkenone producers as compared to those found in marine environments. The range of lake water salinities targeted in this work also suggests a high probability of significant differences in growth rates among sites driven by nutrient supply, anion and cation concentrations, temperature, and other factors in addition to salinity. The apparently limited environmental sensitivity of the magnitude of D/H fractionation by inland alkenone producers

may indicate that δD values of these compounds could serve as useful indicators of paleo-lakewater δD values provided that sites are targeted that have not experienced extreme changes in salinity, and therefore serve as a valuable addition to the growing list of tools for constraining paleohydrology.

It also seems clear that differences in the species distributions and hydrogen isotopic sensitivities of different alkenone producers are in need of further study. Continued phylogenetic work to identify the diversity of species present in individual lake environments, as well as ongoing efforts to culture both lacustrine and marine alkenone producers under a range environmental conditions offer great potential for achieving the required level of understanding to permit accurate quantitative paleoclimate reconstructions from alkenone δD measurements. But such efforts should also be combined with additional studies aimed at constraining the biological mechanisms that control alkenone δD values, as well as field surveys since empirical calibrations are ultimately likely to form the foundation of a well-calibrated quantitative proxy. Alkenones are highly unique biomarkers that have already provided a wealth of information about the climate history of the Earth, and every effort should be made to extend the information that can be recovered from their chemistry.

**Acknowledgments**

This material is based upon work supported by the U.S. National Science Foundation under Grants NSF-EAR-0745982, EAR-0823503 and ESH-0639640, and the U.S. National Oceanic and Atmospheric Administration under Grant No. NA08OAR4310685 to J. Sachs. The authors would like to thank Orest Kawka, Josh Gregersen, S. Nemiah Ladd, Alyssa Atwood, Ines Mügler, Julie Richey, and Jeff Bowman for useful discussions, advice and assistance in the lab. We thank Ariel Townsend for her careful assistance in the lab. We thank Jeff Bowman and Chase Stoudt for assistance in the field, Robert Baskin and the USGS in Salt Lake City for assistance accessing and sampling the Great Salt Lake, Saskatchewan Minerals and the Redberry Lake Biosphere Reserve for allowing site access.

**Chapter 4 References**


Benthien, A., Meer, M.T.J.v.d., Schouten, S., Zondervan, I., Bijma, J., 2009. The effect of growth rate and light intensity on the hydrogen isotopic composition of long-chain alkenones produced by *Emiliania huxleyi*. Geophysical Research Abstracts 11.

Bowman, J.S., Sachs, J.P., 2008. Chemical and physical properties of some saline lakes in Alberta and Saskatchewan. Saline Systems 4.

Brassell, S.C., Brereton, R.G., Eglinton, G., Grimalt, J., Liebezeit, G., Marlowe, I.T., Pflaumann, U., Sarnthein, M., 1986. Palaeoclimatic signals recognized by chemometric treatment of molecular stratigraphic data. Organic Geochemistry 10, 649-660.

Chu, G., Sun, Q., Li, S., Zheng, M., Jia, X., Lu, C., Liu, J., Liu, T., 2005. Long-chain alkenone distributions and temperature dependence in lacustrine surface sediments from China. Geochimica et Cosmochimica Acta 69, 4985-5003.

Conte, M.H., Sicre, M.-A., Ruhlemann, C., Weber, J.C., Schulte, S., Schulz-Bull, D., Blanz, T., 2006. Global temperature calibration of the alkenone unsaturation index (Uk'37) in surface waters and comparison with surface sediments. Geochemistry, Geophysics, Geosystems 7.

Conte, M.H., Thompson, A., Eglinton, G., Green, J.C., 1995. Lipid Biomarker Diversity In The Coccolithophorid Emiliania Huxleyi (Prymnesiophyceae) And The Related Species Gephyrocapsa Oceanica. Journal of Phycology 31, 272-282.

Cranwell, P.A., 1985. Long-chain unsaturated ketones in recent lacustrine sediments. Geochimica et Cosmochimica Acta 49, 1545-1551.

D'Andrea, W.J., Liu, Z., Alexandre, M.D.R., Wattley, S., Herbert, T.D., Huang, Y., 2007. An Efficient Method for Isolating Individual Long-Chain Alkenones for Compound-Specific Hydrogen Isotope Analysis. Analytical Chemistry 79, 3430-3435.

D'Andreaa, W.J., Huanga, Y., Fritz, S.C., Anderson, N.J., 2011. Abrupt Holocene climate change as an important factor for human migration in West Greenland. Proceedings of the National Acadamy of Sciences of the United States of America 108, 9765-9769.

Englebrecht, A.C., Sachs, J.P., 2005. Determination of sediment provenance at drift sites using hydrogen isotopes and unsaturation ratios in alkenones. Geochim. Cosmochim. Acta 69, 4253-4265.

Hayes, J.M., 2001. Fractionation of the Isotopes of Carbon and Hydrogen in Biosynthetic Processes, in: Valley, J.W., Cole, D.R. (Eds.), National Meeting of the Geological Society of America. Geological Society of America, Boston, MA, pp. 1-31.

Kasper, S., Meer, M.T.J.v.d., Mets, A., Zahn, R., Damsté, J.S.S., Schouten, S., 2013. Salinity Changes in the Agulhas leakage area recorded by stable hydrogen isotopes of $C_{37}$ Alkenones during Termination 1 and II. Climate of the Past 9, 3209-3238.

Leduc, G., Sachs, J.P., Kawka, O.E., Schneider, R.R., 2013. Holocene changes in eastern equatorial Atlantic salinity as estimated by water isotopologues. Earth and Planetary Science Letters 362, 151-162.

Liu, W., Liu, Z., Wang, H., He, Y., Wang, Z., Xu, L., 2011. Salinity control on long-chain alkenone distributions in lake surface waters and sediments of the northern Qinghai-Tibetan Plateau, China. Geochimica et Cosmochimica Acta 75, 1693-1703.

Marlowe, I.T., Brassell, S.C., Eglinton, G., Greenb, J.C., 1990. Long-chain alkenones and alkyl alkenoates and the fossil coccolith record of marine sediments. Chemical Geology 88, 349-375.

Nelson, D.B., Sachs, J.P., *Chapter 2*. Concurrent Purification of Sterols, Triterpenols and Alkenones from Sediments for Hydrogen Isotope Analysis using High Performance Liquid Chromatography.

Nelson, D.B., Sachs, J.P., *Chapter 3*. The influence of salinity on D/H fractionation in dinosterol and brassicasterol from globally distributed saline and hypersaline lakes

Pahnke, K., Sachs, J.P., Keigwin, L., Timmermann, A., Xie, S.-P., 2007. Eastern tropical Pacific hydrologic changes during the past 27,000 years from D/H ratios in alkenones. Paleoceanography 22.

Pearson, E.J., Juggins, S., Farrimond, P., 2008. Distribution and significance of long-chain alkenones as salinity and temperature indicators in Spanish saline lake sediments. Geochimica et Cosmochimica Acta 72, 4035-4046.

Polissar, P.J., Freeman, K.H., Rowley, D.B., McInerney, F.A., Currie, B.S., 2009. Paleoaltimetry of the Tibetan Plateau from D/H ratios of lipid biomarkers. Earth and Planetary Science Letters 287, 64-76.

Rontani, J.-F., Prahl, F.G., Volkman, J.K., 2006. Re-Examination Of The Double Bond Positions In Alkenones And Derivatives: Biosynthetic Implications. Journal of Phycology 42, 800-813.

Sachse, D., Billault, I., Bowen, G.J., Chikaraishi, Y., Dawson, T.E., Feakins, S.J., Freeman, K.H., Magill, C.R., McInerney, F.A., van der Meer, M.T.J., Polissar, P., Robins, R.J., Sachs, J.P., Schmidt, H.-L., Sessions, A.L., White, J.W.C., West, J.B., Kahmen, A., 2012. Molecular Paleohydrology: Interpreting the Hydrogen-Isotopic Composition of Lipid Biomarkers from Photosynthesizing Organisms. Annual Review of Earth and Planetary Sciences 40, null.

Schouten, S., Ossebaar, J., Schreiber, K., Kienhuis, M.V.M., Langer, G., Benthien, A., Bijma, J., 2006. The effect of temperature, salinity and growth rate on the stable hydrogen isotopic composition of long chain alkenones produced by *Emiliania huxleyi* and *Gephyrocapsa oceanica*. Biogeosciences 3, 113-119.

Schwab, V.F., Sachs, J.P., 2009. The measurement of D/H ratio in alkenones and their isotopic heterogeneity. Organic Geochemistry 40, 111-118.

Schwab, V.F., Sachs, J.P., 2011. Hydrogen isotopes in individual alkenones from the Chesapeake Bay estuary. Geochimica et Cosmochimica Acta 75, 7552-7565.

Sessions, A.L., Burgoyne, T.W., Hayes, J.M., 2001. Determination of the H3 Factor in Hydrogen Isotope Ratio Monitoring Mass Spectrometry. Analytical Chemistry 73, 200-207.

Sessions, A.L., Burgoyne, T.W., Schimmelmann, A., Hayes, J.M., 1999. Fractionation of hydrogen isotopes in lipid biosynthesis. Organic Geochemistry 30, 1193-1200.

Sun, Q., Chu, G., Liu, G., Li, S., Wang, X., 2007. Calibration of alkenone unsaturation index with growth temperature for a lacustrine species, Chrysotila lamellosa (Haptophyceae). Organic Geochemistry 38, 1226-1234.

Theroux, S., D'Andrea, W.J., Toney, J., Amaral-Zettler, L., Huang, Y., 2010. Phylogenetic diversity and evolutionary relatedness of alkenone-producing haptophyte algae in lakes: Implications for continental paleotemperature reconstructions. Earth and Planetary Science Letters 300, 311-320.

Theroux, S., Huang, Y., Amaral-Zettler, L., 2012. Comparative molecular microbial ecology of the spring haptophyte bloom in a Greenland arctic oligosaline lake. Frontiers in Microbiology 3.

Toney, J.L., Huang, Y., Fritz, S.C., Baker, P.A., Grimm, E., Nyren, P., 2010. Climatic and environmental controls on the occurrence and distributions of long chain alkenones in lakes of the interior United States. Geochimica et Cosmochimica Acta 74, 1563-1578.

Toney, J.L., Leavitt, P.R., Huang, Y., 2011. Alkenones are common in prairie lakes of interior Canada. Organic Geochemistry 42, 707-712.

Toney, J.L., Theroux, S., Andersen, R.A., Coleman, A., Amaral-Zettler, L., Huang, Y., 2012. Culturing of the first 37:4 predominant lacustrine haptophyte: Geochemical, biochemical, and genetic implications. Geochimica et Cosmochimica Acta 78, 51-64.

van der Meer, M.T.J., Baas, M., Rijpstra, W.I.C., Marino, G., Rohling, E.J., Damsté, J.S.S., Schouten, S., 2007. Hydrogen isotopic compositions of long-chain alkenones record freshwater flooding of the Eastern Mediterranean at the onset of sapropel deposition. Earth and Planetary Science Letters 262, 594-600.

van der Meer, M.T.J., Benthien, A., Bijma, J., Schouten, S., Sinninghe-Damsté, J.S., 2013. Alkenone distribution impacts the hydrogen isotopic composition of the C37:2 and C37:3 alkan-2-ones in *Emiliania huxleyi*. Geochimica et Cosmochimica Acta 111, 162-166.

Vasiliev, I., Reichart, G.-J., Krijgsman, W., 2013. Impact of the Messinian Salinity Crisis on Black Sea hydrology—Insights from hydrogen isotopes analysis on biomarkers. Earth and Planetary Science Letters 362, 272-282.

Versteegh, G.J.M., Riegman, R., Leeuw, J.W.d., Jansen, J.H.F.F., 2001. Uk'37 values for Isochrysis galbana as a function of culture temperature, light intensity and nutrient concentrations. Organic Geochemistry 32, 785-794.

Volkman, J.K., Eglinton, G., Corner, E.D.S., Sargent, J.R., 1980. Novel unsaturated straight-chain C37-C39 methyl and ethyl ketones in marine sediments and a coccolithophore *Emiliania huxleyi*. Elsevier, New York.

Winter, A., Almogi-Labin, A., Erez, Y., Halicz, E., Luz, B., Reiss, Z., 1983. Salinity Tolerance of Marine Organisms Deduced From Red Sea Quaternary Record. Marine Geology 53, M17-M22.

Wolhowe, M.D., Prahl, F.G., Probert, I., Maldonado, M., 2009. Growth phase dependent hydrogen isotopic fractionation in alkenone-producing haptophytes. Biogeosciences 6, 1681-1694.

Zhang, Z., Sachs, J.P., Marchetti, A., 2009. Hydrogen isotope fractionation in freshwater and marine algae: II. Temperature and nitrogen limited growth rate effects. Organic Geochemistry 40, 428-439.

# Chapter 5:

# Evaluating the environmental signal in fatty acid δD values in saline and hypersaline lake sediments

[*In prep for Organic Geochemistry*]

**Evaluating the environmental signal in fatty acid δD values in saline and hypersaline lake sediments**

Daniel B. Nelson, Julian P. Sachs

**Abstract**

Salinity is known to influence the magnitude of D/H fractionation in the lipids from phytoplankton, cyanobacteria and mangrove trees, but its effect on lipids from submerged and emergent aquatic vegetation is currently unknown. We sought to address this question through analysis of the hydrogen isotopic composition of fatty acids with 22 carbons in lake sediments from a wide diversity of saline and hypersaline lakes in North America spanning a salinity range from 20-248 ppt. In addition to these compounds we also examined short- and long-chain fatty acids, which, in lake sediments, are presumed to derive from algal and terrestrial higher plant sources, respectively. Our results show no sensitivity to salinity for middle-chain length fatty acids, and maximum overall sensitivity to the δD value of lake water as compared to short- and long-chain length fatty acids. Short chain-length fatty acid δD values appear to show a weak sensitivity to salinity. Long-chain fatty acid δD values are most weakly correlated to lake water δD values and are also insensitive to salinity, consistent with the assumption that these compounds are primarily derived from higher plants and reflect soil water δD values and aridity.

**Keywords:** Hydrogen isotope, δD, biomarker, fatty acid, lipid, saline, lake, sediment, GC-IRMS

## Introduction

Compound-specific hydrogen isotope data are increasingly being used as indicators of hydrologic and environmental change (see Sachse et al., 2012 for a review). *n*-Alkanoic acids often make up a significant fraction of the total solvent-extractable lipids in sediments (Volkman et al., 1980), which has resulted in them being the subject of a large body of research, and frequent targets for hydrogen isotope analysis (e.g. Douglas et al., 2012; Hou et al., 2008; Hou et al., 2007; Hou et al., 2006; Huang et al., 2002, 2004; Smittenberg et al., 2011; Tierney et al., 2010; Tierney et al., 2008). Biologic sources for *n*-alkanoic acids, or "fatty acids" are numerous and varied, but general patterns are observed, and these have been used to argue that particular chain lengths are reflective of a particular classes of organisms and therefore that the hydrogen isotope values of different acids reflect different sources of environmental water. Long-chain ($n$C$_{24}$-$n$C$_{32}$) *n*-alkanoic acids are produced in high abundance in the epicuticular leaf waxes of terrestrial plants, and probably represent the main source of these compounds in most lacustrine sediments (Eglinton and Hamilton, 1967). However, these compounds have also been found in microalgae, and in at least one example 30-80% of $n$C$_{24}$-$n$C$_{28}$ fatty acids (FA) in sediments were attributed to diatoms (Volkman et al., 1980). Middle-chain length *n*-alkanoic acids, typically $n$C$_{22}$FA, have been attributed to submerged and emergent aquatic vegetation in lake environments (Ficken et al., 2000), and in a case study at Blood Pond, MA, up to 97% of the $n$C$_{22}$FA contribution to sediments was attributed to such aquatic vegetation sources (Gao et al., 2011), although these compounds have also been shown to occur in terrestrial plants and grasses (Chikaraishi and Naraoka, 2007; Wiesenberg and Schwark, 2006; Wiesenberg et al., 2004). Short-chain fatty acids are generally produced in high abundance by algae and bacteria, but $n$C$_{16}$FA is ubiquitous in algal, aquatic and terrestrial plants due to its role as a common

biosynthetic precursor to acetogenic compounds (Chikaraishi and Naraoka, 2007; Meyers and Ishiwatari, 1993). However, $n$C$_{16}$FA has also been shown to break down quickly in the terrestrial environment, and it has therefore been argued that the dominant source in lacustrine sediments is within-lake production by algae (Cranwell et al., 1987; Huang et al., 2002, 2004).

The hydrogen isotopic composition of short-, middle- and long-chain fatty acids have all been shown to track the hydrogen isotopic composition of the environmental water source for each of the respective compound classes, which typically means either lake water, sea water, soil water, or precipitation (Hou et al., 2008; Hou et al., 2006; Huang et al., 2002, 2004). In addition to this signal, long-chain length fatty acids and *n*-alkane δD values from leaf waxes have been shown to be influenced by humidity, evapotranspiration rates, salinity, timing of leaf wax production, and changes in vegetation assemblage (Douglas et al., 2012; Hou et al., 2008; Kahmen et al., 2013a; Kahmen et al., 2013b; Ladd and Sachs, 2012; Liu and Yang, 2008; McInerney et al., 2011; Nelson et al., 2013; Polissar and Freeman, 2010; Sachse et al., 2009; Smith and Freeman, 2006; Tipple et al., 2013; Wang et al., 2013; Yang et al., 2011; Yang et al., 2009; Zhou et al., 2011). The δD values from algal lipids, including short-chain fatty acids have been shown to reflect salinity, nutrient stress, growth phase, and temperature (Nelson and Sachs, *Chapter 3*, *Chapter 4;* Sachs and Schwab, 2011; Sachse and Sachs, 2008; Schouten et al., 2006; Smittenberg et al., 2011; van der Meer et al., 2013; Wolhowe et al., 2009; Zhang and Sachs, 2007; Zhang et al., 2009). However, efforts to evaluate the extent to which the δD values of middle-chain length fatty acids or alkanes are sensitive to secondary environmental indicators have been more limited (Nichols et al., 2010). Since salinity has been shown to influence the magnitude of D/H fractionation in higher plant lipids produced by mangrove trees (Ladd and

Sachs, 2012), evaluating the influence of salinity on D/H fractionation in middle-chain length fatty acids, which should be produced primarily by submerged aquatic vegetation is therefore an important question that has yet to be addressed.

In order to assess the influence of salinity on δD values in fatty acids in lake environments we sampled surface sediment and lake water from a variety of sites in North America spanning a range of salinities from 20 - 248 ppt. Although long-chain fatty acids are presumed to derive primarily from terrestrial sources, and therefore should not be influenced by the salinity of nearby lakes, we also measured these compounds to evaluate how their hydrogen isotope values differed from those produced in high abundance by aquatic organisms. All sample sites described here are from North America, and can be categorized into three sub regions, which include a grouping of lakes in the Canadian prairie/grasslands of Saskatchewan and Alberta (CAN), the Great Salt Lake in the Utah desert (GSL), and a series of evaporative ponds for commercial salt production operated by Cargill Incorporated at the southern end of the San Francisco Bay (CAR). Many of the sites described here were also used in our investigations of dinosterol, brassicasterol and alkenones (Nelson and Sachs, *Chapter 3*, *Chapter 4*).

Hydrogen isotope ratios are measured and reported in terms of delta notation, where $\delta D = [(D/H_{sample}/D/H_{standard}) - 1] \times 1000‰$, and D, and H stand for deuterium, and hydrogen, respectively, and the reference standard is Vienna Standard Mean Ocean Water (VSMOW, δD = 0 ‰). The magnitude of the isotopic change imparted over any reaction or series of reactions from substrate to product is defined in terms of a fractionation factor, α. For lipids synthesized by photoautotrophs, the source of all hydrogen is the environmental water, and the combined sequence of biochemical reactions including initial uptake of environmental water into the cell

and photolysis to later elongation and desaturation steps that transfer hydrogen from water to an end product lipid can be represented as $\alpha = (D/H_{lipid})/(D/H_{water}) = (\delta D_{lipid} + 1000)/(\delta D_{water} + 1000)$. The further the $\alpha$ value is from unity, the greater the magnitude of D/H fractionation for a given reaction. Lipids are almost always depleted relative to their source water ($\alpha < 1$), so decreasing fractionation is described by increasing $\alpha$ values.

## Methods

### *Sediment and water sampling*

Sediment samples from the CAN and GSL sites were collected by Van Veen dredge or hand sampler from shallow water, and many of these sites are described in Bowman and Sachs (2008). Van Veen dredge sampling typically resulted in recovery of the upper ~5 - 20 cm of surface sediment, while hand sampler penetration was less than this. Sediment samples were collected from the Cargill (CAR) salt ponds using a hand sampler in the summer of 2008. Lake water conductivity was measured at all sites at the time of sample recovery using a hand held conductivity sensor, and salinities were calculated based on the relationship between seawater conductivity and seawater. Water samples were collected from the lake surface for $\delta D_{water}$ analysis at each site in glass screw-cap vials that were sealed with electrical tape at the time of recovery.

*δD values of water*

Two separate measurement techniques were applied to the lake water samples used in this study depending on the time of sample collection and processing. Some were determined at the University of Washington using a Thermal Conversion Elemental Analyzer (TCEA) interfaced with a Delta V Plus Isotope Ratio Mass Spectrometer (IRMS) (Thermo Scientific, Waltham, MA), and the $H_3^+$ factor was evaluated at the beginning of each sample sequence (Sessions et al., 2001). Each sample was analyzed over six consecutive injections with the first three omitted from reported values due to memory effects from the previous sample. δD values were determined in the Isodat 2.0 software platform relative to monitoring gas hydrogen, and then post-processed using measured values of two standards (0 ‰, and -189.5 ‰) analyzed in the same sequence to reference the data to the VSMOW. Additional water samples were analyzed at the University of Hawaii in the laboratory of Dr. Brian Popp by Cavity Ring Down Spectroscopy (CRDS) (Picarro, Inc., Santa Clara, CA), and are also reported in δD notation. In order to assess consistency between the two methods, nine samples were analyzed using both techniques, and the δD values from each were generally found to differ by less than 2 ‰. Average analytical precision for all water samples was less than 1 ‰, but individual standard deviations of replicate analyses were calculated for each sample. In addition to measured lake water δD values, we also used the Online Isotopes in Precipitation Calculator (OIPC) (Bowen, 2013; Bowen and Revenaugh, 2003; Bowen et al., 2005) to determine model predicted annual average and monthly average δD values of precipitation.

*Lipid extraction, column chromatography and methylation*

Sediment samples were freeze dried and extracted using a 9:1 mixture of dichloromethane (DCM) and methanol (MeOH) with an accelerated solvent extractor (ASE) (Dionex 200) operated at 100 °C and 1500 psi with three five-minute static phases. Excess solvent was evaporated under $N_2$ from the total lipid extract (TLE) on a Turbo-vap system (Caliper, Hopkinton, MA, USA). TLEs were then separated into neutral and acid fractions using 0.5 g of aminopropyl (Supelco) in hand packed glass solid phase extraction (SPE) – type columns. Neutral compounds were eluted with 8 mL of DCM/isopropyl alcohol (IPA) (3:1), acids were eluted with 6 mL of 4% acetic acid in diethyl ether, and a polar fraction was eluted with 6 mL MeOH. Acid fractions as well as a phthalic acid standard of known δD value (standard from Arndt Schimmelmann at Indiana University, Bloomington, IN, USA) were methylated to fatty acid methyl esters (FAMEs) in screw cap glass vials using 2 mL of 10:1 anhydrous methanol and acetyl chloride and 1 mL of dry hexane. After adding the reagents, the headspace was flushed with nitrogen and the vials were sealed and vortexed to ensure mixing and dissolution of the lipids. Vials were then placed in a drying oven overnight at 60 °C to convert free fatty acids to FAMEs. After methylating, the vials were removed from the oven and allowed to cool to room temperature. 2 mL of Nanopure water (Barnstead nanopure infinity water system) was then added to increase the polarity gradient with the 1 mL hexane, and the hexane was then transferred to a new vial with Pasteur pipette. Three additional 2 mL hexane extractions were performed with the methanol, followed by a 3 mL rinse of the hexane with Nanopure water to dilute any residual acidity in the small amount of water dissolved in the hexane. The final FAME-containing hexane solution was then dried over sodium sulfate.

*Gas chromatography – mass spectrometry*

Methylated acid fractions were analyzed by gas chromatography – mass spectrometry (GC-MS) to assess sample purity and to confirm the effectiveness of methylation. Samples were injected in splitless mode at 300°C using helium carrier gas at 1.5 mL/min on an Agilent 6890N GC with 5975 inert mass selective detector equipped with a DB-5ms capillary column (60 m X 0.32 mm X 0.32 μm). The GC oven was held at 110 °C for 4 minutes after sample injection, then increased to 150 °C at 15 °C/min, then increased to 320 °C at 6 °C/min and held for 28 minutes. In cases where coeluting compounds were detected with targeted FAMEs these compounds were not used for hydrogen isotope analysis.

*Gas chromatography – flame ionization detector*

Methylated acids were quantified by gas chromatography – flame ionization detector (GC-FID) by comparing the relative peak areas of analyte targets with that of a 5α-cholestane standard of known concentration that was added after saponification and before GC analysis. Injections were performed on an Agilent 6890N GC using a flame ionization detector (GC-FID). Samples were injected in splitless mode using a programmable temperature vaporization inlet with helium carrier gas at 2.0 mL/min onto a DB-5ms capillary column (60 m X 0.32 mm X 0.32 μm). The GC oven was held at 110 °C for 4 minutes after sample injection, then increased to 150 °C at 15 °C/min, then increased to 320 °C at 6 °C/min and held for 28 minutes.

*Gas chromatography – isotope ratio mass spectrometry*

FAME δD values were measured by gas chromatography-isotope ratio mass spectrometry (GC-IRMS) using a Thermo Delta V Plus isotope ratio mass spectrometer and Thermo Trace GC Ultra interfaced to a gas chromatography combustion interface III. Samples were injected in splitless mode at 330 °C using helium carrier gas at 1.5 mL/min. The GC was equipped with a DB-5ms capillary column (60 m X 0.32 mm X 0.32 μm). The GC oven was increased from an initial temperature of 80 °C to 150 °C at 20 °C/min, then held for 5 minutes, then increased to 170 °C at 20 °C/min, then increased to 320 °C at 3 °C/min and held for 25 minutes. GC column effluent was directed through the pyrolysis reactor and combustion interface to convert all hydrogen to $H_2$ prior to introduction to the mass spectrometer. The $H_3^+$ factor (Sessions et al., 2001) was measured prior to every sample sequence, and was stable and less than 5.

An internal laboratory δD standard was analyzed periodically within each sample sequence. The standard consisted of a range of *n*-alkanes ($n$C$_{14}$ through $n$C$_{37}$, but not $n$C$_{27}$, $n$C$_{31}$, $n$C$_{33}$ or $n$C$_{35}$) with δD values that were individually determined by TC-EA-IRMS relative to purchased *n*-alkane δD standards (standards from Arndt Schimmelmann at Indiana University, Bloomington, IN, USA). Initial isotopic evaluations of all peaks were performed within the Isodat 2.0 software relative to a calibrated reference gas. Secondary corrections were performed based on the regression of Isodat-reported δD values of *n*-alkane standards and their accepted values in order to maintain like treatments of samples and standards, as well as to correct for potential scale compression or stretching as a result of the one-point referencing to VSMOW performed by the Isodat software. Samples were analyzed at least three times, and the average precision calculated as the standard deviation of multiple analyses was less than 4 ‰. Individual

sample uncertainties were calculated as the standard deviation of replicate measurements. Peak areas less than 15 V·s were below the cutoff identified on this GC-IRMS to avoid size dependent δD effects, and were not considered (Polissar et al., 2009).

The δD value of the methylating agent was determined through a mass balance calculation based on the measured and known δD values of the phthalic acid standard and the total number of non-exchangeable hydrogen atoms in the free acid and its FAME derivative. A similar mass balance correction was then performed using the calculated δD value of the methylating agent and the measured δD value of each *n*-alkanoic acid methyl ester to calculate the δD value of the non-exchangeable hydrogen in the original free acid.

## Results and Discussion

### *Salinity*

Salinity at our sample sites ranged from 20 – 248 ppt (Table 1). The common oceanographic method of measuring conductivity and applying a calibrated relationship to determine salinity is in some cases inappropriate in continental interior lakes where the relative abundances of the major ions differ significantly from seawater. We therefore use the absolute salinity values for the CAN sites when possible (Bowman and Sachs, 2008). These values are considered to be more accurate indicators of salinity in lakes where the relative ion concentration differs significantly from seawater (Anati, 1999). Although these values may differ slightly from total dissolved solids measurements determined in g/L or ppt determined by alternate methods owing to the influence of salinity and temperature on water density, in most cases in our sample

set g/L and ppt values are virtually identical to within the uncertainty required for our purposes of ~ ± 5 (Bowman and Sachs, 2008). Field measurements of water salinities at the CAR sites ranged from 32.2 to 201.5 PSU.

**Table 1:** Lake water δD values and OIPC estimated precipitation δD values.

| | | | | OIPC Estimated δD | | | | | | | | | | | | | Measured Water | |
|---|---|---|---|---|---|---|---|---|---|---|---|---|---|---|---|---|---|---|
| Site | Salinity | Salinity error + | Salinity error - | Jan | Feb | Mar | Apr | May | Jun | Jul | Aug | Sept | Oct | Nov | Dec | Annual | δD | σ |
| Manito Lake | 24 | 10 | 10 | -197 | -186 | -163 | -135 | -101 | -99 | -94 | -102 | -108 | -123 | -160 | -189 | -121 | -78.5 | 0.6 |
| Redberry Lake | 20 | 15 | 15 | -199 | -184 | -161 | -129 | -95 | -96 | -92 | -100 | -106 | -123 | -160 | -188 | -119 | -81.1 | 1.2 |
| Big Quill Lake | 43 | 20 | 20 | -199 | -181 | -158 | -122 | -89 | -93 | -88 | -95 | -103 | -121 | -157 | -185 | -115 | -99.7 | 0.2 |
| Freefight Lake | 94.5 | | | -189 | -177 | -152 | -121 | -90 | -91 | -85 | -93 | -100 | -114 | -150 | -178 | -113 | -78.9 | 0.8 |
| Ingebright Lake | 160.0 | | | -188 | -177 | -152 | -121 | -90 | -91 | -85 | -93 | -100 | -114 | -150 | -178 | -113 | -81.3 | 0.7 |
| Chappice Lake | 49 | 57 | 15 | -184 | -175 | -149 | -121 | -91 | -90 | -84 | -93 | -99 | -112 | -148 | -175 | -113 | -75.2 | 0.6 |
| West of West Chaplin Lake NE Division | 140.0 | | | -194 | -179 | -155 | -119 | -87 | -90 | -85 | -92 | -100 | -117 | -153 | -181 | -112 | -49.5 | 0.6 |
| Hughes Bay | 25.6 | | | -194 | -179 | -155 | -119 | -87 | -90 | -85 | -92 | -100 | -117 | -153 | -181 | -112 | -52.6 | 0.3 |
| West Chaplin West Division 1 | 183.7 | | | -194 | -179 | -155 | -119 | -87 | -90 | -85 | -92 | -100 | -117 | -153 | -181 | -112 | -45.0 | 0.7 |
| West Chaplin Center Division | 154.8 | | | -194 | -179 | -155 | -119 | -87 | -90 | -85 | -92 | -100 | -117 | -153 | -181 | -112 | -51.0 | 1.0 |
| West Chaplin Lake SE Division | 125.7 | | | -194 | -179 | -155 | -119 | -87 | -90 | -85 | -92 | -100 | -117 | -153 | -181 | -112 | -50.7 | 1.3 |
| East of West Chaplin Lake NE Division | 54.1 | | | -194 | -179 | -155 | -119 | -87 | -90 | -85 | -92 | -100 | -117 | -153 | -181 | -112 | -57.0 | 0.4 |
| Great Salt Lake (North) | 248.0 | 11 | 49 | -132 | -123 | -112 | -95 | -89 | -78 | -75 | -77 | -85 | -88 | -114 | -122 | -98 | -50.1 | 1.9 |
| Great Salt Lake (South) | 133.0 | 69 | 41 | -132 | -123 | -112 | -95 | -89 | -78 | -75 | -77 | -85 | -88 | -114 | -122 | -98 | -60.7 | 1.2 |
| Cargill Salt Pond 1 | 58.1 | | | -72 | -77 | -73 | -67 | -71 | -55 | -52 | -63 | -76 | -55 | -75 | -69 | -71 | -7.3 | 0.4 |
| Cargill Salt Pond 2 | 32.2 | | | -72 | -77 | -73 | -67 | -71 | -55 | -52 | -63 | -76 | -55 | -75 | -69 | -71 | -3.0 | 0.4 |
| Cargill Salt Pond 3 | 39.6 | | | -72 | -77 | -73 | -67 | -71 | -55 | -52 | -63 | -76 | -55 | -75 | -69 | -71 | 6.3 | 0.4 |
| Cargill Salt Pond 7 | 117.2 | | | -72 | -77 | -73 | -67 | -71 | -55 | -52 | -63 | -76 | -55 | -75 | -69 | -71 | 22.4 | 0.7 |
| Cargill Salt Pond 9 | 197.4 | | | -72 | -77 | -73 | -67 | -71 | -55 | -52 | -63 | -76 | -55 | -75 | -69 | -71 | 10.3 | 1.3 |
| Cargill Salt Pond 12 | 77.7 | | | -72 | -77 | -73 | -67 | -71 | -55 | -52 | -63 | -76 | -55 | -75 | -69 | -71 | 7.2 | 0.4 |
| Cargill Salt Pond 13 | 201.5 | | | -72 | -77 | -73 | -67 | -71 | -55 | -52 | -63 | -76 | -55 | -75 | -69 | -71 | 5.1 | 2.6 |
| Cargill Salt Pond 14 | 158.9 | | | -72 | -77 | -73 | -67 | -71 | -55 | -52 | -63 | -76 | -55 | -75 | -69 | -71 | 8.9 | 0.4 |

The sediments from the CAR sites were collected with a hand sampler and were effective in limiting material to the upper few centimeters of sediment, so we make no effort to account for historical changes in sedimentation. Recovery of surface samples by Van Veen dredge at the CAN and GSL sites results in the collection of material from up to 20 cm deep in the sediments. Lake water salinity was measured during the time of sample collection at the CAN (Bowman and Sachs, 2008) and GSL sites, but these values are unlikely to be representative of the average salinity over the many decades required for the recovered sediment to accumulate in each basin. In order to compensate for this issue, we used historical salinity and sedimentation rates to calculate time-weighted average salinities where possible (Table 1). This results in significant uncertainty, but these estimates are still likely to be more representative of the salinity that corresponds with the sedimentary lipid chemistry than are the snapshot field measurements. This approach is outlined in detail for most sites in our study of phytosterols dinosterol and brassicasterol purified from this sample set (Nelson and Sachs, *Chapter 3*).

Two lakes that are included in this study, but were not described in our previous work include Freefight and Ingebright lakes. Freefight Lake absolute salinity was 94.5 ppt at the time of sample collection (Bowman and Sachs, 2008). This system has been shown to have extreme sedimentation rates on the order of 2 cm/yr (Last and Ginn, 2005), so given the rapid nature of deposition and the lack of precise historical data on salinity, we use the measured salinity in the current study. Ingebright Lake is usually hypersaline, with reported total dissolved solid values ranging from 100 to 300 g/L (Shang, 2000). The absolute salinity that was determined from a water sample recovered at the time of sediment collection was 160.0 ppt (Bowman and Sachs, 2008), so we use this value in the present study since it is consistent with the published range. The Chaplain Lake divisions are the other sites from the CAN sample set from which we present

new lipid δD data. However, we are unaware of detailed estimates of historic salinity changes at these sites, and therefore use the measured values from Bowman and Sachs (2008). In addition to the sample from the southern Great Salt Lake, which we reported on previously (Nelson and Sachs, sterols), in the current study we also include a sample from the northern Great Salt Lake. For this site we take a similar approach to calculate historic average salinity based on available records (Arnow and stephens, 1990; USGS, 2013), and use a value of 248 (+11, -49) ppt. Despite the large uncertainties in many of our salinity estimates, by targeting a very large range of salinities (20 – 248 ppt), our sample set still represents a large and detectable salinity gradient over which to assess the influence of salinity on sedimentary lipid hydrogen isotope geochemistry.

*δD of environmental water*

Measured lake water δD values across the sample set ranged from +22 ‰ to -100 ‰ while OIPC predicted annual values range from -71 ‰ to -121 ‰ (Figure 1a, Table 1). The discrepancy between the predicted precipitation and measured lake water δD values likely arises from seasonal biasing of the measured lake water δD values as well as evaporative enrichment of lake water. The seasonal distribution of OIPC δD values varies between the three sub regions in our sample set (CAN, GSL, CAR) and shows that while the Canadian sites experience an annual range of precipitation δD values spanning approximately 107 ‰, GSL precipitation spans only 62 ‰, and monthly CAR precipitation varies by only 25 ‰ (Figure 1b). Although lake water δD is correlated with annual, as well as individual monthly OIPC δD values across our complete

sample set, the correlations are largely driven by the fact that each sub region is different enough from the others to overcome basin-specific hydrologic factors like evaporative enrichment.

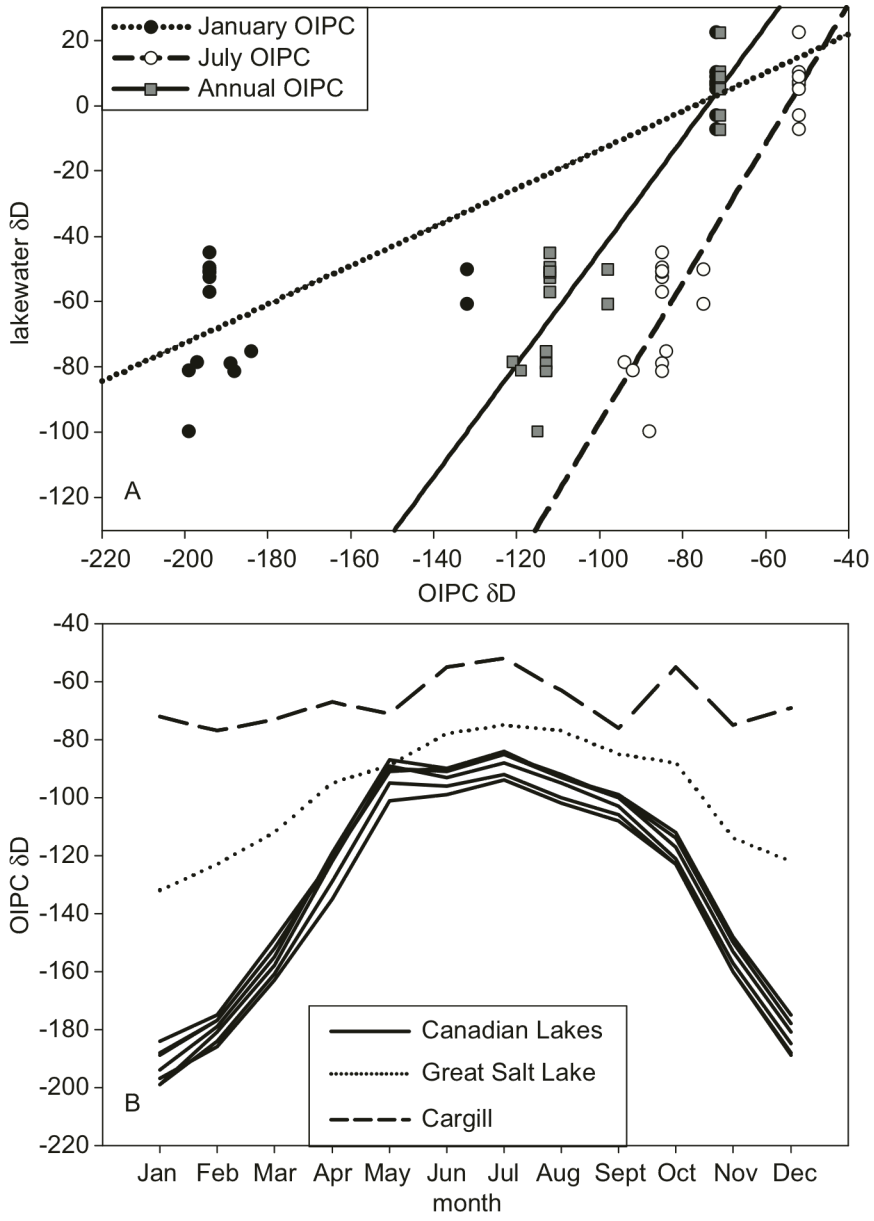


**Figure 1:** A) Lake water δD values vs annual, January and July OIPC precipitation δD value estimates. B) Monthly OPIC precipitation δD value estimates for each site in our study area. All CAR sites and both GSL sites have identical OIPC values.

Within each sub region the correlations between OIPC and lake water δD values are difficult to

compare since the range of OIPC precipitation δD values is small, but it is likely that precipitation and lake water δD values diverge due to lake-specific evaporation and/or other processes that cause lake water δD values to evolve from initial precipitation and groundwater input values.

*Fatty acid and water δD values*

We limit our discussion of fatty acid δD values to $n$C$_{16}$FA, $n$C$_{22}$FA, and $n$C$_{28}$FA as representative compounds, although $n$C$_{24}$FA and $n$C$_{26}$FA δD values are presented (Table 2). At the scale of our entire sample set, the δD values of $n$C$_{16}$FA, $n$C$_{22}$FA, and $n$C$_{28}$FA are all correlated with the δD values of both lake water and annual OIPC precipitation ($R^2 > 0.6$; $P < 0.0001$) (Figure 2). The seasonal timing of maximum fatty acid production is likely to vary as a function of chain length and sample site owing to the wide range of possible source organisms. Without site-specific assessments of these sources, we cannot determine the appropriate seasonal weighting to employ for each lake and therefore choose to use annual OIPC precipitation values to compare to our lipid δD measurements as opposed to monthly or seasonal values. Given that each fatty acid is presumed to derive from a different source in the environment it would be expected that each reflect a different water δD value. However, $n$C$_{16}$FA, $n$C$_{22}$FA, and $n$C$_{28}$FA δD values are all similarly correlated with lake water and OIPC precipitation δD values. This is likely explained by the large distances between the sites since the range in source water precipitation δD values between regions is too great for the isotopic signal to be affected by basin scale by processes that cause lake water, soil water and precipitation δD values to diverge

from one another (e.g. evaporation). Within each subset, correlations between lipid and lake water δD values generally deteriorate as a function of increasing chain length (Figures 2a,c,e), which supports the idea that short and middle-chain length *n*-alkanoic acids are produced within the lakes while long-chain acids are produced on land, and are therefore drawing water from alternate sources. Despite these issues, at regional spatial scales the correlations between the lipid and water δD values are generally good, and the slope and intercept of the regression equations are consistent with previous transect studies of fatty acids in lake sediments in North America (Hou et al., 2006; Huang et al., 2004).

Regional scale correlation patterns between lipid and annual OIPC δD values are more complex than for lake water δD values (Figures 2b,d,f). Within the Canadian and Cargill pond sub regions, the sites are in such close geographic proximity to one another that the OIPC δD values are either very similar or identical (Figure 1b). Even if the OIPC model result is missing small-scale spatial variability and there are real differences in the δD of precipitation at each site, these differences are likely to be minor. For the example of the Cargill sites, this requires that factors other than changes in precipitation δD values be invoked to explain the 62 ‰, 54 ‰, and 52 ‰ range of δD values for $n$C$_{16}$FA, $n$C$_{22}$FA, and $n$C$_{28}$FA, respectively. Possible explanations for $n$C$_{16}$FA and $n$C$_{22}$FA, which should reflect lake water and/or salinity are more forthcoming than are those to explain the variability in the $n$C$_{28}$FA, since there is no obvious reason why the δD value of accumulating terrestrial plant material from the surrounding vegetation should vary so much between adjacent ponds other than to call on complex and coincidental regional vegetation patterns or the possibility that some $n$C$_{28}$FA is being produced by aquatic organisms. Although it is possible that some fraction of the variability in fatty acid δD values might be

attributable to variable precipitation δD values within the Canadian lakes sub region, rigorous evaluation would probably require real measurements of precipitation δD values.

**Table 2:** $n$C$_{16}$FA, $n$C$_{22}$FA, and $n$C$_{28}$FA δD values.

| Site | δD-C16FA | σ | n | δD-C22FA | σ | n | δD-C24FA | σ | n | δD-C26FA | σ | n | δD-C28FA | σ | n |
|---|---|---|---|---|---|---|---|---|---|---|---|---|---|---|---|
| Manito Lake | -227 | 1 | 2 | -226 | 1 | 3 | -228 | 1 | 3 | -239 | 1 | 3 | -235 | 1 | 3 |
| Redberry Lake | -229 | 4 | 2 | -215 | 5 | 2 | -221 | 0 | 2 | -196 | 1 | 2 | -190 | 1 | 2 |
| Big Quill Lake | -230 | 1 | 3 | -195 | 2 | 3 | -175 | 4 | 3 | -194 | 3 | 3 | -201 | 1 | 3 |
| Freefight Lake | -199 | 1 | 3 | -186 | 1 | 3 | -189 | 2 | 3 | -213 | 2 | 3 | -228 | 2 | 3 |
| Ingebright Lake | -211 | 1 | 3 | -196 | 2 | 3 | -174 | 2 | 3 | -215 | 1 | 3 | -219 | 1 | 3 |
| Chappice Lake | -211 | 2 | 3 | -211 | 3 | 3 | -212 | 1 | 3 | -237 | 1 | 3 | -239 | 2 | 3 |
| West of West Chaplin Lake NE Division | -155 | 2 | 3 | -181 | 0 | 3 | -157 | 1 | 3 | -206 | 2 | 3 | -206 | 1 | 3 |
| Hughes Bay | -218 | 3 | 3 | -191 | 3 | 3 | -191 | 2 | 3 | -214 | 1 | 3 | -216 | 3 | 3 |
| West Chaplin West Division 1 | -169 | 3 | 3 | -168 | 1 | 3 | -123 | 5 | 3 | -199 | 7 | 3 | -198 | 4 | 3 |
| West Chaplin Center Division | -185 | | | -172 | 1 | 2 | -128 | 4 | 2 | -196 | 4 | 2 | -194 | 5 | 3 |
| West Chaplin Lake SE Division | -177 | 2 | 3 | -182 | 4 | 3 | -145 | 3 | 3 | -205 | 2 | 3 | -203 | 0 | 3 |
| East of West Chaplin Lake NE Division | -198 | 14 | | -188 | 7 | 3 | -184 | 5 | 3 | -235 | 4 | 3 | -216 | 4 | 3 |
| Great Salt Lake (North) | | | | -153 | 1 | 2 | -160 | 0 | 2 | -167 | 0 | 2 | -175 | 1 | 2 |
| Great Salt Lake (South) | -170 | 3 | 3 | -163 | 2 | 3 | -154 | 2 | 3 | -169 | 1 | 3 | -168 | 1 | 3 |
| Cargill Salt Pond 1 | -175 | 1 | 3 | -135 | 4 | 3 | -143 | 4 | 3 | -165 | 3 | 3 | -171 | 3 | 3 |
| Cargill Salt Pond 2 | | | | -136 | 2 | 3 | -135 | 3 | 3 | -151 | 5 | 3 | -160 | 5 | 3 |
| Cargill Salt Pond 3 | -134 | 1 | 3 | -107 | 4 | 3 | -111 | 2 | 3 | -111 | 4 | 3 | -145 | 4 | 3 |
| Cargill Salt Pond 7 | -122 | 1 | 2 | -110 | 0 | 2 | -83 | 2 | 2 | -118 | 1 | 2 | -141 | 5 | 2 |
| Cargill Salt Pond 9 | -121 | 10 | 3 | -147 | 6 | 3 | -155 | 3 | 3 | -156 | 0 | 3 | -155 | 4 | 3 |
| Cargill Salt Pond 12 | -155 | 5 | 3 | -97 | 6 | 3 | -92 | 2 | 3 | -119 | 3 | 3 | -149 | 3 | 3 |
| Cargill Salt Pond 13 | -183 | 2 | 2 | -108 | 0 | 2 | -88 | 6 | 2 | -134 | | 1 | -119 | | 1 |
| Cargill Salt Pond 14 | -125 | 6 | 3 | -93 | 16 | 3 | -90 | 4 | 3 | -125 | 3 | 3 | -133 | 7 | 3 |

Despite the fact that $n$C$_{16}$FA is produced in high abundance by virtually all aquatic and terrestrial autotrophs, δD values of $n$C$_{16}$FA (δD$_{16}$) show the strongest correlations with lake water δD values within individual sub regions (Figure 2a), but lake water δD$_{22}$ value correlations are strongest at the scale of the entire sample set (Figure 2c). This might suggest that D/H fractionation in $n$C$_{16}$FA is also influenced by salinity, which shows a weak relationship with lake water δD values within the Cargill and Canadian lakes sub regions, but not between them (Figure 3). Regardless of the mechanism, the strength of the regional correlations with lake water δD values supports the idea that the majority of the $n$C$_{16}$FA in lakes is derived from algal production

within the lake (Cranwell et al., 1987; Huang et al., 2002, 2004), at least within our sample set. That $\delta D_{22}$ values are less correlated with lake water δD values within sub regions than are $C_{16}$FA δD values, but at the same time more correlated with lake water at the scale of the entire sample set, suggests that $\delta D_{22}$ values are more directly indicative of lake water δD values without additional variability due to systematic changes in the magnitude of D/H fractionation that are associated with lake water δD value – salinity relationships at the sub region scale.

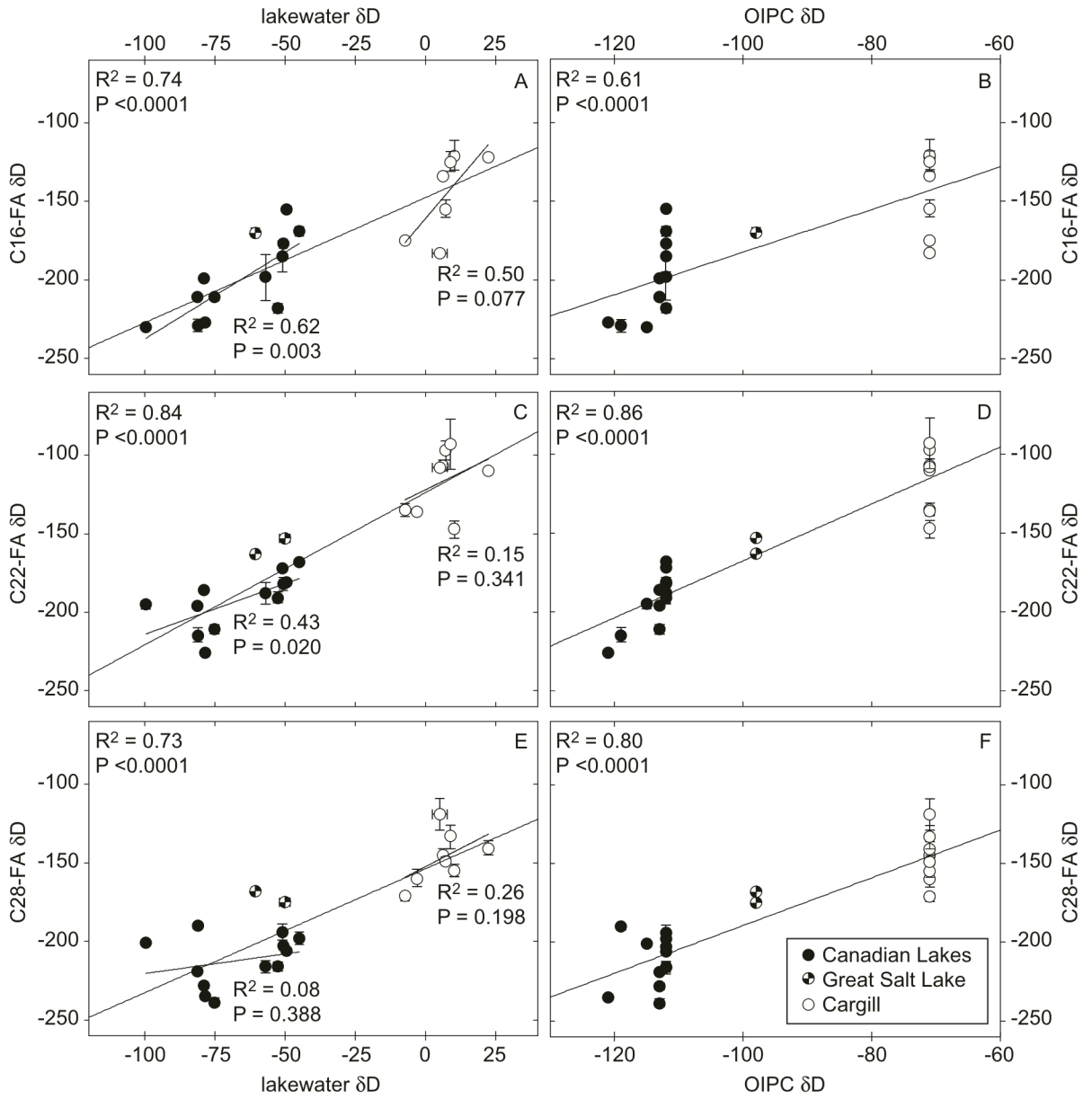


**Figure 2:** Comparison of $n$C$_{16}$FA, $n$C$_{22}$FA, and $n$C$_{28}$FA δD values with lake water δD and annual average OIPC precipitation δD values. Regression statistics in top-left corner of each graph are for the global fit, while statistics for the CAN and CAR sub region regressions are given next to each of the associated lines.

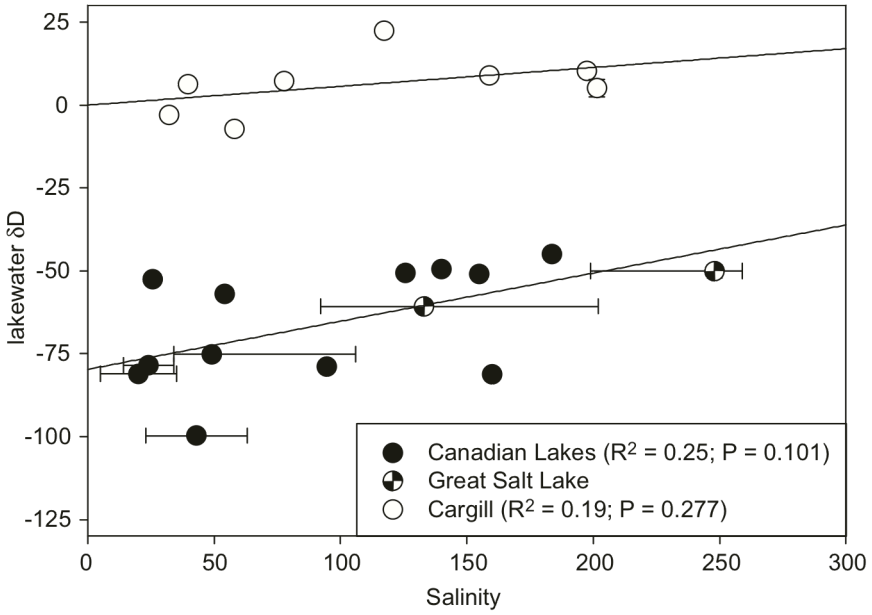


**Figure 3:** Lake water δD values vs Salinity. Regression lines plotted for CAN and CAR sub regions, but not GSL since only two samples were available.

*Influences on D/H fractionation*

In order to evaluate the influence of environmental changes on the magnitude of D/H fractionation, we calculated α values for $n$C$_{16}$FA, $n$C$_{22}$FA, and $n$C$_{28}$FA using both lake water OIPC precipitation δD values (Table 3). Comparing $\alpha_{lipid\text{-}lake}$ values for each compound with the salinity at each of the lake sites, we observe no relationship for $n$C$_{22}$FA or $n$C$_{28}$FA, and a weak relationship for $n$C$_{16}$FA if one high salinity outlier is omitted (Figure 4a). Weak correlations are observed between $\alpha_{lipid\text{-}OIPC}$ values and salinity (Figure 4b), but are likely driven by the fact that OIPC and lake water δD values are themselves correlated.

**Table 3:** $n$C$_{16}$FA, $n$C$_{22}$FA, and $n$C$_{28}$FA α values calculated relative to lake water δD values ($\alpha_{lipid\text{-}lake}$), as well as OIPC precipitation δD values ($\alpha_{lipid\text{-}OIPC}$).

| Site | α - C16-OIPC | σ | α - C16-lake | σ | α - C22-OIPC | σ | α - C22-lake | σ | α - C28-OIPC | σ | α - C28-lake | σ |
|---|---|---|---|---|---|---|---|---|---|---|---|---|
| Manito Lake | 0.880 | 0.002 | 0.839 | 0.001 | 0.880 | 0.003 | 0.840 | 0.002 | 0.870 | 0.002 | 0.830 | 0.001 |
| Redberry Lake | 0.875 | 0.005 | 0.839 | 0.004 | 0.892 | 0.006 | 0.855 | 0.005 | 0.919 | 0.003 | 0.881 | 0.002 |
| Big Quill Lake | 0.870 | 0.002 | 0.855 | 0.001 | 0.909 | 0.003 | 0.894 | 0.003 | 0.903 | 0.002 | 0.888 | 0.001 |
| Freefight Lake | 0.903 | 0.002 | 0.869 | 0.001 | 0.917 | 0.002 | 0.883 | 0.001 | 0.870 | 0.003 | 0.838 | 0.002 |
| Ingebright Lake | 0.890 | 0.003 | 0.859 | 0.002 | 0.906 | 0.003 | 0.875 | 0.002 | 0.880 | 0.003 | 0.850 | 0.002 |
| Chappice Lake | 0.889 | 0.003 | 0.853 | 0.002 | 0.889 | 0.004 | 0.853 | 0.004 | 0.858 | 0.003 | 0.823 | 0.003 |
| West of West Chaplin Lake NE Division | 0.951 | 0.003 | 0.889 | 0.002 | 0.922 | 0.002 | 0.861 | 0.001 | 0.895 | 0.002 | 0.836 | 0.001 |
| Hughes Bay | 0.880 | 0.004 | 0.825 | 0.003 | 0.911 | 0.004 | 0.854 | 0.004 | 0.883 | 0.004 | 0.828 | 0.003 |
| West Chaplin West Division 1 | 0.936 | 0.004 | 0.870 | 0.003 | 0.936 | 0.003 | 0.871 | 0.002 | 0.903 | 0.005 | 0.840 | 0.004 |
| West Chaplin Center Division | | | | | 0.933 | 0.002 | 0.873 | 0.001 | 0.908 | 0.006 | 0.849 | 0.005 |
| West Chaplin Lake SE Division | 0.927 | 0.003 | 0.867 | 0.002 | 0.921 | 0.005 | 0.862 | 0.004 | 0.898 | 0.002 | 0.840 | 0.001 |
| East of West Chaplin Lake NE Division | 0.903 | 0.016 | 0.850 | 0.015 | 0.915 | 0.008 | 0.861 | 0.007 | 0.882 | 0.005 | 0.831 | 0.004 |
| Great Salt Lake (North) | | | | | 0.940 | 0.002 | 0.892 | 0.002 | 0.915 | 0.003 | 0.869 | 0.002 |
| Great Salt Lake (South) | 0.921 | 0.004 | 0.884 | 0.003 | 0.928 | 0.003 | 0.891 | 0.002 | 0.923 | 0.002 | 0.886 | 0.002 |
| Cargill Salt Pond 1 | 0.888 | 0.002 | 0.831 | 0.001 | 0.931 | 0.005 | 0.871 | 0.004 | 0.892 | 0.003 | 0.835 | 0.003 |
| Cargill Salt Pond 2 | | | | | 0.930 | 0.003 | 0.867 | 0.002 | 0.905 | 0.006 | 0.843 | 0.005 |
| Cargill Salt Pond 3 | 0.932 | 0.003 | 0.861 | 0.001 | 0.962 | 0.004 | 0.888 | 0.004 | 0.921 | 0.005 | 0.850 | 0.004 |
| Cargill Salt Pond 7 | 0.945 | 0.002 | 0.858 | 0.001 | 0.958 | 0.002 | 0.871 | 0.001 | 0.925 | 0.005 | 0.840 | 0.004 |
| Cargill Salt Pond 9 | 0.947 | 0.011 | 0.870 | 0.010 | 0.918 | 0.006 | 0.844 | 0.006 | 0.910 | 0.005 | 0.837 | 0.004 |
| Cargill Salt Pond 12 | 0.910 | 0.006 | 0.839 | 0.005 | 0.972 | 0.007 | 0.896 | 0.006 | 0.916 | 0.003 | 0.845 | 0.003 |
| Cargill Salt Pond 13 | 0.879 | 0.003 | 0.813 | 0.003 | 0.960 | 0.002 | 0.888 | 0.002 | 0.948 | 0.002 | 0.877 | 0.002 |
| Cargill Salt Pond 14 | 0.942 | 0.007 | 0.868 | 0.006 | 0.976 | 0.017 | 0.899 | 0.016 | 0.933 | 0.008 | 0.859 | 0.007 |

That $n$C$_{28}$FA $\alpha_{lipid\text{-}lake}$ values are not correlated with salinity is not surprising, since the compounds are presumed to derive from terrestrial plants and not the saline lake water. The weak $n$C$_{16}$FA $\alpha_{lipid\text{-}lake}$ - salinity pattern is somewhat consistent with previous observations of the influence of salinity on D/H fractionation in algae, which has shown that fractionation decreases with increasing salinity (Schouten et al., 2006; Sachse and Sachs, 2008; Sachs and Schwab, 2011; Nelson and Sachs, submitted-sterol; Nelson and Sachs, submitted-alkenone).

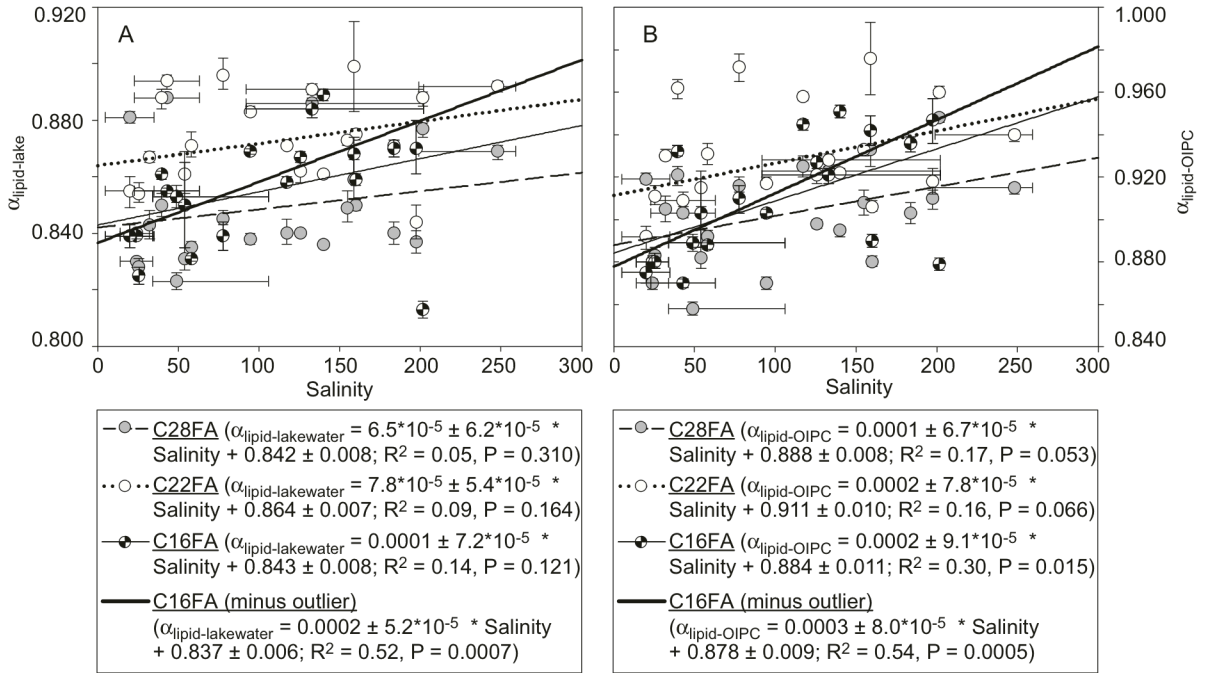


**Figure 4:** A) $\alpha_{lipid\text{-}lake}$ vs salinity for $n$C$_{16}$FA, $n$C$_{22}$FA, and $n$C$_{28}$FA. Regression line and equation for $n$C$_{16}$FA shown with and without S = 200 outlier. B) As in (A), but for $\alpha_{lipid\text{-}OIPC}$.

The slope of 0.0002 is lower than what has been observed for dinosterol, brassicasterol, microbial lipids on Christmas Island, and cultured marine alkenones (Nelson and Sachs, *Chapter 3;* Sachs and Schwab, 2011; Sachse and Sachs, 2008; Schouten et al., 2006), but similar to observations from lacustrine alkenones from the same sample set (Nelson and Sachs, *Chapter 4*). This might suggest that the damped sensitivity of D/H fractionation to salinity observed for lacustrine alkenones is common to acetogenic algal lipids produced in lakes, and that this sensitivity is imparted early in the process of biosynthesis since $n$C$_{16}$FA is a universal precursor compound in the acetogenic pathway. However, if so, this must be reconciled with the steeper $\alpha_{lipid\text{-}lake}$ - salinity slopes observed for microbial acetogenic lipids from saline ponds on Christmas Island (Sachse and Sachs, 2008). Alternatively, the slope may be muted due to the scatter in the data, which is likely caused by the wide variety of source organisms that produce this $n$C$_{16}$FA,

the time varying salinity in the lakes, or possibly different accumulation rates of sediment at each site. That $n$C$_{22}$FA $\alpha_{lipid\text{-}lake}$ values are not correlated with salinity suggests that D/H fractionation may be insensitive to salinity in submerged and emergent aquatic vegetation. If so, a more specific biomarker for submerged aquatic vegetation might prove to be a useful indicator of lake water δD values that is not affected by salinity, which would also help to eliminate the potential that the compounds are coming from terrestrial grass sources that are also known to produce middle-chain length fatty acids in some cases (Chikaraishi and Naraoka, 2007; Wiesenberg and Schwark, 2006; Wiesenberg et al., 2004).

In addition to salinity, we assessed the relationship between $\alpha_{lipid\text{-}lake}$ and $\alpha_{lipid\text{-}OIPC}$ values with climatological evaporation minus precipitation (E-P) (National Center for Atmospheric Research (NCAR) climate analysis section climatology dataset), evapotranspiration (ET) (Food and Agriculture Organization GeoNetwork agrometeorological dataset) and the Normalized Difference Vegetation Index (NDVI) (Pinzon et al., 2005; Tucker et al., 2005) to determine whether any of these factors might help to explain the variability in our fatty acid δD data. We find a weak positive correlation between $\alpha_{lipid\text{-}OIPC}$ values and E-P for $n$C$_{22}$FA and $n$C$_{28}$FA (Figure 5). For $n$C$_{28}$FA this might be driven by enhanced leaf water enrichment in drier areas leading to reduced apparent fractionation with respect to precipitation, which is consistent with growth chamber and field data (Kahmen et al., 2013a; Kahmen et al., 2013b). It might be possible that the similar effect in $n$C$_{22}$FA $\alpha_{lipid\text{-}OIPC}$ values is also being driven by leaf water enrichment in emergent vegetation, but this would require more detailed study to confirm.

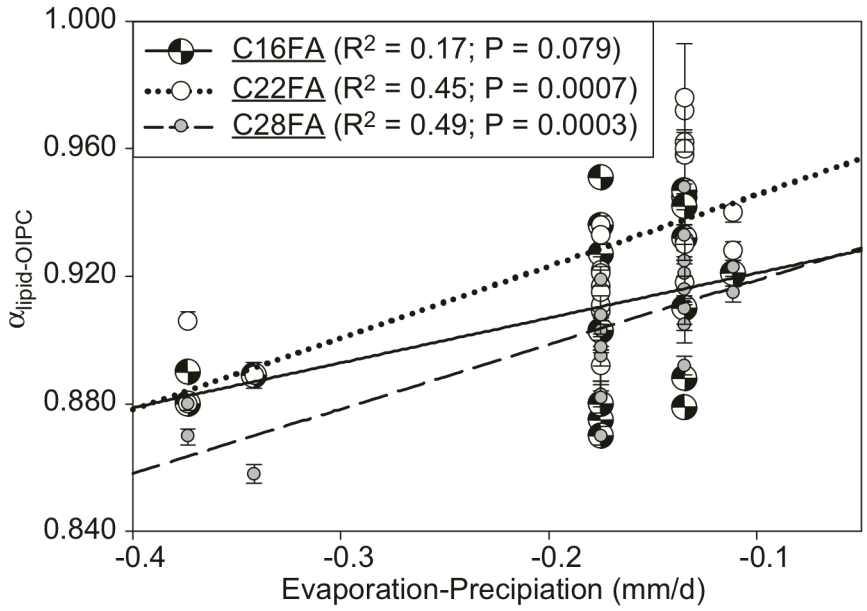


**Figure 5:** $\alpha_{lipid\text{-}OIPC}$ vs. evaporation minus precipitation for $n$C$_{16}$FA, $n$C$_{22}$FA, and $n$C$_{28}$FA.

*Using multiple biomarkers to constrain salinity*

We recently showed that the magnitude of D/H fractionation in the algal biomarkers dinosterol (4α,23,24-trimethyl-5α-cholest-22E-en-3β-ol) and brassicasterol (24-methyl cholest-5,22-dien-3β-ol) is correlated with salinity at the field sites discussed in the present study (Nelson and Sachs, *Chapter 3*), which is consistent with previous investigations on the sensitivity of dinosterol to salinity in the Chesapeake Bay (Sachs and Schwab, 2011). $n$C$_{22}$FA $\alpha_{lipid\text{-}lake}$ values are insensitive to salinity, and $n$C$_{16}$FA $\alpha_{lipid\text{-}lake}$ values show reduced sensitivity to salinity as compared to that for dinosterol and brassicasterol from the same sites (Figure 4) (Nelson and Sachs, *Chapter 3*). Since all of these compounds are presumably being produced primarily by aquatic photoautotrophs that are drawing hydrogen from the same lake water source, it follows that any changes in the difference between sterol and short or middle-chain length fatty acid δD values would be attributable to environmental factors that alter the magnitude of D/H

fractionation differently between these compounds, with salinity being a leading potential cause. To test this possibility we calculated difference values for each of the four possible sterol - fatty acid pairs from our data sets where both lipid δD measurements were available using the same equation that is used to calculate α values [$(\delta D_{sterol} + 1000)/(\delta D_{FA} + 1000)$]. We use this approach instead of a direct subtraction of delta values, or Δ-notation, since the magnitude of Δ will vary as a function of the starting δD values even for equal isotopic differences. But since it is incorrect to consider the δD value difference between sterols and fatty acids in the context of a product and a reactant, we refer to it as $\delta D_{sterol}/\delta D_{FA}$.

Comparing the $\delta D_{sterol}/\delta D_{FA}$ values with salinity we observe generally strong relationships with the exception of some high salinity outlier values (Figure 6). We note greater slopes for the $n$C$_{22}$FA-based terms as opposed to the $n$C$_{16}$FA-based, which is consistent with the observation that $n$C$_{16}$FA $\alpha_{lipid\text{-}lake}$ values display weak salinity dependence, while $n$C$_{22}$FA $\alpha_{lipid\text{-}lake}$ values do not (Figure 4a). Multiple explanations may exist for the cause of an imperfect correlation between $\delta D_{sterol}/\delta D_{FA}$ values and salinity, but leading among these are the variety of additional factors that are known to influence the magnitude of D/H fractionation during lipid synthesis, including the effects of growth rates and species types (Wolhowe et al., 2009; Zhang and Sachs, 2007; Zhang et al., 2009). Since dinosterol, brassicasterol, $n$C$_{16}$FA and $n$C$_{22}$FA are each likely to represent varying sources and degrees of these biases, no individual sterol/fatty acid pairing can be selected as the obvious best choice for a paired lipid salinity reconstruction. However, it can be argued that with enough lipid pairs, the effects of random biases will cancel, assuming all systematic biases, such as salinity, have been individually addressed for each lipid. In order to assess the extent to which our four paired lipid - salinity determinations approach this

target, we also calculated an average reconstructed salinity from these four $\delta D_{sterol}/\delta D_{FA}$-salinity relationships (Figure 7).

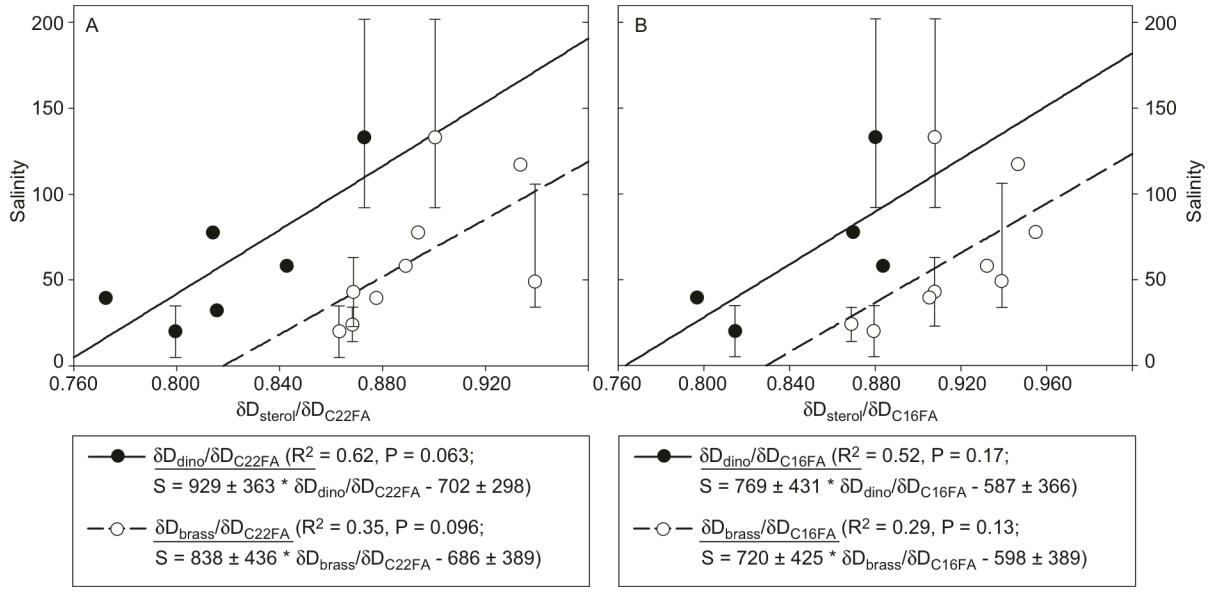


**Figure 6:** $\delta D_{sterol}/\delta D_{FA}$ values vs. historical average salinity at each site and for each lipid pair. A) Values calculated using $n$C$_{22}$FA. B) Values calculated using $n$C$_{16}$FA.

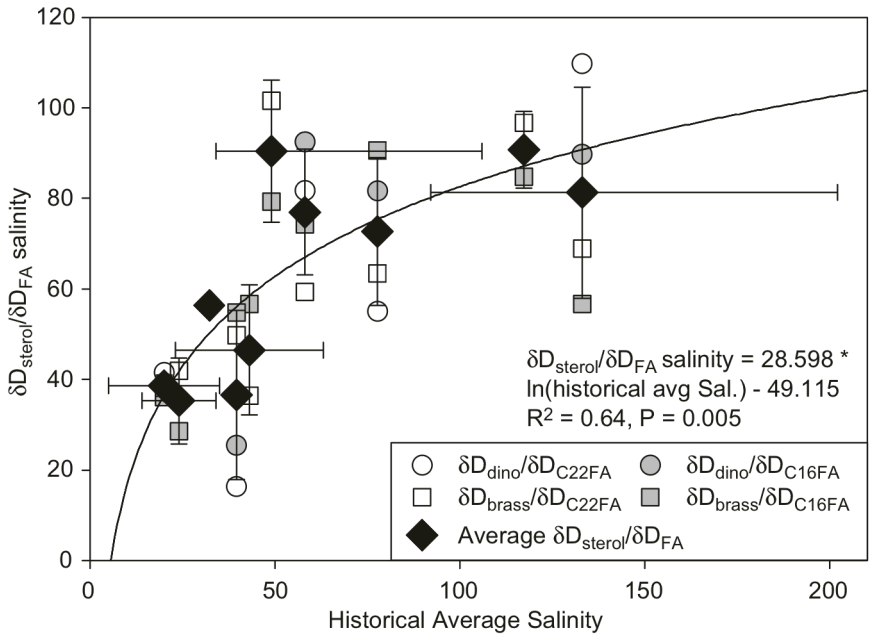


**Figure 7:** $\delta D_{sterol}/\delta D_{FA}$ salinity values vs. historical average salinity at each site. Historic average salinity error bars are only plotted on average $\delta D_{sterol}/\delta D_{FA}$ salinity values for clarity. Average $\delta D_{sterol}/\delta D_{FA}$ salinity value error bars represent the standard deviations of the average values.

The average of each of the four salinity reconstructions fits better with the historic average salinity at each site than does any individual $\delta D_{sterol}/\delta D_{FA}$ – derived salinity value, which is consistent with the notion of random errors canceling each other out. Next, we compare the impact that using the average $\delta D_{sterol}/\delta D_{FA}$ salinity value would have on the $\alpha_{lipid\text{-}lake}$-salinity relationship for brassicasterol and dinosterol as opposed to the historic average for the samples where both sterols and fatty acids were measured (Nelson and Sachs, *Chapter 3*). We observe generally similar regression slopes and intercepts for $\alpha_{lipid\text{-}lake}$ values against both salinity estimates, but for both brassicasterol and dinosterol the slope of the regression line is steeper for the $\delta D_{sterol}/\delta D_{FA}$ salinity as compared to the historic average salinity (Figure 8). While this

might be interpreted as a shortcoming of the paired lipid-salinity reconstruction, it might also be possible that the reconstructed salinities are in fact more representative of the conditions under which the lipids were produced.

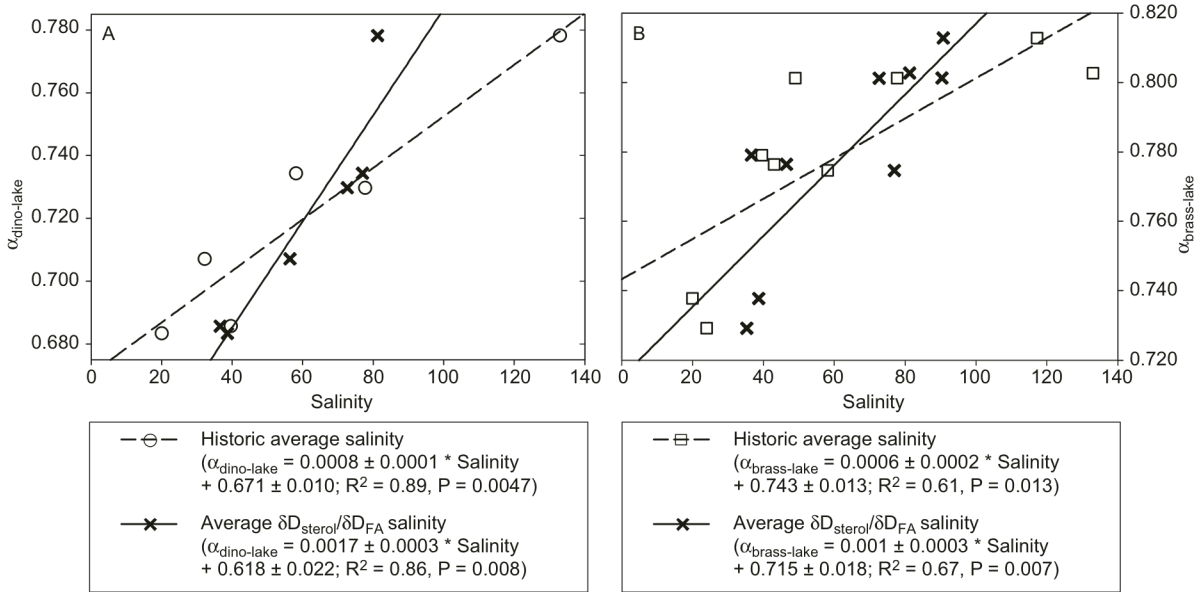


**Figure 8:** A) Comparison of $\alpha_{dino\text{-}lake}$ values with salinity between historic average salinity values and salinity calculated from $\delta D_{sterol}/\delta D_{FA}$ values. B) As in (A) but for brassicasterol.

Salinity in hypersaline lakes is known to vary greatly on seasonal to inter-decadal timescales, and our estimates of historical salinity are probably not perfectly representative of the average conditions under which the dinosterol and brassicasterol in our sediment samples were synthesized. As a final evaluation of the multiple lipid approach to reconstructing lake water δD values we take the calculated average $\delta D_{sterol}/\delta D_{FA}$ salinity value and use this with the $\alpha_{lipid\text{-}lake}$-$\delta D_{sterol}/\delta D_{FA}$ salinity relationships for dinosterol and brassicasterol (Figure 8) to calculate a predicted lake water δD value (Figure 9). In general, these compare well with measured lake water δD values and confirm the internal consistency of this calculation exercise (Figure 9).

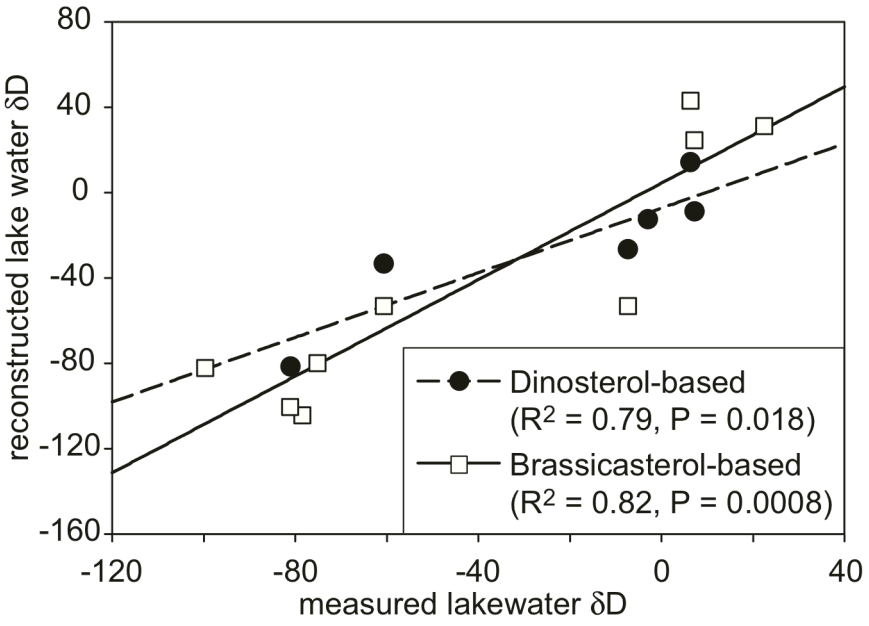


**Figure 9:** Comparison of lake water δD values calculated from $\delta D_{sterol}/\delta D_{FA}$ salinity values and the regression equations for dinosterol and brassicasterol from Figure 8 with measured lake water δD values.

A similar multi-biomarker approach to what we have performed for salinity might also be used with paired higher plant and submerged aquatic vegetation biomarker δD values, since the lake water and leaf water sources of hydrogen for these compounds are both derived from precipitation, but display different sensitivities to aridity (Polissar and Freeman, 2010). However, the extent to which aridity acts to enrich the δD values of lake and leaf water away from precipitation is basin- and plant-specific, respectively, and would therefore also require a local scale hydrologic model (e.g. Steinman et al., 2013) and a detailed understanding of the terrestrial vegetation assemblage. Nevertheless, it appears that as more is learned about the information recorded in each biomarker δD value, we are moving closer to being able to develop site-specific integrated basin-scale ecologic and hydrologic models that will permit quantitative

reconstructions of both precipitation and lake water δD values, as well as salinity, aridity, and perhaps other environmental variables.

**Conclusion**

We have evaluated the extent to which fatty acid δD values from saline and hypersaline lakes can be used to track environmental change. Our results support previous work that has shown that short and middle-chain length fatty acids reflect lake water δD values (Hou et al., 2006; Huang et al., 2004). To our knowledge this is the first assessment of the influence of salinity on these compounds, which are presumed to also derive from autochthonous sources in the lake environment, and our results suggest that these compounds could serve as more reliable indicators of lake water δD values than those from either algae or terrestrial higher plants. Short-chain fatty acids are found to show weak salinity dependence. This supports the idea that $n$$C_{16}$FA in our lake environments is primarily derived from algal sources, and thus is generally consistent with previous assessments of D/H fractionation in algal lipids (Nelson and Sachs, *Chapter 3;* Sachs and Schwab, 2011; Sachse and Sachs, 2008; Schouten et al., 2006). The reduced sensitivity compared to algal sterols (Nelson and Sachs, *Chapter 3;* Sachs and Schwab, 2011), or from acetogenic lipids studied in specialized environments (Sachse and Sachs, 2008), or from batch culture experiments (Schouten et al., 2006) suggests that there may be varying degrees of salinity sensitivity among different algal producers of certain compounds. This is particularly likely for a compound as ubiquitous as $n$$C_{16}$FA, which is a universal precursor in acetogenic lipid biosynthesis and is produced by virtually all organisms. Although our study was not specifically designed to assess the factors that influence D/H fractionation in long-chain fatty

acids, we do observe that they are insensitive to salinity, which is expected since they are not presumed to derive from organisms that use the saline lake water as their hydrogen source. We identify some sensitivity to evaporation minus precipitation, which is consistent with the idea that leaf wax lipids are ultimately controlled by leaf water δD values, which become enriched in arid environments (Kahmen et al., 2013a; Kahmen et al., 2013b).

In an effort to integrate the variety of lipid geochemical and environmental data we have produced at our sample sites we attempt to demonstrate how multiple biomarker δD values might be used together to derive and calibrate empirical fits to multiple environmental signals. In our example, we use the difference between δD values from sterols and fatty acids and calibrate these values against historical average salinity at each site. We then examine how calculating a salinity value from paired lipid isotope measurements using this calibration would impact the relationship between salinity and $\alpha$ values calculated from paired sterol and lake water δD values. As a final check on consistency we assess how lake water δD values calculated from paired lipid δD values using this calibration compare to measured lake water δD values. Although these comparisons are not independent from one another, the fact that we obtain a reasonable measure of internal consistency among the data suggest that our approach may be a useful tool for reconstructing salinity and lake water δD values if it can be tested and confirmed in other locations. The advantage of the $\delta D_{sterol}/\delta D_{FA}$ approach that we outline as opposed to using a calibrated $\delta D_{lipid}$-$\delta D_{water}$ relationship to derive a δD water value, and then using that with a calibrated $\alpha$-salinity relationship for a sterol to derive salinity is that prior knowledge of the $\delta D_{lipid}$-$\delta D_{water}$ relationship is not required. Instead, only an understanding that one lipid is more sensitive to salinity than the other is required to permit local use of paired lipid δD values to

generate at least semi-quantitative or relative records of paleosalinity without extensive calibration.

Efforts to quantify and account for systematic biases in measured δD values through calibration efforts, such as those that we have performed at our sample sites for salinity, represent progress towards moving δD measurements closer to the arena of quantitative paleoclimate proxies. The fact that we observe no apparent salinity effect in D/H fractionation in $n$-$C_{22}$FA suggests that the δD values of lipids form submerged aquatic vegetation may serve as a valuable alternate source of environmental information beyond what can be learned from algal lipids and terrestrial higher plants. Additional effort into searching for more specific biomarkers for these compounds in sediments might therefore prove valuable in working towards direct lake water δD reconstructions.

**Acknowledgments**

This material is based upon work supported by the U.S. National Science Foundation under Grants NSF-EAR-0745982, EAR-0823503 and ESH-0639640, and the U.S. National Oceanic and Atmospheric Administration under Grant No. NA08OAR4310685 to J. Sachs. We thank Orest Kawka, Josh Gregersen, S. Nemiah Ladd, Alyssa Atwood, Ines Mügler, and Julie Richey for useful discussions, advice and assistance in the lab. We thank Ariel Townsend for her careful assistance in the lab. We thank Jeff Bowman and Chase Stoudt for assistance in the field, Robert Baskin and the USGS in Salt Lake City for assistance accessing and sampling the Great Salt Lake. We thank Penny Streff and Terry Lewis at Cargill Incorporated, Saskatchewan Minerals and the Redberry Lake Biosphere Reserve for allowing site access.

**Chapter 5 References**


Anati, D.A., 1999. The salinity of hypersaline brines: Concepts and misconceptions. International Journal of Salt Lake Research 8, 55-70.

Arnow, T., stephens, D., 1990. Hydrologic Characteristics of the Great Salt Lake, Utah: 1847-1986, United States Geological Survey Water-Supply. U.S. Geological Survey.

Bowen, G.J., 2013. The Online Isotopes in Precipitation Calculator, version 2.2. http://www.waterisotopes.org. .

Bowen, G.J., Revenaugh, J., 2003. Interpolating the isotopic composition of modern meteoric precipitation. Water Resources Research 39, 1299.

Bowen, G.J., Wassenaar, L.I., A., H.K., 2005. Global application of stable hydrogen and oxygen isotopes to wildlife forensics. Oecologia 143.

Bowman, J.S., Sachs, J.P., 2008. Chemical and physical properties of some saline lakes in Alberta and Saskatchewan. Saline Systems 4.

Chikaraishi, Y., Naraoka, H., 2007. d13C and dD relationships among three n-alkyl compound classes (n-alkanoic acid, n-alkane and n-alkanol) of terrestrial higher plants. Organic Geochemistry 38, 198-215.

Cranwell, P.A., Eglinton, G., Robinson, N., 1987. Lipids of aquatic organisms as potential contributors to lacustrine sediments--ll*. Organic Geochemistry 11, 513-527.

Douglas, P.M.J., Pagani, M., Brenner, M., Hodell, D.A., Curtis, J.H., 2012. Aridity and vegetation composition are important determinants of leaf-wax dD values in southeastern Mexico and Central America. Geochimica et Cosmochimica Acta 97, 24-45.

Eglinton, G., Hamilton, R.J., 1967. Leaf Epicuticular Waxes. Science 156, 1322-1335.

Ficken, K.J., Li, B., Swain, D.L., Eglinton, G., 2000. An n-alkane proxy for the sedimentary input of submerged/ floating freshwater aquatic macrophytes. Organic Geochemistry 31, 745-749.

Gao, L., Hou, J., Toney, J., MacDonald, D., Huang, Y., 2011. Mathematical modeling of the aquatic macrophyte inputs of mid-chain n-alkyl lipids to lake sediments: Implications for interpreting compound specific hydrogen isotopic records. Geochimica et Cosmochimica Acta 75, 3781-3791.

Hou, J., D'Andrea, W.J., Huang, Y., 2008. Can sedimentary leaf waxes record D/H ratios of continental precipitation? Field, model, and experimental assessments. Geochimica et Cosmochimica Acta 72, 3503-3517.

Hou, J., Huang, Y., Oswald, W.W., Foster, D.R., Shuman, B., 2007. Centennial-scale compound-specific hydrogen isotope record of Pleistocene–Holocene climate transition from southern New England. Geophysical Research Letters 34, L19706.

Hou, J., Huang, Y., Wang, Y., Shuman, B., Oswald, W.W., Faison, E., Foster, D.R., 2006. Postglacial climate reconstruction based on compound- specific D/H ratios of fatty acids from Blood Pond, New England. Geochemistry, Geophysics, Geosystems 7, Q03008.

Huang, Y., Shuman, B., Wang, Y., III, T.W., 2002. Hydrogen isotope ratios of palmitic acid in lacustrine sediments record late Quaternary climate variations. Geology 30, 1103-1106.

Huang, Y., Shuman, B., Wang, Y., III, T.W., 2004. Hydrogen isotope ratios of individual lipids in lake sediments as novel tracers of climatic and environmental change: a surface sediment test. Journal of Paleolimnology 31, 363-375.

Kahmen, A., Hoffmann, B., Schefuß, E., Arndt, S.K., Cernusak, L.A., West, J.B., Sachse, D., 2013a. Leaf water deuterium enrichment shapes leaf wax n-alkane dD values of angiosperm plants II: Observational evidence and global implications. Geochimica et Cosmochimica Acta 111, 50-63.

Kahmen, A., Schefuß, E., Sachse, D., 2013b. Leaf water deuterium enrichment shapes leaf wax n-alkane dD values of angiosperm plants I: Experimental evidence and mechanistic insights. Geochimica et Cosmochimica Acta 111, 39-49.

Ladd, S.N., Sachs, J.P., 2012. Inverse relationship between salinity and n-alkane dD values in the mangrove Avicennia marina. Organic Geochemistry 48, 25-36.

Last, W.M., Ginn, F.M., 2005. Saline systems of the Great Plains of western Canada: an overview of the limnogeology and paleolimnology. Saline Systems 1.

Liu, W., Yang, H., 2008. Multiple controls for the variability of hydrogen isotopic compositions in higher plant n-alkanes from modern ecosystems. Global Change Biology 14, 2166-2177.

McInerney, F.A., Helliker, B.R., Freeman, K.H., 2011. Hydrogen isotope ratios of leaf wax n-alkanes in grasses are insensitive to transpiration. Geochimica et Cosmochimica Acta 75, 541-554.

Meyers, P.A., Ishiwatari, R., 1993. Lacustrine organic geochemistry - an overview of indicators of organic matter sources and diagenesis in lake sediments. Organic Geochemistry 20, 867-900.

Nelson, D.B., Sachs, J.P., *Chapter 3*. The influence of salinity on D/H fractionation in dinosterol and brassicasterol from globally distributed saline and hypersaline lakes

Nelson, D.B., Sachs, J.P., *Chapter 4*. The influence of salinity on D/H fractionation in alkenones from saline and hypersaline lakes in continental North America.

Nelson, D.M., Henderson, A.K., Huang, Y., Hu, F.S., 2013. Influence of terrestrial vegetation on leaf wax dD of Holocene lake sediments. Organic Geochemistry 56, 106-110.

Nichols, J., Booth, R.K., Jackson, S.T., Pendall, E.G., Huang, Y., 2010. Differential hydrogen isotopic ratios of Sphagnum and vascular plant biomarkers in ombrotrophic peatlands as a quantitative proxy for precipitation—evaporation balance. Geochimica et Cosmochimica Acta 74, 1407-1416.

Pinzon, J., Brown, M.E., Tucker, C.J., 2005. Satellite time series correction of orbital drift artifacts using empirical mode decomposition, in: N.Huang (Ed.), Hilbert-Huang Transform: Introduction and Applications, pp. 167-186.

Polissar, P.J., Freeman, K.H., 2010. Effects of aridity and vegetation on plant-wax dD in modern lake sediments. Geochimica et Cosmochimica Acta 74, 5785-5797.

Polissar, P.J., Freeman, K.H., Rowley, D.B., McInerney, F.A., Currie, B.S., 2009. Paleoaltimetry of the Tibetan Plateau from D/H ratios of lipid biomarkers. Earth and Planetary Science Letters 287, 64-76.

Sachs, J.P., Schwab, V.F., 2011. Hydrogen isotopes in dinosterol from the Chesapeake Bay estuary. Geochmica et Cosmochimica Acta 75, 444-459.

Sachse, D., Billault, I., Bowen, G.J., Chikaraishi, Y., Dawson, T.E., Feakins, S.J., Freeman, K.H., Magill, C.R., McInerney, F.A., van der Meer, M.T.J., Polissar, P., Robins, R.J., Sachs, J.P., Schmidt, H.-L., Sessions, A.L., White, J.W.C., West, J.B., Kahmen, A., 2012. Molecular Paleohydrology: Interpreting the Hydrogen-Isotopic Composition of Lipid Biomarkers from Photosynthesizing Organisms. Annual Review of Earth and Planetary Sciences 40, null.

Sachse, D., Kahmen, A., Gleixner, G., 2009. Significant seasonal variation in the hydrogen isotopic composition of leaf-wax lipids for two deciduous tree ecosystems (Fagus sylvativa and Acer pseudoplatanus). Organic Geochemistry 40, 732-742.

Sachse, D., Sachs, J.P., 2008. Inverse relationship between D/H fractionation in cyanobacterial lipids and salinity in Christmas Island saline ponds. Geochim. Cosmochim. Acta 72, 793-806.

Schouten, S., Ossebaar, J., Schreiber, K., Kienhuis, M.V.M., Langer, G., Benthien, A., Bijma, J., 2006. The effect of temperature, salinity and growth rate on the stable hydrogen isotopic composition of long chain alkenones produced by *Emiliania huxleyi* and *Gephyrocapsa oceanica*. Biogeosciences 3, 113-119.

Sessions, A.L., Burgoyne, T.W., Hayes, J.M., 2001. Determination of the H3 Factor in Hydrogen Isotope Ratio Monitoring Mass Spectrometry. Analytical Chemistry 73, 200-207.

Shang, Y., 2000. Mineralogy, Lithostratigraphy and Geochemistry of North lngebright Lake, Saskatchewan, Canada, Department of Geological Sciences. University of Manitoba, Winnipeg, Manitoba, p. 408.

Smith, F.A., Freeman, K.H., 2006. Influence of physiology and climate on delta D of leaf wax n-alkanes from C-3 and C-4 grasses. Geochimica et Cosmochimica Acta 70, 1172-1187.

Smittenberg, R.H., Saenger, C., Dawson, M.N., Sachs, J.P., 2011. Compound-specific D/H ratios of the marine lakes of Palau as proxies for West Pacific Warm Pool hydrologic variability. Quaternary Science Reviews 30, 921-933.

Steinman, B.A., Abbott, M.B., Nelson, D.B., Stansell, N.D., Finney, B.P., Bain, D.J., Rosenmeier, M.F., 2013. Isotopic and hydrologic responses of small, closed lakes to climate variability: Comparison of measured and modeled lake level and sediment core oxygen isotope records. Geochimica et Cosmochimica Acta 105, 455-471.

Tierney, J.E., Oppo, D.W., Rosenthal, Y., Russell, J.M., Linsley, B.K., 2010. Coordinated hydrological regimes in the Indo-Pacific region during the past two millennia. Paleoceanography 25.

Tierney, J.E., Russell, J.M., Huang, Y., Damsté, J.S.S., Hopmans, E.C., Cohen, A.S., 2008. Northern Hemisphere Controls on Tropical Southeast African Climate During the Past 60,000 Years. Science 322, 252-255.

Tipple, B.J., Berke, M.A., Doman, C.E., Khachaturyan, S., Ehleringer, J.R., 2013. Leaf-wax n-alkanes record the plant–water environment at leaf flush. Proceedings of the National Acadamy of Sciences of the United States of America 110, 2659-2664.

Tucker, C.J., Pinzon, J.E., Brown, M.E., Slayback, D.A., Pak, E.W., Mahoney, R., Vermote, E.F., Saleous, N.E., 2005. An Extended AVHRR 8-km NDVI Data Set Compatible with MODIS and SPOT Vegetation NDVI Data. International Journal of Remote Sensing 26, 4485-4498.

USGS, 2013. Great Salt Lake - Salinity and Water Quality (http://ut.water.usgs.gov/greatsaltlake/salinity/index.html). Utah Water Science Center, U.S. Department of the Interior.

van der Meer, M.T.J., Benthien, A., Bijma, J., Schouten, S., Sinninghe-Damsté, J.S., 2013. Alkenone distribution impacts the hydrogen isotopic composition of the C37:2 and C37:3 alkan-2-ones in *Emiliania huxleyi*. Geochimica et Cosmochimica Acta 111, 162-166.

Volkman, J.K., Johns, R.B., Gillan, F.T., Perry, G.J., Jr, H.J.B., 1980. Microbial lipids of an intertidal sediment - I. Fatty acids and hydrocarbons. Geochimica et Cosmochimica Acta 44, 1133-1143.

Wang, Y.V., Larsen, T., Leduc, G., Andersen, N., Blanz, T., Schneider, R.R., 2013. What does leaf wax dD from a mixed C3/C4 vegetation region tell us? Geochimica et Cosmochimica Acta 111, 128-139.

Wiesenberg, G.L.B., Schwark, L., 2006. Carboxylic acid distribution patterns of temperate C3 and C4 crops. Organic Geochemistry 37, 1973-1982.

Wiesenberg, G.L.B., Schwarzbauer, J., Schmidt, M.W.I., Schwark, L., 2004. Source and turnover of organic matter in agricultural soils derived from n-alkane/n-carboxylic acid compositions and C-isotope signatures. Organic Geochemistry 35, 1371-1393.

Wolhowe, M.D., Prahl, F.G., Probert, I., Maldonado, M., 2009. Growth phase dependent hydrogen isotopic fractionation in alkenone-producing haptophytes. Biogeosciences 6, 1681-1694.

Yang, H., Liu, W., Leng, Q., Hren, M.T., Pagani, M., 2011. Variation in n-alkane dD values from terrestrial plants at high latitude: Implications for paleoclimate reconstruction. Organic Geochemistry 42, 283-288.

Yang, H., Pagani, M., Briggs, D.E.G., Equiza, M.A., Jagels, R., Leng, Q., LePage, B.A., 2009. Carbon and hydrogen isotope fractionation under continuous light: implications for paleoenvironmental interpretations of the High Arctic during Paleogene warming. Oecologia 160, 461-470.

Zhang, Z., Sachs, J.P., 2007. Hydrogen isotope fractionation in freshwater algae: I. Variations among lipids and species. Organic Geochemistry 38, 582-608.

Zhang, Z., Sachs, J.P., Marchetti, A., 2009. Hydrogen isotope fractionation in freshwater and marine algae: II. Temperature and nitrogen limited growth rate effects. Organic Geochemistry 40, 428-439.

Zhou, Y., Grice, K., Chikaraishi, Y., Stuart-Williams, H., Farquhar, G.D., Ohkouchi, N., 2011. Temperature effect on leaf water deuterium enrichment and isotopic fractionation during leaf lipid biosynthesis: Results from controlled growth of C3 and C4 land plants. Phytochemistry 72, 207-213.

# Chapter 6:

# A 2 kyr Record of Eastern Tropical Pacific Paleohydrology using Multiple Biomarker Hydrogen Isotope Records from Coastal Lakes on Isabela Island, Galápagos

[*In Prep for Submission*]

**Abstract**

Tropical hydroclimate records from the pre-industrial era are important for understanding the mechanisms of global climate change. Yet continuous records with centennial resolution are rare, and available rainfall proxies are largely qualitative. We use hydrogen isotope measurements of leaf-wax-derived $n$C$_{29}$ alkane, as well as taraxerol from *Rhizophora* mangroves, dinosterol from dinoflagellate phytoplankton, and $n$C$_{24}$ alkanol from cyanobacterial to develop a 2,000-year quantitative reconstruction of lake water δD values and salinity from Poza del Diablo, a brackish coastal lake on Isabela Island in the Galápagos. δD values of these and other lipids from two nearby saline lakes are used to distinguish regional hydroclimate variations from local lake-specific or geomorphological changes. We complement our isotope data with lipid concentration and alkane chain length values to constrain changes in vegetation. The combined changes in lake water δD values and salinity help to differentiate between changes in the El Niño-Southern Oscillation (ENSO) from those cause by changes in the position of the intertropical convergence zone (ITCZ). Together the data suggest that ENSO drove hydrologic changes from approximately 0 – 1200 AD, after which a southward migration of the ITCZ brought increased precipitation and some of the wettest conditions of the past 2 kyr. The Isabela Island lake records offer an improved insight on tropical Pacific climate changes from a sea-level site in a region of key climatic importance, illustrate the potential for quantitative paleohydrologic reconstructions using multiple biomarker hydrogen isotope records, and also identify potential problems that may arise from overreliance on the hydrogen isotope record from a single compound.

## Introduction

The tropical Pacific is a key driver of global climate as the primary heat source for atmospheric and ocean circulation, and changes in this region therefore have substantial global impacts. The El Niño/Southern Oscillation (ENSO) system is the largest mode of interannual climate variability and the consequences of changes in this system are far reaching, while the largest mean precipitation feature on the planet is the Intertropical Convergence Zone (ITCZ). Changes in the distribution of precipitation are arguably the largest and most important component of tropical climate dynamics, and improved understanding of how this distribution has changed over time, and the degree to which the cause of those changes may be attributable to changes in ENSO or ITCZ dynamics is an important focus area of paleoclimate research. Existing paleoclimate records of tropical climate variability have suggested large changes in the mean annual position of the ITCZ (Haug et al., 2001; Sachs et al., 2009), and other paleoclimate records have argued for significant changes in the ENSO over the Holocene (Conroy et al., 2008; Koutavas et al., 2006; Koutavas and Joanides, 2012; Rein et al., 2005; Tudhope et al., 2001), although recent evidence and data synthesis from fossil coral oxygen isotope data indicates that no forced ENSO variability occurred and that the system may instead be characterized by substantial stochastic variability (Cobb et al., 2013). Supporting this result is the fact that mechanistic explanations for the causes of possible changes in ENSO dynamics are often lacking (Chiang, 2009; Vecchi and Wittenberg, 2010), although ITCZ dynamics might be more easily explained through differences in inter-hemispheric mean temperature (Deplazes et al., 2013). Improving the spatial resolution of paleoclimate archives, and striving to improve the quantitative capacity of

hydroclimate proxy data offer two potential means by which to improve our understanding of tropical climate and to work to differentiate between possible ITCZ vs. ENSO forcing.

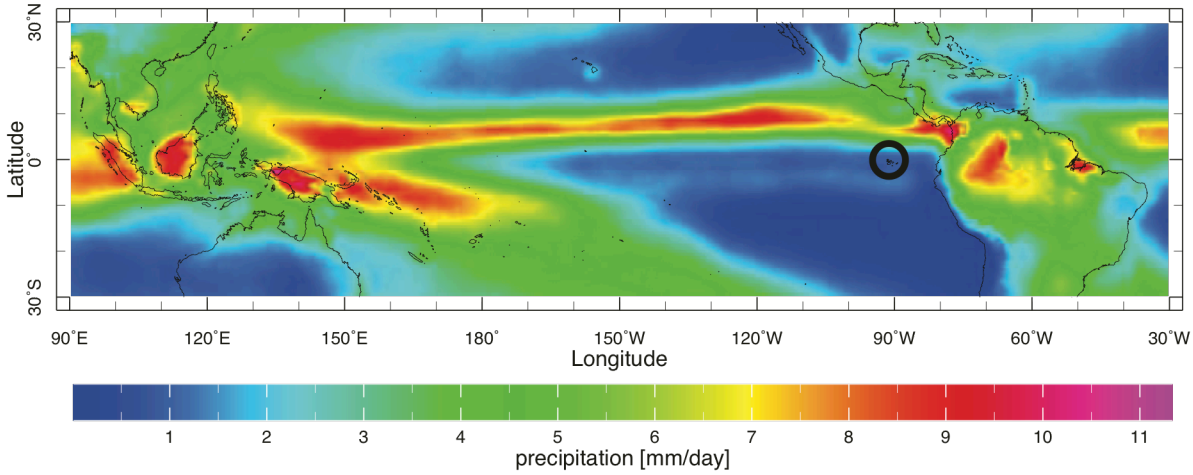


**Figure 1:** Map of the tropical Pacific showing the location of the Galápagos Islands (circled) and mean annual precipitation the NASA GPCP V1DD data set (http://iridl.ldeo.columbia.edu).

The Galápagos Islands are located in the eastern tropical Pacific in a core region for ENSO (Figure 1), and local sea surface temperatures, precipitation, and air temperature are all highly correlated with Nino 1+2, Nino 3, Nino 4, and the multivariate ENSO index (MEI) (Conroy et al., 2008). The islands are south of the modern range of seasonal ITCZ migration (Figure 2), but it has been proposed that during the Little Ice Age (LIA; ~1350 to 1850 AD) the range of ITCZ migration shifted south to cause wetter conditions in the Galápagos (Sachs et al., 2009). However, virtually all millennial-scale information on Galápagos paleohydrology comes from only a few study sites, with the majority coming from El Junco Lake sediment (Colinvaux,

1972; Conroy et al., 2008; Riedinger et al., 2002; Sachs et al., 2009; Seddon et al., 2011). El Junco Lake elevation is approximately 800 m above sea level, and at this elevation it is regularly covered in thick Garúa fog, which was found to account for 26 ± 16 % of incident rainfall at a 650 m site in the Galápagos highlands, but to contribute zero to sea level moisture (Pryeta et al., 2012). Despite these potential complications, paleoclimate evidence from the past 2 kyr from El Junco Lake and Bainbridge crater both suggest similar patterns of ENSO variability, with maximum activity occurring near 2000 cal yr BP (Conroy et al., 2008; Riedinger et al., 2002).

We sought to improve paleoclimate information available from this key climate region by targeting sediment records from coastal lakes on Isabela Island. The primary focus of our work is on Poza del Diablo (Figure 2), a shallow 0.5 – 1 m-deep brackish wetland system that was the target of a paleoecology and diatom study conducted by Seddon et al. (2011) (hereafter S11). We analyzed changes in the concentration and hydrogen isotopic composition of a series of biomarkers from terrestrial plants (*n*-alkanes, taraxerol), cyanobacteria (glycolipids), and dinoflagellates (dinosterol) to produce a comprehensive assessment of paleohydrologic change over the past 2 kyr. We corroborate our results from Poza del Diablo with additional measurements from neighboring lakes Poza Verde and Poza Escondida (Figure 2), and the diatom-based salinity reconstruction from the S11 study performed at Poza del Diablo. Our multiple biomarker isotope approach allows us to extract a coherent paleohydrology signal from Poza del Diablo and to reduce the potential that changes caused by secondary factors known to influence the hydrogen isotope composition of biomarkers are misinterpreted as climate signals, such as growth rates, temperatures, and light levels for algal lipids (Romero-Viana et al., 2013; Sachs and Schwab, 2011; Sachse and Sachs, 2008; Schouten et al., 2006; Wolhowe et al., 2009; Zhang and Sachs, 2007; Zhang et al., 2009), and humidity, evapotranspiration rates, salinity,

timing of leaf wax production, and changes in vegetation assemblage for lipids from terrestrial plants (Douglas et al., 2012; Hou et al., 2008; Kahmen et al., 2013a; Kahmen et al., 2013b; Ladd and Sachs, 2012; Liu and Yang, 2008; McInerney et al., 2011; Nelson et al., 2013; Polissar and Freeman, 2010; Sachse et al., 2009; Smith and Freeman, 2006; Tipple et al., 2013; Wang et al., 2013; Yang et al., 2011; Yang et al., 2009; Zhou et al., 2011). Hydrogen isotope ratios are measured and reported in terms of delta notation, where $\delta D = [(D/H_{sample}/D/H_{standard}) - 1] \times 1000‰$, and D, and H stand for deuterium, and hydrogen, respectively, and the reference standard is Vienna Standard Mean Ocean Water (VSMOW, $\delta D = 0$ ‰).

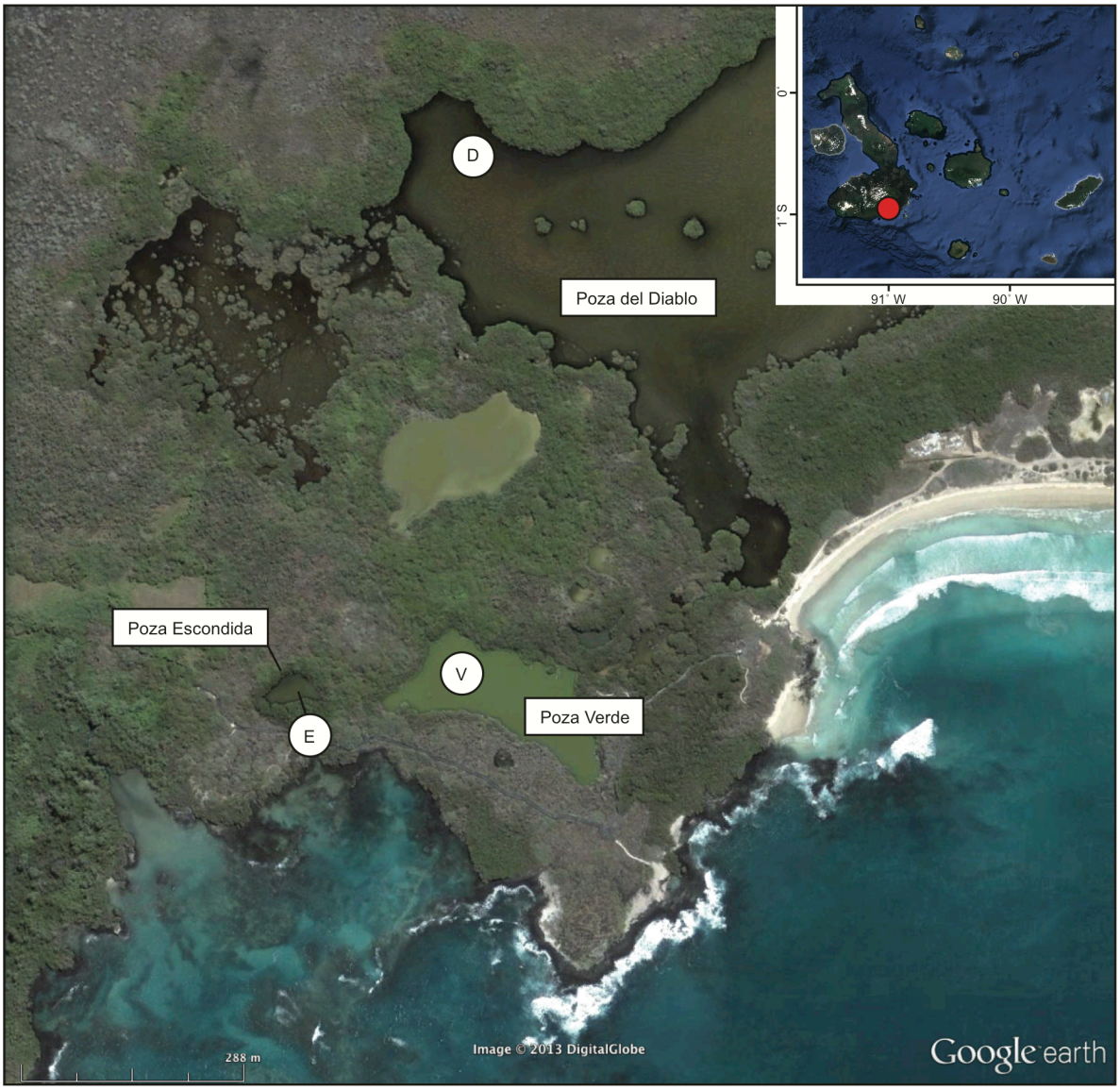


**Figure 2:** Google Earth image showing location of Isabela Island within the Galápagos archipelago (inset) and the location on Isabela Island where samples were collected (red circle). Individual cores were collected at the locations indicated by the white circles.

## Methods

### *Field Sampling*

In June of 2008 a series of sediment cores were collected from the wetland lakes on southern Isabela Island (Figure 2; Table 1). Surface sediments were collected with a universal corer (Aquatic Research, Hope, ID) and sectioned in the field at 1 cm intervals until the sediment became stiff enough to transport in the tube. Longer sediment cores were recovered with a Livingstone-type piston-coring device (Geo-Core, Columbus, OH). Sectioned material was stored on ice in the field or frozen on the day of recovery, while material in core tubes was refrigerated shortly after collection. After transport to the University of Washington, sectioned material was stored at -20 °C while material in core tubes was refrigerated at 4 °C. In total, we recovered overlapping sediment cores at Poza del Diablo to a depth of 8.79 m, a single sediment core with gaps between successive drives to a depth of 5.4 m from Poza Verde, and a single surface sediment core from Poza Escondida spanning 83 cm in length. In addition to the sediment cores, we filtered lake water onto combusted 0.7 μm-pore size glass fiber filters to recover suspended particle samples from the modern lake water in order to aid in the interpretation of down-core geochemical data. We also collected a variety of plant and floating algae samples around each core site for the same purpose as well as water samples for hydrogen isotope analysis. All water isotope and suspended particle sample collection and handling are described elsewhere (Nelson and Sachs, *Chapter 3*). Lake water temperature, pH, conductivity, salinity, and temperature were measured on-site using a portable data sonde.

**Table 1:** Characteristics of Isabela Lakes and locations of sediment cores.

| Site | Salinity (PSS) | δD - Lake Water | σ | Water Depth (m) | Lat (S) | Long (W) |
|---|---|---|---|---|---|---|
| **Poza del Diablo** | 7.4 | 13.2 | 0.6 | 1.3 | 0° 57.145' | 90° 59.431' |
| **Poza Verde** | 43.1 | 10.5 | 0.3 | 0.85 | 0° 57.504' | 90° 59.446' |
| **Poza Escondida** | 32.9 | 4.5 | 0.6 | 0.76 | 0° 57.517' | 90° 59.561' |

*Initial Sediment Processing and Chronology*

Core tube samples were split longitudinally and photographed under controlled light conditions with a reference color bar. A mix of terrestrial macrofossils and bulk sediment total organic carbon was used to develop radiocarbon chronologies in each lake (Table 2). Samples were sent to either the Xi'an Accelerator Mass Spectrometry Center at the Institute of Earth Environment, Chinese Academy of Sciences, or to Direct AMS (Seattle, WA). Samples sent to Direct AMS were pretreated at the University of Washington following and acid-base-acid procedure (Brock et al., 2010), while samples sent to the Xi'an lab were pretreated at that facility prior to analysis. Radiocarbon ages were calibrated using the Calib 5.0 online calibration software (Stuiver and Reimer, 1993), and the Southern Hemisphere 04 calibration curve (McCormac et al., 2004), with the exception of one date from Poza Escondida that contained a small amount of bomb radiocarbon, and was therefore calibrated using the spliced Southern Hemisphere and Southern Hemisphere-Bomb calibration curves (Hua and Barbetti, 2004).

**Table 2:** Radiocarbon dates from Isabela Lakes. Abbreviations: universal core (UC), piston core (PC), terrestrial macrofossil (TM), total organic carbon (TOC), Xi'an AMS Center - Institute of Earth Environment - Chinese Acadamey of Sciences (X), Direct AMS - Seattle, WA (D), southern hemisphere radiocarbon calibration curve (SH04), southern hemisphere bomb radiocarbon calibration curve (Bomb04 SH).

| Lake | Core | Sample Type | Depth (cm) | $^{14}$C age (yr BP) | σ | Med. Cal Age (yr BC/AD) | 2σ Cal Range (yr BC/AD) | Lab | Calibration Curve |
|---|---|---|---|---|---|---|---|---|---|
| Diablo | UC1 | TM | 23.5 | 189 | 22 | 1770 AD | 1660 - 1952 AD | X | SH04 |
| Diablo | PC1 | TOC | 75.5 | 654 | 27 | 1350 AD | 1280 - 1392 AD | X | SH04 |
| Diablo | PC1 | TOC | 149 | 1002 | 24 | 1020 AD | 987 - 1148 AD | X | SH04 |
| Diablo | PC2 | TOC | 231 | 1574 | 24 | 480 AD | 424 - 543 AD | X | SH04 |
| Diablo | PC3 | TM | 356.5 | 2054 | 23 | 70 BC | 162 BC - 2 AD | X | SH04 |
| Diablo | PC4 | TM | 465 | 2352 | 22 | 400 BC | 505 - 384 BC | X | SH04 |
| Verde | PC1 | TM | 52 | 262 | 26 | 1650 AD | 1522 - 1950 AD | D | SH04 |
| Verde | PC2 | TOC | 156.5 | 1202 | 25 | 720 AD | 722 - 891 AD | X | SH04 |
| Escondida | UC1 | TM | 17.5 | 24 | 25 | 1900 AD | 1700 - 1955 AD | D | SH04/Bomb04 SH |
| Escondida | UC1 | TM | 36.5 | 141 | 25 | 1810 AD | 1669 - 1953 AD | D | SH04 |
| Escondida | UC1 | TM | 72.5 | 310 | 28 | 1560 AD | 1489 - 1648 AD | D | SH04 |
| Escondida | UC1 | TM | 80.5 | 409 | 25 | 1460 AD | 1436 - 1616 AD | D | SH04 |

*Lipid Extraction*

Sediment samples for lipid analyses were removed from the split cores or bagged surface sediments in 1 cm-thick samples, with the exception of eight subsamples taken after the initial sampling effort which were collected using 2 cm-thick samples. Subsamples were transferred to combusted glass sample vials, frozen and then freeze dried. Freeze dried material was weighed and then extracted in a 9:1 mixture of dichloromethane (DCM) and methanol (MeOH) on an accelerated solvent extractor (ASE) Dionex 200. Just prior to extraction, an $n$C$_{21}$ alcohol ($n$C$_{21}$-OL), $n$C$_{21}$ acid, and an $n$C$_{36}$ alkane quantification/recovery standard was added to each extraction cell. The ASE was operated at 100 °C and 1500 psi with three five-minute static phases. Following extraction, solvent was evaporated under $N_2$ from the total lipid extract (TLE)

on a Turbo-vap system (Caliper, Hopkinton, MA, USA). After an initial set of 45 samples was extracted and analyzed, an additional 20 samples were extracted following the same protocol. In an effort to improve the yield of some compounds these second-round extracts were saponified by reacting the TLE with 1 N potassium hydroxide (KOH) in MeOH and Nanopure water (Barnstead nanopure infinity water system) at 70 °C overnight. The saponified TLE was then acidified to pH ~2 with HCl to protonate the acid and alcohol potassium salts and then recovered from the aqueous MeOH using a series of hexane liquid-liquid extractions. The hexane was then rinsed once with Nanopure water to dilute the small quantity of low pH water dissolved in this phase, and then dried over sodium sulfate.

*Column Chromatography*

Neutral and acid compounds for the first set of 45 TLEs were separated using 0.5 g of aminopropyl (Supelco) in hand packed glass solid phase extraction (SPE) – type columns. Neutral compounds were eluted with 8 mL of DCM/isopropyl alcohol (IPA) (3:1), acids were eluted with 6 mL of 4% acetic acid in diethyl ether, and a polar fraction was eluted with 6 mL MeOH. Neutral fractions were further separated using the same type of glass hand packed column with 1 g of silica gel 60 (5 % deactivated by weight; EMD chemicals, 35-75 μm). Hydrocarbon fractions were eluted with 10 mL of hexane, ketones/esters with 6 mL DCM/hexane (1:1), alcohols with 8mL ethyl acetate (EtOAc)/hexane (1:4), followed by a polar fraction with 6 mL methanol. For the second set of samples, the aminopropyl columns were not performed in order to save time and improve recoveries of sterols and triterpenols. Instead, saponified TLEs were only separated using the silica gel procedure.

*Hydrocarbon Identification and Quantification*

Hydrocarbon fractions were analyzed by gas chromatography-mass spectrometry (GC-MS) to identify *n*-alkanes suitable for hydrogen isotope analysis. Samples were injected in splitless mode at 300°C using helium carrier gas at 1.5 mL/min on an Agilent 6890N GC with 5975 inert mass selective detector using either an Agilent (formerly Varian) VF-17ms column (60 m X 0.32 mm X 0.25 μm) or an Agilent DB-5ms column with the same dimensions. The oven temperature program began at 110 °C for sample injection, then increased to 170 °C at 15 °C/min, then to 325 °C for the VF-17ms column, or 320 °C for the DB-5ms column at 5 °C/min where it was held for 24 min. Hydrocarbon quantifications were performed by gas chromatography with a flame ionization detector (GC-FID) using an Agilent 6890N. Samples were injected in splitless mode using a programmable temperature vaporization inlet with helium carrier gas at 2.0 mL/min onto a DB-5ms capillary column (60 m X 0.32 mm X 0.32 μm). The GC oven was held at 110 °C for 4 minutes after sample injection, then increased to 150 °C at 15 °C/min, then increased to 320 °C at 6 °C/min and held for 28 minutes. Quantifications were performed by comparing the relative peak areas of target *n*-alkanes with that of the added $n\mathrm{C}_{36}$ standard, and converted to ng/g dry sediment values based on the known mass of standard added prior to extraction. Average chain lengths (ACL) were calculated to determine the amount-weighted average sediment contribution of alkanes from $n\mathrm{C}_{17}$ to $n\mathrm{C}_{35}$. An $n\mathrm{C}_{31}/n\mathrm{C}_{29}$ ratio was calculated by dividing the concentrations, and is termed $\mathrm{C}_{31}/\mathrm{C}_{29}$ in subsequent discussion.

*Alcohol Identification and Quantification*

Alcohol fractions from silica gel were acetylated at 70 °C for 30 minutes in a mixture of 20 μL acetic anhydride of known δD value and 20 μL pyridine. Acetylated alcohols were then analyzed by GC-MS following the same procedure used for the hydrocarbons described above. Although less rigorous than quantification by GC-FID, alcohol fractions were quantified on the GC-MS owing to the need to obtain mass spectral information to identify desired target compounds that were often present at extremely low levels relative to other compounds. The quantification protocol was equivalent to that followed for the *n*-alkanes on the GC-FID, but for the alcohols the $n$$C_{21}$-OL standard was used. Subsamples of the acetylated alcohol fractions were taken for later hydrogen isotope analysis of the compounds present at highest abundance.

*High Performance Liquid Chromatography- Mass Spectrometry Purifications*

All alcohol fractions from silica gel found to contain dinosterol (4α, 23, 24-trimethyl-5α-cholest-22E-en-3β-ol), and some fractions found to contain taraxerol (3β-D-friedoolean-14-en-3-ol), were further purified using high performance liquid chromatography – mass spectrometry (HPLC-MS) following previously described methods (Nelson and Sachs, *Chapter 2*). Briefly, acetylated alcohols were injected on an Agilent 1100 series HPLC using an Agilent ZORBAX Eclipse XDB $C_{18}$ column (4.6 mm X 250 mm X 5 μm) equipped with matching guard column operated at a constant temperature of 30 °C. Acetylated dinosterol and taraxerol were eluted in using a mobile phase composition of 5 % methanol, 10 % ethyl acetate, and 85% acetonitrile.

*Hydrogen Isotope Analysis*

The hydrogen isotopic composition of purified $n$C$_{29}$ alkane ($n$C$_{29}$) $n$C$_{24}$ alkanol ($n$C$_{24}$-OL), dinosterol-acetate, and taraxerol-acetate were measured by gas chromatography – isotope ratio mass spectrometry (GC-IRMS) using a Thermo Delta V Plus isotope ratio mass spectrometer and Thermo Trace GC Ultra coupled with a gas chromatography combustion interface III. Samples were injected in splitless mode at 330 °C using helium carrier gas at 1.5 mL/min. The GC was equipped with either an identical column to the GC-MS, or a similar VF-17ms with slightly narrower diameter (60 m X 0.25 mm X 0.25 μm). Separate GC oven programs were used for different compounds. For dinosterol- and taraxerol acetate, the GC oven was held at an initial temperature of 120 °C for 2 minutes, then increased to 260 °C at 20 °C/min, then to 300 °C at 1 °C/min, then to 325 °C at 20°C/min and held for 8 minutes. For the $n$C$_{29}$ alkane, the GC oven was increased from an initial temperature of 120 °C to 200 °C at 20 °C/min, then held for 10 minutes, then increased to 325 °C at 3 °C/min and held for 12 minutes. For the $n$C24 alkanol, the GC oven was held at an initial temperature of 120 °C for 10 minutes, then increased to 325 °C at 8 °C/min and held for 15 minutes. In all cases, GC column effluent was directed through the pyrolysis reactor and combustion interface to convert organic column effluents to $H_2$ gas prior to introduction to the mass spectrometer. The $H_3^+$ factor was measured prior to every sample sequence (Sessions et al., 2001), and was stable and less than 5. Target compounds were referenced to VSMOW following the procedures described in Nelson and Sachs (*Chapter 4*).

## Results

### *Chronology*

Radiocarbon chronologies for all three lakes show linear relationships between age and depth at each site, with no major changes in sedimentation rates implied in the age/depth plots, or with the extrapolation of the age/depth trends to the coring date at the sediment-water interface (Figure 3; Table 2). This suggests minimal reservoir effect for these shallow lakes, which likely equilibrate rapidly with atmospheric $CO_2$. The linear-interpolated age model for Poza del Diablo indicates sedimentation rates between 1 and 3 mm/yr, with higher rates near the beginning of the approximately 2000-year record that gradually decline towards the most recent sediment. These rates translate to approximately 3 years of deposition for each 1-cm-thick layer in the early part of the record increasing to approximately 10 years per 1-cm-thick layer in the most recent sediment, although bioturbation and wind mixing probably reduces the resolution somewhat. The age/depth relationships from Poza Verde and Poza Escondida are quite similar, and all agree well with the age/depth data from S11 (Figure 3). Additional sediment results are described in relation to age as opposed to depth in most cases.

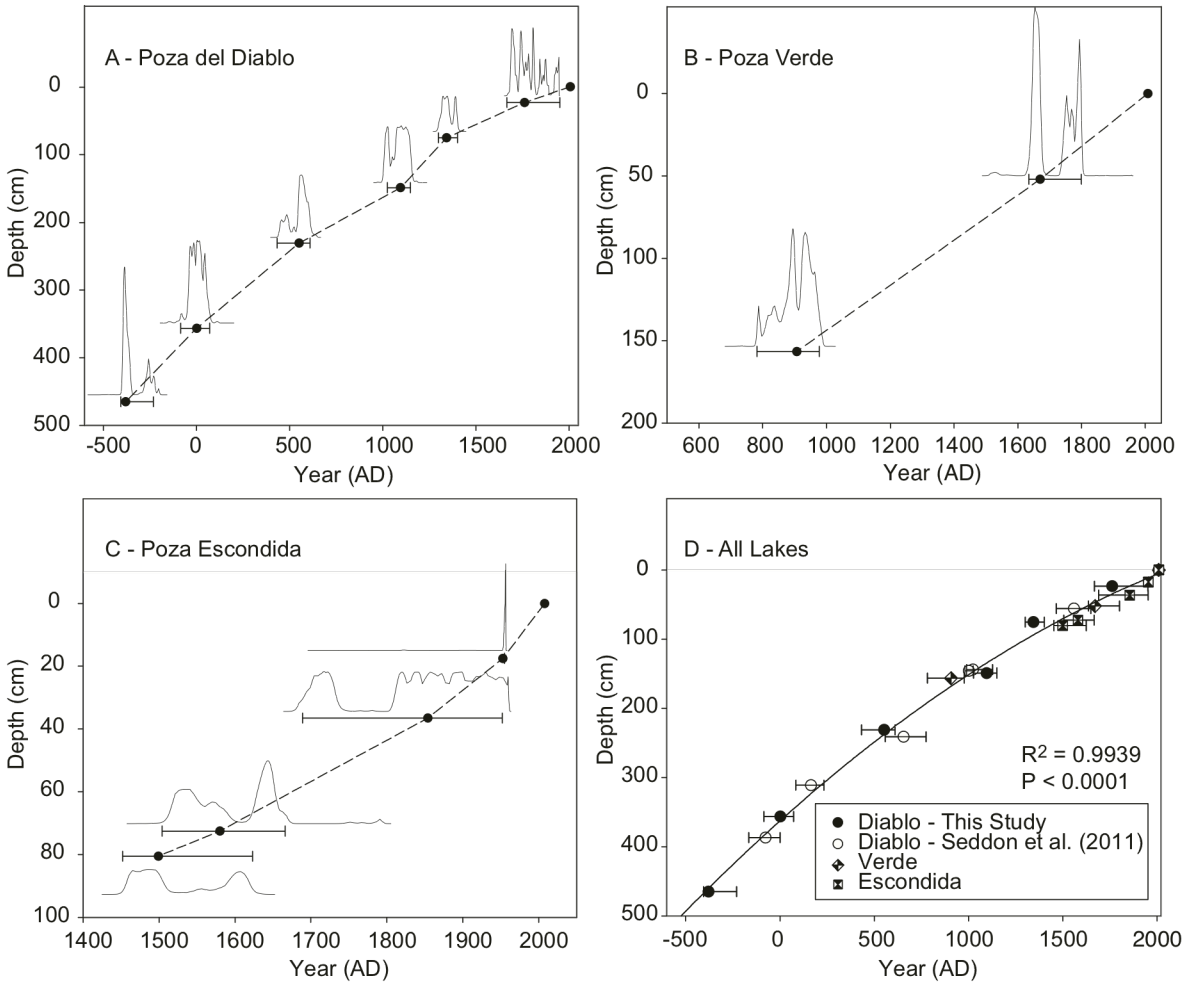


**Figure 3:** Age vs. depth plots for Poza del Diablo, Poza Verde, and Poza Escondida calibrated radiocarbon samples. Probability distributions for each sample are plotted next to the data point in panels A-C using the southern hemisphere atmospheric calibration curve or the spliced southern hemisphere/southern hemisphere bomb calibration curve. Panel D shows all calibrated radiocarbon ages from all samples used in this study as well as the published radiocarbon ages from Seddon et al., 2011. Seddon et al. (2011) radiocarbon ages were recalibrated for this figure to ensure consistent treatment of all samples.

*Lithology*

We observed minimal visually distinct lithological changes in the sediment cores that we recovered from Poza del Diablo (Figure 4). The upper ~ 3.5 m sediment sequence that is the focus of our investigation consists of pink, gelatinous to clay-like matrix material with white nodules or clasts that appear inorganic. Some terrestrial plant macrofossils were present, but the sediments did not resemble peat deposits that would be typical of a mangrove swamp. This is in contrast to the core descried by S11, which was made up of two distinct lithologies characterized by a significant and readily identified visual boundary at 145 cm depth. Above this level the S11 core lithology is similar to that observed in our cores, but below 145 cm the S11 core consists of a dark organic mangrove peat material with abundant roots and shoots preserved.

Sediments from Poza Escondida appear to be representative of mangrove peat throughout the entire 83 cm sequence that was recovered. The Poza Verde surface sedimentary unit is a lightly colored tan, gelatinous material with minimal sedimentary structure to a depth of approximately 50 cm, below which sediments transition to mangrove peat, similar to the transition described in S11 for that Poza del Diablo core at 145 cm.

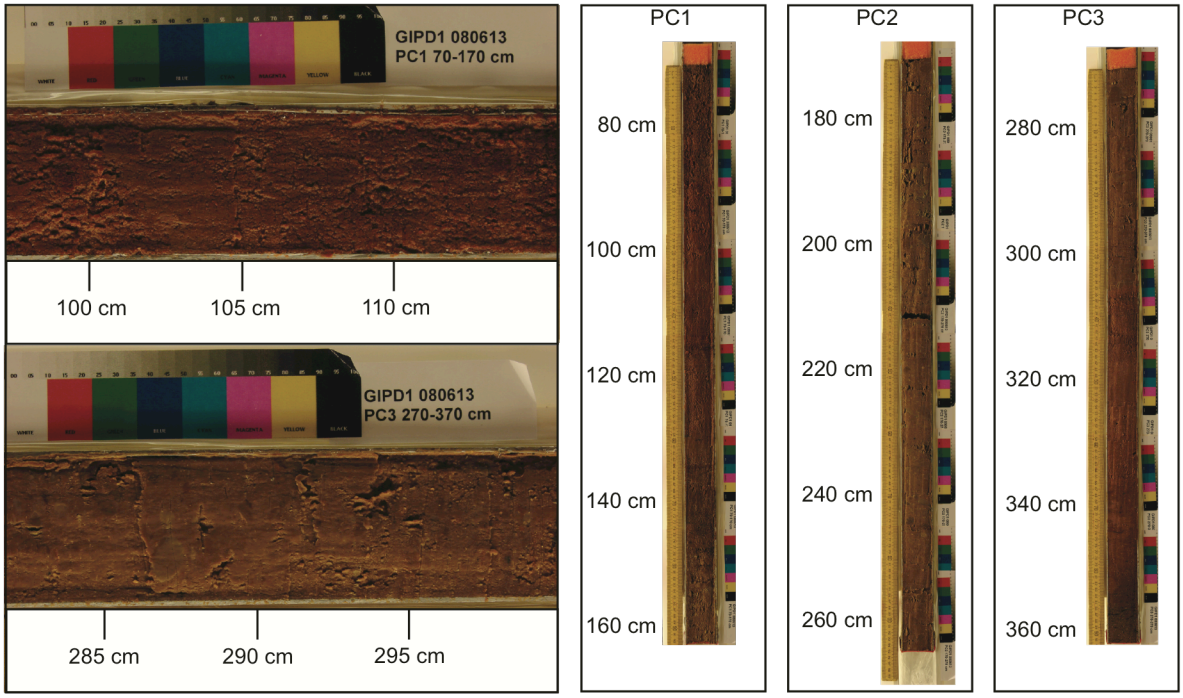


**Figure 4:** Close-up images of two sediment intervals from Poza del Diablo (left) and whole core images (right) showing most of the sediment sequence analyzed at Poza del Diablo.

*n-Alkane Distributions and δD values*

$n$C$_{29}$ is the dominant *n*-alkane over the entire sediment sequence at Poza del Diablo, and typically makes up 30 to 40 % of the sum-total of the *n*-alkanes, with $n$C$_{23}$, $n$C$_{27}$, and $n$C$_{31}$ of secondary importance (Figure 5). A distinct change in *n*-alkane relative abundance occurs after ~ 1550 AD, when $n$C$_{31}$ concentrations increase significantly and reach levels comparable to $n$C$_{29}$. The 400-year period from 1550 – 1950 AD stands out from each of the previous 400-year periods from this perspective (Figure 5).

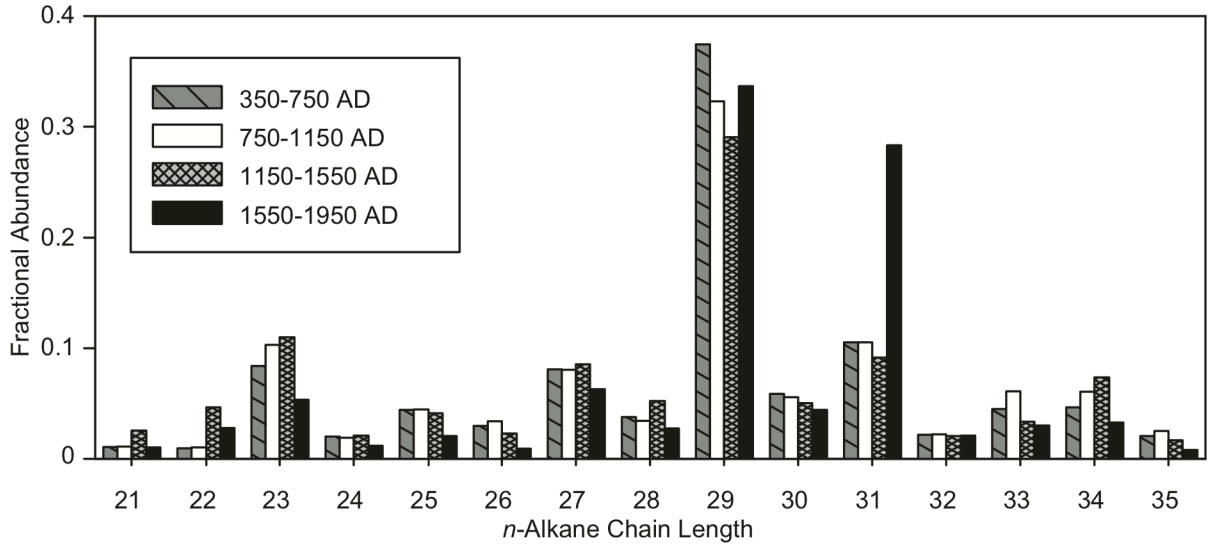


**Figure 5:** Fractional abundance of *n*-alkane distributions in Poza del Diablo sediment for four non-overlapping 400-year time blocks.

Examining the time series records of *n*-alkane concentrations and average chain length illustrates these changes in more detail (Figure 6 B-F). Average chain length (ACL), $C_{31}/C_{29}$, and $nC_{23}$, $nC_{29}$, and $nC_{31}$ abundances are all relatively constant from 0 to 1200 AD, with only minor variations observed (Figure 6 B-F). From ~ 0 – 200 AD, a decrease in $nC_{29}$ concentrations occurred at the same time that $nC_{29}$ δD values ($\delta D_{C29}$) declined from ~ -150 ‰ to -175 ‰, after which both values increased between 200 and 400 AD (Figure 6 A, E). Minimal changes occurred in alkane abundances and ratios between 400 and 1100 AD, after which time $\delta D_{C29}$ values increased to -140 ‰ at 1200 AD. After 1200 AD ACL values decreased from ~ 28 to 26, at the same time that $\delta D_{C29}$ values decreased to ~ -170 ‰, and both $nC_{23}$ and $nC_{29}$ concentrations increased. Neither $nC_{31}$ concentrations nor the $C_{31}/C_{29}$ ratio changed at this time. At approximately 1500 AD, the $nC_{31}$ concentration increased and approached the $nC_{29}$ concentration, which is most clearly observed in the $C_{31}/C_{29}$ ratio (Figure 6 C and D). At this

same time $\delta D_{C29}$ values began a steady increase to the present day maximum values near -130 ‰, while $n C_{23}$ concentrations decreased, causing the ACL value to also increase and reach mean values slightly greater than those prior to 1200 AD due to the contribution from increased $n C_{31}$ deposition (Figure 6 B and F). After 1800 AD, $n C_{29}$ and $n C_{31}$ both declined at approximately the same rate, resulting in little change in the $C_{31}/C_{29}$ ratio and ACL values, and no major change in the rate of increase in the $\delta D_{C29}$ values (Figure 6 A-E). Although we did not measure $\delta D_{C29}$ values in the surface sediments due to the presence of co-eluting compounds, we did measure $\delta D_{C29}$ values in two leaf samples from *Conocarpus erecta*, the dominant mangrove tree surrounding the lagoon at present, and found values of -121 ± 6 ‰ and -106 ± 2 ‰. Although limited, the few $\delta D_{C29}$ values from Poza Escondida are in general agreement with the increasing trend observed at Poza del Diablo, but hydrocarbon concentrations were not measured in Poza Verde or Poza Escondida (Figure 6 A).

**Figure 6:** (next page) Hydrocarbon and taraxerol concentration data from Poza del Diablo and Poza Escondida. A) $\delta D_{C29}$ values from Poza del Diablo (black circles) and Poza Escondida (white circles). Error bars represent the standard deviation of replicate measurements. B) Average chain length from Poza del Diablo calculated as the amount-weighted contribution from *n*-alkanes from $n C_{17} - n C_{35}$. C) The ratio of $n C_{31}$ concentration to $n C_{29}$ from Poza del Diablo. D-F) Concentrations of $n C_{31}$, $n C_{29}$, and $n C_{23}$ alkanes in ng/g dry sediment from Poza del Diablo. G) Taraxerol concentrations from Poza del Diablo in ng/g dry sediment.

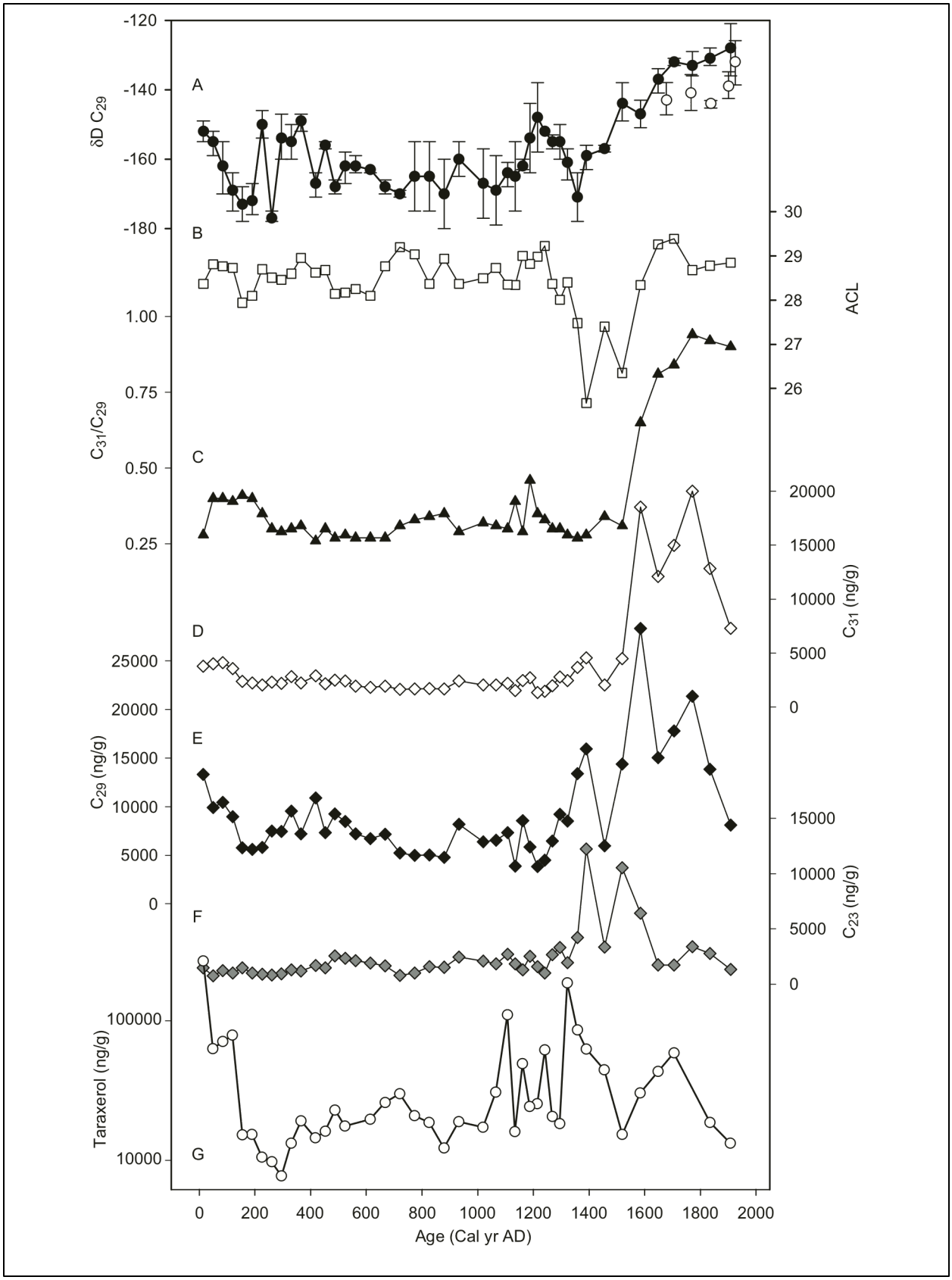
δD C29
-120
-140
-160
-180
A
B
ACL
30
29
28
27
26
C31/C29
1.00
0.75
0.50
0.25
C
D
C31 (ng/g)
20000
15000
10000
5000
0
25000
20000
15000
10000
5000
0
C29 (ng/g)
E
F
C23 (ng/g)
15000
10000
5000
0
Taraxerol (ng/g)
100000
10000
G
0
200
400
600
800
1000
1200
1400
1600
1800
2000
Age (Cal yr AD)

*Alcohol Distributions and δD Values*

Taraxerol concentrations vary greatly over the length of the sediment sequence from Poza del Diablo (Figure 6 G, note log scale). From 0 – 300 AD concentrations fell from more than 100 μg/g dry sediment to less than 3 ug/g in parallel with the decline in $n$C$_{29}$ concentration (Figure 6E) and $\delta D_{C29}$ values (Figure 6 A). Concentrations remained low, but variable until 1000 AD, after which marked increases occurred with values exceeding 10 μg/g. At 1500 AD a local minimum concentration of 2.7 μg/g occurred at the same time that $n$C$_{23}$ concentrations were near maximum, and just prior to the large shifts in $n$C$_{29}$ and $n$C$_{31}$ concentrations and the $n$C$_{31}$/ $n$C$_{29}$ ratio (Figure 6). Taraxerol concentration then increased to more than 35 μg/g near 1700 AD and then declined to very low levels towards the present sediment/water interface.

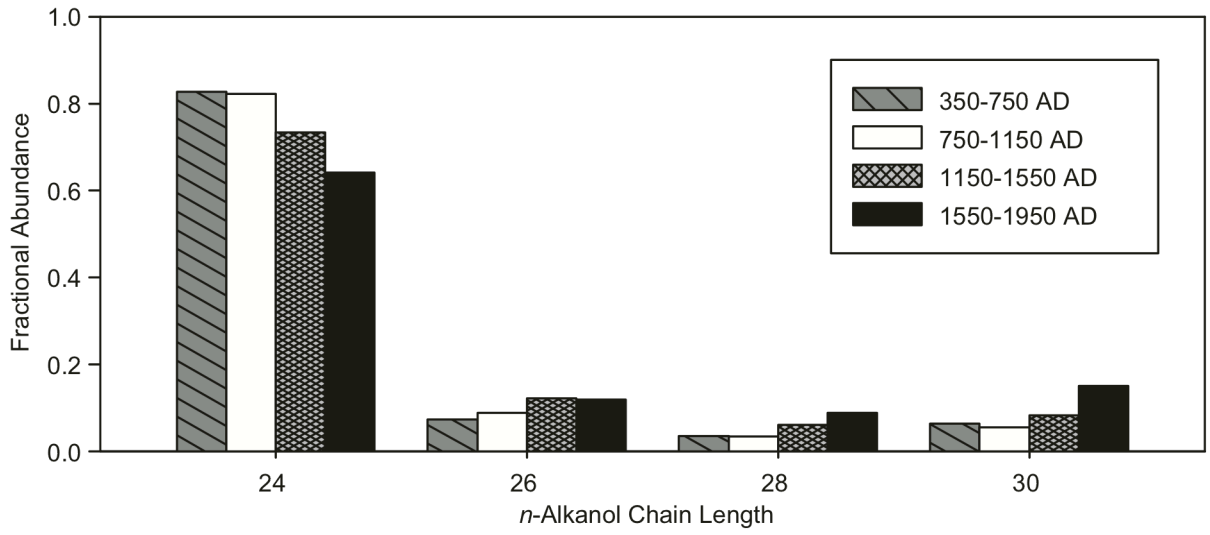


**Figure 7:** Fractional abundance of *n*-alkanol distributions in Poza del Diablo sediment for four non-overlapping 400-year time blocks.

The distribution pattern of *n*-alkanols is dominated in all sediment samples by $n$C$_{24}$-OL. Examining the same 400-year time intervals used to identify changes in the distribution of n-

alkanes shows that the relative abundance of $n$C$_{24}$-OL was consistently highest (Figure 7). At routine sample concentrations, no *n*-alkanols other than even carbon number compounds from $n$C$_{24}$-OL – $n$C$_{30}$-OL were above the detection limit, and examination of a typical neutral fraction chromatogram (after aminopropyl column separation) (Figure 8) shows minimal compounds other than these four *n*-alkanols, taraxerol, and compounds that are tentatively identified as glycolipids based on near identical mass spectra to published values from sediments from Ace Lake, Antarctica (Sinninghe-Damste et al., 2001) and also described in sediments from Lake Malawi (Castañeda et al., 2011). Dinosterol concentrations were generally too low relative to other co-eluting compounds to permit accurate quantification, but qualitatively, concentrations were highest near the sediment/water interface and diminished with depth, and no dinosterol was detected in sediments prior to ~1000 AD.

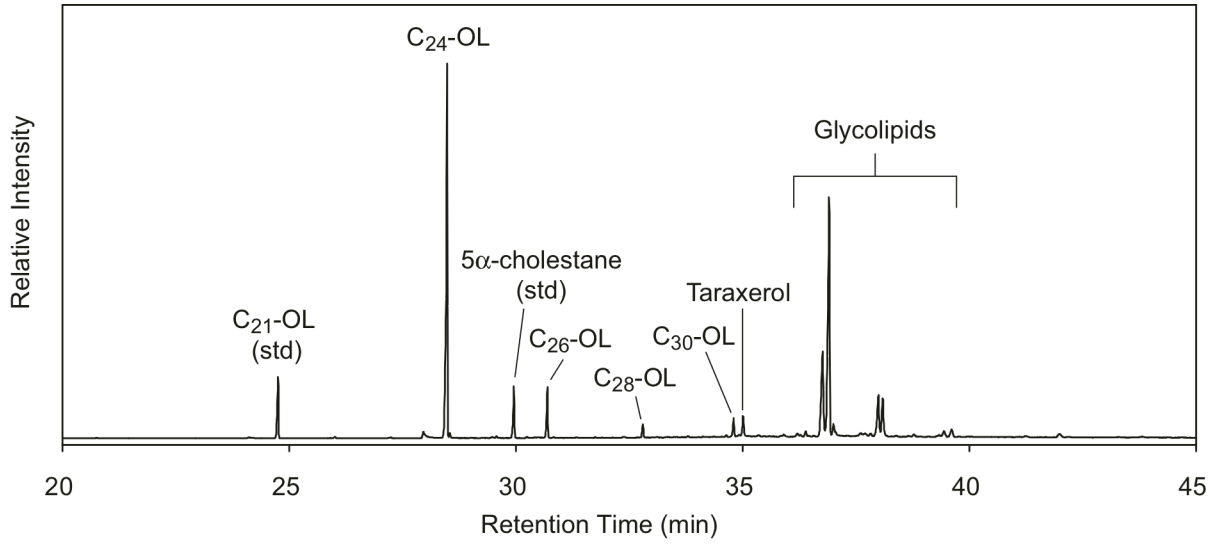


**Figure 8:** Example chromatogram of Poza del Diablo sediment showing neutral fraction after aminopropyl column separation from sample at 113.5 cm depth or 1215 AD. Dinosterol and $n$C$_{29}$ are below the detection limit in this example, but are present.

*n*$C_{24}$-OL δD ($\delta D_{C24OL}$) values and concentration profiles both increased from 0 to 500 AD, after which the rate of increase slowed, but continued until approximately 1000 AD (Figure 9 A and B). Between 1100 and 1500 AD, $\delta D_{C24OL}$ values were more variable and more negative values were measured, while *n*$C_{24}$-OL concentrations declined in a single step excursion to lower values. A local maximum occured in both records at 1500 AD followed by continued decline to approximately 1850 AD. $\delta D_{C24OL}$ values then increased in the surface sediments, but surface *n*$C_{24}$-OL concentrations were not measured. Dinosterol δD values ($\delta D_{Dino}$) from Poza del Diablo generally followed a similar pattern to $\delta D_{C24OL}$ values, although the number of samples decreases with depth due to reduced dinosterol abundance in the sediments (Figure 10 A). $\delta D_{Dino}$ values from Poza Verde and Poza Escondida were similar to one another, but both were more negative than dinosterol from Poza del Diablo (Figure 10 A). Taraxerol δD ($\delta D_{Tarax}$)values from all three lakes were similar during periods where temporal overlap occurs, although the Poza Verde samples show increased variability and more depleted values from 1800 AD to the present (Figure 10 D). The general pattern of $\delta D_{Tarax}$ values from the three lakes is for decreasing values from approximately 1200 to 1400 AD through to 1850 AD, followed by an increase to the present sediment/water interface (Figure 10 D).

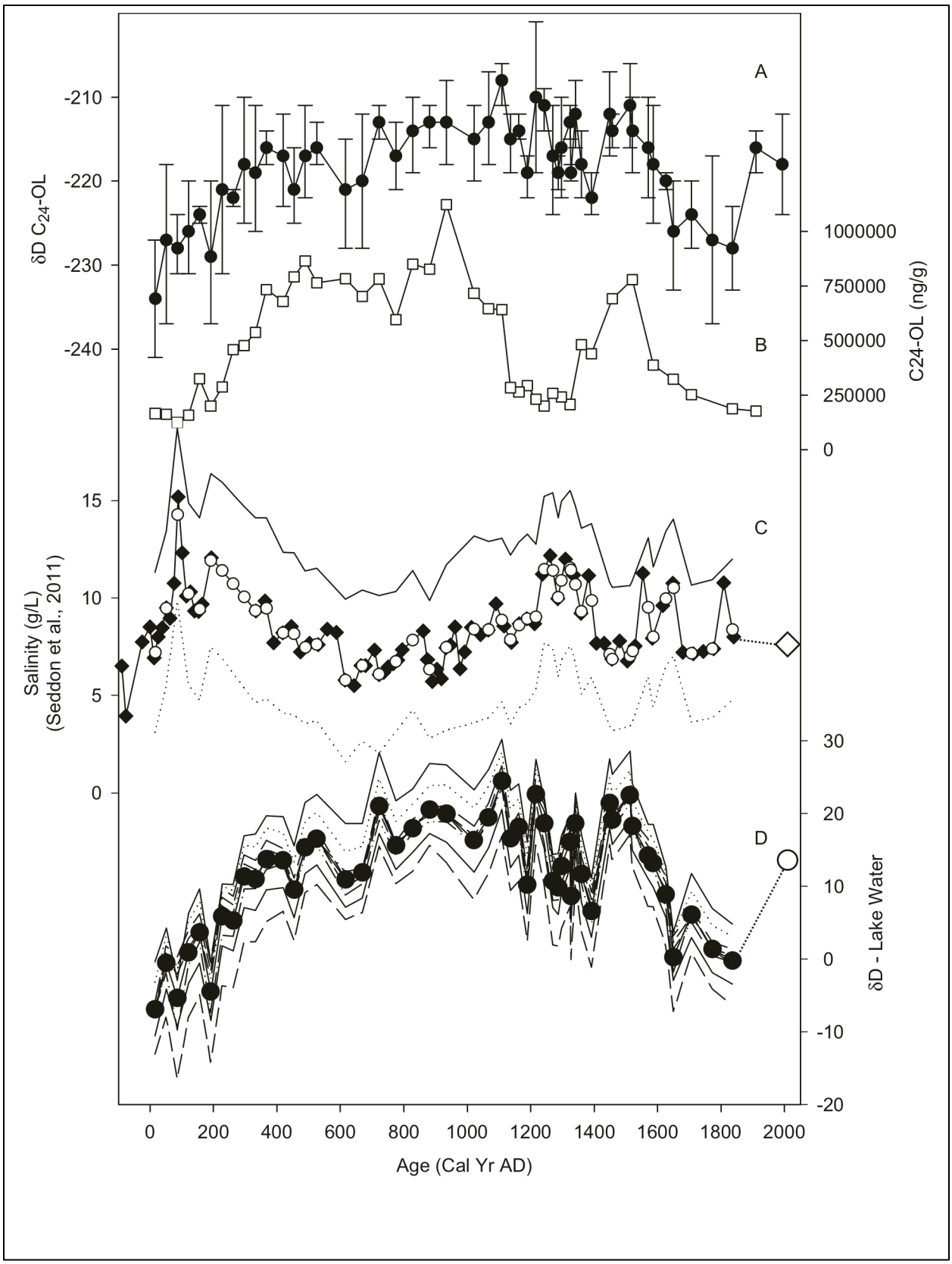
A
B
C
D
δD $C_{24}$-OL
-210
-220
-230
-240
C24-OL (ng/g)
1000000
750000
500000
250000
0
Salinity (g/L)
(Seddon et al., 2011)
15
10
5
0
δD - Lake Water
30
20
10
0
-10
-20
0
200
400
600
800
1000
1200
1400
1600
1800
2000
Age (Cal Yr AD)

**Figure 9:** (preceding page) A) $\delta D_{C24OL}$ values from Poza del Diablo. Error bars are the standard deviation of replicate measurements. B) Concentration of $n$C$_{24}$-OL in ng/g dry sediment from Poza del Diablo. C) Salinity reconstruction from diatom assemblages (black diamonds) (Seddon et al., 2011). White circles are the result from linear interpolation of the salinity reconstruction to match the sampling interval of the $n$C$_{24}$-OL record. Error envelopes are based on the maximum and minimum ranges in the salinity reconstruction after linear interpolation to the $n$C$_{24}$-OL sampling interval. Modern lake water salinity is shown by the large white diamond. D) Poza del Diablo lake water δD values as calculated from (A) and (C) (black circles). Error bars are the range of possible values assuming variable slopes for the relationship of the hydrogen isotope fractionation factor between $n$C$_{24}$-OL and lake water with salinity. White circle is the modern lake water δD value.

**Figure 10:** (next page) A) $\delta D_{Dino}$ record from Poza del Diablo (black circles), Poza Verde (white circles) and Poza Escondida (gray circles) all plotted on the same y-axis. Error bars represent the standard deviation of replicate measurements. B) $\delta D_{Lake}$ value from Figure 9 D replotted here for comparison. C) Salinity plot from Figure 9 C replotted here for comparison. D) $\delta D_{Tarax}$ record from Poza del Diablo (black squares), Poza Verde (white squares) and Poza Escondida (gray squares) all plotted on the same y-axis. Error bars represent the standard deviation of replicate measurements.

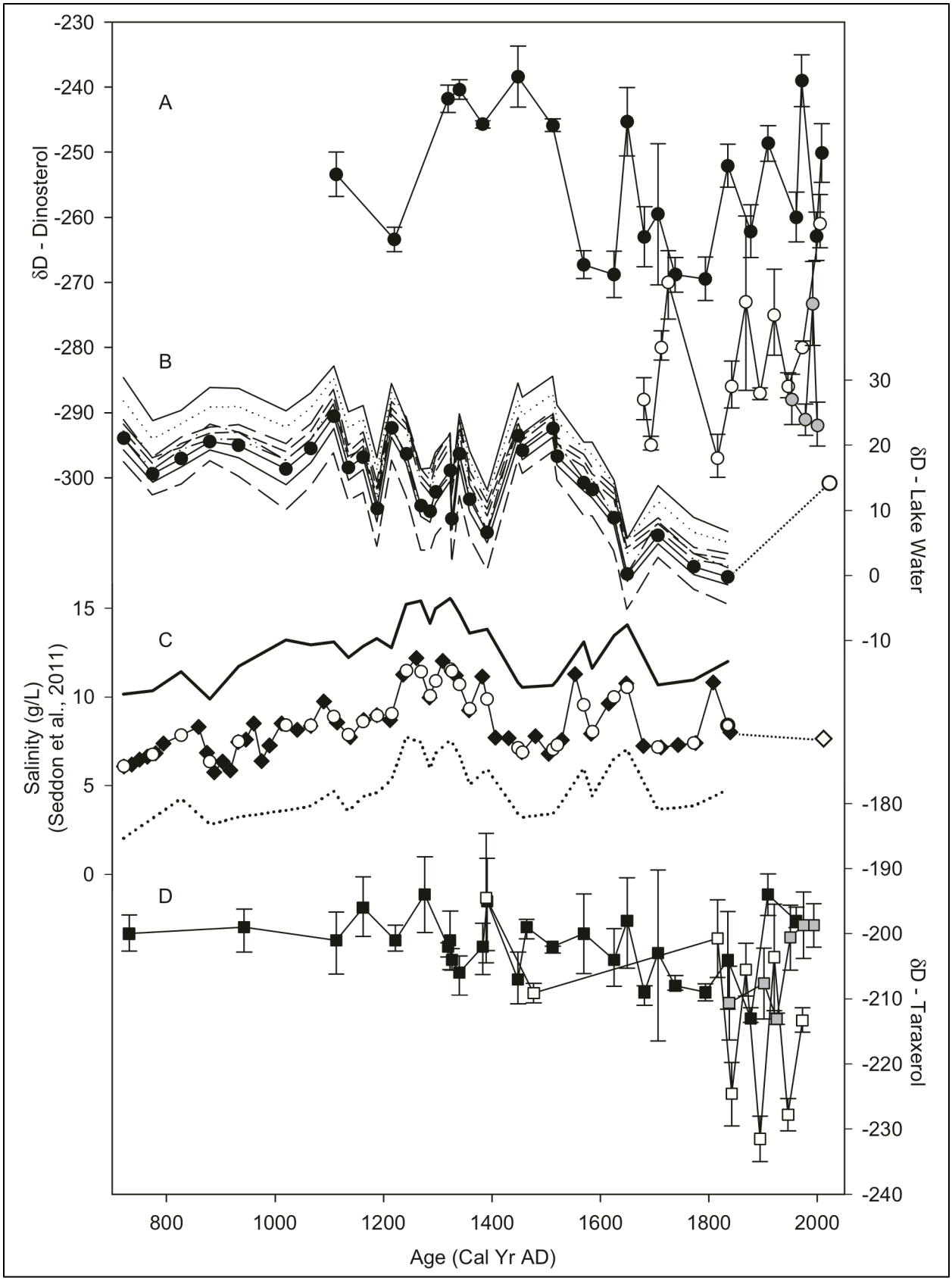
A
B
C
D
δD - Dinosterol
δD - Lake Water
Salinity (g/L)
(Seddon et al., 2011)
δD - Taraxerol
Age (Cal Yr AD)
-230
-240
-250
-260
-270
-280
-290
-300
30
20
10
0
-10
15
10
5
0
-180
-190
-200
-210
-220
-230
-240
800
1000
1200
1400
1600
1800
2000

## Discussion

*Sedimentology and Hydrology*

The most obvious and perplexing feature of the sediments we recovered from Poza del Diablo is the striking dissimilarity from sediment cores described in the recent study of diatoms from the same part of Poza del Diablo by Seddon et al. (2011). As described above, the S11 sediment sequence is characterized by a distinct lithological transition at approximately 145 cm depth that we do not observe in our sediment cores. In order to facilitate accurate comparison of our data with the results from the S11 data we developed a new age model for the S11 samples based on the published radiocarbon ages following the same protocol that we applied to our samples, with the major difference in approach being a forced fit of the surface sediment age to the year of core recovery. The differences in the two sedimentary units described in S11 and characterized with bulk sediment carbon isotope data are clear and distinct between the mangrove peat below 145 cm and the microbial mat material above, and we are doubtful that we have simply overlooked the boundary in our sediment core. At the same time, there is a striking apparent anti-covariance between the S11 diatom-based salinity reconstruction (Figure 9 C) and our $\delta D_{C24OL}$ values and concentration data (Figure 9 A, B). There is also good agreement in the age/depth plots for the two cores (Figure 3D), both of which argue that both sediment cores are recording the same hydrological features. One possible explanation for the differing lithologies in the two closely spaced cores may be the dynamic nature of mangrove swamps in protected and shallow brackish systems. The areal photograph of Poza del Diablo (Figure 2) shows several isolated mangrove tree-stand islands within the lake and in the surrounding vicinity, and the shorelines in the lake are indistinct, with open lake water gradually giving way to permanently

flooded mangrove forest. We suspect that the islands and shorelines may be transient features on centennial timescales, and that perhaps the particular location where the S11 core was recovered was previously in a location similar to the modern flooded mangrove forest even as our coring site remained an open water environment. This would explain the carbon isotope data from S11 showing significantly more depleted values prior to 1000 AD, which might be expected in a flooded mangrove area, while at the same time permitting a diatom-based salinity record that shows similar patterns of variability to those observed in our $n$C$_{24}$-OL concentration and δD records, since the diatoms would be living in the overlying water, and therefore be reflective of the salinity (Figure 9 A-C).

The sediment transition in Poza Verde at ~ 50 cm may result from a similar chance recovery of a former isolated mangrove stand. At the time of sampling for lipid analysis, this transition was interpreted as an indicator of a significant change in basin geomorphology, and no effort was therefore made to purify aquatic lipids from depths below this level, and only minimal terrestrial plant markers were used. However, given the more detailed assessment of the differences in the Diablo core used in this study compared to the one used in S11, and the apparent coherence of the diatom and $n$C$_{24}$-OL records, it might be worthwhile to revisit the Verde sediment in the future and extend the lipid chemistry measurements deeper. Poza Escondida sediments are uniform mangrove peat, and the only limitation at this site was the length of the recovered core; although the sediment deposit was found to be much deeper through probing, recovery of additional material was prevented due to time constraints.

The fact that sedimentation rates for all sediment cores from the present study, as well as the Poza del Diablo core from S11 are all so similar is evidence against the possibility that any

major changes in in the geomorphic setting of the lakes occurred over the period represented in the sediment sequences from each lake. If such changes had occurred, perhaps due to tectonic activity or long-shore drift processes, we would likely observe sediment unconformities or rapid changes in sedimentation rates. For Poza del Diablo, although some changes in the degree of hydrologic communication with the ocean have likely occurred over time, and tenuous surface connection with the ocean probably occurred either permanently or on tidal cycles at various times in the past, the primary factor controlling the balance between the fresh and saltwater sources to the lake is likely to have always been the relative intensity of subsurface groundwater infiltration from the two sources. Freshwater inputs are likely to be controlled by the quantity of groundwater draining from the highlands to the north of the lake site, and therefore the precipitation rate. Saltwater intrusion to the lakes, on the other hand, is likely to have been regulated by relative sea level. Eustatic sea level has changed on millennial timescales in the late Holocene due to continuing planetary isostatic adjustment following major deglaciation. But modeled millennial scale changes in sea level are only 15 cm over the period represented by our Poza del Diablo sediment record and the rate of change is slow (Seddon et al., 2011). Relative sea level has likely changed as a result of changes in shoreline elevation associated with subsidence as the island cools and moves away from the hot spot volcanism, but these changes are not well quantified. On interannual and decadal timescales, the range of sea surface heights recorded since 1960 is approximately 40 cm, with high stands associated with El Niño events (Carton and Giese, 2008). We therefore suggest that ENSO is likely to represent the largest component of decadal and centennial scale changes in relative sea level.

*Terrestrial Biomarkers*

The vegetation surrounding Diablo, Escondida, and Verde is characterized by the mangroves *Conocarpus erecta*, *Rhizophora mangle*, and *Laguncularia racemosa*. Each of these species produces leaf wax with different proportions of *n*-alkanes. $n$C$_{29}$ is the dominant alkane in *L.racemosa* (Rafii et al., 1996), which produces this chain length in much greater quantities than any other and has been reported to make up more than 50% of the total hydrocarbon fraction in these leaves, or to be present at concentrations up to three times greater than $n$C$_{27}$ (Dodd et al., 1998; Silva and Madureira, 2012). However, $n$C$_{29}$ is also the dominant alkane in *C.erecta* and *R.mangle*, although these species also make significant quantities of $n$C$_{31}$ (Dodd et al., 1995; Dodd et al., 1998; Rafii et al., 1996; Versteegh et al., 2004). In contrast, although taraxerol is produced by other terrestrial plant types, among mangroves it is produced in extreme abundance only by the *Rhizophora* genus, and has been shown to covary in sedimentary deposits with *Rhizophora* pollen (Versteegh et al., 2004).

The large changes in the distribution patterns of the *n*-alkanes in the Diablo sediment record are indicative of significant changes in the makeup of the terrestrial plant communities surrounding the lake over time. The most significant change is apparent after 1500 AD in the C$_{31}$/C$_{29}$ ratio, which also coincides with large increases in $n$C$_{23}$, $n$C$_{29}$, and $n$C$_{31}$ (Figure 6 C-F). These distribution and concentration changes also occur at the same time as the largest signal in the $n$C$_{29}$ δD record – an increase of over 30 ‰ (Figure 6 A). While it may be tempting to interpret these isotope changes in the context of changing hydrology, and changing hydrology is probably at least partially responsible for driving this signal, since shifting vegetation assemblage can be the primary driver of changing leaf wax δD values in sediments (e.g. (Nelson

et al., 2013) we cannot differentiate between these two possibilities to draw a definitive explanation for the observed trends. While the straightforward explanation for the large increase might be significant drying, it could also simply be a shift in species composition, which might have been driven by a variety of other factors, including even the possibility of increased precipitation. The increase in the total abundance of *n*-alkanes might also reflect changes in aridity, since overall alkane production and increased leaf thickness has been observed to increase in leaves with increasing aridity (Hoffmann et al., 2013; Naidoo, 2010), but this possibility also cannot be distinguished from the potential influence of species changes. While the alkane concentration and isotope data may be used to identify the timing of changes in the Diablo sediment, determining the exact nature of those changes requires additional proxy records.

In contrast to alkanes, taraxerol is specific to *Rhizophora* in mangrove environments (Versteegh et al., 2004). The decline in taraxerol concentrations from 1500 AD to the present occurred at the same time as the increase in the concentrations of $nC_{29}$ and $nC_{31}$, and the increase in the $C_{31}/C_{29}$ ratio, as well as the $nC_{29}$ δD values (Figure 6). The decline in taraxerol implies a declining fractional contribution from *Rhizophora* mangroves to the $nC_{29}$ alkanes in the sediment, and could potentially be the cause of the entire $\delta D_{C29}$ value signal after 1500 AD. The gradual decline in $\delta D_{Tarax}$ values in Poza del Diablo from ~ 800 AD to 1850 AD (Figure 10 D) could be attributable to a steady decrease in the δD of source water over the same interval, or it might also be attributable to an increase in the salinity of lake water over that time, since increasing salinity has been linked to increasing isotope fractionation for *n*-alkanes from mangrove leaves (Ladd and Sachs, 2012), and would presumably extend to taraxerol from mangrove trees as well. The salinity effect may explain the more negative values for Poza Verde taraxerol, since salinity in

that lake is 44 PSU compared to 7.4 in Diablo (Table 1). Why the Escondida $\delta D_{Tarax}$ data is more or less equivalent to the Diablo data is less clear, although we point out that Escondida is much smaller than either Verde or Diablo (Figure 2), and may therefore receive a greater proportion of terrestrial organic matter that is not relying on the lake as source water. In any case, the reduced ambiguity surrounding the possible sources of taraxerol makes the δD record more easily interpretable in the context of regional hydrology. A more complete assessment of Galápagos hydroclimate in the preindustrial era can be obtained by combining the mangrove δD variations with those in algal biomarkers.

*Algal Biomarkers*

The most abundant compounds detected by gas chromatography in the Poza del Diablo sediments were $n$C$_{24}$–OL and the compounds we tentatively identify as glycolipids based on the near identical mass spectra for these compounds to those published from samples collected at Ace Lake, Antarctica (Sinninghe-Damste et al., 2001). In our acetylated sample we observe major ion fragments at *m*/z 57, 74, 85, 116, 153, and 245 at nearly identical relative abundances to published spectra. The Ace Lake GC-MS mass spectra also contained a fragment at *m*/z 368, which the authors identified a 22-carbon unit aliphatic side chain that was ether-bound to the sugar moiety characterized by the other ion fragments. Glycolipid presence in the core was associated with high concentrations of $n$C$_{22}$–OL, and the authors used this observation to argue that this *n*-alkanol occurred as a degradation product of the associated glycolipids. The mass spectra for the glycolipids in the Diablo sediment does not contain a major ion fragment at *m*/z 368, but does contain a major fragment at *m*/*z* 396. This difference implies a carbon chain that is

28 daltons larger than that described in Ace Lake, which would support the notion that the $n$C$_{24}$–OL in the Diablo sediment is a degradation product of this compound, since $n$C$_{24}$–OL is also 28 daltons larger than $n$C$_{22}$–OL due to the presence of two additional methylene groups. Given the near perfect match for the mass spectra from the Ace Lake sediments we identify this glycolipid as tetracosanyl 3-O-methyl-α-rhamnopyranoside. Although it might be unusual to consider that a compound found in an Antarctic lake could also be found in the Galápagos, these compounds have also been detected in tropical Lake Malawi (Castañeda et al., 2011). The fact that we observe *n*-alkanol moieties with a different carbon number may itself be something that is worthy of additional study if these compounds can be found elsewhere in high abundance. But given the overwhelming dominance of $n$C$_{24}$–OL in the Diablo sediments over other *n*-alkanols, and the associated extreme abundance of tetracosanyl 3-O-methyl-α-rhamnopyranoside and other associated glyclolipids, we interpret the $n$C$_{24}$–OL in the Diablo sediments as deriving primarily from cyanobacteria, especially since $n$C$_{24}$–OL is typically not the most abundant *n*-alkanol produced by higher plants, and those that are more common to higher plants, such as $n$C$_{28}$–OL and $n$C$_{30}$–OL, are present only at low concentration.

Dinosterol is a known biomarker for dinoflagellates, although it is also produced by other types of aquatic organisms including certain diatoms (Rampen et al., 2010; Volkman, 2003; Volkman et al., 1998). Among algal biomarkers, dinosterol δD values have received considerable attention, and these have been the subject of regional and global calibration efforts to understand the influence of salinity on D/H fractionation in algae (Nelson and Sachs, *Chapter 3;* Sachs and Schwab, 2011), as well as application as a proxy for paleohydrology in Palau (Sachse et al., 2009; Smittenberg et al., 2011). Interestingly, dinosterol fractionation factors

calculated from surface sediment and suspended particle sample δD values and measurements of δD values from modern lake water collected at Poza del Diablo show an anomalous relationship with salinity compared to virtually all other sample locations (Nelson and Sachs, *Chapter 3*). Two other dinosterol fractionation factors calculated from surface sediment and lake water δD values are also outliers in the otherwise apparently global trend of decreasing D/H fractionation with increasing salinity, but these are both freshwater sites (Nelson and Sachs, *Chapter 3*). The anomalous nature of the α vs. salinity relationship for dinosterol in Poza del Diablo might suggest the presence of more freshwater-adapted dinosterol producers in the relatively low salinity environment of Poza del Diablo (S = 7.4). Given this complication, we do not attempt to interpret the Diablo $\delta D_{Dino}$ record in the context of a paleosalinity signal. However, we also note that within a calibration set from surface sediments in tropical Pacific lakes, that $\delta D_{Dino}$ values were well correlated with lake water δD values, including the sample from Poza del Diablo (Nelson and Sachs, *Chapter 3*). Modern dinosterol fractionation factors from surface sediment in Poza Verde and Poza Escondida also do agree with the global trend of decreased fractionation at higher salinity (Nelson and Sachs, *Chapter 3*).

Given the known importance of salinity in influencing the magnitude of D/H fractionation in algal lipids, it is especially beneficial to the interpretation of our isotope data that a recent paleosalinity record was generated based on changing diatom assemblages in Poza del Diablo sediment (Figure 10 C) (Seddon et al., 2011). The record indicates that although some changes in salinity occurred over time, it remained relatively stable over the past 2 kyr, fluctuating between 5 and 10 g/L. This suggests that the $nC_{24}$–OL and $\delta D_{Dino}$ records may be interpreted without having to consider very large changes in salinity as a potential driving factor.

Qualitatively, the fact that $n$C$_{24}$–OL and dinosterol δD values from Poza del Diablo both declined from approximately 1500 to 1850 AD, and that those changes coincided with decreases in mangrove-derived taraxerol δD values, together suggest that the same external factors drove the common signal in all three lipids (Figure 9A, 10A, D).

Changing growth rates are a factor that must be considered in attempting to understand the δD records from the algal markers, but unfortunately what is known about this effect is complex and contradictory. Isoprenoid compounds produced by algae grown in batch cultures were shown to exhibit significant differences in D/H fractionation between nitrogen-limited and nitrogen-replete conditions, with the latter resulting in increased fractionation. Yet, acetogenic lipids from the same algal cultures were apparently insensitive to growth rate changes (Zhang et al., 2009). This finding was broadly consistent with a previous batch culture experiment with coccolithophorids that showed that higher growth rates were associated with lowered δD values (Schouten et al., 2006). The apparent difference between isoprenoid and acetogenic compounds could not be assessed since only acetogenic compounds were analyzed (Schouten et al., 2006). In contrast, growth stage has been shown to influence D/H fractionation dramatically, with alkenones produced during the exponential growth phase in culture experiments enriched by up to 40 ‰ over lipids produced during stationary growth (Wolhowe et al., 2009).

In a recent study, salinity-induced growth rate changes were cited to explain the apparently contradictory relationship observed between precipitation and δD values from an *n*-alkyl diol that was thought to be produced by eustigmatophytes (Romero-Viana et al., 2013). Increased precipitation at this site is correlated with decreased precipitation δD values and decreased salinity, both of which should contribute to decreased lipid δD values according to

conventional understanding (e.g. Sachse et al., 2012), yet the opposite relationship was observed. The complexities of growth rate changes might be called upon to explain some of the features of the $\delta D_{C24OL}$ and $\delta D_{Dino}$ records from Poza del Diablo, especially given the fact that $\delta D_{C24OL}$ values show opposing trends with salinity over much of the record. However, given the complementary data from the other biomarkers, we consider changes in the δD value of the lake water to offer the most plausible explanation, since a similar growth rate effect is unlikely to extend to mangroves. The $\delta D_{Tarax}$ signal would thus not be expected to mimic changes in the algal lipid (dinosterol and $n C_{24}$-OL) δD values if growth rate was a primary influence on the latter (Figure 9A, 10 A, D). At the same time, the lower δD values observed for the Poza Verde and Poza Escondida $\delta D_{Dino}$ records are consistent with a more conventional relationship between D/H fractionation and salinity, implying increased fractionation as compared to dinosterol from Poza del Diablo (Nelson and Sachs, *Chapter 3*).

*Quantitative isotope reconstructions from multiple biomarkers*

We attempted to combine the multiple isotope records and the available diatom-based salinity reconstruction (Seddon et al., 2011) to produce a single, internally consistent record of lake water δD values ($\delta D_{Lake}$) over time. Salinity is known to influence the magnitude of D/H fractionation in algal lipids, and although the slope of the regression between the fractionation factor and salinity is similar in most cases, it has not been definitively proven as a constant (Nelson and Sachs, *Chapter 3*). Slopes for hydrocarbons from cyanobacteria from Christmas Island were measured in the range of 0.007 to 0.009 per unit change in salinity (Sachse and

Sachs, 2008), while the slope for Chesapeake Bay dinosterol was 0.009 per unit change in salinity (Sachs and Schwab, 2011) and North American and global calibration efforts for brassicasterol and dinosterol gave slopes on the order of 0.007 (Nelson and Sachs, *Chapter 3*). If the slope of the relationship between D/H fractionation factor and salinity were known precisely, it would be possible to constrain the exact relationship between $\alpha$ and salinity with one $\alpha$ value that can be calculated using the surface sediment $\delta D_{C24OL}$ value in combination with the modern $\delta D_{Lake}$ value and salinity. This relationship could then be applied to down-core lipid isotope data provided that an independent constraint were available for salinity. We performed this calculation, but since the slope is not precisely known we used a range of possible values from 0.0002 to 0.0012 per unit change in salinity. This exceeds the probable range of slopes based on published calibrations, and is therefore a conservative estimate (Nelson and Sachs, *Chapter 3;* Sachs and Schwab, 2011; Sachse and Sachs, 2008). We then used this range of possible calibrations with the S11 salinity reconstruction to calculate a range of possible $\delta D_{Lake}$ values for the past 2 kyr (Figure 9 C, 10 B). In order to perform this calculation it was necessary to do a linear interpolation of the S11 salinity record to match the sampling interval of the $\delta D_{C24OL}$ record (Figure 9 C). Not surprisingly, given the small range of salinity variations implied by the S11 diatom record, the resulting $\delta D_{Lake}$ record shows similar trends and variability to the $\delta D_{C24OL}$ record (Figure 9 A, D). Nevertheless, the range of variability and absolute values of the reconstruction are now more easily interpreted in the context of modern hydrology. The $nC_{24}$–OL /S11 reconstructed $\delta D_{Lake}$ record also compares favorably with the independent dinosterol and taraxerol δD records from each lake (Figure 10).

To further evaluate the consistency and coherence of the environmental signal preserved in

the multiple biomarker isotope records, we followed the approach employed for $n$C$_{24}$–OL to constrain the relationship between taraxerol α values and salinity using an α value calculated from modern lipid and water δD values and the published slope of -0.0015 per unit change in salinity for *n*-alkanes from mangrove leaves (Ladd and Sachs, 2012). In this case, we assumed a possible range of slopes from -0.001 to -0.002 per unit change in salinity, which is also a wide margin based on the available data. Given these two calibrations for the relationship for D/H fractionation factor as a function of salinity, it is also possible to independently reconstruct both $\delta D_{Lake}$ and salinity using only the lipid isotope data since both mangroves and microautotrophs ought to use water with the same δD value and salinity. If the fractionation factor, α, is defined as $(\delta D_{lipid} + 1000)/(\delta D_{water} + 1000)$, and α may be described as a linear function of salinity for taraxerol and $n$C$_{24}$-OL, then these α-salinity calibrations may be substituted into the definition of α to give:

$$m_{Tarax}*salinity+b_{Tarax} = (\delta D_{Tarax} + 1000)/(\delta D_{Lake} + 1000)$$

$$m_{C24OL}*salinity+b_{C24OL} = (\delta D_{C24OL} + 1000)/(\delta D_{Lake} + 1000)$$

where $m_x$ and $b_x$ are the respective slope and intercept values of the α-salinity relationships for each lipid, $\delta D_{Lake}$ is the unknown δD value of the lake water, and $\delta D_{tarax}$ and $\delta D_{C24OL}$ are the measured values from the sediment biomarkers. This leaves two equations with two unknowns, $\delta D_{Lake}$ and salinity, which can be solved for. Assuming the range of possible slope and intercept values as constrained by measured modern surface sediments and $\delta D_{Lake}$ values we calculate a range of possible paleo-$\delta D_{Lake}$ values that agree well with the $\delta D_{Lake}$ values calculated from the

$\delta D_{C24OL}$ and the diatom-based salinity reconstruction from S11 (Figure 11A). The salinity reconstruction based on $\delta D_{Tarax}$ and $\delta D_{C24OL}$ values also agrees quite well with the independent salinity reconstruction based only on diatom assemblages, and performed on a different sediment core with a different sampling interval (Figure 11B). Given these reproducible results with different techniques we base further discussion of the environmental and climatic significance of our isotope data on these composite and quantitative records of past salinity and $\delta D_{Lake}$ values.

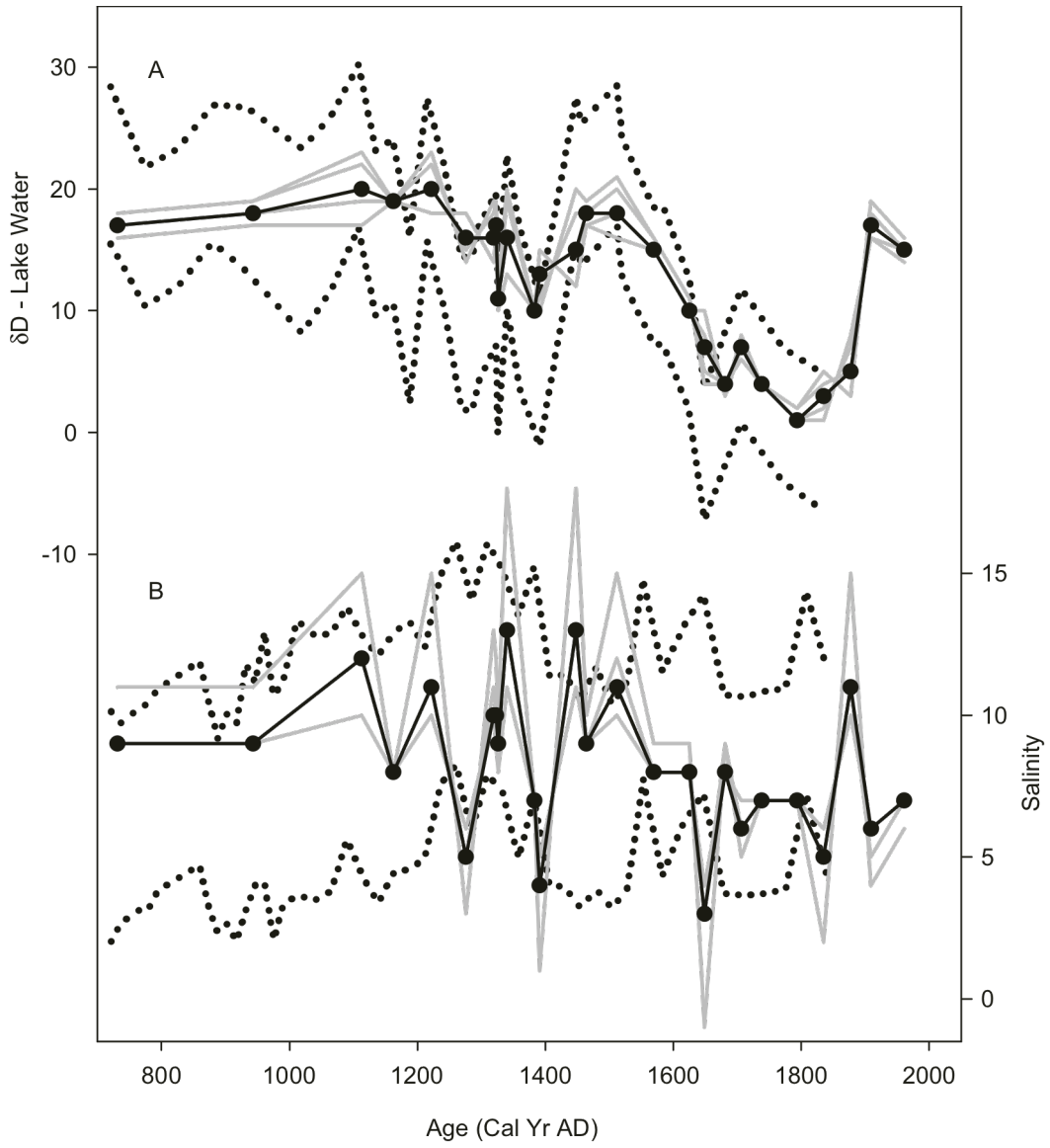


**Figure 11:** A) Reconstructed Poza del Diablo $\delta D_{Lake}$ values calculated from $n C_{24}$-OL and $\delta D_{Tarax}$ values (black circles) assuming a range of possible slopes for the relationship of α-salinity relationship for each lipid. Dotted lines are the maximum and minimum error envelopes from $\delta D_{Lake}$ as calculated from $\delta D_{C24OL}$ and S11 salinity. B) Salinity calculated from $\delta D_{C24OL}$ and $\delta D_{Tarax}$ (black circles). Error shown in gray as in (A). Dotted lines are the error envelopes in the published S11 salinity reconstruction on the original sampling interval.

*Galápagos hydroclimate variations during the last 2,000 years*

An intriguing result from our work at Poza del Diablo is the observation that increasing $\delta D_{Lake}$ values correspond with decreasing salinity over much of the 2 kyr record, particularly for the period prior to ~1500 AD (Figure 12 A, B). An explanation for this counterintuitive result might be found in the relationship between precipitation intensity, El Niño events, and sea surface height anomalies. Since Poza del Diablo is very near to the sea in both distance and elevation, the amount of salt-water intrusion into the system is a function of the position and height of the coastline, the hydraulic head from groundwater draining into the sea, and the local sea level. Changes in the position of the coastline are certainly a possibility, but one would expect major breaks in the coast to significantly alter the sedimentation rates and sediment character, of which we observe neither (Figures 3 and 4). Increases in rainfall in the absence of other changes would be expected to cause a decrease in the δD value of precipitation according to the amount effect (Dansgaard, 1964; Risi et al., 2008), while at the same time possibly increasing the freshwater head, which should either cause salinity to decrease or remain unchanged. If, however, the increases in precipitation were driven by El Niño events, they would be accompanied by transient increases in sea surface height on the order of up to 0.4 m for strong events (Carton and Giese, 2008), which could explain how the lake water could become saltier at the same time that $\delta D_{Lake}$ values decline.

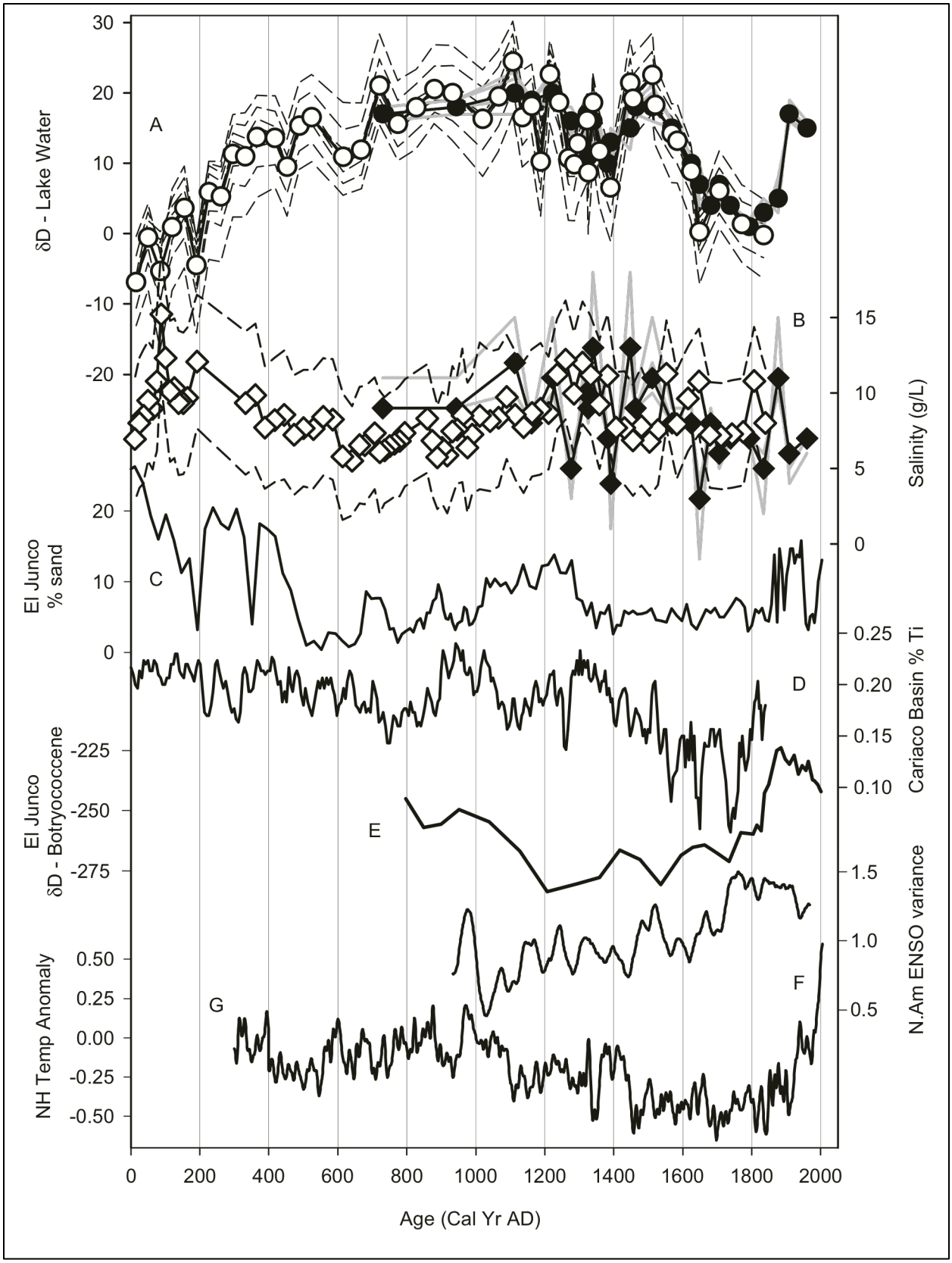
δD - Lake Water
A
B
Salinity (g/L)
El Junco
% sand
C
D
Cariaco Basin % Ti
El Junco
δD - Botryococcene
E
N.Am ENSO variance
NH Temp Anomaly
F
G
Age (Cal Yr AD)

**Figure 12:** (previous page) A) Reconstructed $\delta D_{Lake}$ from Poza del Diablo using the $n$$C_{24}$-OL/taraxerol approach (black circles) as well as the $n$$C_{24}$-OL/diatom salinity record from Seddon et al. (2011) approach (white circles). Errors are represented as in previous figures. B) Reconstructed salinity from Poza del Diablo showing the Seddon et al. (2011) diatom-based record (white diamonds) with the $n$$C_{24}$-OL and taraxerol based reconstruction (black diamonds). Errors are represented as in previous figures. C) Grain size record of % sand from El Junco Lake (Conroy et al., 2008). D) Cariaco Basin % titanium record (Haug et al., 2001). E) Botryococcene δD record from El Junco Lake (Sachs et al., 2009). F) ENSO variance reconstructed from the gridded network of tree ring – based Palmer Drought Severity Index reconstructions from North America (Li et al., 2011). G) Northern hemisphere temperature anomaly (Mann et al., 2008).

Comparing the Diablo $\delta D_{Lake}$ record with other records of paleoclimate changes in the region helps to confirm this interpretation. At El Junco Lake, on San Cristóbal Island, ~160 km to the east, increases in the contribution of sand size grains to the sediments are interpreted as an increase in strong El Niño, with one of the most active episodes of the Holocene peaking near 0 AD (Figure 12 C) (Conroy et al., 2008). The decline in percent sand from 0 to 700 AD at El Junco Lake was interpreted to mark decreasing precipitation due to decreasing El Niño activity, which is consistent with the observed increase in $\delta D_{Lake}$ values and decreasing salinity over this interval. Similarly, the increasing sand concentrations from ~ 1000 AD to 1300 AD corresponds with increasing salinity and decreasing $\delta D_{Lake}$ values in Poza del Diablo, although the decreasing trend in $\delta D_{Lake}$ values continues until approximately 1400 AD (Figure 12 A). After this time, the

coherence between the El Junco sand record and the Diablo salinity and $\delta D_{Lake}$ data become less clear, and the major decrease in $\delta D_{Lake}$ values from Poza del Diablo are not recorded in the El Junco sand. It may therefore be the case that while the period prior to 1500 AD is driven largely by variability of strong ENSO events, after 1500 AD the variability is attributable to other causes. Another possibility is that human disturbance in the El Junco watershed acted obscured the relationship between precipitation and grain size (Conroy et al., 2008).

In addition to any possible trends in ENSO is the potential for changes in precipitation as a result of migration in the mean annual or seasonal position of the ITCZ. Indeed, over the past ~ 1kyr the percentage of titanium in the sediments of the Cariaco Basin, which was interpreted primarily as an ITCZ signal, show strong similarity to the changes in Poza del Diablo $\delta D_{Lake}$ values (Figure 12 A, D) (Haug et al., 2001). In this record increased titanium is inferred to correspond to increased erosion as a result of increased precipitation in northern South America, so the decrease in titanium from ~ 1000 to 1800 AD would indicate drying in the northern tropics, which was interpreted as a southward shift of the ITCZ (Haug et al., 2001). Such migration would have brought wetter conditions to the Galápagos, which would have not been associated with El Niño-driven changes in sea surface height, and therefore might explain the decrease in $\delta D_{Lake}$ in Poza del Diablo without a corresponding increase in salinity (Figure 12 A, B). In fact, if anything there is a weak decline in salinity in the Diablo sediment record (Figure 12 B), which would be consistent with increased influx of freshwater without changes in sea level. It is also possible that reductions in global sea level over this period acted to reduce the sensitivity of the salinity to ENSO driven changes in sea surface height. However, if the changes over the last millennium in the eastern tropical Pacific were entirely ENSO driven the Poza del

Diablo $\delta D_{lake}$ record would still be consistent with the Cariaco titanium record since the two regions also display an opposing hydrologic response to ENSO conditions.

The botryococcene δD record from El Junco Lake (Sachs et al., 2009) also indicates a wetter interval prior to 1850 AD, but in contrast to the Diablo record, the onset is earlier at ~ 1000 AD, with the wettest conditions observed near 1200 AD (Figure 12 E). Although this coincides with a wet interval at Diablo as well, Diablo is even wetter between ~1600 and 1850 AD, which corresponds more closely with the maximum northern hemisphere cooling (Figure 12 G) (Mann et al., 2008). The El Junco $\delta D_{botryo}$ record was originally interpreted to support the idea that the ITCZ was south of its present position during the Little Ice Age, and the data from Poza del Diablo may in fact support this assertion given the significant depletion in $\delta D_{Lake}$ values with minimal accompanying changes in salinity (Figure 12 A, B). However, a recent continuous and annually resolved record of ENSO variance derived from the gridded network of tree ring-based reconstructions of the Palmer Drought Severity Index in North America suggests increases from 1000 AD to the present (Li et al., 2011), which could be called on to explain the decrease in Diablo $\delta D_{Lake}$ values if the salinity sensitivity were reduced by falling sea levels. It is also possible that the changes in the *n*-alkane concentrations and the $\delta D_{C29}$ values can be explained by wetter conditions after 1500 AD, since these changes may have altered the hydroclimate enough to permit a significant shift in the dominant mangrove groups (Figure 6).

**Conclusion**

The data we present from Poza del Diablo using multiple lipid biomarker concentration

and hydrogen isotope data provide new insights on climate variability in the eastern tropical Pacific over the past 2 kyr. We use sediment records from three lakes, δD values from $n$C$_{29}$ alkanes, $n$C$_{24}$ alkanols, taraxerol and dinosterol, and alkane and taraxerol concentration profiles to produce a coherent characterization of hydrologic change. Our data agree favorably with an independent salinity reconstruction based on changes in diatom species assemblages preserved in the sediments from Poza del Diablo (Seddon et al., 2011). We apply calibrated relationships between the salinity and hydrogen isotopic fractionation in algal and mangrove lipids to calculate a record of changing $\delta D_{Lake}$ and salinity values. Our data support the interpretation that pre-Little Ice Age hydroclimate variability may have been driven by ENSO or ENSO-like climate events, while the changes since ~ 1200 AD are more likely to have been caused by migration of the ITCZ.

Our data also demonstrate the importance of considering the source of compounds used for hydrogen isotope based paleoclimate records, since the common leaf wax biomarker $n$C$_{29}$ alkanes, yielded δD values that were inconsistent with those from three other compounds at three separate lakes. Rather than reflecting a direct hydrologic signal, the $\delta D_{C29}$ values likely represent changing vegetation patterns, which are also reflected in changing relative concentrations of other alkanes in the sediments.

Using the multiple biomarker approach we have attempted to recover a coherent assessment of regional hydroclimate changes from a complicated hydrologic and sedimentary setting. Our apparently successful efforts should help to open the door for continued exploration of coastal lakes, lagoons, and estuaries in tropical environments as sources of paleoclimate proxy records. This helps to expand the range of potential study sites beyond the limited number of

true lakes on tropical islands. Basin scale hydrologic models are the next logical step in recovering the maximum quantitative climate information from records of lake water salinity and δD values, which may permit estimates of parameters that can be incorporated into climate models, such as precipitation δD values.

**Acknowledgements**

This material is based upon work supported by the U.S. National Science Foundation under Grants ESH-0639640, and the U.S. National Oceanic and Atmospheric Administration under Grant No. NA08OAR4310685 to J. Sachs. We also thank the University of Washington School of Oceanography for funding the field work. The authors would like to thank Orest Kawka, Josh Gregersen, Nemiah Ladd, Alyssa Atwood, and Julie Richey for useful discussions, advice and assistance in the lab. We thank Ariel Townsend for her careful assistance in the lab. We thank Alyssa Atwood, and Simon Haberle for assistance in the field.

**Chapter 6 References**

Brock, F., Higham, T., Ditchfield, P., Ramsey, C.B., 2010. Current Pretreatment Methods For Ams Radiocarbon Dating At The Oxford Radiocarbon Accelerator Unit (Orau). Radiocarbon 52, 103-112.

Carton, J.A., Giese, B.S., 2008. A Reanalysis of Ocean Climate Using Simple Ocean Data Assimilation (SODA). Monthly Weather Review 136, 2999-3017.

Castañeda, I.S., Werne, J.P., Johnson, T.C., Powers, L.A., 2011. Organic geochemical records from Lake Malawi (East Africa) of the last 700 years, part II: Biomarker evidence for recent changes in primary productivity. Palaeogeography, Palaeoclimatology, Palaeoecology 303, 140-154.

Chiang, J.C.H., 2009. The Tropics in Paleoclimate. Annual Review of Earth and Planetary Sciences 37, 263-297.

Cobb, K.M., Westphal, N., Sayani, H.R., Watson, J.T., Lorenzo, E.D., Cheng, H., Edwards, R.L., Charles, C.D., 2013. Highly Variable El Niño–Southern Oscillation Throughout the Holocene. Science 339, 67-70.

Colinvaux, P.A., 1972. Climate and the Galapagos Islands. Nature 240, 17-20.

Conroy, J.L., Overpeck, J.T., Cole, J.E., Shanahan, T.M., Steinitz-Kannan, M., 2008. Holocene changes in eastern tropical Pacific climate inferred from a Gala´pagos lake sediment record. Quaternary Science Reviews 27, 1166-1180.

Dansgaard, W., 1964. Stable Isotopes in Precipitation. Tellus 16, 436-468.

Deplazes, G., Lückge, A., Peterson, L.C., Timmermann, A., Hamann, Y., Hughen, K.A., Röhl, U., Laj, C., Cane, M.A., Sigman, D.M., Haug, G.H., 2013. Links between tropical rainfall and North Atlantic climate during the last glacial period. Nature Geoscience 6, 213-217.

Dodd, R.S., Fromard, F., Rafii, Z.A., Blasco, F., 1995. Biodiversity among West African Rhizophora: Foliar Wax Chemistry. Biochemical Systematics and Ecology 23, 859-868.

Dodd, R.S., Radii, Z.A., Fromard, F., Blasco, F., 1998. Evolutionary diversity among Atlantic coast mangroves. Acta Oecologica 3, 323-330.

Douglas, P.M.J., Pagani, M., Brenner, M., Hodell, D.A., Curtis, J.H., 2012. Aridity and vegetation composition are important determinants of leaf-wax dD values in southeastern Mexico and Central America. Geochimica et Cosmochimica Acta 97, 24-45.

Haug, G.H., Hughen, K.A., Sigman, D.M., Peterson, L.C., Röhl, U., 2001. Southward Migration of the Intertropical Convergence Zone Through the Holocene. Science 293, 1304-1308.

Hoffmann, B., Kahmen, A., Cernusak, L.A., Arndt, S.K., Sachse, D., 2013. Abundance and distribution of leaf wax n-alkanes in leaves of Acacia and Eu‐calyptus trees along a strong humidity gradient in northern Australia. Organic Geochemistry doi: http://dx.doi.org/10.1016/j.orggeochem.2013.07.003.

Hou, J., D'Andrea, W.J., Huang, Y., 2008. Can sedimentary leaf waxes record D/H ratios of continental precipitation? Field, model, and experimental assessments. Geochimica et Cosmochimica Acta 72, 3503-3517.

Hua, Q., Barbetti, M., 2004. Review Of Tropospheric Bomb 14C Data For Carbon Cycle Modeling And Age Calibration Purposes. Radiocarbon 46, 1273-1298.

Kahmen, A., Hoffmann, B., Schefuß, E., Arndt, S.K., Cernusak, L.A., West, J.B., Sachse, D., 2013a. Leaf water deuterium enrichment shapes leaf wax n-alkane dD values of angiosperm plants II: Observational evidence and global implications. Geochimica et Cosmochimica Acta 111, 50-63.

Kahmen, A., Schefuß, E., Sachse, D., 2013b. Leaf water deuterium enrichment shapes leaf wax n-alkane dD values of angiosperm plants I: Experimental evidence and mechanistic insights. Geochimica et Cosmochimica Acta 111, 39-49.

Koutavas, A., deMenocal, P.B., Olive, G.C., Lynch-Stieglitz, J., 2006. Mid-Holocene El Niño−Southern Oscillation (ENSO) attenuation revealed by individual foraminifera in eastern tropical Pacific sediments. Geology 34, 993-996.

Koutavas, A., Joanides, S., 2012. El Niño–Southern Oscillation extrema in the Holocene and Last Glacial Maximum. Paleoceanography 27, doi:10.1029/2012PA002378.

Ladd, S.N., Sachs, J.P., 2012. Inverse relationship between salinity and n-alkane dD values in the mangrove Avicennia marina. Organic Geochemistry 48, 25-36.

Li, J., Xie, S.-P., Cook, E.R., Huang, G., D'Arrigo, R., Liu, F., Ma, J., Zheng, X.-T., 2011. Interdecadal modulation of El Niño amplitude during the past millennium. Nature Climate Change 1, 114-118.

Liu, W., Yang, H., 2008. Multiple controls for the variability of hydrogen isotopic compositions in higher plant n-alkanes from modern ecosystems. Global Change Biology 14, 2166-2177.

Mann, M.E., Zhang, Z., Hughes, M.K., Bradley, R.S., Miller, S.K., Rutherford, S., Ni, F., 2008. Proxy-based reconstructions of hemispheric and global surface temperature variations over the past two millennia. Proceedings of the National Acadamy of Sciences of the United States of America 105, 13252-13257.

McCormac, F.G., Hogg, A.G., Blackwell, P.G., Buck, C.E., Higham, T.F.G., Reimer, P.J., 2004. SHCal04 Southern Hemisphere Calibration 0-11.0 cal Kyr BP. Radiocarbon 46, 1087-1092.

McInerney, F.A., Helliker, B.R., Freeman, K.H., 2011. Hydrogen isotope ratios of leaf wax n-alkanes in grasses are insensitive to transpiration. Geochimica et Cosmochimica Acta 75, 541-554.

Naidoo, G., 2010. Ecophysiological differences between fringe and dwarf Avicennia marina mangroves. Trees 24, 667-673.

Nelson, D.B., Sachs, J.P., *Chapter 2*. Concurrent Purification of Sterols, Triterpenols and Alkenones from Sediments for Hydrogen Isotope Analysis using High Performance Liquid Chromatography.

Nelson, D.B., Sachs, J.P., *Chapter 3*. The influence of salinity on D/H fractionation in dinosterol and brassicasterol from globally distributed saline and hypersaline lakes

Nelson, D.M., Henderson, A.K., Huang, Y., Hu, F.S., 2013. Influence of terrestrial vegetation on leaf wax dD of Holocene lake sediments. Organic Geochemistry 56, 106-110.

Polissar, P.J., Freeman, K.H., 2010. Effects of aridity and vegetation on plant-wax dD in modern lake sediments. Geochimica et Cosmochimica Acta 74, 5785-5797.

Pryeta, A., Domínguez, C., Tomaia, P.F., Chaumont, C.d., d'Ozouville, N.m., Villacís, M., Violette, S., 2012. Quantification of cloud water interception along the windward slope of Santa Cruz Island, Galapagos (Ecuador). Agricultural and Forest Meteorology 161, 94-106.

Rafii, Z.A., Dodd, R.S., Fromard, F., 1996. Biogeographic Variation in Foliar Waxes of Mangrove Species. Biochemical Systematics and Ecology 24, 341-345.

Rampen, S.W., Abbas, B.A., Schouten, S., Sinninghe-Damsté, J.S., 2010. A comprehensive study of sterols in marine diatoms (Bacillariophyta): Implications for their use as tracers for diatom productivity. Limnology and Oceanography 55, 91-105.

Rein, B., Lückge, A., Reinhard, L., Sirocko, F., Wolf, A., Dullo, W.-C., 2005. El Niño variability off Peru during the last 20,000 years. Paleoceanography 20, doi:10.1029/2004PA001099.

Riedinger, M.A., Steinitz-Kannan, M., Last, W.M., Brenner, M., 2002. A ~6100 14C yr record of El Niño activity from the Galápagos Islands. Journal of Paleolimnology 27, 1-7.

Risi, C., Bony, S., Vimeux, F., 2008. Influence of convective processes on the isotopic composition ( $\delta$ 18O and $\delta$ D) of precipitation and water vapor in the tropics: 2. Physical interpretation of the amount effect. Journal of Geophysical Research 113.

Romero-Viana, L., Kienel, U., Wilkes, H., Sachse, D., 2013. Growth-dependent hydrogen isotopic fractionation of algal lipid biomarkers in hypersaline Isabel Lake (Mexico). Geochimica et Cosmochimica Acta 106, 490-500.

Sachs, J.P., Sachse, D., Smittenberg, R.H., Zhang, Z., Battisti, D.S., Golubic, S., 2009. Southward movement of the Pacific intertropical convergence zone AD 1400–1850. Nature Geoscience 2, 519-525.

Sachs, J.P., Schwab, V.F., 2011. Hydrogen isotopes in dinosterol from the Chesapeake Bay estuary. Geochmica et Cosmochimica Acta 75, 444-459.

Sachse, D., Billault, I., Bowen, G.J., Chikaraishi, Y., Dawson, T.E., Feakins, S.J., Freeman, K.H., Magill, C.R., McInerney, F.A., van der Meer, M.T.J., Polissar, P., Robins, R.J., Sachs, J.P., Schmidt, H.-L., Sessions, A.L., White, J.W.C., West, J.B., Kahmen, A., 2012. Molecular Paleohydrology: Interpreting the Hydrogen-Isotopic Composition of Lipid Biomarkers from Photosynthesizing Organisms. Annual Review of Earth and Planetary Sciences 40, null.

Sachse, D., Kahmen, A., Gleixner, G., 2009. Significant seasonal variation in the hydrogen isotopic composition of leaf-wax lipids for two deciduous tree ecosystems (Fagus sylvativa and Acer pseudoplatanus). Organic Geochemistry 40, 732-742.

Sachse, D., Sachs, J.P., 2008. Inverse relationship between D/H fractionation in cyanobacterial lipids and salinity in Christmas Island saline ponds. Geochim. Cosmochim. Acta 72, 793-806.

Schouten, S., Ossebaar, J., Schreiber, K., Kienhuis, M.V.M., Langer, G., Benthien, A., Bijma, J., 2006. The effect of temperature, salinity and growth rate on the stable hydrogen isotopic composition of long chain alkenones produced by *Emiliania huxleyi* and *Gephyrocapsa oceanica*. Biogeosciences 3, 113-119.

Seddon, A.W.R., Froyd, C.A., Leng, M.J., Milne, G.A., Willis, K.J., 2011. Ecosystem Resilience and Threshold Response in the Galápagos Coastal Zone. Plos One 6, e22376.

Sessions, A.L., Burgoyne, T.W., Hayes, J.M., 2001. Determination of the H3 Factor in Hydrogen Isotope Ratio Monitoring Mass Spectrometry. Analytical Chemistry 73, 200-207.

Silva, C.A., Madureira, L.A.S., 2012. Source correlation of biomarkers in a mangrove ecosystem on Santa Catarina Island in southern Brazil. Annals of the Brazilian Acadamy of Sciences 84, 589-604.

Sinninghe-Damste, J.S., Dongen, B.E.v., Rijpstra, W.I.C., Schouten, S., Volkman, J.K., Geenevasen, J.A.J., 2001. Novel intact glycolipids in sediments from an Antarctic lake (Ace Lake). Organic Geochemistry, 321-332.

Smith, F.A., Freeman, K.H., 2006. Influence of physiology and climate on delta D of leaf wax n-alkanes from C-3 and C-4 grasses. Geochimica et Cosmochimica Acta 70, 1172-1187.

Smittenberg, R.H., Saenger, C., Dawson, M.N., Sachs, J.P., 2011. Compound-specific D/H ratios of the marine lakes of Palau as proxies for West Pacific Warm Pool hydrologic variability. Quaternary Science Reviews 30, 921-933.

Stuiver, M., Reimer, P.J., 1993. Radiocarbon calibration program. Radiocarbon 35, 215-230.

Tipple, B.J., Berke, M.A., Doman, C.E., Khachaturyan, S., Ehleringer, J.R., 2013. Leaf-wax n-alkanes record the plant–water environment at leaf flush. Proceedings of the National Acadamy of Sciences of the United States of America 110, 2659-2664.

Tudhope, A.W., Chilcott, C.P., McCulloch, M.T., Cook, E.R., Chappell, J., Ellam, R.M., Lea, D.W., Lough, J.M., Shimmield, G.B., 2001. Variability in the El Niño–Southern Oscillation Through a Glacial-Interglacial Cycle. Science 291, 1511-1517.

Vecchi, G.A., Wittenberg, A.T., 2010. El Niño and our future climate: where do we stand? Wiley Interdisciplinary Reviews: Climate Change 1, 260-270.

Versteegh, G.J.M., Schefuss, E., Dupont, L., Marret, F., Damste, J.S.S., Jansen, J.H.F., 2004. Taraxerol and Rhizophora pollen as proxies for tracking past mangrove ecosystems. Geochimica et Cosmochimica Acta 68, 411-422.

Volkman, J.K., 2003. Sterols in microorganisms. Applied Microbiology and Biotechnology 60, 495-506.

Volkman, J.K., Barrett, S.M., Blackburn, S.I., Mansour, M.P., Sikes, E.L., Gelin, F., 1998. Microalgal biomarkers: A review of recent research developments. Organic Geochemistry 29, 1163-1179.

Wang, Y.V., Larsen, T., Leduc, G., Andersen, N., Blanz, T., Schneider, R.R., 2013. What does leaf wax dD from a mixed C3/C4 vegetation region tell us? Geochimica et Cosmochimica Acta 111, 128-139.

Wolhowe, M.D., Prahl, F.G., Probert, I., Maldonado, M., 2009. Growth phase dependent hydrogen isotopic fractionation in alkenone-producing haptophytes. Biogeosciences 6, 1681-1694.

Yang, H., Liu, W., Leng, Q., Hren, M.T., Pagani, M., 2011. Variation in n-alkane dD values from terrestrial plants at high latitude: Implications for paleoclimate reconstruction. Organic Geochemistry 42, 283-288.

Yang, H., Pagani, M., Briggs, D.E.G., Equiza, M.A., Jagels, R., Leng, Q., LePage, B.A., 2009. Carbon and hydrogen isotope fractionation under continuous light: implications for paleoenvironmental interpretations of the High Arctic during Paleogene warming. Oecologia 160, 461-470.

Zhang, Z., Sachs, J.P., 2007. Hydrogen isotope fractionation in freshwater algae: I. Variations among lipids and species. Organic Geochemistry 38, 582-608.

Zhang, Z., Sachs, J.P., Marchetti, A., 2009. Hydrogen isotope fractionation in freshwater and marine algae: II. Temperature and nitrogen limited growth rate effects. Organic Geochemistry 40, 428-439.

Zhou, Y., Grice, K., Chikaraishi, Y., Stuart-Williams, H., Farquhar, G.D., Ohkouchi, N., 2011. Temperature effect on leaf water deuterium enrichment and isotopic fractionation during leaf lipid biosynthesis: Results from controlled growth of C3 and C4 land plants. Phytochemistry 72, 207-213.